

Batch en continue bezinking van actief slib:
doorgedreven experimenten en ID compressie modellering

Batch and Continuous Settling of Activated Sludge:
In-Depth Monitoring and ID Compression Modelling

Jeriffa De Clercq

Promotoren: prof. dr. ir. J. Defrancq, prof. dr. ir. P. A. Vanrolleghem
Proefschrift ingediend tot het behalen van de graad van
Doctor in de Ingenieurswetenschappen: Chemische Technologie

Vakgroep Chemische Proceskunde en Technische Chemie
Voorzitter: prof. dr. ir. G. B. Marin
Faculteit Ingenieurswetenschappen
Academiejaar 2005 - 2006



ISBN 90-8578-093-4

NUR 973

Wettelijk depot: D/2006/10.500/51

Voor mijn lieve schat
Wim

PROMOTOREN:

Prof. dr. ir. Jacques Defrancq	Universiteit Gent
Prof. dr. ir. Peter A. Vanrolleghem	Universiteit Gent

EXAMENCOMMISSIE:

Prof. dr. ir. Ronny Verhoeven, voorzitter	Universiteit Gent
Dr. ir. Ingmar Nopens, secretaris	Universiteit Gent
Prof. dr. ir. Geraldine Heynderickx	Universiteit Gent
Prof. dr. ir. Peter Troch	Universiteit Gent
Prof. dr. ir. Willy Verstraete	Universiteit Gent
Prof. dr. ir. Jean-Luc Vassel	Université de Liège
Ir. Martijn Devisscher	Aquafin NV

Universiteit Gent
Faculteit Ingenieurswetenschappen
Vakgroep Chemische Proceskunde en Technische Chemie
Technologiepark 914
9052 Zwijnaarde
België

Dit werk is tot stand gekomen dankzij:



Faculteit
Bio-ingenieurswetenschappen



Copyright

The author and the promotor give the authorization to consult and to copy parts of this work for personal use only. Any other use is limited by the Laws of Copyright. Permission to reproduce any material contained in this work should be obtained from the author.

De auteur en de promotor geven de toelating dit werk voor consultatie beschikbaar te stellen en delen ervan te kopiëren voor persoonlijk gebruik. Elk ander gebruik valt onder de beperkingen van het auteursrecht, in het bijzonder met betrekking tot de verplichting uitdrukkelijk de bron te vermelden bij het aanhalen van resultaten uit dit werk.

Gent, 6 juli 2006

De promotoren:

De auteur:

Prof. dr. ir. Jacques
Defrancq

Prof. dr. ir. Peter A.
Vanrolleghem

ir. Jeriffa De Clercq

Dankwoord

Professor Jacques Defrancq, promotor, ik wil je bedanken voor het vertrouwen en de steun en vooral voor de vrijheid die je me gaf. Ik kon ook steeds op je rekenen voor de praktische kant van de zaak. Ik zal proberen je vanaf nu met Jacques (iplv professor) aan te spreken... Ik denk ook dat je een fantastische opa bent voor je kleinkinderen. Peter (professor Vanrolleghem, promotor), bedankt dat je op de vraag wou ingaan om promotor te zijn van mijn doctoraat. Zonder jou was het echt nooit gelukt om tot dit werk te komen. Je bleef steeds vertrouwen hebben in mijn kunnen en je kon me ook steeds motiveren. Ik kon ook steeds bij jou terecht met vanalles en nog wat. Je slaagde erin om tussen al je werkzaamheden op Biomath in toch nog steeds tijd te vinden voor onze maandelijkse vergaderingen, het nalezen van de artikels en het doctoraat. Petje af hoor voor je energie, je gedrevenheid en je managementcapaciteiten. Bovenop al deze (en nog vele andere) capaciteiten blijf je gewoon en begripvol. Ik snap echt niet hoe je alles wat je doet, doet... Jij hebt ook een groep in het leven geroepen om alle activiteiten rond bezinking binnen Biomath en binnen de groep van professor Van der Meeren te bundelen: Sedifloc. De maandelijkse vergaderingen brachten nieuwe inzichten en kritische vragen met zich mee. Ook bedankt om er op het laatste wat vaart achter te zetten, anders was ik misschien nog wel voor een paar maanden zoet geweest..., en om de laatste loodjes wat lichter te maken.

Dank u, professor De Vynck, voorzitter vakgroep en hoofd van het labo, omdat je me de kans hebt gegeven om aan jouw labo te doctoreren en omdat je steeds bereid was de nodige centen op te hoesten.

Professor Heynderickx, bedankt dat je lid wou zijn van mijn doctoraatsbegeleidingscommissie en examencommissie. Je geruststellende woorden en je hulp hebben deugd gedaan.

Professor Vassel, *il était toujours très intéressant de discuter avec vous de la sédimentation et de la compression. Merci!*

Ook alle andere leden van de examencommissie wens ik te bedanken voor hun kritische input.

Toen ik net begon als assistent, had ik me voorgenomen om eens te polsen bij Aquafin en aanverwante bedrijven wat ik voor hen zou kunnen betekenen. En ik was aangenaam verrast dat ze mij dan ook een aantal voorstellen hebben gedaan. Bedankt hiervoor Chris, Ivo en Herwig. Ik vond en vind het nog steeds een heel leuk onderwerp en zou er graag nog verder aan werken... En uiteraard wil ik jullie ook bedanken voor het ter beschikking stellen van de installaties, meetapparatuur e.d.. Martijn, jij bent de drijvende kracht geweest achter de volschalige experimenten. Zonder jou was dit nooit gelukt. Ook dankjewel aan de operatoren van RWZI Heist, Essen, Destelbergen en Deinze en aan Cedric en Marc voor jullie aandeel in de metingen. Het was aangenaam

met jullie samen te werken.

Dan zijn er ook nog de andere collega's van op het labo: Paul, Erik, Maria, Hugo, Anny, Herwin, Willy, Michel, Ann en Carl. Paul, bedankt voor het mee helpen ontwerpen en maken van de pilootopstelling, voor je interesse in en hulp bij computerprogramma's, schrijven van macro's in Excel om al de data te extraheren en te verwerken en om mijn loopmaatje te zijn, om er steeds voor mij te zijn. Maria, bedankt voor alle administratieve hulp. Hugo, bedankt voor de analyses. Anny, bedankt voor je interesse en voor je moederlijke aandacht. Herwin, bedankt voor het maken van onze eigen settlometer. Willy en Michel, ook bedankt voor je interesse. Ann, bedankt voor de dagelijkse portie gezelligheid. Carl, jammer dat we niet langer hebben kunnen samenwerken. En Erik, last but not least: bedankt voor je nooit aflatende hulp bij vanalles en nog wat (piloootopstelling, slib halen, ...). Het was toch wel echt gezellig om samen in je rode autootje een koffietje drinken en een koekje te eten. En dan mag ik zeker het samen verorberen van frietjes niet vergeten... Als mijn been in het gips zat, heb jij ook met mij rondgereden in een rolstoel.

Dan zijn er ook nog de thesisstudenten: Joris, Krishna, Stijn, Philippe en Kristof. Bij de ene ging de samenwerking al wat vlotter dan de andere. Maar ik heb in elk geval genoten van de samenwerking en er ook veel van geleerd. Dankjewel. En het was ook leuk dat er dan nog 's wat jong bloed aan de koffiepauze zat...

Twee leden van Sedifloc, Bob en Ingmar, wil ik in het bijzonder bedanken.

Bob, we hebben vele keren de vraag gekregen of we een koppel waren (zelfde familienaam)... Het was steeds verhelderend om met jou te discussiëren over mijn werk. Ook bedankt om delen van mijn literatuurstudie grondig en kritisch na te lezen. Jij hebt deze als eerste doorgenomen. Je bent echt wel een verstandige kerel. Ingmar, bedankt voor het kritisch nalezen van mijn tekst. Het was echt aangenaam met je samen te werken. Met o.a. jouw managerscapaciteiten zou je een waardige vervanger zijn voor Peter in Biomath (ik hoop en duim mee)...

Op een van de vele conferenties is Peter Dave Kinnear tegen het lijf gelopen. A man with a lot of knowledge about settling and flocculation. And Peter could arrange it that Dave came to work at Biomath for a few months. This was evidently a very fertile time for my research. His questions about compression and the theory behind it are perhaps a bit answered now... Dave went with me to Oxford to see how professor Sills studied the settling of sediments with X-rays. Professor Sills had a few ideas to study the settling of activated sludge, one of those was finally used in this work: tracing of the activated sludge.

Hans (lid van Sedifloc) heeft ons naar het UZ geleid, waar ik in contact ben gekomen met Filip De Vos en Filip Jacobs. Filip J., het was aangenaam met je samen te werken, bedankt om elk weekend nog 's naar je werk te komen.

En dan is er nog het thuisfront... Tja, hiervoor zijn er geen woorden genoeg. Dankjewel mama en papa om me de kans te hebben gegeven om verder te studeren en om er steeds voor me te zijn en me te soigneren en de kindjes op te vangen als ik nog maar eens dringend moest verderwerken. Ook mijn schoonouders, broers, schoonbroers en schoonzussen, dankjewel om me te blijven motiveren en om me mijn werk te doen relativeren.

En dan is er nog mijn allerliefste Wim, jij hebt me steeds de moed gegeven om verder te doen. Door onze babbeltjes over mijn doctoraatsproblemen kwam ik vaak al tot

nieuwe ideeën. Ge zijt echt nen heel verstandige kerel, moest je het nog niet weten... Toen ik met mijn been in het gips zat en/of mogelijks zwanger was, moest jij de experimenten in het UZ opstarten en beëindigen. Vooral op vrijdag was het niet evident om dit te combineren met jouw werk. Maar toch stond je er steeds, merci! En dan is er ook nog het laatste jaar, waarin ik mijn werk moest combineren met mijn doctoraat en met ons gezin. Dankjewel om mij hiervoor de tijd te geven en er te blijven in geloven. Het is niet evident geweest... In mijn doctoraatsperiode zijn er twee wondertjes (na een lijdensweg) in ons leven gekomen, Cas en Nande. Het is echt merkwaardig hoe zij je doen inzien waar het leven eigenlijk om draait.

Ik had dit nooit durven dromen...

Gent, 6 juli 2006
Jeriffa De Clercq

Summary

In municipal wastewater treatment, the wastewater is transformed in clean water and solid matter. In order to get the clean water the solids are most often separated from it by gravity in a clarifier. The clarifier is therefore crucial for the overall performance; improper operation results in a washout of solids, increasing the concentration of effluent particulate pollutants and involuntarily wasting mixed liquor. Violation of effluent permits and deterioration of the receiving waters is then the unavoidable result, with long-term release of nitrogen, phosphorus and COD as the solids degrade. The settling characteristics of activated sludge are obviously important for the performance of the clarifier and, hence, the efficiency of the wastewater treatment plant. The operation of a clarifier can be improved by a better understanding of the settling properties.

This dissertation focuses on the settling properties and a 1D batch/continuous settling model. It aimed at finding a model that describes this settling behaviour, i.e. a batch settling model, and to develop, to this end, measurement techniques that give more information about the settling behaviour. Two detailed full-scale measuring campaigns were performed and used as input for a 1D continuous settling model that describes the full-scale behaviour of a circular clarifier and that incorporates the batch settling model.

Novel measurement techniques were developed, which give solids concentration profiles and pressure profiles with sufficient accuracy during the batch settling of activated sludge.

A novel non-invasive measurement technique borrowed from nuclear medicine, using a solids radiotracer and gamma cameras was used to obtain high time and spatial resolution solids concentration profiles during the batch settling of activated sludge in a pilot-scale column with a height of 1 m. This non-invasive technique does not disturb the settling process, does not alter the settling characteristics of the activated sludge, gives profiles every minute, and is capable of measuring in a range of 0-25 g/l with high accuracy. Dynamic solids concentration profile measurements were performed for sludges of 2 different municipal wastewater treatment plants, and at 3 different initial solids concentrations. The high-resolution profiles give a quantitative representation of the settling process and can be used for a better understanding and modelling of the process. The results reveal hindered and compression settling and show a time-dependent compression solids concentration.

For measuring the excess pore pressure profiles during batch settling of activated sludge, a pilot-scale set-up has been built, which consists of a settling column, a water-filled column and a differential pressure transducer with sufficient accuracy. The pressure of the water in the sludge, i.e. the pore pressure, was measured at 15 points

along the height of the settling suspension. The measurements are however not as good and as detailed as the concentration profile measurements but they confirm compression settling from the sludge blanket height downwards. More work is needed to improve this measurement technique.

The high-resolution batch settling experiments were used to develop a fundamental batch settling model, i.e. a model which is based on the fundamental mass and force balances for water and solids. Such a model is generally described by two functions, a hindered settling flux function and an effective solids stress function. Observed initial settling velocities and inverse modelling calculations of the experimental data were used to obtain a relationship for these two functions. This resulted in the power function of Cole (1968), limited by imposing a maximum settling velocity, for the hindered settling flux function and a logarithmic function for the effective solids stress function, together with a time-dependent compression solids concentration. This time-dependent compression solids concentration is located at the sludge blanket height and can be readily calculated. The resulting batch settling model excellently describes the settling behaviour and this for sludges originating from two different wastewater treatment plants. When the settling behaviour, i.e. the parameters of the batch settling model, is identified, it can be used as the basis for (1D, 2D or 3D) models which attempt to describe the full-scale behaviour of a clarifier. Since the batch settling model describes the settling behaviour better than any other reported model, these (1D, 2D or 3D) models can be used e.g. to make better designs and set-up better control strategies.

For calibration and validation of a 1D continuous settling model, which incorporates this batch settling model, two detailed full-scale measuring campaigns were performed, one for building and testing and one for validating. These provided measurements of solids concentration profiles in the clarifier, sludge blanket heights, concentrations of the relevant flows (feed, recycle and effluent), and batch settling curves at different solids concentrations and sludge volume index (SVI). One campaign was performed on an operational secondary circular centre-fed clarifier of a municipal WWTP. The other one was performed on a primary circular centre-fed clarifier of another municipal WWTP, which was used as a secondary clarifier. Since the effluent of this test clarifier was sent to the aeration tanks, the latter set-up allowed to have overflow of sludge (no effluent restrictions). During the studied period, the feed and recycle flow rates were changed frequently and the settling properties changed. The study showed that it is not straightforward to perform full-scale experiments: it is impossible to set all variables to desired values (feed solids concentration, settling properties) and the daily operation of the WWTP may not be disturbed, but on the other hand it influences the experiments (e.g. maintenance works had effect on settling properties and feed solids concentration). There is not always someone present on-site to solve problems, one needs reliable and appropriate sensors/pumps that remain stable with time, Nevertheless, the results were very satisfying. The effect of variations in recycle and feed flow, feed solids concentrations and settling properties could in most cases be clearly identified and confirmed the expectations. The two sets of full-scale experimental data were used to build, test and validate a 1D continuous settling model.

The settling behaviour of the activated sludge of the full-scale experimental data was predicted with the batch settling model on the basis of the measured batch settling curves. Instead of using a maximum settling velocity for the Cole (1968) hindered

settling flux function, the Vesilind function (Vesilind, 1968) was used for the lower solids concentrations, together with the condition that the flux function is differentiable at a transition solids concentration between both functions. The agreement with the experimental batch settling curves is excellent. The batch settling model is incorporated in the 1D continuous settling model by the following modifications: (i) setting the compression solids concentration equal to the concentration that is found at a location of 5 layers below the location of the highest concentration gradient of the simulated solids concentration profile, (ii) defining the feed layer location at the compression solids concentration location and (iii) making a parameter of the effective solids stress function dependent on the average solids concentration in the clarifier. Simulations with the 1D continuous settling model showed the need for the addition of a dispersion term to the model. Two dispersion coefficients, one in the clarification zone and the other in the thickening zone, were added to the model and estimated with measured solids concentration profiles. Dispersion clearly improved the simulation results but the model needs further improvement. When this is done, the 1D continuous settling model can be used for operation and control.

Samenvatting

In rioolwaterzuivering wordt het afvalwater omgezet tot schoon water en zwevende deeltjes, het actief slib. Het schoon water wordt meestal van het slib gescheiden in een nabezinker. De nabezinker is essentieel voor de prestaties van de hele zuiveringsinstallatie. Een niet-optimale afscheidingsefficiëntie resulteert immers in de lozing (en dus ook verlies) van slib. Lozingsnormen worden overschreden en de kwaliteit van het ontvangende water verslechtert (het afbreken van het actief slib resulteert immers in afgifte van stikstof, fosfor en COD). De bezinkingseigenschappen van het actief slib zijn aldus belangrijk voor de prestaties van de nabezinker en uiteindelijk ook voor de efficiëntie van de hele waterzuiveringsinstallatie. De werking van de nabezinker kan verbeterd worden door een betere kennis van deze bezinkingseigenschappen.

Dit proefschrift concentreert zich op de bezinkingseigenschappen van het actief slib en op een batch en 1D continu bezinkingsmodel. Het beoogt een model te vinden dat het bezinkingsgedrag kan beschrijven, i.e. een batch bezinkingsmodel en daartoe meettechnieken te ontwikkelen welke meer informatie verschaffen over dit bezinkingsgedrag. Twee gedetailleerde meetcampagnes zijn ook uitgevoerd en gebruikt voor het opstellen van een 1D continu bezinkingsmodel dat het volschalig gedrag van een cirkelvormige nabezinker beschrijft en welke het batch bezinkingsmodel bevat.

Nieuwe meettechnieken met voldoende nauwkeurigheid werden ontwikkeld welke slibconcentratieprofielen en drukprofielen opmeten tijdens de batchbezinking van het actief slib.

Een nieuwe niet-invasieve meettechniek, afkomstig van de kerngeneeskunde, en gebruik makende van een radioactieve slibtracer en gammacamera's, werd aangewend om slibconcentratieprofielen met hoge tijds- en ruimteresolutie op te meten in een 1 m hoge kolom gedurende de batchbezinking van het actief slib. Deze niet-invasieve techniek verstoort het bezinkingsproces niet, verandert de bezinkingseigenschappen niet, genereert elke minuut concentratieprofielen, en kan meten met hoge nauwkeurigheid in een bereik van 0-25 g/l. Dynamische slibconcentratieprofielen zijn opgemeten voor actief slib van 2 verschillende rioolwaterzuiveringsinstallaties en bij 3 verschillende initiële slibconcentraties. Dergelijke hoge-resolutie profielen geven een kwantitatieve beschrijving van het bezinkingsproces en zijn tot op heden de meest geschikte data voor het verkrijgen van een beter inzicht in en het modelleren van het proces. De metingen tonen gehinderde en compressiebezinking en een tijdsafhankelijke compressieconcentratie.

Er werd een pilootopstelling gebouwd om de waterdrukprofielen te meten tijdens de batchbezinking van actief slib. De opstelling bestaat uit een bezinkingskolom, een kolom gevuld met water en een differentiële drukkometer met voldoende nauwkeurigheid. De druk van het water in de suspensie, i.e. de poriedruk, werd gemeten op 15 plaat-

sen langsheen de hoogte van de bezinkende suspensie. De metingen zijn echter niet zo goed en gedetailleerd als de concentratieprofielmetingen maar ze bevestigen wel compressiebezinking neerwaarts vanaf het slibbed. Deze meettechniek dient echter verbeterd te worden.

Deze hoge-resolutie batchbezinkingsexperimenten werden vervolgens gebruikt om een fundamenteel batch bezinkingsmodel op te stellen, i.e. een model dat gebaseerd is op de fundamentele massa- en krachtbalansen voor het water en het slib. Dergelijk model wordt doorgaans beschreven door 2 functies, i.e. een gehinderde bezinkingsfluxfunctie en een effectieve slibspanningsfunctie. Gemeten initiële bezinkingsnelheden en inverse modelleringsberekeningen op de experimentele data zijn gebruikt om een relatie te bekomen voor deze 2 functies. Dit resulteerde in de machtsfunctie van Cole (1968), begrensd door een maximum bezinkingsnelheid, voor de gehinderde bezinkingsfluxfunctie en in een logaritmische functie voor de effectieve slibspanningsfunctie en dit gecombineerd met een tijdsafhankelijke compressieconcentratie. Deze tijdsafhankelijke compressieconcentratie bevindt zich ter hoogte van het slibbed en kan op eenvoudige wijze worden berekend. Het bekomen batch bezinkingsmodel beschrijft het bezinkingsgedrag uitstekend en dit voor actief slib afkomstig van 2 verschillende waterzuiveringsinstallaties. Wanneer het bezinkingsgedrag, i.e. de parameters van het batch bezinkingsmodel geïdentificeerd zijn, kan het model gebruikt worden als basis voor (1D, 2D of 3D) modellen welke pogen het volschalig gedrag van een nabezinker te beschrijven. Vermits het batch bezinkingsmodel het bezinkingsgedrag beter beschrijft dan de andere gepubliceerde modellen, kunnen dergelijke (1D, 2D en 3D) modellen gebruikt worden om o.a. betere ontwerpen te maken en betere controlestrategieën op te zetten.

Er werden 2 gedetailleerde volschalige meetcampagnes uitgevoerd voor de calibratie en de validatie van een 1D continu bezinkingsmodel welke het batch bezinkingsmodel integreert: één campagne voor het bouwen en testen en één voor het valideren. Deze campagnes bestonden uit metingen van slibconcentratieprofielen in de nabezinker, slibbedhoogtes, slibconcentraties van voeding, recycle en effluent en batchbezinkingscurves bij verschillende slibconcentraties en slibvolumeindices (SVI). Een meetcampagne werd uitgevoerd op een operationele cirkelvormige centraal-gevoede nabezinker van een rioolwaterzuiveringinstallatie. De andere meetcampagne werd uitgevoerd op een cirkelvormige centraal-gevoede voorbezinker van een andere rioolwaterzuiveringinstallatie, welke werd ingezet als nabezinker. Gezien het effluent van deze testbezinker naar het actief slibbekken stroomde, liet deze laatste opstelling toe dat er slib overstortte aangezien er geen beperking inzake lozingsnormen gold voor de bestudeerde nabezinker. Gedurende de meetcampagnes werden de voedings- en recycledebieten frequent gewijzigd en wijzigden de slibbezinkingseigenschappen. Dergelijke studie toonde aan dat het niet zo evident is om volschalige experimenten uit te voeren: het is immers onmogelijk om alle variabelen (voedingsconcentratie, bezinkingseigenschappen) te controleren, en de dagelijkse werking van de waterzuiveringinstallatie mag niet verstoord worden maar beïnvloedt wel de experimenten (onderhoudswerken bijvoorbeeld hadden een invloed op de bezinkingseigenschappen en op de voedingsconcentratie). Er is niet altijd iemand ter plaatse om problemen op te lossen, er is nood aan betrouwbare en geschikte sensoren en pompen welke stabiel blijven in de tijd, Niettemin waren de resultaten zeer goed. De invloed van wijzigingen in recycle en voedingsdebieten, voedingsconcentraties en bezinkingseigenschappen kon in de meeste gevallen duidelijk geïdentificeerd worden en bevestigden de verwachtingen. De 2 gedetailleerde volschalige experimentele data sets werden vervolgens gebruikt om een 1D continu

bezinkingsmodel te bouwen, te testen en te valideren.

Het bezinkingsgedrag van het actief slib van de volschalige experimentele data werd beschreven met het batch bezinkingsmodel aan de hand van de gemeten batchbezinkingscurves. In plaats van het opleggen van een maximale bezinkingsnelheid voor de Cole (1968) gehinderde bezinkingsfluxfunctie, werd de Vesilind functie (Vesilind, 1968) gebruikt voor de lagere slibconcentraties. De fluxfunctie dient wel differentieerbaar te zijn bij de overgang tussen beide functies, i.e. de Vesilind functie en de machtsfunctie van Cole (1968). De overeenkomst met de gemeten batchbezinkingscurves is uitstekend. Het batch bezinkingsmodel werd vervolgens geïntegreerd in het 1D continu bezinkingsmodel door volgende wijzigingen aan te brengen: (i) de compressieconcentratie wordt gelijkgesteld aan de concentratie welke zich bevindt op 5 lagen onder de laag waar zich de hoogste concentratiegradiënt van het gesimuleerde slibconcentratieprofiel bevindt, (ii) de voedingslaag wordt gelijkgesteld aan de laag waar zich de compressieconcentratie bevindt en (iii) een parameter van de effectieve slibspanningsfunctie wordt afhankelijk gemaakt van de gemiddelde slibconcentratie in de nabezinker. Simulaties met het 1D continu bezinkingsmodel toonden de behoefte aan het opnemen van een dispersieterm in het model. Twee dispersiecoëfficiënten, één in de klaringszone en de andere in de indikkingszone, werden toegevoegd aan het model en werden geschat met behulp van de gemeten slibconcentratieprofielen. Dispersie verbeterde duidelijk de simulatieresultaten, maar het model verdient nog verder onderzoek. Eens dit gebeurd is, kan het model gebruikt worden voor het voorspellen van het gedrag van de nabezinker en voor sturing ervan.

Contents

Copyright	iii
Dankwoord	v
Summary	ix
Samenvatting	xiii
List of abbreviations and symbols	xxi
1 Introduction and Objectives	1
1.1 Description and Performance of a Clarifier	2
1.1.1 Configuration	2
1.1.2 Performance	4
1.1.3 Modelling	6
1.2 Goals and Outline of Dissertation	7
1.2.1 Goals	7
1.2.2 Outline	7
2 Modelling of batch settling	9
2.1 Settling behaviour of suspensions	9
2.1.1 Batch settling	11
2.1.2 Fundamental model structure for batch settling	12
2.2 Modelling of activated sludge settling	15
2.2.1 Settling velocity function of Cacossa and Vaccari (1994)	16
2.2.2 Settling velocity function of Kinnear (2002)	17
2.3 Modelling of flocculated suspension settling	19
2.3.1 Properties of the suspensions, experiments and differences with activated sludge	19
2.3.2 Models for flocculated suspension settling	22
2.3.3 Experimental results and model predictions	24
2.4 Conclusion	35
3 1D modelling of continuous settling	39
3.1 Introduction	39
3.2 General Model Description	40
3.3 Models with limitation of the settling flux	43
3.4 Models with dispersion	47
3.5 Models that consider compression settling	50

3.6	Model with a by-pass from inlet to recycle (Dupont and Dahl, 1995)	53
3.7	Conclusion	53
4	Numerical integration and estimation	57
4.1	Numerical integration of the model equations	57
4.1.1	Properties of the mathematical models	57
4.1.2	Numerical integration algorithm	59
4.2	Estimation of the model parameters	62
4.3	Implementation software	63
5	Non-invasive monitoring of activated sludge during batch settling	65
5.1	Introduction	65
5.1.1	Measurement of solids concentration profiles	65
5.1.2	Measurement of excess pore pressure profiles	67
5.2	Material and methods	67
5.2.1	Experimental set-up	67
5.2.2	Origin of the sludge	71
5.2.3	Analytical procedures	71
5.2.4	Experimental procedure for P- and C-set-up	73
5.3	Preliminary experiments	74
5.3.1	Concentration profiles (C-set-up)	74
5.3.2	Pressure profiles (P-set-up)	76
5.4	Pilot-scale experiments: results and discussion	77
5.4.1	Concentration profiles	78
5.4.2	Pressure profiles	85
5.5	Conclusion	87
6	Activated sludge batch settling model	89
6.1	Initial settling velocity and induction period	89
6.2	Kynch batch density function $f_{bk}(C)$	90
6.3	Effective solids stress function $\sigma_e(C)$	91
6.3.1	Inverse modelling: theory and application	95
6.3.2	Evolution of the compression solids concentration	98
6.3.3	Effective solids stress function	98
6.4	Prediction/simulation	100
6.5	Practical use of the improved model	111
6.6	Conclusion	113
7	Continuous settling experiments	115
7.1	Essen WWTP	115
7.1.1	Material and methods	115
7.1.2	Results of the measurements at the Essen WWTP	118
7.1.3	Discussion of the measurement results at the Essen WWTP	121
7.2	Heist WWTP	126
7.2.1	Material and Methods	126
7.2.2	Results of the measurements at the Heist WWTP	130
7.2.3	Discussion of the measurement results at the Heist WWTP	135
7.3	Conclusion	153

8	Activated sludge 1D continuous settling model	155
8.1	Building and testing	155
8.1.1	Determining the settling behaviour of the Heist data	155
8.1.2	Building a 1D continuous settling model	162
8.1.3	Testing a 1D continuous settling model	173
8.2	Validation using the Essen data	178
8.2.1	Determining the settling behaviour of the Essen data	178
8.2.2	Simulating the Essen data with the 1D continuous settling model	178
8.3	Conclusion	182
9	Conclusions and perspectives	185
9.1	Batch settling of activated sludge	185
9.1.1	Non-invasive monitoring of batch settling	185
9.1.2	Batch settling model	188
9.2	Continuous settling of activated sludge	190
9.2.1	Full-scale continuous settling experiments	190
9.2.2	1D Continuous settling model	191
A	Radioactivity profiles	195
B	Initial Kynch batch density values: calculations and functions	197
C	Heist data: Vesilind function	201
	Bibliography	205
	Curriculum Vitae	215

List of abbreviations and symbols

Abbreviations

1D, 2D, 3D	one-, two-, three-dimensional	
BOD	Biological Oxygen Demand	$M L^{-3}$
COD	Chemical Oxygen Demand	$M L^{-3}$
CATScan	Computerized Axial Tomography Scan	
DWA	Dry Weather Supply	
MLSS	Mixed Liquor Suspended Solids	
ODE	Ordinary Differential Equation	
PDE	Partial Differential Equation	
PE	Population Equivalent	
RWA	Rain Weather Supply	
SBH	Sludge Blanket Height	L
SSE	Sum of Squared Errors	
SVI	Sludge Volume Index	$L^3 M^{-1}$
WWTP	WasteWater Treatment Plant	

English symbols

a	settling parameter	
A	cross sectional area	L^2
b	settling parameter	
B_1	Tracy (1973) parameter	$MT^{-1}L^{-2}$
B_2	Tracy (1973) parameter	ML^{-3}
C	solids concentration	ML^{-3}
$C_{average}$	average solids concentration	ML^{-3}
C_C	compression solids concentration	ML^{-3}
C_{crit}	Watts <i>et al.</i> (1996) dispersion parameter	ML^{-3}
C_e	effluent solids concentration	ML^{-3}
C_f	feed solids concentration	ML^{-3}
C_{min}	non-settleable solids concentration	ML^{-3}
C_o	initial solids concentration	ML^{-3}
C_r	recycle solids concentration	ML^{-3}
C_t	threshold solids concentration	ML^{-3}
C_{tr}	transition solids concentration	ML^{-3}

Cnts	counts	-
Cnts _o	counts of the completely mixed suspension	-
Cnts _l	counts of the supernatant	-
D	dispersion coefficient	L ² T ⁻¹
D ₁	Watts <i>et al.</i> (1996) dispersion parameter	L ² T ⁻¹
F	flux	ML ⁻² T ⁻¹
f _{bk}	Kynch batch density function	ML ⁻² T ⁻¹
f _{bk} ^{EO}	Engquist-Osher Kynch batch density function	ML ⁻² T ⁻¹
g	gravity constant	LT ⁻²
H	total depth	L
H _{centre}	depth at the centre of the clarifier	L
J	objective function	
K	compressibility function	L ² M ⁻¹
K _m	(Cacossa, 1994) parameter	L ² M ⁻¹
m	Kinnear (2002) parameter	-
n	Vesilind (1968) settling parameter	L ³ M ⁻¹
N	number of observations	
n ₁	Dupont and Dahl (1995) settling parameter	L ³ M ⁻¹
n ₂	Dupont and Dahl (1995) settling parameter	-
no	number of layers	
p _{diff}	differential pore pressure	MT ⁻² L ⁻¹
p _e	excess pore pressure	MT ⁻² L ⁻¹
p _f	liquid phase pressure	MT ⁻² L ⁻¹
p _{pore}	pressure within the fluid in the voids	MT ⁻² L ⁻¹
p _o	total pressure at the bottom	MT ⁻² L ⁻¹
P _o	Kinnear (2002) parameter	MT ⁻² L ⁻¹
p _s	solids pressure	MT ⁻² L ⁻¹
Q _e	effluent flow rate	L ³ T ⁻¹
Q _f	feed flow rate	L ³ T ⁻¹
Q _u	underflow rate	L ³ T ⁻¹
Q _r	recycle flow rate	L ³ T ⁻¹
R	recycle ratio	-
r	resistance coefficient	MT ⁻¹ L ⁻²
r _h	Takács settling parameter	L ³ M ⁻¹
r _p	Takács settling parameter	L ³ M ⁻¹
s	source term to the clarifier, $\frac{Q_f}{A\partial z} C_f \Delta(z)$	ML ⁻³ T ⁻¹
S	Cacossa (1994) parameter	ML ⁻³
S _o	specific surface area of the primary particle	L ⁻¹
t	time	T
V _{f,1}	Watts <i>et al.</i> (1996) dispersion parameter	LT ⁻¹
V _f	feed velocity	LT ⁻¹
V _{hindered}	hindered settling velocity	LT ⁻¹
v _o	surface load	LT ⁻¹
V ₀	Vesilind (1968) settling parameter	LT ⁻¹
V _{0max}	Takács settling parameter	LT ⁻¹
v _f	liquid velocity	LT ⁻¹
v _s	solids velocity	LT ⁻¹
V _S	settling velocity	LT ⁻¹
V _{stokes}	Stokes settling velocity	LT ⁻¹

y	observation	
\hat{y}_i	model prediction	
z	depth in settling column	L
z_f	feed layer location	L

Greek Symbols

α	effective solids stress parameter	$MT^{-2}L^{-1}$
β	effective solids stress parameter	ML^{-3}
β	Watts <i>et al.</i> (1996) dispersion parameter	L^3M^{-1}
β_1	effective solids stress parameter	ML^{-3}
β_2	effective solids stress parameter	-
γ	Watts <i>et al.</i> (1996) dispersion parameter	T
δ	Dirac pulse function	
ϵ	porosity	-
ϕ	volumetric solids concentration	-
ϕ_C	volumetric compression solids concentration	-
ϕ_{max}	maximum volumetric solids concentration	-
ϕ_o	initial volumetric solids concentration	-
ρ_f	floc mass density	ML^{-3}
ρ_l	liquid mass density	ML^{-3}
ρ_s	solids mass density	ML^{-3}
ρ_{super}	supernatant mass density	ML^{-3}
μ	dynamic viscosity of the liquid	$MT^{-1}L^{-1}$
σ_e	effective solids stress	$MT^{-2}L^{-1}$
θ	parameter set	
$\Delta\rho$	difference between solid and fluid mass densities	ML^{-3}

Chapter 1

Introduction and Objectives

Every community produces both liquid and solid wastes and air emissions. The liquid waste, i.e. the wastewater, contains water, organic matter, mineral nutrients, microorganisms and pathogens. For ecological and public health reasons, the wastewater is treated before it is released into a river, lake, or ocean (receiving water).

The **treatment** of municipal and some industrial wastewaters generally uses a combination of primary, secondary and tertiary treatment. The primary treatment, also called mechanical purification, removes coarse constituents by simple screens, settles large particles (such as sand and gravel) and skims off floating greases and oil. Secondary treatment biologically degrades dissolved and colloidal organic matter. Tertiary treatment attempts to limit the microorganisms and other pathogens in the treated water by membrane filtration or deep-bed filters and some form of disinfection using chlorine, ozone or ultraviolet light.

The secondary or **biological treatment** includes primarily biological purification processes and processes for settling and clarification. The biological reactors involve several reaction types (anaerobic fermentation, anaerobic activated sludge, anoxic activated sludge, aerobic activated sludge) and an increasing number of physical configurations (mixed and partially mixed tanks, tanks with loose or fixed packings, fixed-film processes and sequential batch reactors). This work focusses on the clarifier of the aerated activated sludge process. The clarifier separates the purified water from the biomass.

The **activated sludge process** was developed in England in 1914 by Arden and Lockett (1914) and was so named because of the production of an active mass of microorganisms capable of stabilizing a wastewater aerobically. It consists of a continuously operated aeration tank and a clarifier, as shown in Figure 1.1. The organic matter is introduced into the aeration tank where a mixed bacterial culture is maintained in suspension, i.e. the "mixed liquor". The latter carries out the conversion of the waste, i.e. a portion is used in a series of biochemical oxidation-reduction reactions in order to yield energy while the remaining part is used for cell growth and reproduction. The aerobic environment is achieved by the use of diffused or mechanical aeration, which also serves to maintain the mixed liquor in a completely mixed regime. The mixed liquor flows then to a clarifier, where the bacteria are separated from the treated wastewater by sedimentation. The settled bacteria are partly recycled

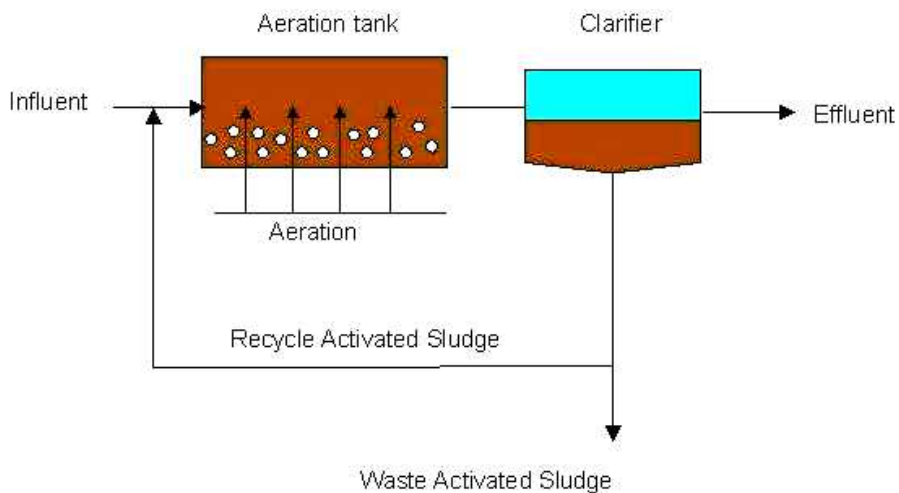


Figure 1.1: Activated sludge process

to maintain the desired concentration of microorganisms in the aeration tank and a portion, corresponding to the new growth of bacteria, is wasted.

The **clarifier** separates the flocculent microbial mass from the treated wastewater: the solid phase is removed from the wastewater by means of gravity. A settling tank is a vital component of the activated sludge system. It combines the function of (i) a thickener, to produce thickened sludge for return to the biological reactor, (ii) a clarifier to produce a clarified final effluent and (iii) a storage tank to store sludge during peak flows. Should the tank fail in any of these functions, suspended solids will carry over to the effluent. Besides delivering an effluent of poor quality, excessive loss of suspended solids could affect the behaviour of the biological process by an uncontrolled decrease in MLSS. The separation of the activated sludge thus determines the quality of the effluent and, to an important extent, the efficiency of the whole purifying process as well.

Since the clarifier forms the last step in the production of a well-clarified, stable effluent, low in BOD and suspended solids, it represents a critical link in the operation of the whole activated sludge treatment process and, as such, determines its efficiency. (Ekama *et al.*, 1997)

1.1 Description and Performance of a Clarifier

1.1.1 Configuration

The most commonly used types of activated sludge clarifiers are either circular or rectangular (Figures 1.2 and 1.3).

Circular clarifiers have been constructed with diameters ranging from 3 to 60 m, although the more common range is from 10 to 40 m. There are two basic types of circular tanks: the center-feed and the rim-feed clarifier. Both types use a revolving mechanism to transport and remove the sludge from the bottom of the clarifier. There

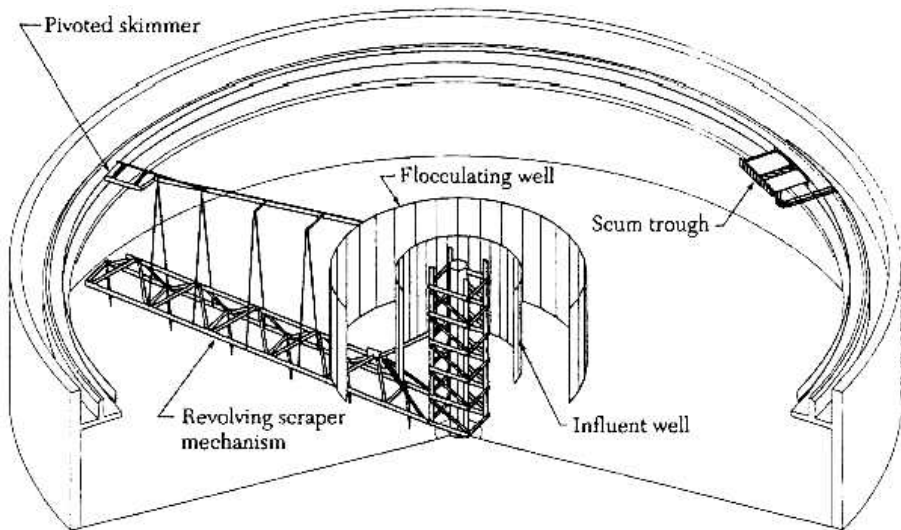


Figure 1.2: Circular center-feed clarifier with scraper mechanism and flocculator (Ekama *et al.*, 1997)

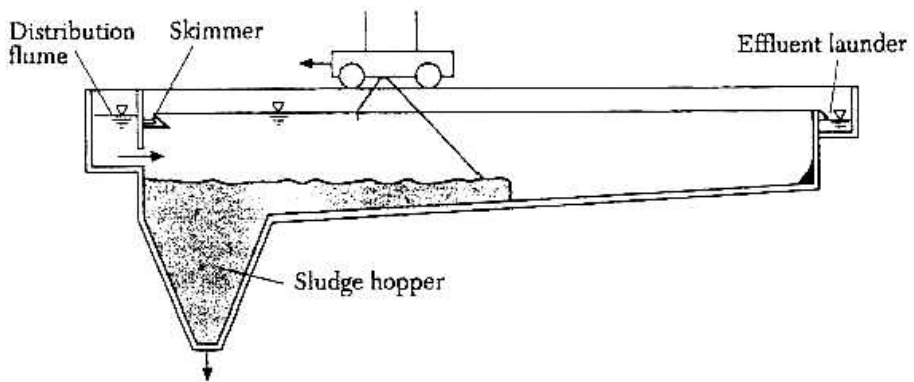


Figure 1.3: Rectangular clarifier with travelling-bridge collector mechanism (Ekama *et al.*, 1997)

Table 1.1: Factors affecting the solid/liquid separation in a clarifier (Ekama *et al.*, 1997)

Hydraulic load features and external tank dimensions	Internal physical features
Wastewater flow	Presence of flocculation zone
Surface area and overflow rate	Sludge collection arrangement
Depth and retention time	Inlet arrangement
Underflow recycle ratio	Weir type, length and position
	Tank configuration and baffling
	Hydraulic flow pattern and turbulence
	Density and convection currents
Site conditions	Sludge characteristics
Wind and wave action	MLSS concentration
Water and air temperature variation	Flocculation and settling characteristics
	Biological processes, e.g. denitrification

are two types of mechanisms: those that scrape or plow the sludge to a central hopper and those that remove the sludge directly from the tank bottom through suction orifices that serve the entire bottom of the tank in each revolution.

Rectangular clarifiers must be well-proportioned to achieve a proper distribution of incoming flow so that horizontal velocities are not excessive. It is recommended that the maximum tank length does not exceed 10 to 15 times the tank depth, although lengths up to 90 m have been used successfully in large plants. When tank widths exceed 6 m, multiple sludge collection mechanisms may be used to permit tank widths up to 24 m. The sludge collector should be allowed to meet the following two operational conditions: (i) exhibit a high capacity to avoid channeling of the overlying liquid through the sludge when a high sludge recirculation rate is desired, and (ii) the mechanism should be sufficiently rugged to allow transport and removal of very dense sludges that could accumulate in the tank during periods of mechanical breakdown or power failure. Two types of sludge collectors are commonly used: (i) traveling flights and (ii) traveling bridges.

There is no basis for establishing the superiority of a rectangular unit over a circular unit (Parker, 1995; Parker *et al.*, 2001) but circular clarifiers are most commonly used (Tchobanoglous and Burton, 1991; Parker, 1983). **Center-feed circular clarifiers are the subject of this work.**

1.1.2 Performance

The performance of the clarifier is influenced by the factors listed in Table 1.1. The main processes occurring in a clarifier, i.e. settling, flocculation, density currents and turbulence (Zhou and McCorquodale, 1992; Vitasovic *et al.*, 1997; Ekama *et al.*, 1997; Ozinsky and Ekama, 1995; Lakehal *et al.*, 1999; Deininger *et al.*, 1998) are briefly discussed. The effectiveness of the activated sludge process is of course primarily related to the **settling** characteristics of the mixed liquor during settling. The influent wastewater composition, the conditions of the aeration tank influence the composition of the

microbial floc and subsequently the settling characteristics. Knowledge of the settling characteristics of the mixed liquor is essential for the proper design and operation of clarifiers (Jin *et al.*, 2003; Mines *et al.*, 2001). Those characteristics are commonly measured in batch settling tests. This PhD focusses on the modelling of this batch settling behaviour.

Flocculation is another important process which influences the behaviour of the clarifier. Mixed liquor is naturally flocculent under most conditions. The purpose of flocculation is to form aggregates, or flocs, from dispersed solid particles. Flocculation of the mixed liquor is necessary not only to produce flocs of sufficient mass to settle in the clarifier, but also to decrease the concentration of small, dispersed solids that do not have sufficient mass to settle in the clarifier. Process determinants affecting activated sludge flocculation include: (i) solids retention time, (ii) MLSS concentration, (iii) dissolved oxygen level in the aeration tank, (iv) cations, (v) aeration tank and mixed liquor transfer system turbulence. In a clarifier where hydraulic flow currents do not impact the effluent quality, the success of the clarification function depends on the extent to which the mixed liquor has been flocculated before settling and any additional flocculation that occurs during settling (Clauss *et al.*, 1998; Wahlberg *et al.*, 1994). Primary particles and small flocs can impinge onto the floc as settling occurs and are as such incorporated into the sludge blanket. Primary particles that are not trapped by the sludge blanket, are not removed because of their very low settling velocity. Poor mixed liquor flocculation characteristics can result in higher effluent suspended solids concentrations.

Flow non-idealities in clarifiers are usually associated with circulating flows generated by excess energy in the feed. This has two main sources: the kinetic energy associated with the inlet flow velocity and the gravitational potential energy associated with the higher concentration of the mixed liquor relative to the clarified water in the clarifier (Brouckaert and Buckley, 1999). Thermal and sediment-driven **density currents** exist in clarifiers (Brouckaert and Buckley, 1999; Wells and Laliberte, 1998; Anderson, 1945; Larsen, 1977; Taebi-Harandy and Schroeder, 2000). Research has even shown that the density current, besides the sludge characteristics, is one of the main features in the design of clarifiers (Ueberl and Hager, 1997). **Thermal density currents** occur due to temperature differences between the ambient air and the influent (Taebi-Harandy and Schroeder, 2000; Wells and Laliberte, 1998). When the air temperature is lower than the influent, there is surface cooling which results in the tank contents having lower temperatures than the influent and a horizontal surface current is formed. When the air temperature is higher than the influent, a horizontal bottom current is formed. Surface temperatures are often about 1 °C cooler than bottom temperatures during winter (Wells and Laliberte, 1998). A **sediment-driven density current** is formed due to differences in suspended solids concentration between the inlet mixed liquor and the fluid in the clarifier. The inlet flow falls quickly down to the sludge blanket height (Anderson, 1945) or to the depth where the suspended solids concentration is the same as the one in the inlet mixed liquor (Larsen, 1977). This so-called "waterfall-effect" interferes with the separation of the solids and the thickening of the sludge. Velocity profile measurements in full-scale clarifiers (Deininger *et al.*, 1996, 1998) confirm these sediment-driven density currents. A sediment-driven density current (with influent of greater density than clarifier contents) results in a circulating current, as shown in Figure 1.4: the influent sinks to the sludge blanket and flows towards the tank rim (bottom current), in the rim region the flow is directed to the tank surface, from where it returns towards the tank inlet (return current) (Deininger *et al.*, 1998; Taebi-Harandy and Schroeder, 2000). It is clear that the flow pattern and suspended

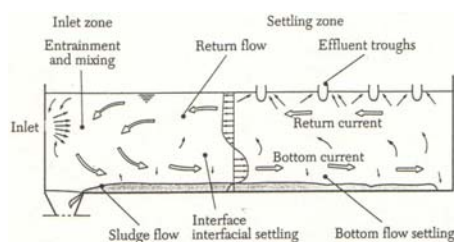


Figure 1.4: Typical clarifier flow pattern with a density current

solids transport in a clarifier are not only vertically distributed but that they also vary in the horizontal dimension. Strong density currents can result in higher effluent suspended solids concentration when they resuspend previously settled flocs and they can also result in short-circuiting of the sludge to the effluent or to the recycle.

1.1.3 Modelling

Clarifier models attempt to represent the physical, chemical and biological phenomena occurring in the clarifier and are of great theoretical, practical and economical interest because of their use in the following applications:

- to increase the understanding of the underlying mechanisms
- in the design of full-scale processes, and of control and operating strategies
- for the training of operators and process engineers.

There are different type of models depending on the objective for which they are used or the information sources they are based on. Some models are developed to yield a very detailed description of the involved processes whereas other models are developed for prediction and control purposes.

Most clarifier (or continuous settling) models are based on the most important physical, chemical and biological relations and contain empirical terms to account for uncertainties in model formulation as well as in observations. Most of the empiricism comes in through the definition of the settling behaviour of the activated sludge (Ekama *et al.*, 1997). A theoretical description of compression settling (i.e. the interaction between the activated sludge flocs is so large that a floc structure is formed which exhibits compressive yield strengths) would allow the models to approach reality more closely (Ekama *et al.*, 1997). Modelling of the well-known hindered settling and compression settling, as measured in batch settling tests, is the subject of this PhD.

1D, 2D and 3D continuous settling models have been formulated (using 1, 2 or 3 spatial dimensions). The current 2D and 3D models describe the internal flow pattern and the solids transport phenomena to a certain extent and are closest to reality. Since their use is computationally very demanding, they are not yet used for control or optimisation purposes. 1D models only describe the processes in the vertical dimension and are a gross simplification of reality. Unlike the higher dimensional models, 1D models can be used for operation and control (Ekama *et al.*, 1997) and answer mass inventory questions, questions related to the recycling of activated sludge and questions about sludge blanket levels. Such 1D continuous settling models are the subject of this PhD.

1.2 Goals and Outline of Dissertation

1.2.1 Goals

The settling characteristics of activated sludge are important for the performance of the clarifier and, hence, the efficiency of the wastewater treatment plant. Currently, however, no (mechanistic) model is available in wastewater industry that can accurately describe the (batch) settling behaviour of activated sludge, measured with batch settling tests. This dissertation aims at finding a model that describes this settling behaviour, i.e. a **batch settling model**, and to develop, to this end, measurement techniques that give more information about the settling behaviour.

Having a batch settling model, the next goal of this dissertation is finding a **1D continuous settling model** which describes the full-scale behaviour of a circular clarifier and that incorporates the batch settling model. To this end, 2 detailed full-scale measuring campaigns were performed.

It is not intended to investigate the effect of the biology of the activated sludge on the settling behaviour nor to include flocculation in the models.

1.2.2 Outline

Generally, empirical approaches are applied to model the settling behaviour of activated sludge. Exceptions are the models of Kinnear (2002) and Cacossa and Vaccari (1994). The approach of Kinnear (2002) is based on the fundamental properties of the suspension (e.g. density, viscosity) and continuity and momentum balance equations for the liquid and the solids. This approach is however commonly used for the settling of other flocculated suspensions, like clay, talc, calcium carbonate suspensions, ... More in-depth batch settling experiments have been performed in these areas too. Since similarities exist between activated sludge settling and settling/consolidation of these flocculated slurries (Behn, 1957) and a huge amount of literature is available about the settling of this type of slurries, the settling of these suspensions can broaden the insight in the activated sludge settling. These aspects are discussed in Chapter 2. As will be shown in Chapter 2, there is a need for measured continuous solids concentration and pressure profiles during batch settling to develop a good settling model. Conventional measuring techniques have difficulties in recording this kind of data, either because they are invasive, or because of the low solids concentration and/or solids density of activated sludge. Chapter 5 investigates a novel non-invasive measurement technique borrowed from nuclear medicine, using a solids radiotracer and gamma cameras, to obtain high resolution solids concentration profiles during the batch settling of activated sludge. Chapter 5 also investigates the possibility to measure pressure profiles with sufficient accuracy.

Next, the batch settling experiments of Chapter 5 are used as an input for a model that can describe the batch settling process. This modelling is subject of Chapter 6. The numerical integration of the model equations and estimation of model parameters on the basis of the experimental data are discussed in Chapter 4.

The current 1D continuous settling models, together with their characteristics and their ability to predict the full-scale behaviour, are discussed in Chapter 3. This discussion leads to the conclusion that none of the current 1D continuous settling models combines a founded description of the settling behaviour, a suitable numerical algorithm and a calibration and validation with full-scale dynamic data.

The description of the settling behaviour is already mentioned, the numerical algorithm is discussed in Chapter 4. The full-scale dynamic data are discussed in Chapter 7. The batch settling model of Chapter 6 and the full-scale dynamic data of Chapter 7 are finally used as input for a 1D continuous settling model. This modelling is subject of Chapter 8.

Chapter 2

Modelling of batch settling

The settling characteristics of activated sludge are, as already stated, important for the performance of the clarifier and, hence, the efficiency of the wastewater treatment plant. Since the settling characteristics are commonly measured in batch settling tests/experiments, the modelling of batch settling is discussed here. First, the settling behaviour of suspensions, the batch settling process and the fundamental model structure for batch settling are discussed. Next, it is demonstrated how environmental engineers model batch settling of activated sludge revealing a trend to model batch settling more fundamentally. Subsequently, an overview of the different approaches used in other scientific areas, together with the simulated versus the experimental batch settling curves, illuminate how researchers model the settling behaviour of slurries and reveal which mathematical relations are capable of describing the complete batch settling curve.

2.1 Settling behaviour of suspensions

Suspended particles can settle in one of four markedly different regimes. At low solids concentrations, the distance between the flocs is large compared to the size of the flocs and the flocs are able to settle independently. Collisions between the flocs still occur, despite the relatively sparse concentration. If the flocs aggregate, larger flocs are formed which settle at increased rates. If the flocs fail to aggregate, each floc will continue to settle at its characteristic rate. The flocs are not identically shaped. Instead, some of the flocs may appear as spherical flocs that settle readily, while others may be filamentous. These filaments may exhibit worse settling behaviour. In addition, there are often dispersed organisms that will not settle. The settling of the flocs at low concentrations is called **discrete settling** (no aggregation)(class I) and **flocculent settling** (aggregation)(class II).

At higher solids concentrations, the distance between the flocs decreases. The conditions within the suspension modify considerably; the upward velocity of the fluid displaced by the settling particles is much greater and the flow patterns are appreciably altered. The particles no longer settle as individuals. The particles or flocs do not make contact, but are prevented from behaving as individuals by the close proximity of neighbouring particles. The same relative position of the flocs to one another is preserved and, hence, they settle collectively as a zone at essentially the same rate. This process is known as **hindered settling or zone settling** (class III). This type of

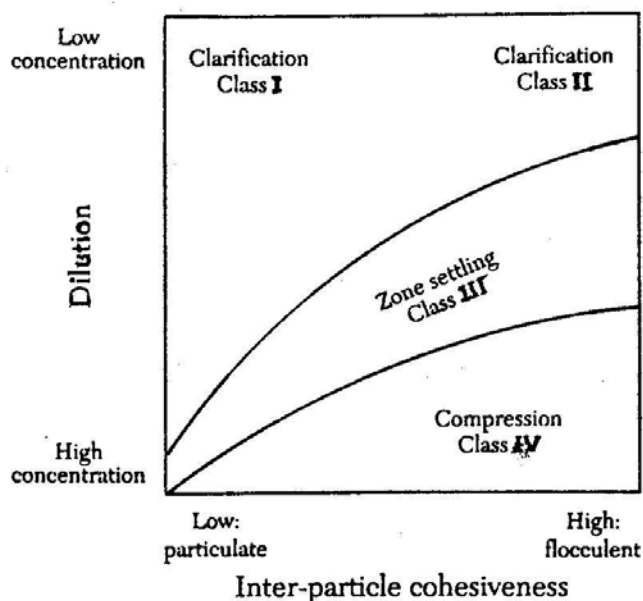


Figure 2.1: Relation between concentration and flocculation, and four settling regimes (Ekama *et al.*, 1997)

settling behaviour is characterised by the presence of a distinct interface between the clear supernatant in the upper region of the thickener and the subsiding floc structure. The zone settling velocity can be evaluated by measuring the interface settling rate from batch settling tests at different solids concentrations; this velocity is inversely related to the solids concentration.

When the solids concentration further increases, a new phenomenon takes place: **compression** (class IV). The interaction between flocs becomes so large that the floc geometry will be influenced. A floc structure is formed which exhibits compressive yield strengths. As opposed to free settling and hindered settling, where the flocs move due to gravity and the drag force resulting from the relative movement of the flocs and surrounding water, the flocs are additionally subjected to a force resulting from the interparticle compressive stress. As the solids concentration increases due to the compaction of the floc structure, the hydrodynamic force decreases while the compressive force increases. The knowledge (Olsson and Newell, 1999) of these phenomena is still insufficient to result in adequate models. Apart from a few exceptions, such as Zheng and Bagley (1998), Cacossa and Vaccari (1994) and Kinnear (2002), the wastewater industry typically neglects compressive effects in designing and modelling secondary clarifiers.

The relation between concentration and flocculation and the four regimes of settling is shown in Figure 2.1.

All four settling regimes (discrete, flocculent, hindered and compressive) occur simultaneously in a secondary clarifier: discrete and flocculent in the top and upper middle region, hindered in the lower middle region and compressive in the bottom region.

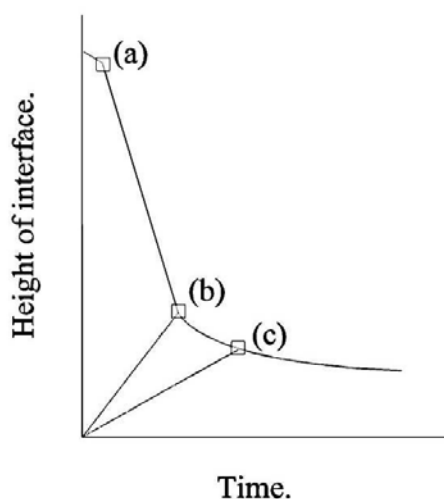


Figure 2.2: Typical shape of a batch settling curve (Rushton *et al.*, 2000)

2.1.1 Batch settling

Batch settling experiments are an interesting information source on settling characteristics as the data are the result of only the physical properties of the measuring device and the settling properties of the sludge. Batch settling is used for studying hindered settling, process monitoring attempting to measure sludge thickenability in a continuous thickening/settling process, as well as to validate thickening/settling models.

During a batch settling experiment, usually the suspension-supernatant interface height is recorded. Figure 2.2 shows the progress of the suspension-liquid interface. Four distinct settling regimes can be detected: the lag stage or induction period (up to point (a)), the zone settling stage (from point (a) to (b)), the transition stage or first falling rate section (from point (b) to (c)) and the compression or second falling rate section (from point (c)).

The initial period, up to point (a), represents an **induction period** in which the suspension recovers from initial disturbances or, if it is a flocculating or coagulating suspension, in which the loosely aggregated particles called flocs are formed. Ekama *et al.* (1997) stated though that this stage should not be regarded as a reflocculation stage, because the shear velocities and duration are far too low for this to take place at any significant degree.

From points (a) to (b), a **constant rate of fall** of the interface is observed. The solids settle at a uniform velocity under zone settling conditions. An equilibrium is established between the gravitational forces causing the particles to settle and the hydrodynamic friction forces resisting this motion.

Initially, all particles settle at apparently the same velocity (constant rate of fall) and higher concentrations than the initial one build up at the base of the settling tank. Eventually, a layer with a solids concentration in excess of the original will build up from the base and will, eventually, be present at the settling interface-point (b). At point (b), a transition occurs to a **first falling rate** section that ends at point (c), the "compression point", beyond which the second falling rate section begins. Since the settling rate is inversely related to the solids concentration, the observed settling

rates begin to slow down (change in slope).

At the compression point (c) it is believed that the particles are now in physical contact with one another. The **second falling rate** period begins; further decrease in height is effected solely by flow of liquid out of the compaction zone because of the unbalanced buoyed weight of the solid particles; when the cake structure carries the entire weight of particulates, liquid pressure gradients attain a null state and no further compression occurs.

When such a batch settling curve (as in Figure 2.2) can be modelled, the governing equations may be subsequently used to describe the settling behaviour of activated sludge in a secondary clarifier.

2.1.2 Fundamental model structure for batch settling

The basic settling model is based on the conservation of mass and momentum of both water and solids. These are the most general equations that all suspensions must obey, no matter how different their particular properties are. The forces acting on the solids are gravity, buoyancy, liquid pressure, friction and effective solids stress (Figure 2.3). The following assumptions are introduced (Bustos *et al.*, 1999):

1. The solid particles are small (with respect to the settler) and of the same density
2. The solids and the fluid are incompressible, i.e. the densities of the liquid and the solids are constant during settling
3. The suspension is completely flocculated prior to settling, this dissertation does not include flocculation in the model, although this could occur during settling; some research has been done on the dynamics of flocculation (Govoreanu, 2004) and modelling of flocculation (Nopens, 2005) and in future research flocculation will be incorporated in a 2D/3D-model since a 1D-model can not describe such behaviour
4. No mass transfer exists between the solid and the fluid during sedimentation
5. Gravity is the only body force
6. The solids and the fluid are contained in an impervious vessel with frictionless walls, in which all variables are constant across any cross-sectional area
7. The solids and the liquid can perform a one-dimensional compressive motion only
8. The friction between the fluid particles is much smaller than that associated with the solid-fluid interaction force
9. The solid component is isotropic
10. The effective solids stress $\sigma_e(\phi)$, i.e. the stress supported by the solid skeleton, is assumed to be constant during hindered settling, i.e. for a volumetric solids concentration ϕ lower than the volumetric compression solids concentration ϕ_C , and is assumed to increase monotonically for $\phi > \phi_C$
11. Because the flocs are small and their sedimentation velocity is small, the solid-fluid interaction force depends linearly on the solid-fluid relative velocity and on the concentration gradient: $p_{pore} \frac{\partial \phi}{\partial z} + V_{ST}(\phi)$ with p_{pore} the pore pressure, i.e.

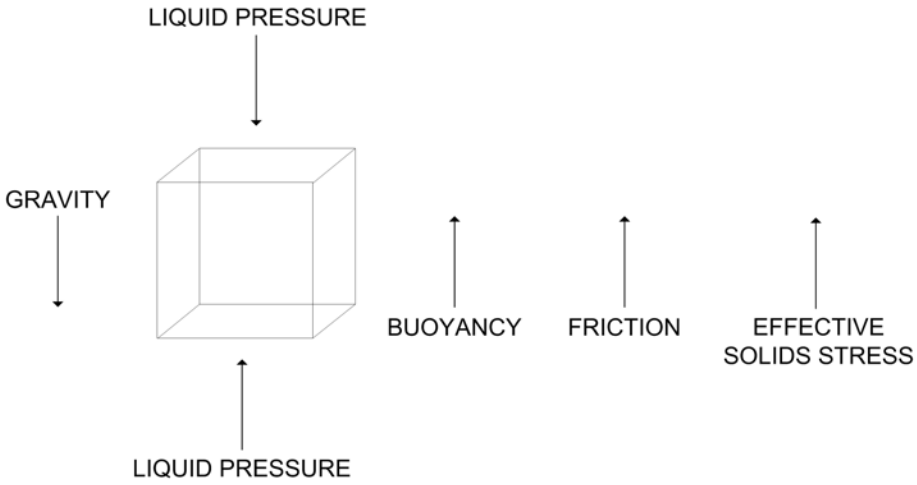


Figure 2.3: Forces acting on a solids control volume during batch settling

the pressure within the fluid in the voids, V_S the settling velocity and $r(\phi)$ the resistance coefficient

12. The acceleration terms are neglected (because the Froude number, i.e. ratio of inertial to gravitational force, is small)

These assumptions lead to the following continuity equations for the solids and liquid:

$$\frac{\partial \phi}{\partial t} + \frac{\partial (v_s \phi)}{\partial z} = 0 \quad (2.1)$$

$$\frac{\partial (1 - \phi)}{\partial t} + \frac{\partial (v_l (1 - \phi))}{\partial z} = 0 \quad (2.2)$$

with ϕ the volumetric solids concentration, $v_s = V_S - v_f$ the solids velocity, v_f the liquid velocity and z the depth in settling column, and the following linear momentum balances for solids and liquid:

$$0 = -\frac{\partial p_s}{\partial z} + \rho_s \phi g + p_{pore} \frac{\partial \phi}{\partial z} + V_S r(\phi) \quad (2.3)$$

$$0 = -\frac{\partial p_f}{\partial z} + \rho_f (1 - \phi) g - p_{pore} \frac{\partial \phi}{\partial z} - V_S r(\phi) \quad (2.4)$$

with ρ_l the density of the liquid, ρ_s the density of the solids, p_s the solids pressure and p_f the fluid phase pressure. The total pressure p_t is given by the equations:

$$p_t = p_s + p_f \quad (2.5)$$

$$p_t = p_{pore} + \sigma_e(\phi) \quad (2.6)$$

Assuming that all variables are constant across any cross-sectional area, the following equations are obtained for p_s and p_f :

$$p_s = \phi p_{pore} + \sigma_e(\phi) \quad (2.7)$$

$$p_f = (1 - \phi) p_{pore} \quad (2.8)$$

The linear momentum balances are rewritten in terms of p_{pore} and σ_e :

$$0 = -\frac{\partial(\phi p_{pore} + \sigma_e(\phi))}{\partial z} + \rho_s \phi g + p_{pore} \frac{\partial \phi}{\partial z} + V_S r(\phi) \quad (2.9)$$

$$0 = -\frac{\partial((1-\phi)p_{pore})}{\partial z} + \rho_f(1-\phi)g - p_{pore} \frac{\partial \phi}{\partial z} - V_S r(\phi) \quad (2.10)$$

and are subsequently solved for p_{pore} and σ_e :

$$\frac{\partial(p_{pore})}{\partial z} = \rho_f g - \frac{V_S r(\phi)}{1-\phi} \quad (2.11)$$

$$\frac{\partial \sigma_e}{\partial z} = \Delta \rho \phi g + \frac{V_S r(\phi)}{1-\phi} \quad (2.12)$$

with $\Delta \rho$ the difference between solid and fluid mass densities. The resistance coefficient $\alpha(\phi)$ is replaced by the Kynch batch density function (hindered settling flux) $f_{bk}(\phi)$:

$$f_{bk}(\phi) = -\frac{\Delta \rho \phi^2 g (1-\phi)^2}{r(\phi)} \quad (2.13)$$

The function $f_{bk}(\phi)$ should satisfy the conditions as stated by Kynch (1952):

$$f_{bk}(0) = f_{bk}(\phi_{max}) = 0 \quad (2.14)$$

$$f_{bk}(\phi) > 0 \quad \text{for } 0 < \phi < \phi_{max} \quad (2.15)$$

$$\frac{df_{bk}}{d\phi}(0) > 0$$

$$\frac{df_{bk}}{d\phi}(\phi_{max}) < 0$$

with ϕ_{max} the maximum volumetric solids concentration

The equation for σ_e (equation 2.12) is rewritten as follows:

$$V_S(\phi) = \frac{f_{bk}(\phi)}{\phi(1-\phi)} \left(1 - \frac{1}{\Delta \rho \phi g} \frac{\partial \sigma_e}{\partial z}\right) \quad (2.16)$$

This relationship is inserted in the continuity equation for the solids, considering that in batch settling the total velocity, i.e. $\phi v_s + (1-\phi)v_l$, equals zero: (Bustos *et al.*, 1999)

$$\frac{\partial \phi}{\partial t} = -\frac{\partial f_{bk}(\phi)}{\partial z} + \frac{\partial}{\partial z} \left(f_{bk}(\phi) \frac{1}{\Delta \rho g \phi} \frac{d\sigma_e(\phi)}{d\phi} \frac{\partial \phi}{\partial z} \right) \quad (2.17)$$

When $\phi \leq \phi_C$, the second term on the right-hand side is zero and only hindered settling exists. When $\phi > \phi_C$, an effective solids stress exists and the settling is comprised of a downward hindered settling term and an upward term due to the effective solids stress.

Inserting the excess pore pressure p_e , i.e. the fluid pressure in excess of the hydrostatic pressure ($=p_{pore} - \rho_f g z$), in the momentum balance for the liquid, solving this equation

for p_e and inserting this subsequently in the momentum balance for the solids, the effective solids stress $\sigma_e(\phi)$ can be calculated as follows (Bustos *et al.*, 1999):

$$\frac{\partial p_e}{\partial z} = \Delta\rho g\phi - \frac{d\sigma_e(\phi)}{d\phi} \frac{\partial\phi}{\partial z} \quad (2.18)$$

The equation for the volumetric solids concentration (equation 2.17) a second-order parabolic differential equation degenerating into a first-order hyperbolic type for the interval $[0, \phi_C]$. This hyperbolic equation corresponds to the hindered settling regime. The initial and (non-linear) boundary conditions are:

$$\phi(z, 0) = \phi_o(z) \quad \text{for } 0 \leq z \leq H \quad (2.19)$$

$$f_{bk}(\phi) \left(1 - \frac{1}{\Delta\rho g\phi} \frac{d\sigma_e(\phi)}{d\phi} \frac{\partial\phi}{\partial z} \right) = 0 \quad \text{for } z = 0, z = H \text{ and } t > 0 \quad (2.20)$$

In literature, different expressions/approaches are used for the hindered settling flux and/or effective solids stress. Firstly, the activated sludge settling models are discussed, and next an overview of the different approaches in other research areas is given.

2.2 Modelling of activated sludge settling

In activated sludge settling, the settling velocity V_S is generally used instead of the settling flux, $V_S\phi$:

$$V_S(\phi)\phi = f_{bk}(\phi) \left(1 - \frac{1}{\Delta\rho g\phi} \frac{d\sigma_e(\phi)}{d\phi} \frac{\partial\phi}{\partial z} \right) \quad (2.21)$$

Quite a number of settling velocity functions have been presented in literature (Vesilind, 1968; Takacs *et al.*, 1991; Dupont and Henze, 1992; Hartel and Popel, 1992; Otterpohl and Freund, 1992; Cho *et al.*, 1993; Cacossa and Vaccari, 1994; Kinnear, 2002). The functions describe hindered settling and/or compression settling and/or settling at low solids concentrations. The Vesilind and Takács function are most frequently used in clarifier modelling (Takacs *et al.*, 1991; Hamilton *et al.*, 1992; Grijspeerd *et al.*, 1995; Watts *et al.*, 1996; Ekama *et al.*, 1997; Diehl and Jeppsson, 1998; Lee *et al.*, 1999; Joannis *et al.*, 1999) and are given by the following relationship $V_S(C)$, respectively:

$$V_S(C) = V_0 e^{-nC} \quad (2.22)$$

$$V_S(C) = \min \left(V_{0max}, V_0 \left(e^{-r_h(C-C_{min})} - e^{-r_p(C-C_{min})} \right) \right) \quad (2.23)$$

with V_0 , n , V_{0max} , r_h , and r_p parameters and C_{min} the non-settleable solids concentration.

Most of these settling velocity functions are still very empirical in nature (Vanderhasselt and Vanrolleghem, 2000) and the (lumped) parameters of these functions are obtained by curve fit. The settling velocity is expected to be a function of various physical characteristics of the activated sludge flocs and water interactions including particle shape and size distribution, fluid and floc density, floc interaction forces, fluid viscosity and hydrodynamic resistance (drag force). Fortunately there is a trend to derive these functions from the fundamental mass and force balances for both phases (Cacossa and Vaccari, 1994; Kinnear, 2002). In this respect, the models of Cacossa and Vaccari (1994) and of Kinnear (2002) are discussed below.

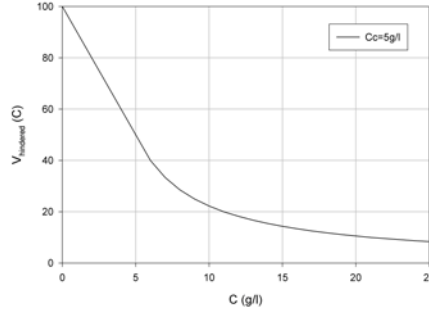


Figure 2.4: The hindered settling velocity versus solids concentration for the Cacossa and Vaccari (1994) settling velocity function

2.2.1 Settling velocity function of Cacossa and Vaccari (1994)

Cacossa and Vaccari (1994) derived the following empirical settling velocity function V_S (as function of the solids concentration C and its gradient):

$$V_S(C) = V_{hindered}(C) \left(1 - \frac{\partial C}{\partial z} \frac{1}{K} \right) \quad (2.24)$$

with K the compressibility function. The empirical Tracy equation (Tracy, 1973)

$$V_{hindered}(C) = \left(\frac{B_1}{C - B_2} \right) \quad (2.25)$$

with B_1 and B_2 parameters is only applicable at concentrations greater than or equal to C_C (i.e. the lowest solids concentration at which interparticle compressive stresses still exist) and was used for $V_{hindered}$ because calibration of this function with experimental data gave good results.

The linear extension of the Tracy equation was used for $V_{hindered}$ for concentrations lower than C_C :

$$V_{hindered}(C) = \left(2 - \frac{C}{C_C} \right) \left(\frac{B_1}{C_C - B_2} \right) \quad (2.26)$$

Figure 2.4 gives an example of the evolution of $V_{hindered}$ versus solids concentration. The following empirical expression for the compressibility function K gave adequate model results compared to the experimental data (Cacossa, 1994):

$$K = K_m e^{-\frac{C}{S}} \quad (2.27)$$

with K_m and S parameters. The parameters of the settling velocity function were calibrated from batch experiments (recording of suspension-liquid interface). Some experimental and simulated batch curves are shown in Figure 2.5.

This settling velocity function, however, does not give satisfactory results for the compression phase as can be seen in the simulated batch settling curves. Several curves tend to overpredict the height of the solids-liquid interface in the compressive region of the curve. Cacossa (1994) suggested that the batch thickening behaviour could be more accurately predicted if the simple empirical expression for the compressibility function (K) was replaced with a more elaborate expression.

The resulting settling velocity function (equation 2.24) contains empirical functions which are derived by calibration of experimental data and the settling parameters no longer have a relationship with the particle shape and size distribution, fluid and solids density, solids interaction forces, fluid viscosity and drag force.

2.2.2 Settling velocity function of Kinnear (2002)

Kinnear (2002) attempted to improve the work of Cacossa and Vaccari (1994) by using more fundamental properties, such as the dry solids density, the floc density, the permeability and the compressive resistance to represent the settling characteristics of activated sludge. Water in activated sludge is present in the form of free water and bound water. The bound water is the water associated with the floc matrix. This includes the stagnant water trapped within the floc structure, water of hydration, cellular water and water absorbed and adsorbed by the solid phase (Vaccari, 1984). Consequently, the bound water moves with the floc matrix during settling and should be considered as a part of the particle phase, i.e. the two phases are the floc phase and the (free) water phase. The difference between solids and flocs (i.e. solids and bound water) was recognized and a relationship between concentration and porosity as a function of the dry solids density and the floc density was derived.

A settling velocity function was developed from the continuity and momentum equation for the liquid and the flocs. The friction force was described by Darcy's law. The permeability was described with the empirical Kozeny equation and the effective solids stress with the empirical function of Buscall and White (1987). The final settling velocity functions as function of the porosity ϵ are:

$$V_S(\epsilon) = \frac{(\rho_f - \rho_l)g\epsilon^3}{5S_o^2(1 - \epsilon)\mu} \quad \text{for } C < C_C \quad (2.28)$$

$$V_S(\epsilon) = \frac{(\rho_f - \rho_l)g(1 - \epsilon) + P_o \left(\frac{1 - \epsilon}{1 - \epsilon_C} \right)^m \frac{\partial \epsilon}{\partial z}}{5S_o^2(1 - \epsilon)^2 \mu} \epsilon^3 \quad \text{for } C \geq C_C \quad (2.29)$$

with

$$\epsilon(C) = 1 - \left(1 + \frac{\rho_s - \rho_f}{\rho_f - \rho_l} \right) \frac{C}{\rho_s} \quad (2.30)$$

and ρ_f the density of the floc, S_o the specific surface area of the primary particle, μ the dynamic viscosity of the liquid and P_o and m empirical coefficients.

For model calibration, the following information is required: (i) the measurement of the dry solids and floc density using density gradient centrifugation or other techniques, e.g. pycnometer (Malisse *et al.*, 2004), (ii) the determination of S_o using observed initial settling velocities and (iii) the determination of the effective solids stress parameters using measured equilibrium concentration profiles. Experimental batch settling curves were simulated and one of them is shown in Figure 2.6 (left).

Initially, the settling velocity function accurately predicts the interface height (i.e. in the hindered settling regime). In the transitional range, between approximately 20 and 150 minutes, the predictions are poorer however. The simulation fails to exhibit transitional behaviour and the simulated interface height decreases at the hindered settling velocity until settling and compression no longer occur. The results are similar to the

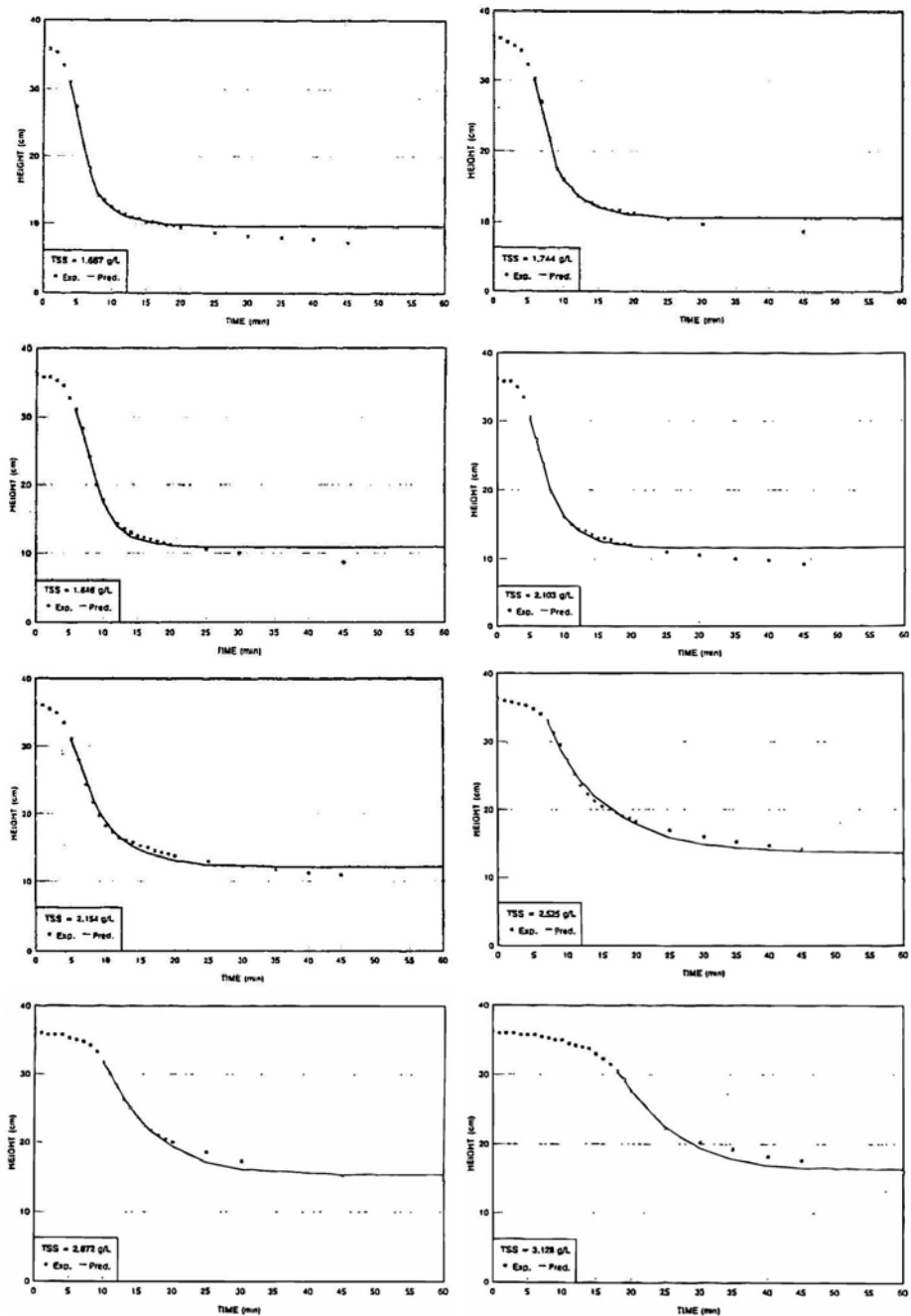


Figure 2.5: Experimental (symbol) and simulated (line) batch settling curves for different initial concentrations (Cacossa, 1994)

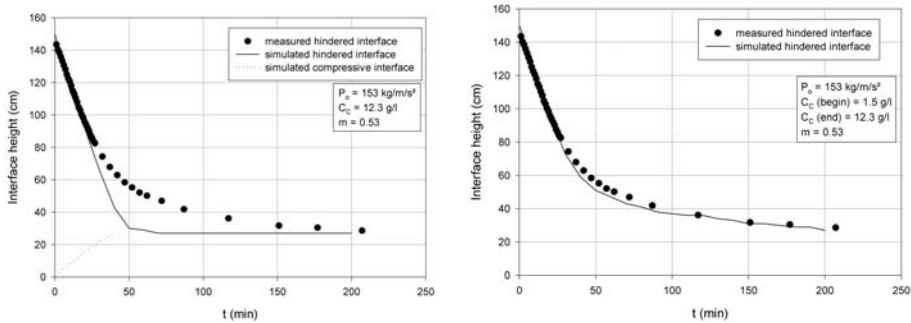


Figure 2.6: Measured and simulated batch settling curve (left: simulation with constant compression solids concentration; right: simulation with a linear time-dependent compression solids concentration) (Kinnear, 2002)

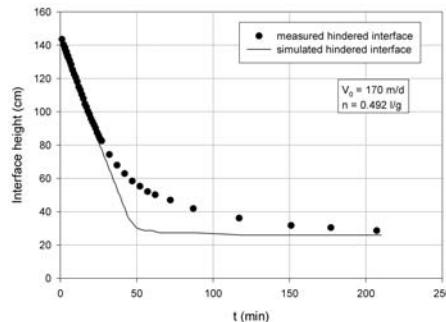


Figure 2.7: Measured and simulated batch settling curve; measurements are from Kinnear (2002) and simulations are done with Vesilind settling velocity function

best fit obtained with the Vesilind settling velocity function, as shown in Figure 2.7. Kinnear (2002) showed that the simulation can be improved if C_C does not remain constant in the course of a batch simulation. Figure 2.6 (right) shows a simulation with a linear time-dependent C_C . He suggested that C_C in the effective solids stress function is not a function of only the solids fraction and should be modified.

In summary, neither the settling velocity function of Cacossa and Vaccari (1994) nor the one of Kinnear (2002) can accurately simulate a complete batch settling curve.

2.3 Modelling of flocculated suspension settling (different from activated sludges)

2.3.1 Properties of the suspensions, experiments and differences with activated sludge

In literature, a large number of models can be found that describe settling of flocculated suspensions. Only the models which have been confronted with experimental

batch settling data are reviewed here.

In Table 2.1, an overview is given of the conducted experiments. As can be seen, the density difference (i.e. $\Delta\rho = \rho_s - \rho_f$) for those materials is significantly higher than for activated sludge (around 800 kg/m^3 for dry solids (Kinnear, 2002)), except for the Al(OH)-flocs-experiments of Bhargava and Rajagopal (1990). The same holds for the initial solids concentration (ϕ_o), which is also higher than the solids concentration of activated sludge (around 0.1-0.2 vol%).

In *activated sludge* batch settling, usually only the batch settling curve is recorded, whereas in almost all cases of Table 2.1 (exceptions: Tiller (1981), Font (1988), Bhargava and Rajagopal (1990)), more in-depth measurements were performed. Mostly, the dynamic profiles of density or concentration were measured over time and some of them even measured excess pore pressure profiles over time (Shirato *et al.*, 1970; Been and Sills, 1981; Dreher, 1997). Those two measurements, i.e. solids concentration and excess pore pressure profiles, can be used directly in the model equations and give a lot more information about the settling process than recording the suspension-liquid interface only.

Because of the significantly lower concentration and density of the *activated sludge* solids, it is less evident to measure the solids concentration and excess pore pressure profiles during batch settling compared to the suspensions of Table 2.1.

On the other hand, there are only few that performed experiments at different initial solids concentrations (Font, 1988; Bhargava and Rajagopal, 1990; Wells, 1990; Been and Sills, 1981), which is common practice in activated sludge settling tests. The compression solids concentration ϕ_C in the anorganic sludge settling is usually mentioned though. Some of the experiments were performed with initial concentrations higher than ϕ_C (Shirato *et al.*, 1970; Shih *et al.*, 1986; Bergstrom, 1992; Holdich and Butt, 1997), whereas for *activated sludge*, it can be assumed that the operational activated sludge concentration (i.e. the concentration in the biological reactor) is lower than the compression solids concentration.

The time-scale of settling for the suspensions in Table 2.1 is generally considerably larger than the one for activated sludge and is in the range of hours to days (exceptions: Shih *et al.* (1986), Karl and Wells (1999)) compared to one or several hours for activated sludge.

Non-invasive techniques, such as gamma-ray (Bergstrom, 1992; Scott, 1968; Dreher, 1997) and X-ray (Shih *et al.*, 1986; Been, 1980; Been and Sills, 1981; Wells, 1990; Tiller *et al.*, 1991) imaging, have been applied for the measurement of the solids concentration profiles. However those suspensions (Table 2.1) all have a higher solids concentration and solids density than activated sludge. Some authors mentioned the accuracy of the measurement, i.e. 0.25 and 0.5 vol% (Been and Sills, 1981; Bergstrom, 1992). This accuracy is too low for activated sludge batch settling with a solids concentration around 0.1-0.2 vol%. Chu *et al.* (2003) used CATScan measurements for wasted activated sludge but the measurement uncertainty of the solids volume fraction was only 0.1 vol% while the initial solids concentration was 0.8 vol%. Again the accuracy was low in comparison with the concentration used which, moreover, is significantly higher than the typical solids concentration of the activated sludge. It has to be investigated which non-invasive technique can be used to measure the solids concentration profiles during the batch settling of activated sludge. This will be the subject of Chapter 5.

Table 2.1: Overview of the experiments used by different modellers

Model	Experimental data	Materials	$\Delta\rho$ (kg/m^3)	ϕ_o (vol%)	ϕ_C (vol%)
Shirato <i>et al.</i> (1970)	Shirato <i>et al.</i> (1970)	ZnO/water	4640	2.5	1.5
		$F_{e_2O_3}$ /water	4160	15.9	5.9
Shih <i>et al.</i> (1986)	Shih <i>et al.</i> (1986)	Illite/toluene	1590	4.8	$\phi_o > \phi_C$
Font (1991)	Font (1988)	CaCO_3 /water	1580	2.0; 4.4; 8.8	22.5
Bergstrom (1992)	Bergstrom (1992)	Alumina/decalin	3089	15	15
Holdich and Butt (1997)	Holdich and Butt (1997)	Talc/potassium nitrate	1690	5.2	4
Diplas and Papanicolaou;	Tiller (1981)	Attapulgite/water	1300	3.0	6.5
Papanicolaou and Diplas	Been (1980)	Kaolin-bentonite/water	1630	9.1	Nm
Zheng and Bagley (1999)	Bhargava and Rajagopal (1990)	Al(OH)-flocs/water#	1071	4.4; 3.5; 2.7; 2.6; 2.3; 1.6 \otimes	Na
	Bhargava and Rajagopal (1990)	Bentonite/water	1051	3.0; 2.8; 2.3; 1.9; 1.6; 1.0	Na
	Scott (1968)	Gold ore/water	1700	2.2	Na
Karl and Wells (1999)	Wells (1990)	Kaolin/water	1616	12.0; 18.0; 5.7	Nm
Burger <i>et al.</i> (2000)	Tiller <i>et al.</i> (1991)	Kaolin/water	1562	5.0	7
	Bergstrom (1992)	Alumina/decalin	3089	15.0	15
	Been and Sills (1981)	Estuarine mud/water	1690	2.9	8.3
			1536	9.2	8.3
	Dreher (1997)	Kaolin/water	1560	7.0	9.6

Nm: not mentioned in article; Na: not needed for the model; #: since it is not clear whether the flocs are pure solid or solids and bound water, the volumetric solids concentration and density difference cannot be calculated with certainty; \otimes : suspended solids concentration in g/l

For determining the excess pore pressure profiles, i.e. the fluid pressure in excess of the hydrostatic pressure, pore pressure profiles, i.e. fluid pressure profiles, have been measured with manometers (Shirato *et al.*, 1970; Dreher, 1997) and pressure transducers (Been and Sills, 1981), and subsequently the excess pore pressure profiles are determined by subtracting the pore pressure from the hydrostatic pressure. To ensure that only the fluid pressure is measured, filters are placed in the column walls and the fluid is connected through these filters with the sensors.

Only Been and Sills (1981) mentioned the accuracy of this measurement, i.e. 30 Pa. In more recent work of Sills (1998), accuracies of 10 Pa are reported. Note that it cannot be expected that the accuracy of the other studies (Shirato *et al.*, 1970; Dreher, 1997) will be better, since the manometers used will not have a better accuracy than transducers. Hence, the accuracy is again too low for determining the excess pore pressure profiles of activated sludge. For example, if the activated sludge has a solids density of 1800 kg/m^3 and a solids concentration of 0.2 vol% and settling is performed in a column of 1 m height, then the excess pore pressure at the bottom at the beginning of the settling experiment is about 20 Pa ($\Delta\rho g\phi H$) while the hydrostatic pressure is about 10 kPa. Since there is a big difference in absolute value between the excess pore pressure and the hydrostatic pressure, a very accurate device (accuracy of about 0.001 % of the maximum range) for measuring pore pressure profiles is needed for activated sludge batch settling. The potential of measuring directly the excess pore pressure by measuring the pressure difference between the settling column and a water-filled column, with sufficient accuracy will therefore be investigated in Chapter 5.

2.3.2 Models for flocculated suspension settling

Different models for flocculated suspension settling, i.e. the Kynch batch density function and the effective solids stress function for the different suspensions are shown in Table 2.2.

Kynch batch density function For the Kynch batch density functions $f_{bk}(\phi)$, a variety of equations have been used as seen in Table 2.2. By inspecting the functions a bit closer, they can be divided into 5 categories:

- Shirato *et al.* (1970), Holdich and Butt (1997), Diplas and Papanicolaou (1997), Karl and Wells (1999) used **Darcy's law** for the friction force. The difference between those models is the permeability, which is described either by the Kozeny equation, an effective solids stress power-law function or a concentration-dependent exponential function. In one case, the Kozeny constant K is function of the volumetric solids concentration.
- Other researchers (Shih *et al.*, 1986; Font, 1991; Burger *et al.*, 2000) used the **Richardson and Zaki (1954)** equation or an extension of it (i.e. the exponent in the equation is not always 4.65, but is considered a parameter which has to be calibrated, or the V_{stokes} is a parameter to be calibrated and/or is a function of the volumetric solids concentration, or the proportionality factor between the brackets is different).
- Bergstrom (1992) and Burger *et al.* (2000) used the **permeability model of Brinkman (1947)** to derive the Kynch batch density function. Burger *et al.* (2000), though, did not use V_{stokes} but a parameter which has to be calibrated.

Table 2.2: Different Kynch batch density functions and effective solids stress functions presented in literature (a, b, d, d_i , n_i , h, α , α_i , β , β_i , λ , γ , τ , θ and ω are parameters which have to be calibrated)

Authors	Kynch batch density function $f_{bk}(\phi)$	Effective solids stress function $\sigma_e(\phi)$
Shirato <i>et al.</i> (1970)	$\frac{(1-\phi)^3}{\alpha} \frac{g(\rho_s - \rho_l)}{\mu}$	$\left(\frac{1-\phi}{a}\right)^b + d$
Shih <i>et al.</i> (1986)	$V_{stokes} e^{-\alpha\phi} \phi (1-\phi)^2$	$a e^{b\phi}$
Font (1991)	for $\phi < \phi_C$: $\alpha\beta^\gamma \phi (1-\beta\phi)^{4.65}$ for $0 < \phi < \phi_1$: $\beta = \beta_1$ for $\phi_1 < \phi < \phi_C$: $\beta = \beta_2 - \beta_3\phi + \beta_4\phi^2$ for $\phi > \phi_C$: $\tau(\omega - \phi)$	for $\sigma_e < \sigma_{e1}$: $\phi = a + b\sigma_e - d\sigma_e^2$ for $\sigma_e > \sigma_{e1}$: $\phi = h$
Bergstrom (1992)	$V_{stokes} \phi \frac{(2-3\phi)^2}{3\phi+4+3(8\phi-3\phi^2)^{0.5}}$	$\frac{a\phi^b}{\phi_{max}-\phi}$
Holdich and Butt (1997)	$\frac{(1-\phi)^3}{K(\phi)S_o^2} \frac{g(\rho_s - \rho_l)}{\mu}$	$\left(\frac{\phi}{a}\right)^b$
Diplas and Papanicolaou (1997)	$\frac{k}{\mu} \phi^2 g(\rho_s - \rho_l)$ with $k = \alpha(1 + \beta\sigma_e)^\gamma$; $\alpha = \alpha_1 + \alpha_2 t$	$-a + a\left(\frac{\phi}{\phi_C}\right)^b$ with $\phi_C = d_1 + d_2 t$; $\frac{1}{b} = n_1(n_2 - d_1)^h$
Zheng and Bagley (1998, 1999)	$\alpha e^{\beta\phi} \phi$	$\frac{g(\rho_s - \rho_l)\phi^2}{\rho_s a e^{b\phi}} \frac{\partial V_s}{\partial z}$
Karl and Wells (1999)	for $\phi > \phi_1$: $\frac{\alpha_1 e^{-\beta_1 \phi^x}}{\mu} \phi^2 g(\rho_s - \rho_l)$ for $\phi \leq \phi_1$: $\frac{\alpha_2 e^{-\beta_2 \phi^x}}{\mu} \phi^2 g(\rho_s - \rho_l)$ if $\phi < \phi_{initial}$, $\phi^x = \phi_{initial}$; else $\phi^x = \phi$	$a e^{b\phi}$
Burger <i>et al.</i> (2000)	$\alpha\phi \left(1 - \frac{\phi}{\phi_{max}}\right)^\beta$ $\alpha\phi \frac{(2-3\phi)^2}{3\phi+4+3(8\phi-3\phi^2)^{0.5}}$ for $0 \leq \phi \leq \phi_C$: $\alpha\phi(1-\gamma\phi)^\beta$ for $\phi > \phi_C$: $\frac{\lambda e^{\frac{\omega(1-\phi)}{\mu}}}{\mu} \phi^2$	$a \left(\left(\frac{\phi}{\phi_C} \right)^b - 1 \right)$ $a\phi^b$ $a\phi^b$
	for $0 \leq \phi \leq \phi_{initial}$: $\alpha\phi^2 + \beta\phi$ for $\phi_{initial} \leq \phi \leq \phi_C$: $\gamma\phi^2 + \lambda\phi + \omega$ for $\phi > \phi_C$: $\tau \frac{\phi^2 e^{-\theta\phi}}{1-\phi}$	$a \left(\left(\frac{\phi}{\phi_C} \right)^b - 1 \right)$

- Only one model (Zheng and Bagley, 1999) used the **Vesilind settling velocity function**, which is frequently used in activated sludge settling.
- Burger *et al.* (2000) used a special kind of function to describe the data of Dreher (1997), as can be seen in Table 2.2.

The model of Cacossa and Vaccari (1994) for *activated sludge* does not belong to one of those categories, whereas that of Kinnear (2002) for activated sludge belongs to the first category.

Some models used different batch density functions for different concentration ranges (Font, 1991; Karl and Wells, 1999; Burger *et al.*, 2000). Those models resulted in improved predictions of the measurements, as will be shown in the next section.

Mostly, the parameters of the Kynch batch density function were obtained from observed initial settling velocities.

Effective solids stress function To describe the effective solids stress, most reported models use power or exponential laws, similar to the model of Kinnear (2002) for *activated sludge* settling. Exceptions are the models of Font (1991) and Zheng and Bagley (1998, 1999).

In Zheng and Bagley (1998, 1999), the effective solids stress is a function of both the local concentration and the rate of change in concentration ($d\phi/dt$), which equals $\phi\partial V_S/\partial z$. This is in contrast with the traditionally used functions for the effective solids stress that only depend on the solids concentration. By its dependence on the rate of change in concentration, the effective solids stress is zero in the zone settling regime because there is simply no concentration gradient. In all the other approaches, it is assumed that the effective solids stress is a constant or zero in the zone settling regime.

Concerning the compression solids concentration ϕ_C , all models, except one, had a constant value, even for different initial concentrations (e.g. in Font (1991), Zheng and Bagley (1999) and Karl and Wells (1999)). The exception is the model of Diplas and Papanicolaou (1997), where the compression solids concentration was time-dependent. This was also suggested by Kinnear (2002) in order to improve the model predictions for activated sludge settling.

Mostly, the parameters of the effective solids stress function were obtained from the observed equilibrium solids concentration profiles.

2.3.3 Experimental results and model predictions

Besides reviewing the different results, it is pointed out in this section whether (i) the measurements, performed for the flocculated suspensions different than activated sludge, give more insight into the settling process compared to the *activated sludge* settling measurements and (ii) the models perform better compared to the *activated sludge* settling models.

The performance of the model of Shirato *et al.* (1970) is shown in Figure 2.8 for zinc oxide and in Figure 2.9 for ferric oxide. The concentration and excess pore pressure profiles are predicted rather accurately. The model performs well in general, but it has to be noted that the experiments were performed at a volumetric solids concentration higher than ϕ_C . Even though the initial concentration was higher than ϕ_C , a sludge bed is observed in the experiments with a constant concentration equal to ϕ_o .

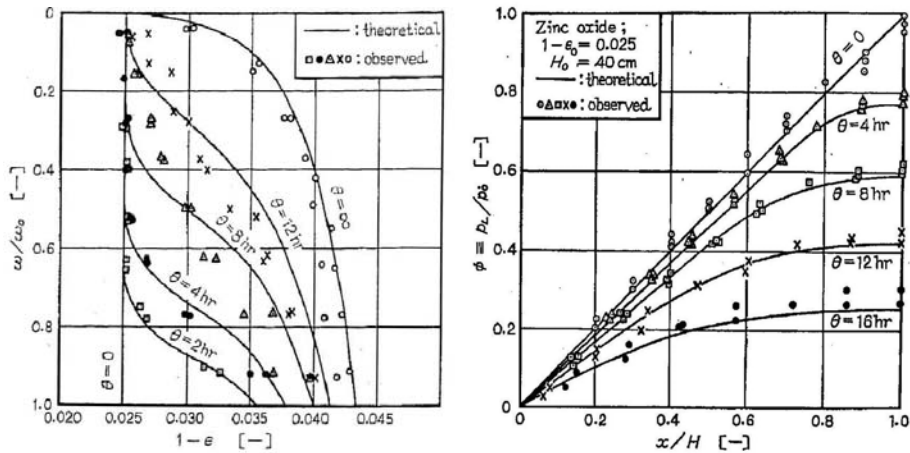


Figure 2.8: Experimental and simulated solids concentration (left) and excess pore pressure profiles (right) for zinc oxide (with H : sludge blanket height at time θ ; ω : volume of solids per unit area in distance x from H , i.e. $x = 0$ corresponds to the sludge blanket height; $x = H$ corresponds to the bottom of the settler; ω_o : total volume of solids per unit area, i.e. $\omega = 0$ corresponds to the sludge blanket height; $\omega = \omega_o$ corresponds to the bottom of the settler; p_L : local value of excess pore pressure; p_o : total pressure at the bottom) ($\phi_o = 2.5$ vol%; $\phi_C = 1.5$ vol%) (Shirato *et al.*, 1970)

(hindered settling). At the bottom, compression is already occurring: the pressure profiles from 4 hrs on for zinc oxide and from 8 hrs on for ferric oxide show that the total pressure at the bottom (p_o) is larger than the excess pore pressure (p_L), i.e. $p_L < p_o$. Both suspensions show the same settling behaviour. The measurements give of course much more information than the recording of the suspension-liquid interface, e.g. the compression is clearly observed by the pressure measurements. The model results are clearly better than the performance of the activated sludge settling models available up to now.

In Figure 2.10, the model predictions of Shih *et al.* (1986) and the measurements of the concentration profiles of illite settling in toluene are shown. The model describes the experiments at 3 and 5 minutes reasonably well; larger discrepancies are observed at 1.5 minutes. Shih *et al.* (1986) claimed that this is due to the uncertainty of the stress function. However, the time scope of the measurements was very limited. The initial solids concentration is again higher than the compression solids concentration ϕ_C and a sludge bed with constant concentration is observed in the experiments as well as in the model predictions. The suspension-liquid interface is well described by the model, but this does not guarantee better model results for *activated sludge* since the time scope of the measurements was very limited. For such short term experiments, the *activated sludge* settling models give good results too.

The model predictions of Font (1991) along with the experimental results (liquid-suspension and suspension-sediment interfaces over time at different initial solid concentrations ϕ_o) for the settling of commercial carbonate suspensions are shown in

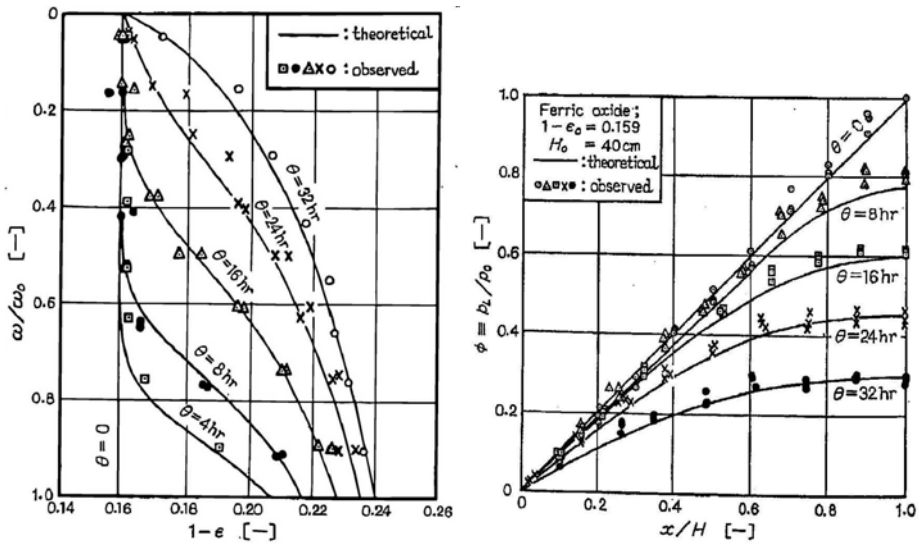


Figure 2.9: Experimental and simulated solids concentration (left) and excess pore pressure profiles (right) for ferric oxide (nomenclature is the same as in the previous figure) ($\phi_o=15.9$ vol%; $\phi_C=5.9$ vol%) (Shirato *et al.*, 1970)

Figure 2.11. A good agreement is found for the different initial solids concentrations: the measured suspension-sediment interface coincides with the simulations for the different initial concentrations. The initial solids concentration ϕ_o was lower than the compression solids concentration ϕ_C for all three experiments. The experimental results show the same settling behaviour as activated sludge but the model is doing a much better job than any of the activated sludge settling models.

The model predictions of Bergstrom (1992) and measured concentration profiles for the settling of alumina in decalin are shown in Figure 2.12 for two flocculation states (strongly flocculated: propionic acid is adsorbed at the alumina/decalin interface; weakly flocculated: oleic acid as adsorbant). Both suspensions (weakly and strongly flocculated) show the same settling behaviour. If the suspension is more strongly flocculated, the strong particle network resists compression, even at low concentrations. This is taken into account by the model by varying the parameters of the effective solids stress function (a , b and ϕ_{max}) according to the flocculation state. The model only partly describes the settling process accurately, and does not predict the slow increase in solids concentration observed in the top portion of the settling suspension. It is not clear why this happened in the experiments (not purely hindered settling) but this phenomenon is also seen in other experimental results (see further). For the weakly flocculated suspension, the simulated profiles at the bottom have a completely different shape than the measured ones but show the same trend as the profile for 172 days. Unfortunately, no simulations have been performed at 75 and 172 days. It can be concluded that the model is not suitable for weakly flocculated suspensions. Bergstrom (1992) suggested that the model needs to be modified by the introduction of an additional time- and stress-dependent compression process. The suspension-liquid interface is predicted well by the model, even in the non-hindered settling regime (at time 16 days for the weakly flocculated suspension), so this model is performing better

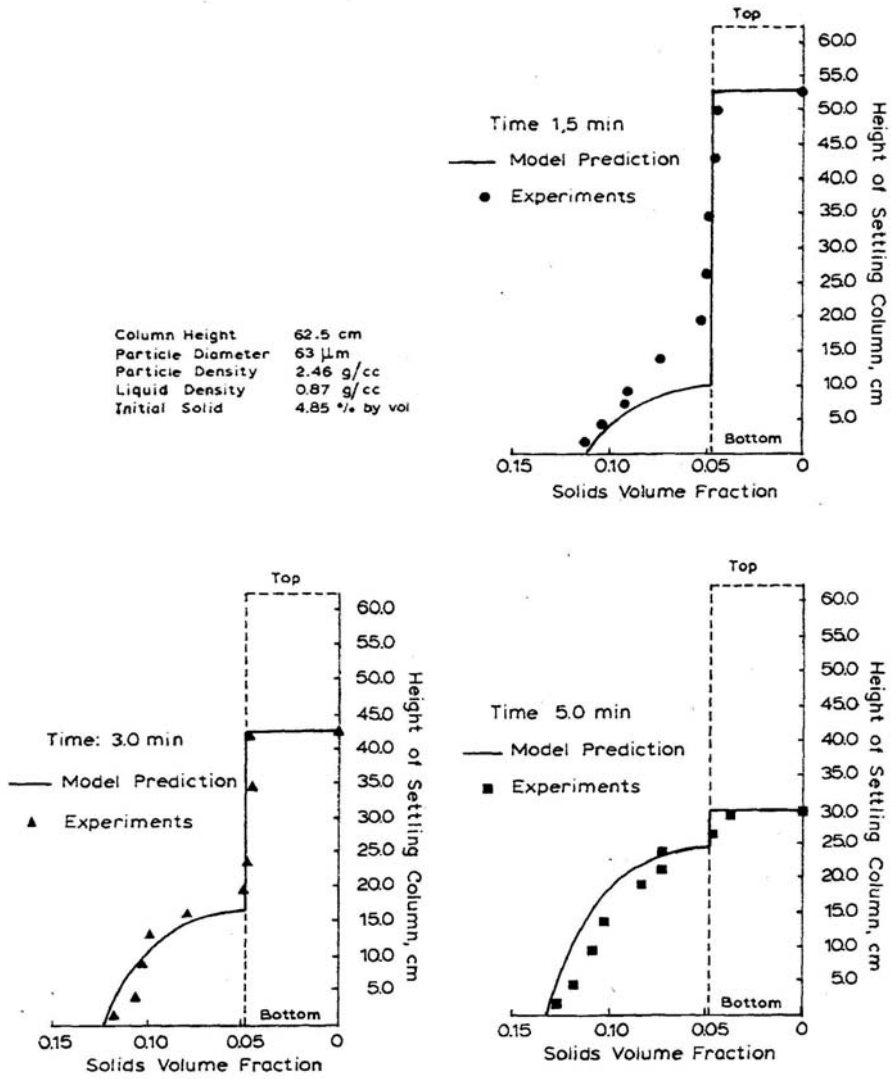


Figure 2.10: Comparison of simulated and experimental concentration profiles of the settling of illite in toluene ($\phi_o=4.85 \text{ vol}\% > \phi_C$) (Shih *et al.*, 1986)

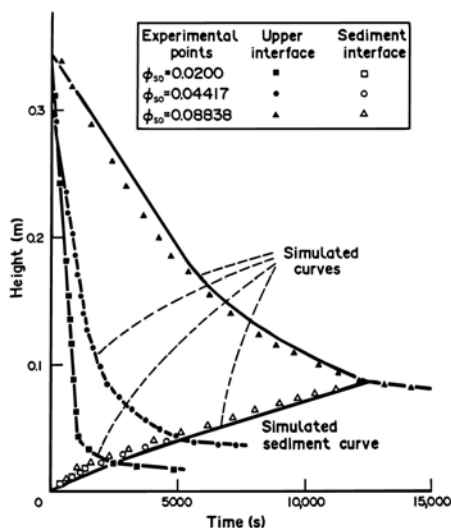


Figure 2.11: Experimental (symbol) and simulated (solid line) liquid-suspension and suspension-sediment interfaces versus time for the settling of commercial calcium carbonate suspensions (ϕ_o is indicated in legend; $\phi_C = 22.5$ vol%) (Font, 1991)

than the *activated sludge* settling models. Concerning the influence of flocculation on the *activated sludge* settling behaviour, Chu *et al.* (2003) experienced that flocculated activated sludge was less compressible and that flocculation enhanced the settleability.

The model predictions of Holdich and Butt (1997) are compared with measurements of mineral talc settling in Figure 2.13. The model describes the compression of the talc well. However, the initial solids concentration ϕ_o was higher than the compression solids concentration ϕ_C . Without considering this, the model gives better results than the *activated sludge* settling models.

The model simulations of Diplas and Papanicolaou (1997) and Papanicolaou and Diplas (1999) versus measurements are shown in Figures 2.14 and 2.15. The model predictions are in good agreement with the experimental data, except for the concentration profile at 97 h and 264 h. This shows that although the batch curve can be simulated very well, the concentration profiles cannot. In Figure 2.15, an increase in the concentration is seen in the top portion of the settling suspension in the experiments as well as in the simulations. The model is able to do this because of the time-dependency of the permeability. The suspension-liquid interface shows the same behaviour as the *activated sludge* batch settling curve but this model is performing better than the *activated sludge* settling models. This suggests that profile measurements are necessary for proper modelling of the *activated sludge* settling process.

In Figure 2.16 the experimental and predicted settling data for various suspensions of Zheng and Bagley (1999) are given. The model predicts the interfaces very well, even for different initial solids concentrations, and seamlessly moves from the zone settling regime to the compression regime. This is not the case with the existing *activated sludge* settling models, although the suspensions show the same settling behaviour

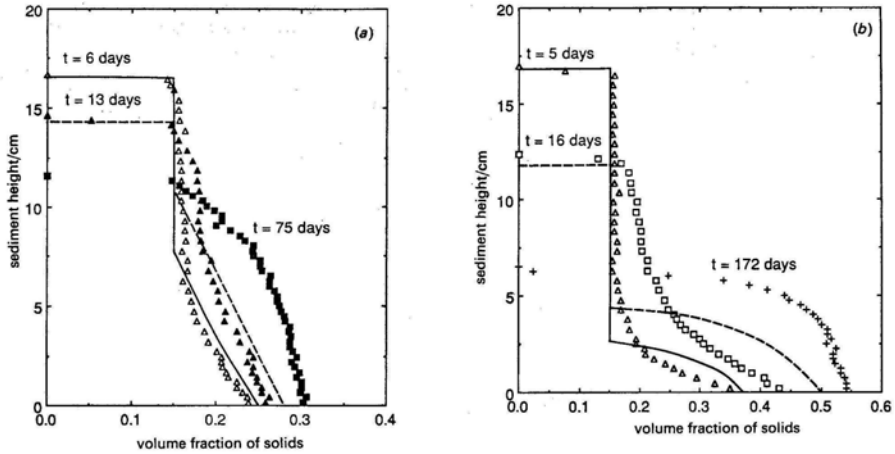


Figure 2.12: Measured (symbol) and predicted (line) solids concentration profiles of the settling of alumina in decalin ((a): strongly flocculated suspension; (b): weakly flocculated suspension) ($\phi_o = \phi_C = 15$ vol%) (Bergstrom, 1992)

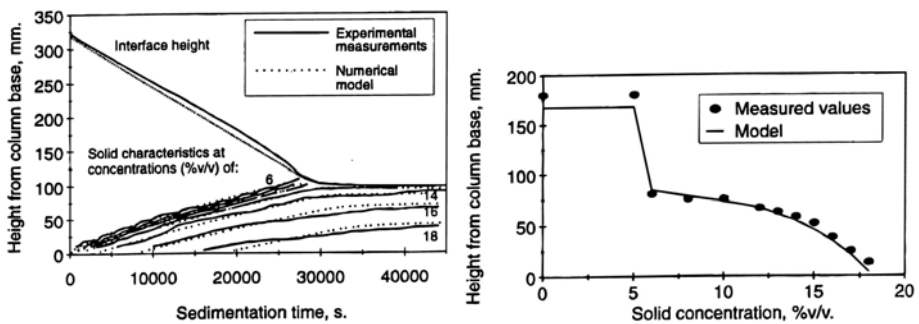


Figure 2.13: Measured and predicted lines of constant solids concentrations (left) and concentration profile (right) for the settling of mineral talc in a potassium nitrate solution ($\phi_o = 5.2$ vol%; $\phi_C = 4$ vol%) (Holdich and Butt, 1997)

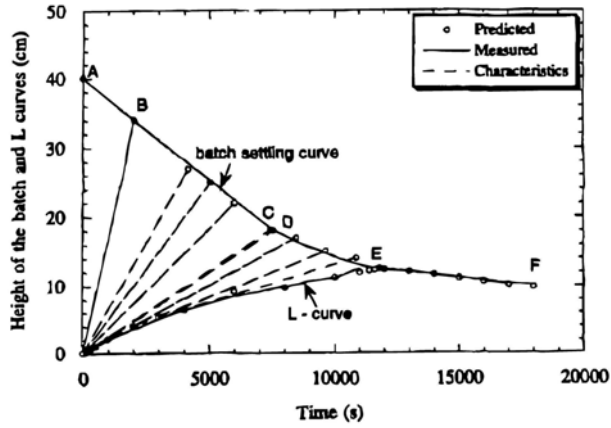


Figure 2.14: Simulated and measured suspension-liquid and sediment-suspension interface for the settling of attapulgite ($\phi_o=3$ vol%; $\phi_C=6.5$ vol%) (Diplas and Papanicolaou, 1997)

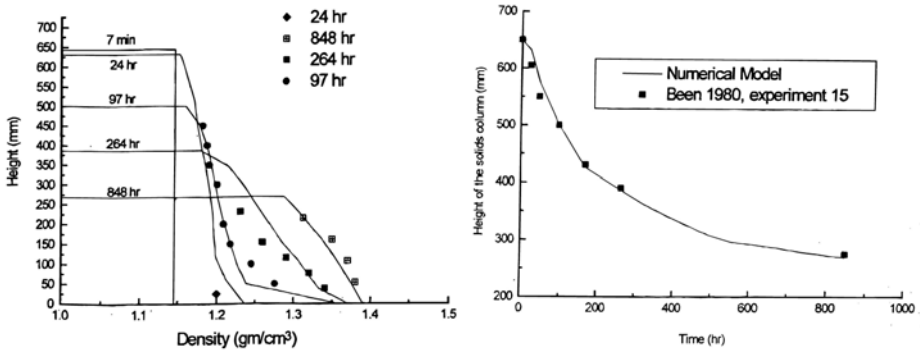


Figure 2.15: Simulated (line) and measured (symbol) density profiles (left) and batch settling curve (right) for the settling of kaolin-bentonite ($\phi_o=9.1$ vol%; ϕ_C =not mentioned) (Papanicolaou and Diplas, 1999)

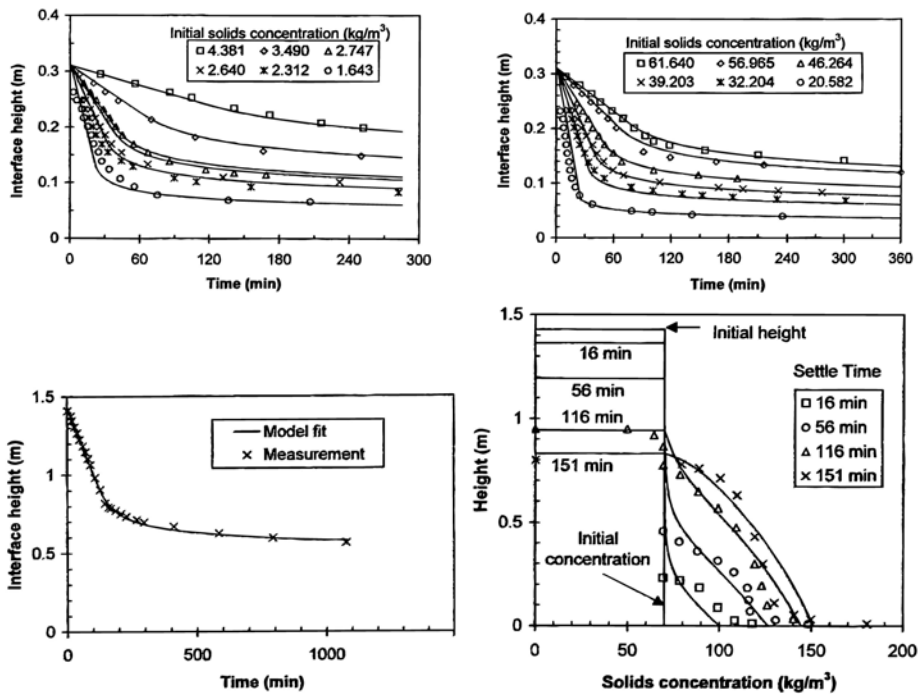


Figure 2.16: Experimental and predicted height versus time for settling of aluminum hydroxide flocs (top left, solids concentrations in legend), bentonite (top right, solids concentrations in legend) and desanded gold ore pulp (bottom left, $\phi_o=2.2$ vol%) and experimental and predicted concentration profiles for settling of desanded gold ore pulp (bottom right, $\phi_o=2.2$ vol%) (symbols: experimental data; lines: model predictions) (Zheng and Bagley, 1999)

as the *activated sludge*. Zheng and Bagley (1999) were one of the few that used measurements at different concentrations, even though these measurements consisted of only the suspension-liquid interface evolution (similar as typical *activated sludge* measurements). The concentration profiles are reasonably predicted as well, but only for the profiles collected at 116 and 151 minutes.

The predictions from the Karl and Wells (1999) model and measured concentration profiles for the settling of kaolin are shown in Figure 2.17. Karl and Wells (1999) were one of the few that tried to validate the model with other experimental data. Unfortunately the results were not satisfying: the agreement between the model predictions and the experimental data was not very good when the parameters calibrated from another data set were used. For the bottom left and right graph of Figure 2.17 the concentration profiles are underpredicted in the compression phase. The profiles were measured at small times, i.e. a few minutes, in comparison with the other data obtained for the settling of kaolin (Tiller *et al.*, 1991; Dreher, 1997): all experiments are still in the hindered settling regime. Note that the highest initial concentration ($\phi_o=18$ vol%) shows other behaviour in the lower portion. Karl and Wells (1999) concluded that the model was extremely sensitive to the constitutive relationships used and that further research was necessary to understand and determine slurry con-

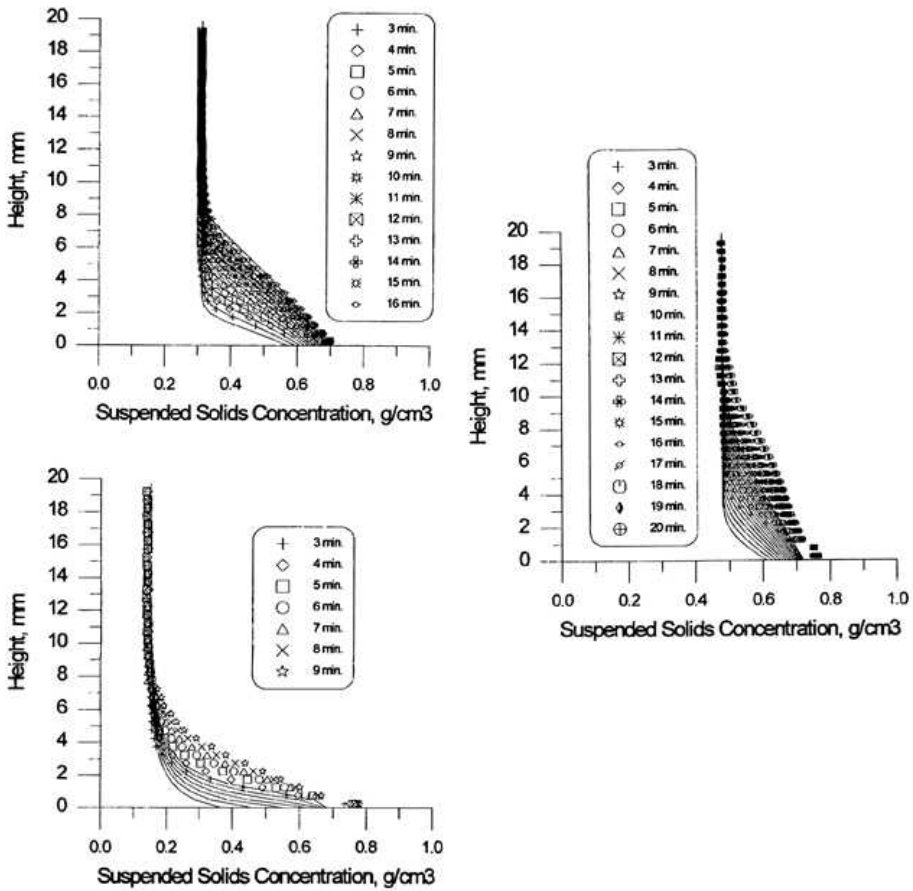


Figure 2.17: Predicted/simulated (line) and measured (symbol) concentration profiles at different initial concentrations for the settling of kaolin (top left: calibrated parameters; right and bottom left: parameters obtained from first figure, validation) (top left: $\phi_o=12$ vol%, right: $\phi_o=18$ vol%, bottom left: $\phi_o=5.7$ vol%) (Karl and Wells, 1999)

stitutive properties. These results cannot be compared with *activated sludge* results because the suspension-liquid interface is not shown. However, they are important to mention since Karl and Wells (1999) were the only ones who tried to validate their model.

The model simulations of Burger *et al.* (2000) and measured (Tiller *et al.*, 1991) concentration profiles for the settling of kaolin are shown in Figure 2.18. A good agreement is found but the model predicts clear liquid above the liquid-suspension interfaces while the measurements indicated that the supernatant was not completely clear. The simulated sludge blanket height is decreasing too rapidly at the beginning (up to 1800 s, in the hindered settling regime). Also, the concentration gradient in the sediment layer is overestimated, except for the data at 2 days. From 3000 s on, there is no more hindered settling. Before 3000 s, a discontinuity in the measurements and simulations is seen around the compression solids concentration of 7 vol%. So

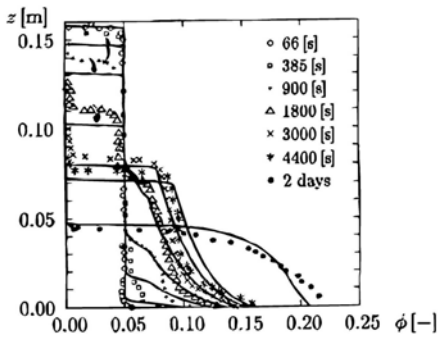


Figure 2.18: Simulated (line) and measured (symbol) concentration profiles of the batch settling of kaolin ($\phi_o=5$ vol%; $\phi_C=7$ vol%) (Burger *et al.*, 2000)

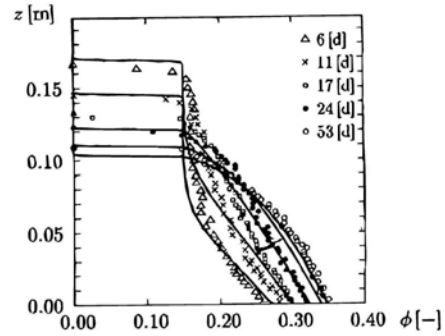


Figure 2.19: Simulated (line) and measured (symbol) concentration profiles of the batch settling of alumina in decalin ($\phi_o=\phi_C=15$ vol%) (Burger *et al.*, 2000)

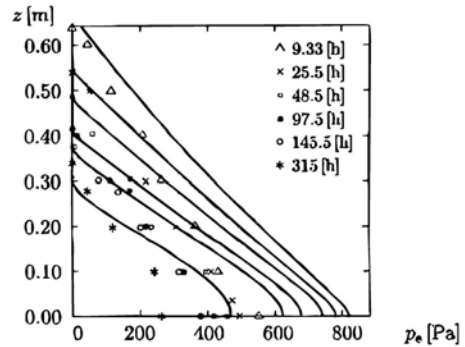
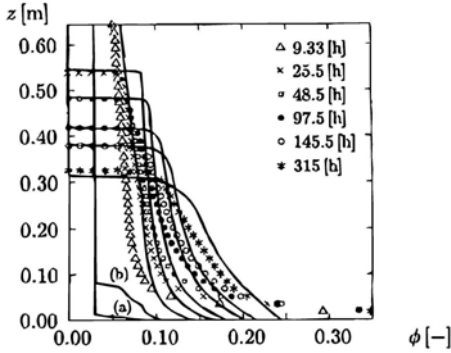


Figure 2.20: Simulated (line) and measured (symbol) concentration profiles (left) and excess pore pressure profiles (right) of estuarine mud settling ($\phi_o=2.9$ vol%; $\phi_C=8.3$ vol%) (Burger *et al.*, 2000)

the model gives better results for the suspension-liquid interface in the non-hindered settling regime but not in the hindered settling regime, which is in contrast with the *activated sludge* settling results.

The simulations of Burger *et al.* (2000) and the measured (Bergstrom, 1992) concentration profiles for settling of alumina in decalin are shown in Figure 2.19. A good agreement is found, except for the slow increase in the concentration in the top portion of the settling suspension (same as the model of Bergstrom (1992)). The results are better than the simulations of Bergstrom (1992) as shown in Figure 2.12. The simulations show a more continuous profile inside the sludge blanket than the ones of Bergstrom (1992). The difference between the two models is the V_{Stokes} -value and the effective solids stress function. The model gives better results than the *activated sludge* settling models.

The simulations of Burger *et al.* (2000), measured (Been and Sills, 1981) concentration and excess pore pressure profiles for the settling of estuarine mud are given in

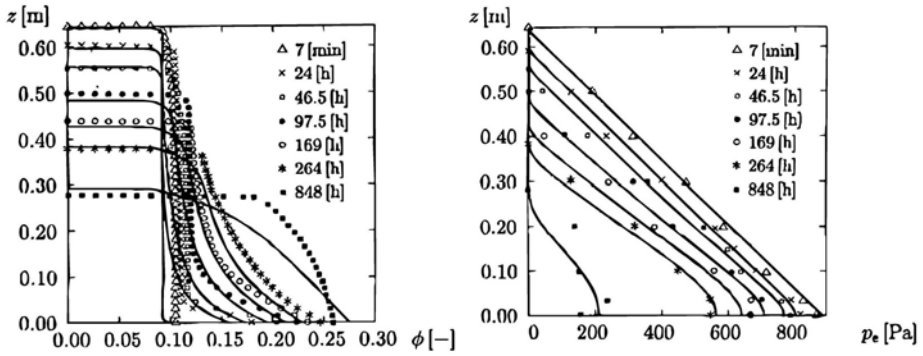


Figure 2.21: Simulated (line) and measured (symbol) concentration profiles (left) and excess pore pressure profiles (right) of estuarine mud settling ($\phi_o=9.2$ vol%; $\phi_C=8.3$ vol%) (Burger *et al.*, 2000)

Figures 2.20 and 2.21 for two different initial solids concentrations (one below and one above ϕ_C). The sludge blanket heights are simulated well for the whole duration of the experiments, which is in the range of days. This (simulation over a long period) cannot be said about the *activated sludge* settling models though.

For low initial concentration ($< \phi_C$), a slight overestimation of the profiles for the upper heights (higher than 0.1 m) and an underestimation for the lowest 0.1 m are observed. Burger *et al.* (2000) argued that this was due to the plastic deformation of sediment at high loads, i.e. near the bottom of large columns (in this case: 1.8 m). The excess pore pressure simulation for the low initial concentration is not very good, but Burger *et al.* (2000) claimed that this was due to the formation of vertical channels, which were not modelled. On the other hand, Been and Sills (1981) did not mention anything about plastic deformation at high loads and formation of vertical channels.

The simulated concentration profiles at high initial concentration ($> \phi_C$) provide fairly good approximations of the measured ones, except for the profile at 848 h (also for the excess pore pressure profiles). Here too, an increase in the concentration in the top portion of the settling suspension is observed and is not predicted by the model. Clearly, additional work is needed to determine the constitutive function for the effective solids stress more accurately. Again, the results show that even if the sludge blanket heights are predicted well, this does not imply that the entire process is modelled well since the concentration and excess pore pressure profiles are not predicted accurately. This is a very important finding for *activated sludge* settling models, since most modelling efforts are based on prediction of the sludge blanket heights only.

Figures 2.22 and 2.23 shows the simulations of Burger *et al.* (2000), measured (Dreher, 1997) concentration and excess pore pressure profiles for kaolin settling. The measured concentration data are scattered, but it can be concluded that the simulated profiles approximate the measurements well. The excess pore pressure is simulated fairly well, except for the largest time (13.27 days), where the simulated values are much higher than the measured ones. This is not reflected in the concentration profiles though. At 0.312 days, the suspension is still in hindered settling at the top and a discontinuity at the compression solids concentration can be seen in the simulated concentration profile. From 0.87 days on, there is no pure hindered settling any more. The model

gives better suspension-liquid interface predictions than the *activated sludge* settling models.

2.4 Conclusion

A mechanistic model describing the batch settling of activated sludge may be used to predict the settling behaviour of activated sludge in a secondary clarifier. However, in the wastewater industry, no such mechanistic model is currently available. Most models are empirical and have no relationship with the physical properties of activated sludge flocs and solid-water interaction. Kinnear (2002) recognized this and considered densities, viscosity, ... Unfortunately, his mechanistic model was not capable of predicting a complete batch curve. Hence, there is a need to describe the batch settling behaviour of activated sludge in a more fundamental and correct way.

In other application areas more fundamental research has been performed on the modelling of batch settling, including more in-depth batch settling measurements. Therefore, a review of this research provides insight into the activated sludge batch settling, both for the modelling as for the experimental aspects. Concerning the experimental part, not only the suspension-liquid interface is recorded as in activated sludge batch settling, but the solids concentration and the excess pore pressure profiles have been measured. Those measurements give much more information about the process of batch settling and reveal some interesting phenomena:

- even with an initial concentration higher than the compression solids concentration, a zone with a constant concentration (equal to the initial concentration) is observed, although this is not always experienced: in some cases a slight increase in solids concentration ... occurs in the top portion of the settling suspension
- for different initial concentrations of the same suspension, the sediment-suspension interfaces coincide
- when the flocculation state is different for the same suspension, the more flocculated suspension is less compressible.

The solids concentration and excess pore pressure profile measurements are, furthermore, the most appropriate measurements for the validation of a mechanistic model. It is investigated in this PhD study whether these measurements can be done for activated sludge which has a lower density than the suspensions that were reviewed.

Concerning the modelling part, all models are based on the same fundamental mass and force balances for water and solids, similar to the model of Kinnear (2002). However, they use different Kynch batch density functions and effective solids stress functions. Even for the same material, such as kaolin and alumina, different constitutive functions are used in literature (e.g. Bergstrom (1992) and Burger *et al.* (2000)). All reviewed models give better performance in terms of suspension-liquid interface predictions than the activated sludge settling models. However, when the batch settling curves are predicted accurately, the solids concentration profiles may not correctly describe the settling process. This emphasizes the importance of solids concentration profile measurements for activated sludge batch settling. For the reviewed model results, good predictions are obtained when

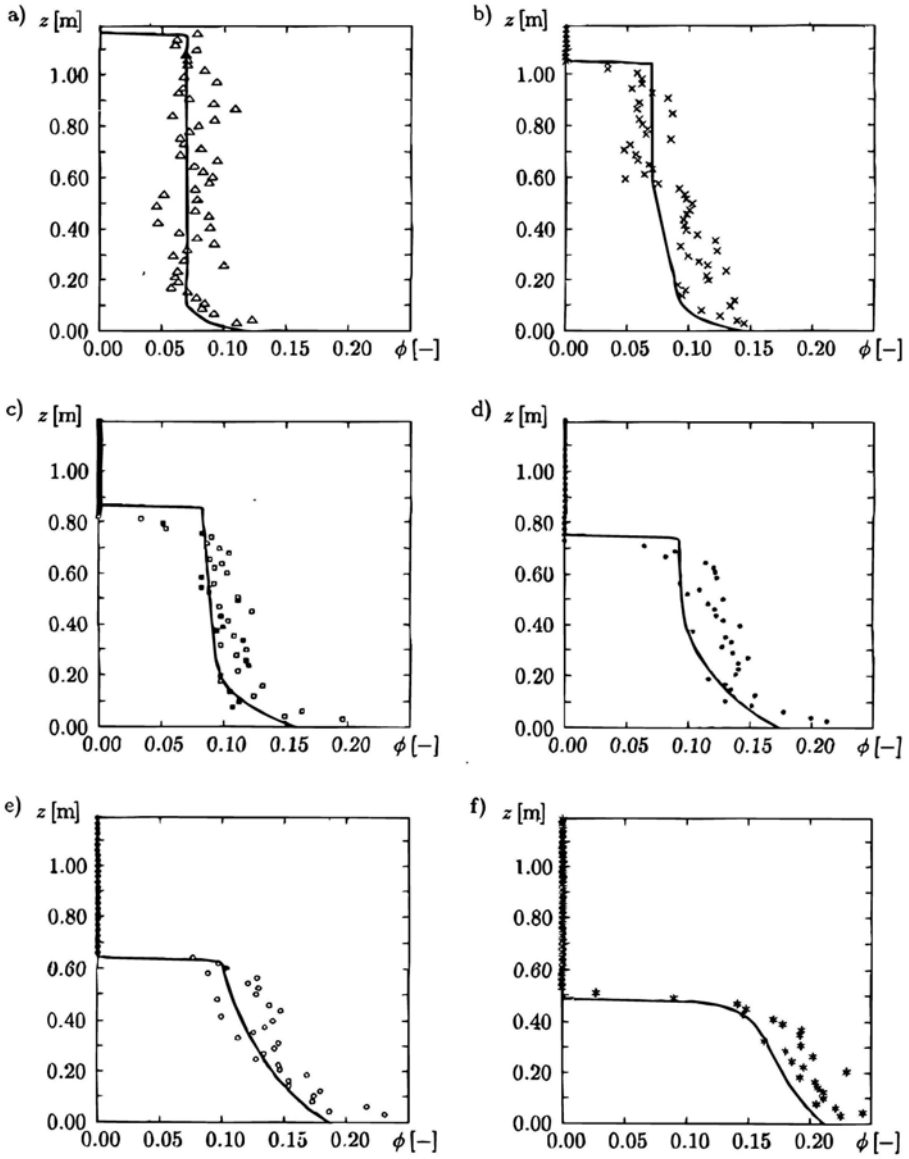


Figure 2.22: Simulated (line) and measured (symbol) concentration profiles of kaolin settling ($\phi_o=7$ vol%; $\phi_C=9.6$ vol%) (a) at 0.052d; b) at 0.312d; c) at 0.87d; d) at 2.13d; e) at 3.91d; f) at 13.27d) (Burger *et al.*, 2000)

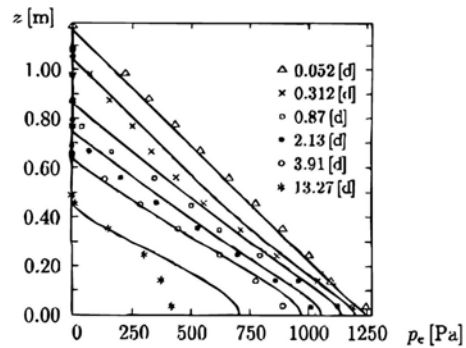


Figure 2.23: Simulated (line) and measured (symbol) excess pore pressure profiles of kaolin settling ($\phi_o=7$ vol%; $\phi_C=9.6$ vol%) (Burger *et al.*, 2000)

- a time-varying compression solids concentration is used, like Kinnear (2002) suggested (Diplas and Papanicolaou, 1997)
- the effective solids stress is a function of the local concentration and concentration gradient (Zheng and Bagley, 1998, 1999)
- the initial concentration is higher than the compression solids concentration (Shirato *et al.*, 1970; Holdich and Butt, 1997; Burger *et al.*, 2000), even though this does not always result in good predictions (Shih *et al.*, 1986; Bergstrom, 1992)
- different batch density functions are used for different concentration ranges (Karl and Wells, 1999; Font, 1991; Burger *et al.*, 2000)

It is investigated in this PhD study whether one of these models or functions gives better predictions of the settling behaviour of activated sludge. The activated sludge settling model should also be capable of describing different batch settling data of sludge with the same properties. Only Karl and Wells (1999) investigated this by using the same model parameters, but their work showed poor performance in this respect.

The resulting sludge settling model should subsequently be the basis for models which attempt to describe the behaviour of a clarifier.

Chapter 3

1D modelling of continuous settling

3.1 Introduction

There are different type of models, e.g. black box, white box and grey box models, depending on the objective for which they are used or the information sources they are based on. Some models are developed to yield a very detailed description of the involved processes whereas other models are developed for prediction and control purposes.

Black box models describe input-output relations by equations that do not reflect physical, chemical, biological etc. considerations and are not considered here. White box models are developed from the idea that a full understanding of nature can be obtained by identifying and describing all the physical, chemical and biological laws that govern the system concerned. The models solve the differential equations of continuity, momentum, energy, mass transport and chemical and biological reactions with realistic boundary conditions. No such model exists yet for clarifiers since all current models are based on some kind of empirical input. Most of this empiricism is introduced by the description of the settling behaviour of the sludge, which is used in all current clarifier models.

Hence, most clarifier models are **grey box** models. Grey box models are based on the most important physical, chemical and biological relations and contain empirical terms to account for uncertainties in model formulation as well as in observations. 1D, 2D and 3D models have been formulated (using 1, 2 or 3 spatial dimensions).

The current 2D and 3D models describe the internal flow pattern and the solids transport phenomena to a certain extent and are closest to reality. Since their use is computationally very demanding, they are not yet used for control or optimisation purposes. 1D models only describe the processes in the vertical dimension and are a gross simplification of reality. Unlike the higher dimensional models, 1D models can be used for operation and control (Ekama *et al.*, 1997) and answer mass inventory questions, questions related to the recycling of activated sludge and questions about sludge blanket levels. Those models are the subject of this research and hence, are discussed here.

Several 1D models are reported in literature. These can be roughly classified as:

- models with limitation of the settling flux (Vitasovic, 1989; Takacs *et al.*, 1991)
- models with dispersion (Hamilton *et al.*, 1992; Watts *et al.*, 1996; Lee *et al.*, 1999; Joannis *et al.*, 1999)
- models considering compression settling (Hartel and Popel, 1992; Otterpohl and Freund, 1992; Cacossa and Vaccari, 1994; Kinnear, 2002)
- models with a by-pass from inlet to recycle (Dupont and Dahl, 1995)

The detailed discussion of these models includes the specific characteristics (settling velocity function, the presence/absence of a dispersion coefficient, other features) and the ability of the model to predict the full-scale behaviour in the clarifier. This behaviour is dynamic because of the variation of flow rates (e.g. diurnal, seasonal, ...), waste content of the wastewater, settling properties,

The behaviour cannot be imitated in a down-scaled version of the clarifier because down-scaling is not possible. For down-scaling purposes, geometric (similarity in form or shape), kinematic (similarity of motion) and dynamic similarity (forces at corresponding points are similar) is required and complete dynamic similarity is impossible unless the down-scaled clarifier is almost the same size as the full-scale one. This implies that the calibration and validation of the 1D-models are preferably done using dynamic full-scale measurements. The measurements used for modelling are, consequently, considered too in the discussion of the different models. In Table 3.1, the different aspects of the described models are shown. Before discussing these models in more detail, a general model description is given.

3.2 General Model Description

The continuity equation for sludge in the clarifier is a non-linear PDE

$$\frac{\partial C(z,t)}{\partial t} = -\frac{\partial F(C(z,t), z, t)}{\partial z} + \frac{\partial}{\partial z} \left(D(z,t) \frac{\partial C(z,t)}{\partial z} \right) + s(z,t) \quad (3.1)$$

where $C(z,t)$ is the solids concentration (dependent on depth z and time t) and $D(z,t)$ is the dispersion coefficient, which is possibly dependent on local variables and/or on input variables, such as flow rates, feed concentration $C_f(t)$, ... (e.g. Watts *et al.* (1996), Joannis *et al.* (1999)). The discontinuous flux $F(C(z,t), z, t)$, which is dependent on depth z (with $z=0$ at the top, z_f the feed layer location and $z=H_{centre}$ at the bottom), is composed of the bulk vertical movement of water and settling:

$F(C(z,t), z, t) =$

$$\begin{cases} \left(V_S(C(z,t), t) - \frac{Q_e(t)}{A(z)} \right) C(z,t) & 0 \leq z < z_f \\ \left(V_S(C(z,t), t) - \frac{Q_e(t)}{A(z)} + \frac{Q_u(t)}{A(z)} \right) C(z,t) & z = z_f \\ \left(V_S(C(z,t), t) + \frac{Q_u(t)}{A(z)} \right) C(z,t) & z_f < z \leq H_{centre} \end{cases} \quad (3.2)$$

with $V_S(C(z,t), t)$ the settling velocity function, $Q_e(t)$ the effluent flow rate, $Q_u(t)$ the underflow rate and $A(z)$ the cross sectional area. The latter is dependent on height in some models (Watts *et al.*, 1996). The source term $s(z,t)$ is described with a point source $\frac{Q_f(t)}{A(z)} \frac{\partial C_f(t)}{\partial z} \delta(z - z_f)$, where $Q_f(t)$ is the feed flow rate.

Table 3.1: Settling velocity function, dispersion coefficient, other features and experimental data of the described 1D-models

Authors	Settling velocity function (V_S)	Dispersion coefficient and Other features	Experimental data
Vitasovic (1989)	$V_0 e^{-nC}$	Limitation of settling flux 10 layer discretisation	
Takacs et al. (1991)	$\min(V_{0max}, V_0 (e^{-r_h(C-C_{min})} - e^{-r_p(C-C_{min})}))$	Limitation of settling flux 10 layer discretisation	Full-scale steady-state concentration profiles for calibration
Hamilton et al. (1992)	$V_0 e^{-nC}$	$D(z, t) = \text{constant}$ 24 layer discretisation	Full-scale SBH for calibration Pilot-scale SBH for validation
Watts et al. (1996)	$\min(V_{0max}, V_0 (e^{-r_h(C-C_{min})} - e^{-r_p(C-C_{min})}))$	$D(z, t) = f(C(z, t), Q_f(t))$ 50 layer discretisation $A(z)$ Density current Special recycle mode	Full-scale steady-state concentration profiles for calibration
Joannis et al. (1999)	$V_0 e^{-nC}$	$D(z, t) = \text{constant}$ Dilution coefficient Dilution zone Density current Special recycle mode	Full-scale dynamic concentration profiles for calibration; Full-scale dynamic SBH for validation
Lee et al. (1999)	$\min(V_{0max}, V_0 (e^{-r_h(C-C_{min})} - e^{-r_p(C-C_{min})}))$	$D(\text{clarification zone}, t) = \text{constant}_1$ $D(\text{thickening zone}, t) = \text{constant}_2$ 20 layer discretisation	Full-scale steady-state concentration profiles for calibration and validation

Authors	Settling velocity function (V_S)	Dispersion coefficient and Other features	Experimental data
Hartel and Popel (1992)	$V_0 e^{-n_C C}$	Compression settling Clarification zone is one volume with $V_S = V_0$	Full-scale steady-state concentration profiles and effluent concentrations for validation
Otterpohl and Freund (1992)	Macroflocs: $V_0 e^{-n_C C}$ Microflocs: $0.1m/hr$	Compression settling Limitation of settling flux	Full-scale dynamic effluent concentrations for validation
Cacosa and Vaccari (1994)	$V_{hindered}(C) \left(1 - \frac{\partial C}{\partial z} \frac{1}{K}\right)$ with $K = K_m e^{-\frac{C}{S}}$ For $C \geq C_C$: $V_{hindered} = \frac{C-B_1}{C}$ For $C < C_C$: $V_{hindered} = \left(2 - \frac{C}{C_C}\right) \left(\frac{B_1}{C_C - B_2}\right)$	Compression settling	Pilot-scale steady-state concentration profiles for validation
Kinnear (2002)	For $C < C_C$: $\frac{(p_f - p_l) g e^3}{5S_2^2(1-\epsilon)\mu}$ For $C \geq C_C$: $\frac{(p_f - p_l) g (1-\epsilon) + P_0 \left(\frac{1-\epsilon}{1-\epsilon_C}\right)^m \frac{\partial \epsilon}{\partial z}}{5S_2^2(1-\epsilon)^2 \mu} e^3$		Pilot-scale steady-state concentration profiles for validation
Dupont and Dahl (1995)	$V_0 e^{-0.5 \left(\frac{\ln(n_1 C)}{n_2}\right)^2}$	Density current Short-circuiting	Full-scale steady-state concentration profiles for calibration

with D the dispersion coefficient and n_1 and n_2 parameters

At the boundaries, the solids transport reduces to its convective part and $C(z,t)$ has to be continuous. This implies the following non-linear boundary conditions:

$$V_S(C(z,t), t) C(z,t) - D(z,t) \frac{\partial C(z,t)}{\partial z} \Big|_{z=0, z=H_{centre}} = 0 \quad (3.3)$$

The initial condition is given by

$$C(z, 0) = C_o(z) \quad (3.4)$$

A schematic drawing of a clarifier is shown in Figure 3.1, together with the different fluxes and in- and outputs.

The relationship of $V_S(C(z,t), t)$ with the $f_{bk}(\phi)$ of section 2.1.2 is:

$$V_S(C(z,t), t) C(z,t) = f_{bk}(C(z,t), t) \left(1 - \frac{\rho_s(t)}{\Delta\rho(t)g} \frac{\partial \sigma_e(C(z,t), t)}{\partial C(z,t)} \frac{\partial C(z,t)}{\partial z} \right) \quad (3.5)$$

considering (1) the simple relationship $C(z,t) = \phi(z,t) \rho_s(t)$ and (2) time-varying settling properties.

3.3 Models with limitation of the settling flux

Vitasovic (1989) used the Vesilind settling velocity function and Takacs *et al.* (1991) used the settling velocity function of Patry and Takacs (1992) (see Table 3.1 for the structure of these functions). The Vesilind settling velocity function only applies to hindered settling conditions, while the Takács settling velocity function applies both to the hindered settling and settling at more diluted concentrations.

The model equation 3.1 is solved by discretizing the partial derivatives by splitting up the tank into horizontal layers. Both authors used 10 layers. A limitation of the settling flux is introduced to ensure that a shock wave cannot be created and the concentration profile will never show an inverse gradient, i.e. the concentration in a certain layer is never higher than that of a layer below. This limitation is interpreted as follows: the settling flux into a differential volume cannot exceed the settling flux the volume is capable of passing, nor can it exceed the settling flux of the lower adjoining differential volume. This limitation exists throughout the thickening zone. In the clarification zone, the limitation only holds if the concentration is higher than the threshold concentration C_t . It is presumed that C_t corresponds to the onset of hindered settling behaviour. The value of this threshold concentration is equal to 3 g/l (Takacs *et al.*, 1991; Vitasovic, 1989) or 1 g/l (Ekama *et al.*, 1997). This limitation is in fact an ad hoc assumption based on empirical considerations and without any founded background.

Takacs *et al.* (1991) applied the model to the full-scale measurements of Pflanz (1969), assuming that steady-state prevailed (Figure 3.2). Concentration profiles at 10 points were measured at 3 different loads (low, medium and high). The settling parameters, which are assumed different for every load, are determined by minimizing the sum of squares of differences between measured and calculated concentration profiles. The model predicts the measurements fairly well, but a validation of the model with full-scale dynamic concentration profiles is not performed yet.

Watts *et al.* (1996) tested the same model but with more than 10 layers to the

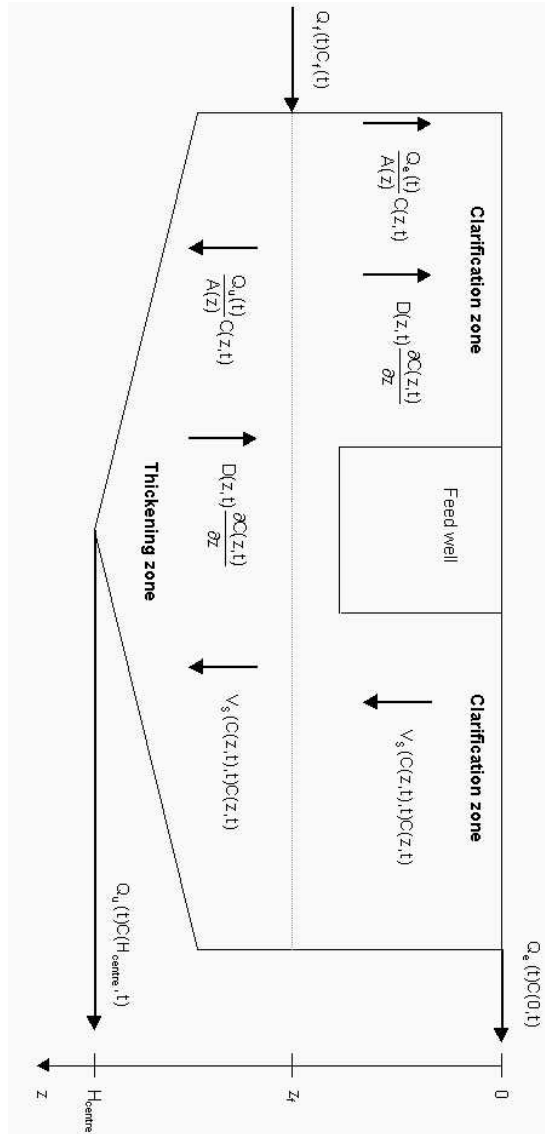


Figure 3.1: Schematic drawing of the clarifier with fluxes and in- and output(s)

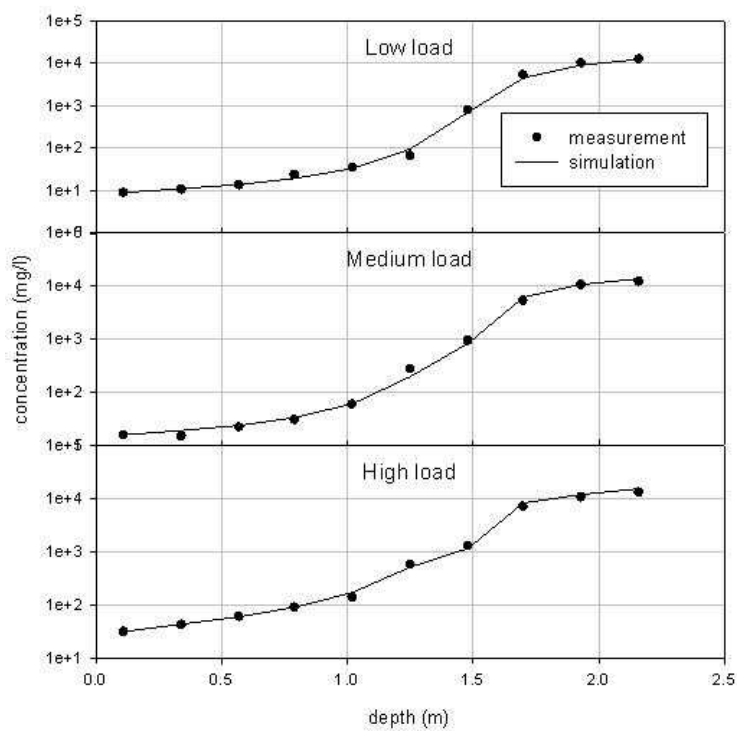


Figure 3.2: Observed and simulated concentration profiles (Takacs *et al.*, 1991)

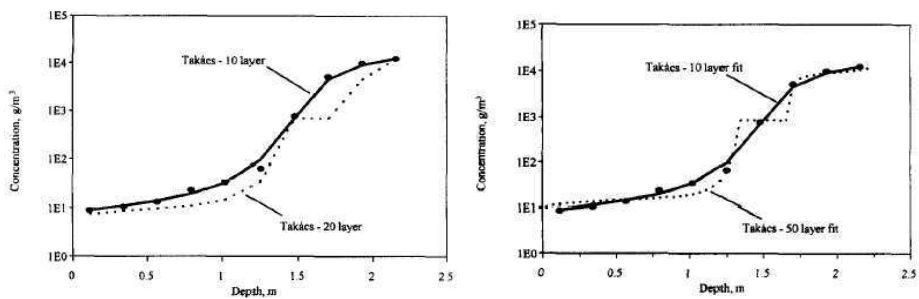


Figure 3.3: Comparison of 10- and 20-layer versions of the Takacs *et al.* (1991) model with same settling parameters (left) and of 10- and 50-layer versions of the Takacs *et al.* (1991) model with recalibrated settling parameters (right) (Watts *et al.*, 1996)

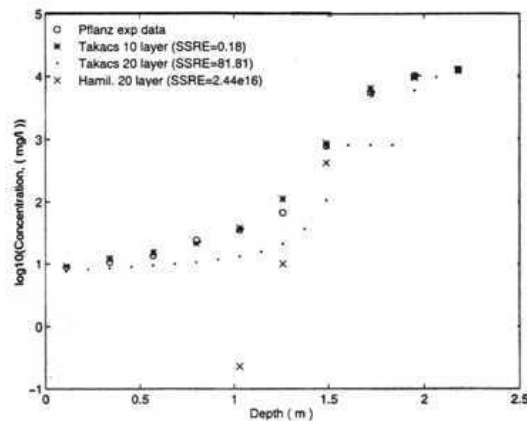


Figure 3.4: Predicted and measured concentration profiles for the Takacs *et al.* (1991) and Hamilton *et al.* (1992) model and the Pflanz low load experimental data (Lee *et al.*, 1999)

same Pflanz-data (Figure 3.3). For 20 layers and the same settling parameters and for 50 layers and recalibrated settling parameters, the model gave worse predictions. This is contradictory to the basic rule that a model should perform better when the discretisation becomes finer. Lee *et al.* (1999) too predicted the low-load experiment of Pflanz (1969) with the model of Takacs *et al.* (1991) and found the same results (Figure 3.4): the fit was excellent for 10 layers, but for 20 layers the model failed to give reasonable predictions in the thickening zone.

There is clearly something wrong with the inclusion of the limiting settling flux since a finer discretisation should normally give a better model result. This was also shown by Jeppsson and Diehl (1996). Since the model equation 3.1 is a non-linear PDE, a specific numerical integration for non-linear PDE's is required, i.e. simple finite differences, as in Vitasovic (1989) and Takacs *et al.* (1991), even if they are combined with the ad hoc limiting flux condition, cannot be used. The numerical integration of the non-linear PDE is discussed more thoroughly in section 4.1. Vitasovic (1989) and Takacs *et al.* (1991) were correct in a way that the shock wave may not be created but they had to use a more fundamental way to obtain this behaviour.

3.4 Models with dispersion

Hamilton *et al.* (1992) used the Vesilind settling velocity function and included a Fickian dispersion term instead of using the limiting settling flux (Table 3.1). This inclusion converts the first-order partial differential equation into a parabolic differential equation, which of course results in a more continuous concentration profile.

Hamilton *et al.* (1992) recognized the fact that theoretically an infinite number of layers is needed to exactly model the continuous phenomena of settling and concentration variation with height. In practice, however, a finite number of layers can simulate the clarifier, giving a good estimate of effluent and recycle concentration, as well as the sludge blanket height. Those 3 variables were in fact used to determine the required number of layers and this investigation gave 24 layers as a result.

The parameters of the settling velocity function and the dispersion coefficient were determined by minimizing the sum of squares of differences between measured and calculated sludge blanket heights of a full-scale clarifier. Steady-state pilot-scale experiments were conducted at the same plant and used for validation of the model. The model successfully predicted the sludge blanket level.

Lee *et al.* (1999) predicted the low-load experimental data of Pflanz (1969) with the model of Hamilton *et al.* (1992) (Figure 3.4): the model failed to predict the concentration profile in the clarification zone. This could be caused by the Vesilind settling velocity function which does not consider the settling at low solids concentrations and gives a too high settling velocity for low solids concentrations.

Watts *et al.* (1996) reinterpreted the approach of Takacs *et al.* (1991), i.e. the limiting flux constraint, as modelling with a concentration-dependent dispersion coefficient (Table 3.1). Both interpretations gave different results if the number of layers is changed. For the finer discretisations, the dispersion interpretation led to better predictions of the experimental data. The concentration-dependent dispersion coefficient was then simplified and a dependency on clarifier feed velocity was incorporated:

$$D_{i,i+1}(C_i, C_{i+1}) = \begin{cases} D_{max}(1 + \beta(\sqrt{C_i C_{i+1}} - C_{crit})e^{-\beta(\sqrt{C_i C_{i+1}} - C_{crit})}) & \text{for } \sqrt{C_i C_{i+1}} > C_{crit} \\ D_{max} & \text{for } \sqrt{C_i C_{i+1}} \leq C_{crit} \end{cases} \quad (3.6)$$

with

β, C_{crit} parameters

$$D_{max} = \begin{cases} D_1 + \gamma(V_f - V_{f,1})^2 & \text{for } V_f \geq V_{f,1} \\ D_1 & \text{for } V_f < V_{f,1} \end{cases}$$

$D_1, \gamma, V_{f,1}$ parameters

V_f the feed velocity

The model was also modified by including a conical section at the bottom of the cylindrical section, i.e. $A(z)$ was made dependent on depth z . Since in the clarifier studied, the recycle is removed by a hydraulic suction system which has intake pipes spaced along the sloping floor of the bottom, this is also considered by the model: in

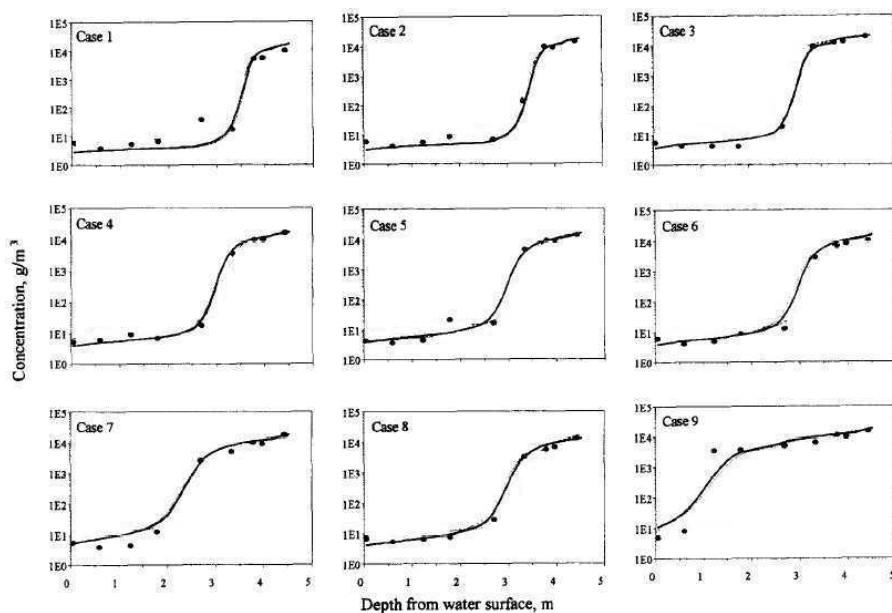


Figure 3.5: Predicted (lines) and measured (symbols) concentration profiles (Watts *et al.*, 1996)

each of the layers of the conical section, sludge is withdrawn at a rate equal to the change in cross-sectional area from the top to the bottom of the layer multiplied by the underflow velocity.

The clarifier was divided into 50 layers and the partial derivatives were discretized. Since Anderson (1945) observed that the clarifier feed falls as a density current to the top of the sludge blanket, the feed layer was assumed to be the layer with a concentration equal to the feed concentration. This was considered by setting the feed layer at a position immediately above the uppermost layer having a concentration greater than that of the mixed liquor entering the clarifier. This layer was located according to a recursive procedure. The hindered settling parameters of the Takács settling velocity function were determined from observed initial settling velocities. The parameter C_{min} was determined from the measurement of the 60-min non-settleable suspended solids concentration of the mixed liquor. The other parameters were obtained by least-squares non-linear regression on concentration profiles.

Full-scale steady-state concentration profiles were predicted nicely (Figure 3.5), but the model was never validated.

Joannis *et al.* (1999) used the Vesilind settling velocity function (Table 3.1). The model includes dispersion, a dilution coefficient and an upper limit of the dilution zone. Dilution was added to the model since solids concentration measurements, conducted in the sinking plume, showed that the sludge experienced strong dilution as it went out of the feeding well and travelled towards the top of the sludge blanket level. The feed layer was placed at the top of the sludge blanket.

The parameters of the settling function were derived from a settleability index by an empirical relationship. The other parameters, i.e. the dilution coefficient, the upper limit for the dilution zone and the dispersion coefficient, were determined from a non-

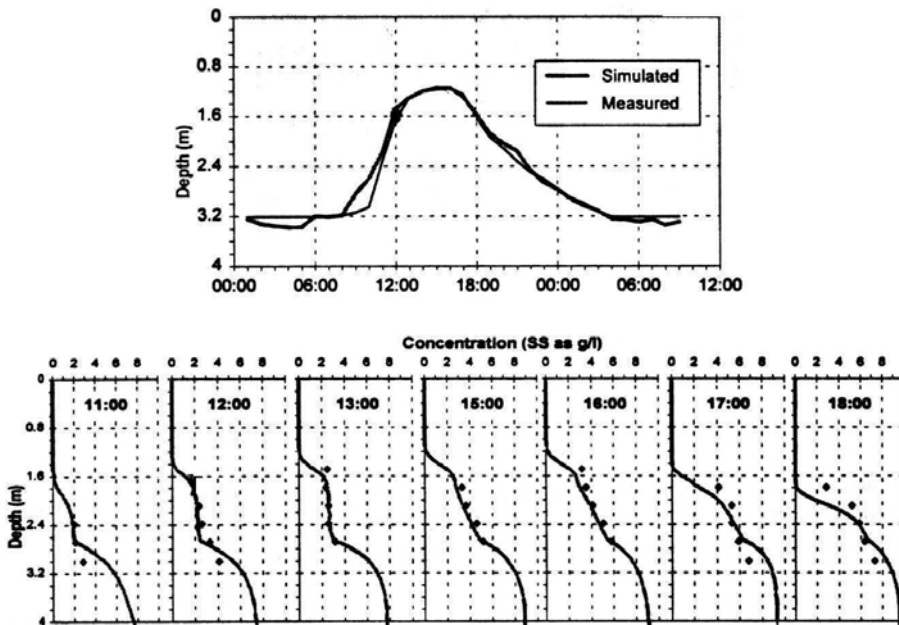


Figure 3.6: Model-calibrated and measured sludge blanket height (top) and concentration profiles (bottom) (Joannis *et al.*, 1999)

linear regression of concentration profiles and sludge blanket heights.

Full-scale controlled overload experiments were used for the calibration of the model. Joannis *et al.* (1999) were the only ones that used full-scale dynamic data for modelling. Concentration profiles and sludge blanket heights were predicted nicely except for the two last profiles where the simulated discontinuity at 6 g/l is not present in the measurements (Figure 3.6). This disagreement may be caused by a non-suitable numerical integration. To validate the model, the DSVI (diluted sludge volume index) was recalibrated if necessary. A 6-month validation gave good predictions of the sludge blanket height (Figure 3.7).

Lee *et al.* (1999) used the Takács settling velocity function and two dispersion coefficients, one for the clarification zone and one for the thickening zone (Table 3.1). The model equation was solved numerically using a finite difference scheme and 20 layers. The settling and dispersion parameters were determined from non-linear regression of concentration profiles.

The full-scale steady-state data of Pflanz (1969) were used for calibration and validation. The low-load data were used for calibration of the model parameters. The medium- and high-load data were used for validation of the model. The concentration profile was well predicted for the medium load, but for the high load the profile in the clarification zone was underpredicted (Figure 3.8).

The same remark as for the models with the settling flux limitation, holds here: the numerical integration of the model equation cannot be done with simple finite differences because of the non-linear PDE (Burger *et al.*, 2000; Diehl, 1995). Considering the kind of experiments used for modelling (full-scale or pilot-scale, dynamic or steady-

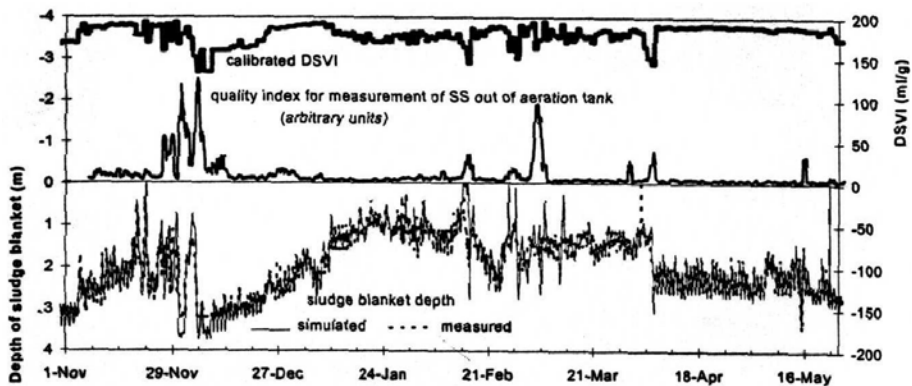


Figure 3.7: Simulated and measured sludge blanket height (bottom) and calibration results for DSVI (top) (Joannis *et al.*, 1999)

state) and whether the model was validated or not, the model of Joannis *et al.* (1999) performed best among the 3 models including dispersion.

3.5 Models that consider compression settling

Hartel and Popel (1992) used the Vesilind settling velocity function. This function was multiplied by a corrective function to account for transition and compression settling. This corrective function is a function of height and is zero at the bottom of the clarifier where there is no hindered nor compression settling and is one at the hindered settling zone. Hartel and Popel (1992) developed the corrective function as a function of height, sludge volume index, feed height and feed concentration. The clarification zone was modelled as one completely mixed volume and the settling velocity of the discrete flocs within this volume was the maximum hindered settling velocity, i.e. V_0 . The Vesilind parameters were determined from the sludge volume index by empirical relationships.

The model equations themselves were not described by Hartel and Popel (1992). Figure 3.9 shows the comparison of predicted and measured steady-state concentration profiles. The agreement was only good for the first graph.

Otterpohl and Freund (1992) modified the model of Hartel and Popel (1992) by making a distinction between the settling velocity for macroflocs and microflocs. The solids concentration was divided in a concentration of microflocs and one of macroflocs. For each type of flocs, a continuity equation was used. The settling velocity of the microflocs was set equal to 0.01 m/hr. For the macroflocs, the settling velocity of Hartel and Popel (1992) was used. The limiting flux constraint was applied in the thickening zone for both kind of flocs.

Again, the Vesilind parameters were related to the SVI.

The model results were compared with measured effluent concentrations (Figure 3.10) at full-scale treatment plants. However, the agreement was only good for the first 0.5 days.

The settling velocity function of Cacossa and Vaccari (1994) was already discussed in

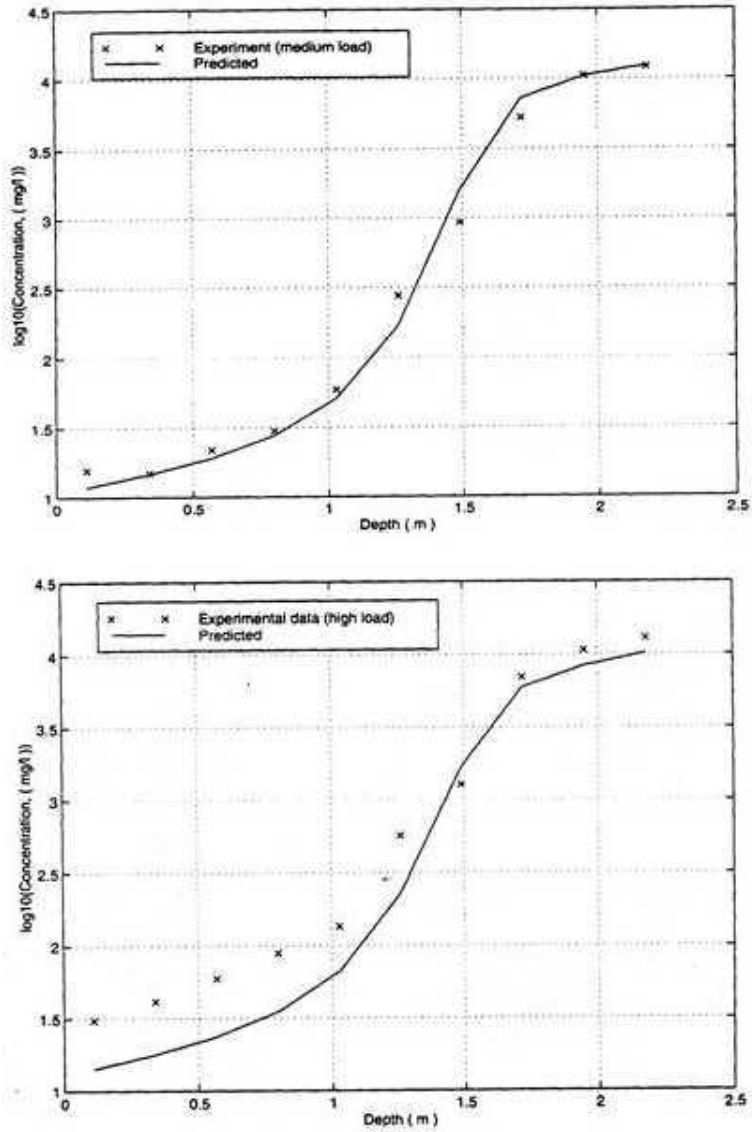


Figure 3.8: Predicted and measured concentration profiles for the Pflanz's medium load case (top) and the high load case (bottom) using the Lee *et al.* (1999) model

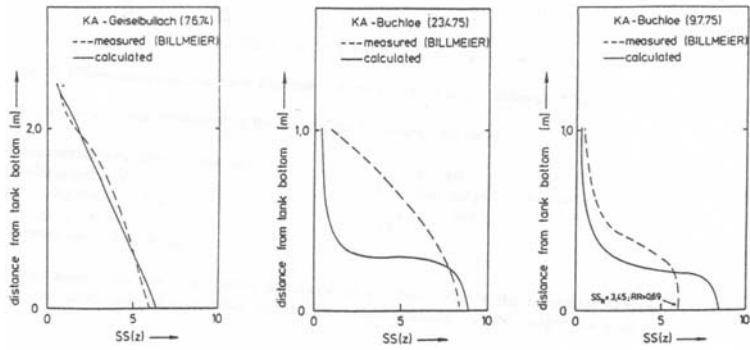


Figure 3.9: Predicted (full line) and measured (dotted line, Billmeier (1978)) concentration profiles using the Hartel and Popel (1992) model

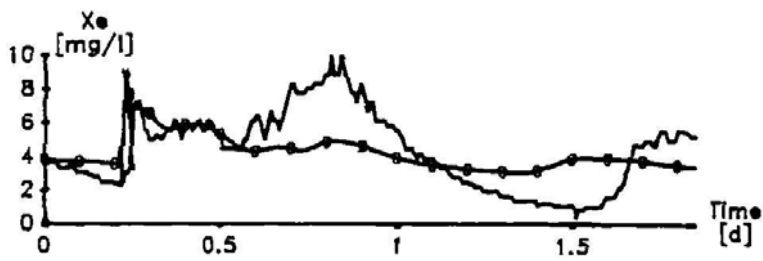


Figure 3.10: Simulated (●) and measured (line) effluent concentrations (Otterpohl and Freund, 1992)

section 2.2.1. The same holds for the model of Kinnear (2002).

Cacossa and Vaccari (1994) calibrated the settling parameters with batch settling data and used these parameters to simulate steady-state pilot-scale concentration profiles (Figure 3.11). The experimental data were not always well predicted, especially the ones of the upper two graphs of Figure 3.11. The predicted discontinuity is not seen in the measurements.

Steady-state pilot-scale concentration profiles were not predicted well by the model of Kinnear (2002), especially when a sludge blanket was formed. Some of the profiles are shown in Figure 3.12.

In summary, none of the models with compression gives good predictions of the behaviour in the clarifier.

3.6 Model with a by-pass from inlet to recycle (Dupont and Dahl, 1995)

The settling velocity function used by Dupont and Dahl (1995) covers the free settling zone and the hindered settling zone, i.e. it gives an increasing settling velocity for increasing concentrations at low solids concentrations and a decreasing settling velocity for increasing concentrations at high solids concentrations (Table 3.1).

The model considers density currents by changing the feed layer to the layer which has the same concentration as the feed. Short-circuiting is also taken into account by introducing a short-circuiting factor. This factor is simply the necessary dilution factor for the simulated concentration to obtain the measured recycle concentration.

The settling parameters were determined from free settling experiments and batch settling experiments.

The model predicted steady-state full-scale concentration profiles nicely, with the short-circuiting factor being calculated from mass balances over the clarifier (Figure 3.13). However, work is still required to establish a good relationship between the short-circuiting factor and other parameters, since this factor is now being calculated from mass balances. Hence, the model cannot be used for predicting clarifier behaviour.

3.7 Conclusion

The models of Lee *et al.* (1999); Otterpohl and Freund (1992); Cacossa and Vaccari (1994); Kinnear (2002) do not give satisfying results. Some models (Takacs *et al.*, 1991; Hamilton *et al.*, 1992; Watts *et al.*, 1996; Joannis *et al.*, 1999; Dupont and Dahl, 1995) give good predictions in their original application (i.e. as described in the original reference). But if the discretisation of the model of Takacs *et al.* (1991) becomes finer or other experimental data are used with the model of Hamilton *et al.* (1992), then the models perform significantly worse (Watts *et al.*, 1996; Joannis *et al.*, 1999). Another issue is the validation of these well performing models: not all models have been validated (Watts *et al.*, 1996; Dupont and Dahl, 1995).

The following aspects have been discussed: (i) settling velocity function, (ii) numerical integration and (iii) the kind of experiments used for calibration and validation of the model.

All 1D-models aimed at describing hindered settling and some of them tried to capture settling at lower concentrations and compression settling. In order to achieve this,

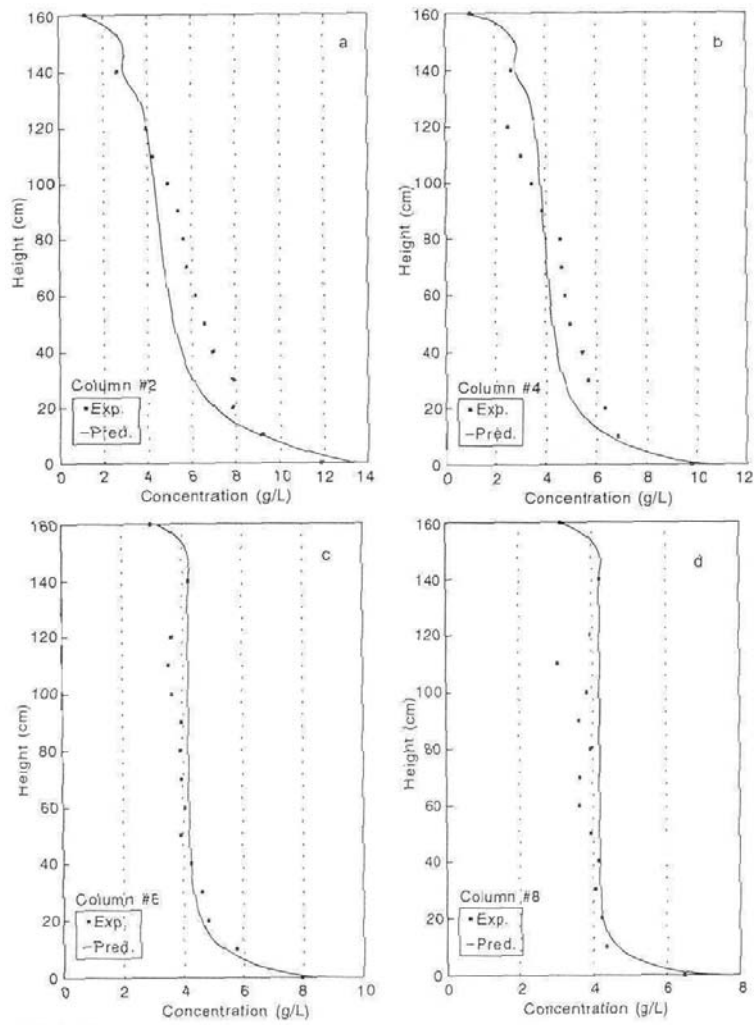


Figure 3.11: Simulated and measured concentration profiles using batch calibration (Cacossa and Vaccari, 1994)

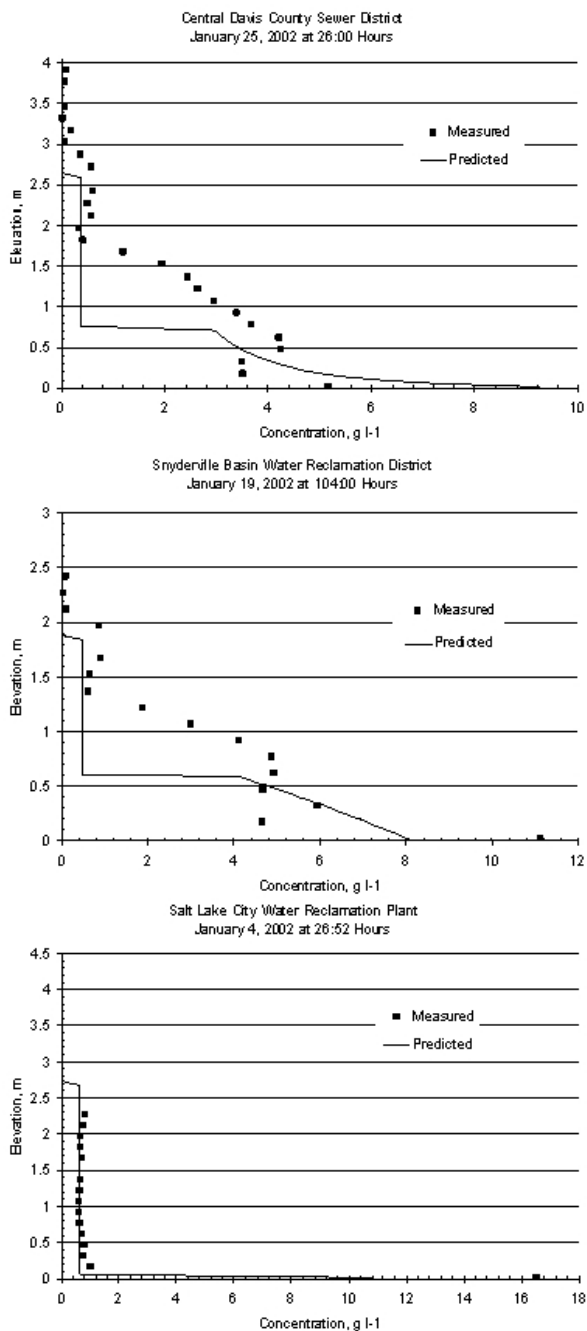


Figure 3.12: Predicted and measured concentration profiles (Kinnear, 2002)

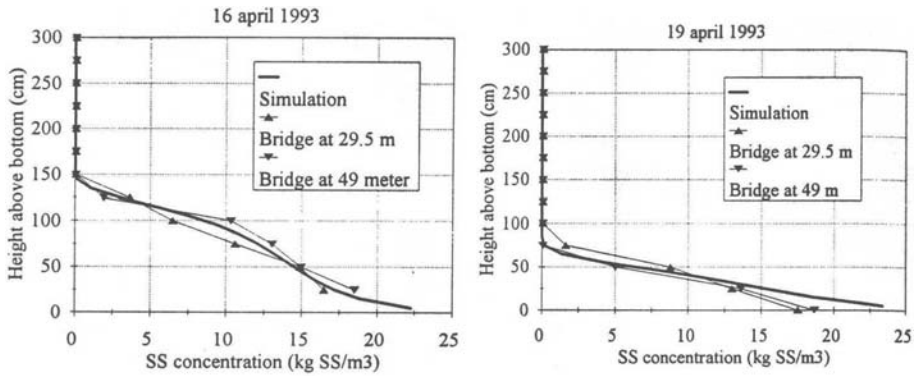


Figure 3.13: Measured and simulated concentration profiles for the model of Dupont and Dahl (1995)

most models used empirical **settling velocity functions**, except for Kinneer (2002), as was stated in Chapter 2. This Chapter clearly demonstrated that there are more fundamental approaches to model hindered and compression settling.

The model equation 3.1 is a non-linear PDE, which implies that the **numerical integration** of the model equation cannot be pursued by simple differences (Burger *et al.*, 2000; Diehl, 1995). However, none of the modellers recognized this, except for the ones that used a limiting settling flux (Vitasovic, 1989; Takacs *et al.*, 1991; Otterpohl and Freund, 1992). The latter is empirical and not the correct way to deal with this non-linearity, as will be shown in Chapter 4.

As stated in the introduction of this Chapter, calibration and validation of the model is preferably done with **full-scale dynamic data**. Not many modellers used such data, except for Joannis *et al.* (1999). Others used full-scale steady-state or pilot-scale/lab-scale data. This deficiency of model calibration/validation with full-scale dynamic data (Dupont and Dahl, 1995; Lee *et al.*, 1999; Olsson and Newell, 1999) makes that there is currently no dynamic 1D-model available that accurately predicts the full-scale dynamic solids concentration profiles. Joannis *et al.* (1999) used such data for calibration but not for validation and the results of the calibration showed some flaws. Other researchers (Deininger *et al.*, 1996, 1998; Samstag *et al.*, 1992; Lyn *et al.*, 1992; De Clercq, 2003) measured full-scale concentration profiles, but only under steady-state conditions. In order to guarantee practically usable results, clarifier models require extensive testing with high-quality field data.

To conclude, none of the currently available models combines a fundamental description of the hindered and compression settling, a suitable numerical algorithm and a calibration and validation with full-scale dynamic data.

Chapter 4

Numerical integration and estimation of model parameters

4.1 Numerical integration of the model equations

4.1.1 Properties of the mathematical models

As stated in Chapter 2, the **model for batch settling** is an initial-boundary value problem of a partial differential equation of second order parabolic type for the solids concentration as a function of depth and time. The model in terms of solids concentration and whereby $z=0$ corresponds to the top, is given by

$$\frac{\partial C}{\partial t} = -\frac{\partial f_{bk}(C)}{\partial z} + \frac{\partial}{\partial z} \left(f_{bk}(C) \frac{\rho_s}{\Delta \rho g C} \frac{d\sigma_e(C)}{dC} \frac{\partial C}{\partial z} \right) \quad (4.1)$$

with boundary conditions and initial condition

$$f_{bk}(C) \left(1 - \frac{\rho_s}{\Delta \rho g C} \frac{d\sigma_e(C)}{dC} \frac{\partial C}{\partial z} \right) = 0 \quad \text{for } z = 0, z = H \text{ and } t > 0 \quad (4.2)$$

$$C(z, 0) = C_o \quad \text{for all } z \quad (4.3)$$

The equation simplifies into a first order hyperbolic type if the solids concentration is less than the compression solids concentration as the second term of the right hand side of equation 4.1 vanishes. The first order spatial term (i.e. the Kynch batch density function) and the boundary conditions of the model are non-linear. It is well known that non-linear hyperbolic equations give rise to discontinuities (Press *et al.*, 1992). An example of such a discontinuity during settling is the suspension-liquid interface. The 1D **model for continuous settling** of Chapter 3 is also an initial-boundary value problem of a partial differential equation of second order parabolic type for the solids concentration as a function of depth and time. The model in terms of solids concentration and whereby $z=0$ corresponds to the top, is given by

$$\frac{\partial C}{\partial t} = -\frac{\partial \left(\frac{Q_i}{A} + f_{bk}(C) \right)}{\partial z} + \frac{\partial}{\partial z} \left(\left(D + f_{bk}(C) \frac{\rho_s}{\Delta \rho g C} \frac{d\sigma_e(C)}{dC} \right) \frac{\partial C}{\partial z} \right) + s \quad (4.4)$$

with

$$Q_i(t) = \begin{cases} -Q_e(t) & 0 \leq z < z_f \\ Q_u(t) & z_f < z \leq H_{centre} \end{cases} \quad (4.5)$$

with boundary conditions and initial condition

$$f_{bk}(C) - \left(D + f_{bk}(C) \frac{\rho_s}{\Delta\rho g C} \frac{d\sigma_e(C)}{dC} \right) \frac{\partial C}{\partial z}_{z=0} = 0 \quad (4.6)$$

$$f_{bk}(C) - \left(D + f_{bk}(C) \frac{\rho_s}{\Delta\rho g C} \frac{d\sigma_e(C)}{dC} \right) \frac{\partial C}{\partial z}_{z=H} = 0 \quad (4.7)$$

$$C(z, 0) = C_o(z) \quad (4.8)$$

The model equation stays parabolic as long as dispersion is occurring and it contains the same non-linearities as the model for batch settling. A special feature of this model is that it has a point source and a discontinuous flux function.

Due to

the mixed hyperbolic-parabolic nature of the batch settling model,

the discontinuous fluxes of the continuous model,

the non-linearity of the Kynch batch density function in both models,

the solutions are discontinuous and difficulties arise if one tries to construct these solutions by classical numerical methods (Burger *et al.*, 2000). Diehl (1996) also addressed this but only for continuous settling without compression settling and dispersion. The problem becomes even more complicated when the cross-sectional area is varying (Burger *et al.*, 2004), as in full-scale circular clarifiers.

Before discretizing the model equations of batch settling and continuous settling, they are grouped into one general equation and reformulated in the conservative form, on which the numerical discretisation algorithm is based:

$$\frac{\partial(A(z)C(z,t))}{\partial t} = - \frac{\partial(Q_i(t)C(z,t) + A(z)f_{bk}(C(z,t),t))}{\partial z} + \frac{\partial}{\partial z} \left(A(z) \left(D(z,t) + sig(C(z,t),t) \right) \frac{\partial C(z,t)}{\partial z} \right) + A(z)s(z,t) \quad (4.9)$$

with

$$sig(C(z,t),t) = f_{bk}(C(z,t),t) \frac{\rho_s(t)}{\Delta\rho(t)gC(z,t)} \frac{\partial\sigma_e(C(z,t),t)}{\partial C(z,t)} \quad (4.10)$$

The boundary conditions are given by

$$f_{bk}(C(0,t),t) - (D(0,t) + sig(C(0,t),t)) \frac{\partial C(z,t)}{\partial z}_{z=0} = 0 \quad (4.11)$$

$$f_{bk}(C(H_{centre},t),t) - \left(D(H_{centre},t) + sig(C(H_{centre},t),t) \right) \frac{\partial C(z,t)}{\partial z}_{z=H_{centre}} = 0 \quad (4.12)$$

and initial condition by

$$C(z,0) = C_o \text{ for all } z \quad (4.13)$$

Those equations hold for both continuous and batch settling. For batch sedimentation, the convective and dispersion fluxes and the source term are zero.

4.1.2 Numerical integration algorithm

Conservative methods are needed for integrating the model equations (4.9-4.13). It is common knowledge that a conservative method will compute discontinuities with the correct jump conditions, whereas a non-conservative scheme will compute discontinuities with the incorrect strength and the incorrect position.

Upwind differencing is such a conservative discretisation and is used for the first order terms: it stabilizes profiles which are liable to undergo sudden changes, such as discontinuities and other large gradient profiles (Press *et al.*, 1992). Since the Kynch batch density function is a non-monotone function, the generalised **upwind flux of Engquist and Osher (1981)** is used for this term (Evje and Karlsen, 2000; Burger and Karlsen, 2001; Burger *et al.*, 2004). Conservative discretisation of the second order term is done with **central differencing**.

The discretisation of the spatial derivatives, with a mesh size $\Delta z > 0$ ($no\Delta z = H_{centre}$ with no : number of layers), results in the following expressions for the first order convective terms (equations 4.14 and 4.15), the first order settling term (equation 4.16), the second order dispersion term (equation 4.17) and the second order settling term (equation 4.18), respectively:

$$\frac{\partial(-Q_e(t)C(z,t))}{\partial z} = \frac{Q_e(t)C(z+\Delta z,t) - Q_e(t)C(z,t)}{\Delta z} \quad (4.14)$$

$$\frac{\partial(Q_u(t)C(z,t))}{\partial z} = \frac{Q_u(t)C(z-\Delta z,t) - Q_u(t)C(z,t)}{\Delta z} \quad (4.15)$$

$$\begin{aligned} \frac{\partial(A(z)f_{bk}(C(z,t),t))}{\partial z} = & \\ & \frac{1}{\Delta z} \left(A(z - \frac{1}{2}\Delta z)f_{bk}^{EO}(C(z-\Delta z,t), C(z,t), t) \right. \\ & \left. - A(z + \frac{1}{2}\Delta z)f_{bk}^{EO}(C(z,t), C(z+\Delta z,t), t) \right) \quad (4.16) \end{aligned}$$

$$\begin{aligned} \frac{\partial}{\partial z} \left(A(z)D(z,t) \frac{\partial C(z,t)}{\partial z} \right) = & \\ & \frac{1}{(\Delta z)^2} \left(A(z - \frac{1}{2}\Delta z)D(z - \frac{1}{2}\Delta z,t)(C(z-\Delta z,t) - C(z,t)) \right. \\ & \left. + A(z + \frac{1}{2}\Delta z)D(z + \frac{1}{2}\Delta z,t)(C(z+\Delta z,t) - C(z,t)) \right) \quad (4.17) \end{aligned}$$

$$\begin{aligned} \frac{\partial}{\partial z} \left(A(z) \text{sig}(C(z, t), t) \frac{\partial C(z, t)}{\partial z} \right) = \\ \frac{1}{(\Delta z)^2} \left(A(z - \frac{1}{2} \Delta z) \left(\int_0^{C(z-\Delta z, t)} \text{sig}(u) du - \int_0^{C(z, t)} \text{sig}(u) du \right) \right. \\ \left. + A(z + \frac{1}{2} \Delta z) \left(\int_0^{C(z+\Delta z, t)} \text{sig}(u) du - \int_0^{C(z, t)} \text{sig}(u) du \right) \right) \quad (4.18) \end{aligned}$$

with

$$f_{bk}^{EO}(C(z, t), C(z + \Delta z, t), t) = f_{bk}^+(C(z, t), t) + f_{bk}^-(C(z + \Delta z, t), t) \quad (4.19)$$

$$f_{bk}^+(C(z, t), t) = f_{bk}^+(0) + \int_0^{C(z, t)} \max(f'_{bk}(s), 0) ds \quad (4.20)$$

$$f_{bk}^-(C(z + \Delta z, t), t) = \int_0^{C(z+\Delta z, t)} \min(f'_{bk}(s), 0) ds \quad (4.21)$$

The number of layers is a parameter of the numerical integration. From the author's experience, **200** layers are suitable to trade-off convergence and calculation time. To ensure convergence of the resulting scheme to the physically relevant solution of the model, the following stability condition must be satisfied (Burger *et al.*, 2004):

$$\begin{aligned} \frac{1}{\min_z(A(z))} \left(\left(\max_t |Q_{u/e}(t)| + \max_z(A(z)) \max_C |f'_{bk}(C, t)| \right) \frac{\Delta t}{\Delta z} \right. \\ \left. + 2 \left(\max_C \left| f_{bk} \frac{\rho_s}{\Delta \rho g C} \frac{\partial \sigma_e(C, t)}{\partial C} \right| + \max_{z,t}(D(z, t)) \right) \frac{\Delta t}{(\Delta z)^2} \right) \leq 1 \quad (4.22) \end{aligned}$$

The spatial discretisation of the model equations gives the following system of first order ODE's:

top layer ($i=1$):

$$\begin{aligned} \frac{\partial C_1(t)}{\partial t} = \\ \frac{1}{A_1 \Delta z} \left(Q_e(t) C_2(t) - Q_e(t) C_1(t) - A_{1+\frac{1}{2}} f_{bk}^{EO}(C_1(t), C_2(t), t) \right) \\ + \frac{A_{1+\frac{1}{2}}}{A_1 \Delta z^2} \left(D_{1+\frac{1}{2}}(t) (C_2(t) - C_1(t)) + \text{compr}_2(t) - \text{compr}_1(t) \right) \quad (4.23) \end{aligned}$$

i -th layer in the overflow zone ($1 < i < m$):

$$\begin{aligned} \frac{\partial C_i(t)}{\partial t} = \frac{1}{A_i \Delta z} \left(Q_e(t) C_{i+1}(t) - Q_e(t) C_i(t) \right. \\ \left. + A_{i-\frac{1}{2}} f_{bk}^{EO}(C_{i-1}(t), C_i(t), t) - A_{i+\frac{1}{2}} f_{bk}^{EO}(C_i(t), C_{i+1}(t), t) \right) \\ + \frac{1}{A_i \Delta z^2} \left(A_{i-\frac{1}{2}} \left(D_{i-\frac{1}{2}}(t) \left(C_{i-1}(t) - C_i(t) \right) + \text{compr}_{i-1}(t) - \text{compr}_i(t) \right) \right. \\ \left. - A_{i+\frac{1}{2}} \left(D_{i+\frac{1}{2}}(t) \left(C_{i+1}(t) - C_i(t) \right) + \text{compr}_{i+1}(t) - \text{compr}_i(t) \right) \right) \quad (4.24) \end{aligned}$$

feed layer ($i = m$):

$$\begin{aligned} \frac{\partial C_m(t)}{\partial t} = & \frac{1}{A_m \Delta z} \left(-Q_u(t)C_m(t) - Q_\epsilon(t)C_m(t) + Q_f(t)C_f(t) \right. \\ & \left. + A_{m-\frac{1}{2}} f_{bk}^{EO}(C_{m-1}(t), C_m(t), t) - A_{m+\frac{1}{2}} f_{bk}^{EO}(C_m(t), C_{m+1}(t), t) \right) \\ + & \frac{1}{A_m \Delta z^2} \left(A_{m-\frac{1}{2}} \left(D_{m-\frac{1}{2}}(t)(C_{m-1}(t) - C_m(t)) + compr_{m-1}(t) - compr_m(t) \right) \right. \\ & \left. - A_{m+\frac{1}{2}} \left(D_{m+\frac{1}{2}}(t)(C_{m+1}(t) - C_m(t)) + compr_{m+1}(t) - compr_m(t) \right) \right) \end{aligned} \quad (4.25)$$

i -th layer in the underflow zone ($m < i < no$):

$$\begin{aligned} \frac{\partial C_i(t)}{\partial t} = & \frac{1}{A_i \Delta z} \left(Q_u(t)C_{i-1}(t) - Q_u(t)C_i(t) \right. \\ & \left. + A_{i-\frac{1}{2}} f_{bk}^{EO}(C_{i-1}(t), C_i(t), t) - A_{i+\frac{1}{2}} f_{bk}^{EO}(C_i(t), C_{i+1}(t), t) \right) \\ + & \frac{1}{A_i \Delta z^2} \left(A_{i-\frac{1}{2}} \left(D_{i-\frac{1}{2}}(t)(C_{i-1}(t) - C_i(t)) + compr_{i-1}(t) - compr_i(t) \right) \right. \\ & \left. - A_{i+\frac{1}{2}} \left(D_{i+\frac{1}{2}}(t)(C_{i+1}(t) - C_i(t)) + compr_{i+1}(t) - compr_i(t) \right) \right) \end{aligned} \quad (4.26)$$

bottom layer ($i=no$):

$$\begin{aligned} \frac{\partial C_{no}(t)}{\partial t} = & \frac{1}{A_n \Delta z} \left(Q_u(t)C_{no-1}(t) - Q_u(t)C_{no}(t) + A_{no-\frac{1}{2}} f_{bk}^{EO}(C_{no-1}(t), C_{no}(t), t) \right) \\ + & \frac{A_{no-\frac{1}{2}}}{A_{no} \Delta z^2} \left(D_{no-\frac{1}{2}}(t)(C_{no-1}(t) - C_{no}(t)) + compr_{no-1}(t) - compr_{no}(t) \right) \end{aligned} \quad (4.27)$$

with

$$C_i(t) = C(i\Delta z - \frac{\Delta z}{2}, t)$$

$$A_i = A(i\Delta z - \frac{\Delta z}{2})$$

$$D_{i+\frac{1}{2}}(t) = D(i\Delta z, t)$$

$$compr_i(t) = \int_0^{C_i(t)} sig(u) du$$

With the functions obtained in Chapters 6 and 8, the integral $compr_i(t)$ is numerically calculated. The temporal concentration gradient is subsequently integrated and the time-step Δt is usually determined by setting equation 4.22 equal to 0.98.

4.2 Estimation of the model parameters

Parameter estimation is a technique that allows to determine the optimum values of the model parameters present in a mathematical description in order to minimize the discrepancy between model predictions and experimental data. It is assumed that the structure of the model, i.e. the relationships between the variables and the parameters, is explicitly known. The objective function for parameter estimation, J , which has to be minimized, is often taken to be the sum of squared errors function:

$$J(\theta) = \sum_{i=1}^N \left(y_i - \widehat{y}_i(\theta) \right)^2 \quad (4.28)$$

with y_i the observations, N the number of observations, \widehat{y}_i the model predictions and θ the parameter set. The observations y can either be measured solids concentrations or measured sludge blanket heights. The parameters can be the parameters of the Kynch batch density function, the effective solids stress function and/or the dispersion coefficient. The estimation process is non-linear in the current case because the parameters are non-linear in the model. For such non-linear parameters, the best estimates are found with numerical optimization algorithms that search the parameter space in a systematic way. Typical for non-linear objective functions is that the minimum can either be global or local. The optimization algorithm can eventually end up in a local minimum instead of the global minimum, i.e. the fit is best within a limited range around this set of parameter values found, but there is a significantly better fit obtainable with another set of parameter values. No perfect optimization algorithm for non-linear objective functions exists (so far) and consequently, finding the global minimum for non-linear problems cannot be guaranteed. A property of non-linear function estimation is that the minimum found by the algorithm can be influenced by the choice of the starting values for the parameters θ . Press *et al.* (1992) presented the Levenberg-Marquardt (Marquardt, 1963) algorithm as the algorithm that works very well in practice and has become the standard of the non-linear least-squares algorithms. It can be thought of as a combination of the steepest descent and the Gauss-Newton method. When the current solution is far from the correct one, the algorithm behaves like a steepest descent method: slow, but guaranteed to converge. When the current solution is close to the correct solution, it becomes a Gauss-Newton method. The algorithm almost always converges and does not slow down its search as the steepest descent method often does. This algorithm is used for the estimation of the model parameters in this work. The algorithm also provides a statistical analysis of the parameter estimation results if the number of observations does not exceed 1000. The overall procedure for non-linear parameter estimation is as follows. Initially, the model structure and the experimental data need to be specified, together with first estimates of the parameters. The minimisation algorithm will then request for model predictions corresponding to the first parameter set. These model predictions are obtained by solving the set of model equations with this parameter set and are passed to the routine where the objective function is calculated by confronting the predictions with the data. On the basis of rules which are different for each optimization algorithm, either a new proposal for parameters is made and sent to the model solver or, if certain criteria are met, the parameter values are passed on to the user as best estimates. Stopping criteria may be that the maximum number of iterations is reached or that no improvement in objective function is found in recent iterations.

4.3 Implementation software

A computer program was written in FORTRAN, which contains the numerical integration and optimization algorithm. The program consists of 3 major parts: input, main program and output, as presented schematically in Figure 4.1.

The **input** consists generally of the initial condition(s), (the time-evolution of) the settling parameters, the geometry of the clarifier and the number of layers. In case of continuous settling, additionally, the time-evolution of the feed solids concentration, feed and recycle flow rate and the dispersion parameters need to be stated. In case of optimization, the parameters of the optimization algorithm, the observations and the initial parameter values are required.

For the **main program**, the cross sectional area at every height is first calculated. In case of **simulation**, the time-step Δt is first calculated according to equation 4.22. Next, for each time-step, the Engquist-Osher Kynch batch density function f_{bk}^{EO} for each concentration $C_i(t)$ is calculated according to equation 4.19. Knowing these values, the concentration profile at time $t + \Delta t$ is calculated with the system of ODE's given by equations 4.23-4.27. From the calculated concentration profile, the sludge blanket height is calculated at time $t + \Delta t$.

In case of **optimization**, the optimization algorithm is called. For every parameter set, given by the optimization algorithm, model predictions, i.e. simulations, are required to calculate the objective function. When the objective function does not change with respect to its value in the former iteration or when the maximum number of iterations is reached, the algorithm returns the best parameter values and a statistical analysis to the main program.

The statistical analysis consists of

- the tabulated t-value for the test concerning the significance of the individual parameters, the tabulated F-value for the test concerning the significance of the regression
- information about the parameter estimates: optimum value, standard deviation, lower and upper limit of the individual confidence interval at the 95 % probability interval and calculated t-value
- analysis of variance table: total sum of squares, regression sum of squares, residual sum of squares, each with their degrees of freedom and the calculated F-value
- estimate of the standard deviation
- square of multiple correlation coefficient
- variance-covariance matrix of the parameter estimates
- correlation coefficients between parameter estimates
- enveloping beam of confidence interval
- intercept axes with probability region
- linearity coefficient

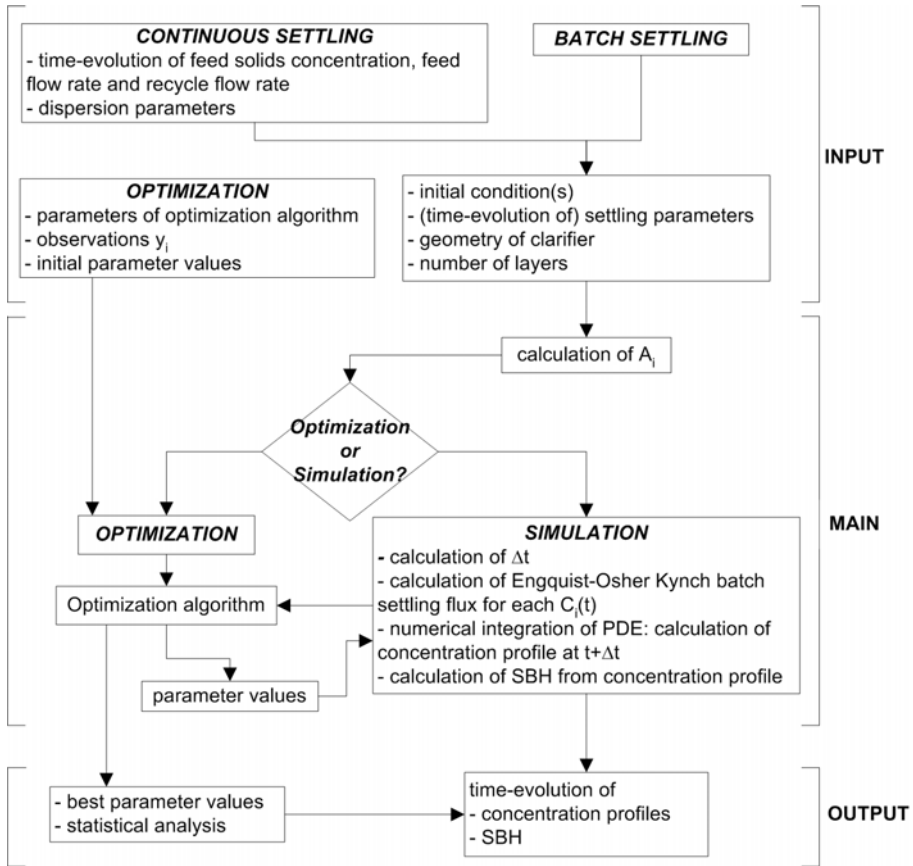


Figure 4.1: Flow-chart of the computer code

The **output** consists of the time-evolution of the concentration profiles and the sludge blanket heights and in case of optimization, the best parameter values and a statistical analysis.

Chapter 5

Non-invasive monitoring of activated sludge during batch settling

5.1 Introduction

As shown in Chapter 2, there is a need for measured continuous solids concentration and pressure profiles during batch settling to develop a good settling model. This Chapter investigates (1) a novel measurement technique to obtain solids concentration profiles during the batch settling of activated sludge ¹ and (2) the possibility to measure pressure profiles with sufficient accuracy during the batch settling of activated sludge.

5.1.1 Measurement of solids concentration profiles

A measurement technique for dynamic solids concentration profiles for activated sludge batch settling should fulfill the following requirements:

- the settling process may not be disturbed
- the settling characteristics of the sludge may not be altered
- solids concentrations in the range 0-25 g/l need to be measured
- on-line analysis at high spatial and temporal resolution

Non-invasive techniques, such as gamma-ray (Bergstrom, 1992; Scott, 1968; Dreher, 1997) and X-ray (Shih *et al.*, 1986; Been, 1980; Been and Sills, 1981; Wells, 1990; Tiller *et al.*, 1991) have been applied for the measurement of solids concentration profiles during batch settling of suspensions other than activated sludge. However, those suspensions all have a higher solids concentration and solids density than activated sludge. Moreover, the reported accuracy of the measurement, i.e. 0.25 and 0.5 vol% (Been and Sills, 1981; Bergstrom, 1992) is too low for activated sludge that has a

¹This part of the Chapter is published as Jeriffa De Clercq, Filip Jacobs, David J. Kinnear, Ingmar Nopens, Rudi A. Dierckx, Jacques Defrancq, Peter A. Vanrolleghem (2005). Detailed spatio-temporal solids concentration profiling during batch settling of activated sludge using a radiotracer. *Water Research*, 39(10), 2125-2135

solids concentration of only 0.1-0.4 vol% (i.e. for a solids concentration between 3 and 6 g/l and a solids density around 1700-1900 kg/m³, as found in the present case). Hence, the techniques are unsuitable for studying activated sludge settling.

Chu *et al.* (2003) used CATScan measurements for the monitoring of activated sludge settling, but the measurement accuracy obtained was only 0.1 vol%, which is again too low for activated sludge.

In wastewater treatment processes, optical devices, ultrasound and dielectric spectrometry are commonly used for the measurement of the solids concentration (Vanrolleghem and Lee, 2003). However, such sensors cannot be used for monitoring the solids concentration profile during batch settling since they are commonly positioned inside the clarifier (Olsson and Nielsen, 1997), disturbing the settling process.

To overcome this problem, a characteristic of a substance which adsorbs to the solids can be measured. Solids tracers have already been used before to determine sludge residence time distributions:

- Lumley and Balmer (1990) used MnCl₂ (Lumley and Horkeby, 1989) in a secondary clarifier (off-line analysis)
- Bailey and Harkness (1978) used radioactive Au-198 in a primary clarifier (on-line analysis)
- Audic *et al.* (1993) used the same tracer, i.e. radioactive Au-198, but in a secondary clarifier (on-line analysis)
- Grijspeerdt and Verstraete (1995) used pyrene in a lab-scale secondary clarifier (off-line analysis)
- IAEA (2001) used radioactive La-140 in an aeration tank (on-line analysis)

The radioactive tracers (Au-198 and La-140) have the advantage over Mn and pyrene that they can be measured on-line. Besides radioactive Au-198 and La-140, other radiotracers such as Br-82, I-131 and Tc-99m have been used as a liquid tracer to investigate wastewater treatment processes (Borroto *et al.*, 2003; Farooq *et al.*, 2003; Chmielewski *et al.*, 1998; IAEA, 2001). Among those 5 radiotracers, Tc-99m is the only one that can be produced in a generator. Such a generator for the Tc-99m consists of Mo-99 (67 hr half-life) that decays by β^- -emission to Tc-99m (6 hr half-life). The Tc-99m can be extracted by flushing physiological saline through the generator. This radionuclide is the most commonly used radioisotope in nuclear medicine (Vucina and Lukic, 2002), because of (1) its optimal half-life (long enough to perform a study and short enough to limit the radioactive dose received by patients), (2) the monochromatic gamma-ray energy it emits, and (3) its broad range of oxidation states (from +1 to +7 in radiopharmaceuticals). Those radiopharmaceuticals can be anionic, neutral or cationic. A cationic Tc-99m complex could be used to trace the solids of activated sludge since these are negatively charged.

One such positively charged complex is Tc-99m Sestamibi (Methoxy IsoButyl Isonitritil), which could be produced and detected at the Department of Nuclear Medicine of the Ghent University Hospital, since a Mo-99/Tc-99m generator and different gamma cameras are available. Its structure is shown in Figure 5.1. Tc-99m Sestamibi behaves in a similar way as potassium in viable myocardial tissue (Geatti, 1999). Hence, it is not unlikely that activated sludge possesses a strong binding affinity for Tc-99m

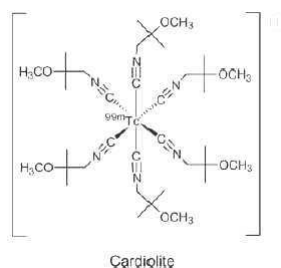


Figure 5.1: Structure of Tc-99m Sestamibi

Sestamibi just like it has for binding potassium (Wang *et al.*, 2000). However, the latter might also be disadvantageous as it may alter the settling properties of activated sludge (Muller *et al.*, 2002; Novak *et al.*, 1998; Murthy and Novak, 1998).

Therefore, it will first be investigated whether Tc-99m Sestamibi adsorbs onto the solids of activated sludge without altering the settling properties. The influence of the radiotracer on the settling properties is determined by comparing the batch settling curve with and without radiotracer, in a way similar to Grijpsperdt and Verstraete (1995). Secondly, it will be investigated whether the on-line analysis of the Tc-99m Sestamibi can be converted into solids concentration profiles. Finally, pilot-scale batch settling experiments are performed and discussed.

5.1.2 Measurement of excess pore pressure profiles

As mentioned in section 2.3.1, a very accurate measuring device for **excess pore pressure profile measurements** is needed for activated sludge batch settling. This is partly due to the big difference in range between the excess pore pressure and the hydrostatic pressure. In this Chapter, the possibility to measure the differential pressure, i.e. the pressure difference between a settling column and a water-filled column, with sufficient accuracy is investigated.

5.2 Material and methods

5.2.1 Experimental set-up

2 set-ups will be used in this Chapter: a first one for the measurement of the excess pore pressure profiles and a second one (located at the Ghent University Hospital) for the measurement of the solids concentration profiles. The first one will be referred to as the **P-set-up**, the second one as the **C-set-up**. Before describing the set-ups, the specifications of the identical settling columns are given.

Specifications of the settling columns

An important requirement for a settling column is that it is large enough to avoid wall effects (Vesilind, 1968). Different rules concerning a minimum diameter have been proposed in literature to avoid these effects:

- according to Matsui *et al.* (1978), no wall effects occur when the settling is performed in a cylinder of 170 mm internal diameter and 600 mm in height (activated sludge)
- Behn (1957) found in literature minimum diameters of 40 mm and 63 mm and used 152 mm in his experiments (digested sludge of a wastewater treatment plant)
- Chen *et al.* (1996) reported negligible wall effects when the ratio of the settling column diameter and the floc mean diameter is in the range of 200-1000 (wasted activated sludge)

The batch settling columns used here are made of polymethyl methacrylate (Stokvis Plastics bv, Ghent, Belgium) and have an inner diameter of 386 mm. Two such columns (one for the P-set-up and one for the C-set-up) have a height of 1.6 m, the third one (for the C-set-up) has a height of 1.2 m. The reason for having 2 columns of different height for the C-set-up is explained below.

P-set-up

The P-set-up consists of a settling column, a water-filled column (height of 1.6 m and inner diameter of 100 mm) and a differential pressure transducer (Druck LPX9481, Dimed electronic engineering, Ghent) with a range of 200 Pa and an accuracy of 0.2 Pa (the transducer is calibrated by the manufacturer). Fifteen holes were drilled in the settling column at specified heights (every 50 mm in the lower 0.5m and every 100 mm in the upper 0.5m) and in those ports a cigarette filter was inserted, to ensure that only the pressure of the water in the sludge is transmitted, i.e. the pore pressure. Tubes with valves connect the ports in the columns with a distributor. The latter is connected to the high pressure port of the transducer. Each of the fifteen ports in the column is connected in turn with the transducer. It takes about 15 minutes to measure a profile. The low pressure port of the transducer is connected to the water-filled column. In Figure 5.2, a schematic diagram of the P-set-up is shown. The differential pressure indicated by the transducer is a measure for the excess pore pressure.

C-set-up

Since the largest gamma camera available has a field of view of 508 mm by 381 mm, only 500 mm height of one settling column can be scanned per experiment. To simultaneously scan the complete height (1 m) with the same sludge, 2 experiments were always performed in parallel, using 2 gamma cameras and 2 settling columns: one gamma camera for detection of the lower 0.5 m of one column (Marconi Prism 1500 XP, single-headed gamma camera, Philips Medical Systems, Netherlands) and the other one for the upper 0.5 m of the other column (Marconi AXIS, two-headed gamma camera, Philips Medical Systems, Netherlands). The lowest 20 mm of the column could not be scanned because of the presence of a metallic aerator (needed for initial mixing of the sludge) which interfered with the gamma radiation. An overlap of 50 mm between the 2 columns was provided to evaluate the coherence of the 2 parallel settling tests. A third settling column in the lab was used to verify the influence of the tracer on the settling properties. Thus, the set-up consists of 3 settling columns and 2 gamma cameras. The experimental set-up at the Ghent University Hospital is

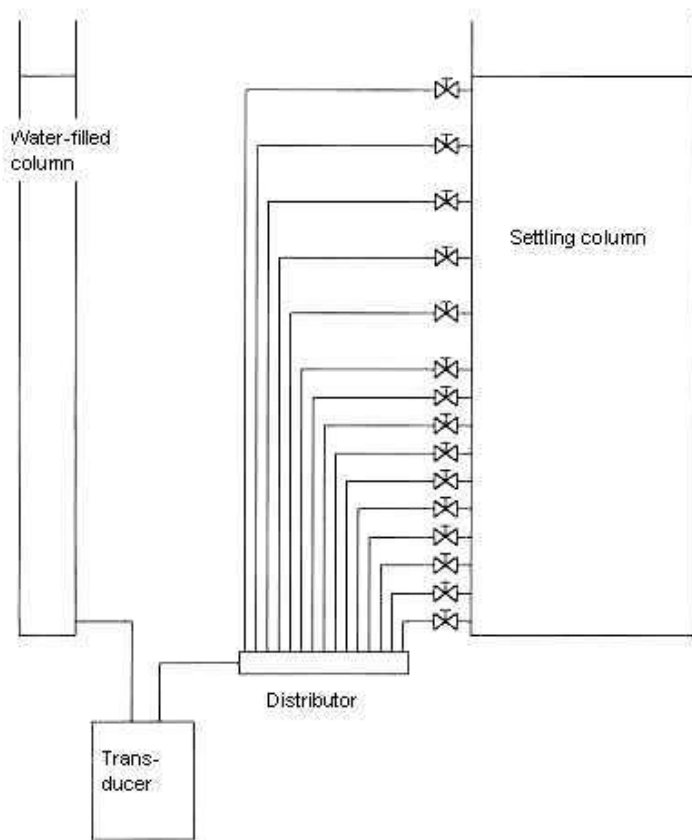


Figure 5.2: A schematic diagram of the P-set-up to measure differential pore pressure profiles



Figure 5.3: Experimental C-set-up at the Ghent University Hospital (left: lower section, 1500XP camera; right: upper section, AXIS camera)

shown in Figure 5.3. The column for detection of the lower 0.5 m (Figure 5.3, left) was shorter than the other columns because the set-up had to be passed through a door opening. There was also a covering placed on top of each column to ensure that no aerosols escaped during aeration.

The principle of the gamma camera's operation is shown in Figure 5.4. The gamma camera detects the 140 keV photons emitted from Tc-99m during a chosen time interval. The first object that an emitted gamma photon encounters is the collimator. The collimator is a pattern of holes with gamma ray absorbing material that allows the projection of the gamma ray image onto the detector crystal. The collimator only allows those gamma rays traveling along certain directions to reach the detector; this ensures that the position on the detector accurately depicts the originating location of the gamma ray. Scintillation detectors are used to detect the gamma photon. They consist of a Thallium-activated Sodium Iodide [NaI(Tl)] detector crystal. The gamma ray photon interacts with the NaI crystal and light is created. Analysis of these light pulses produces a 2-dimensional projection of the radioactivity of the emitting object, i.e. an image. Images are produced every 30 or 60 seconds, which results in radiotracer images over time. The images have a resolution of 256 by 256 pixels (65536). The size of each pixel is 2.33 by 2.33 mm. An example of such an image is shown in Figure 5.5.

With a Co-57 flood source it is determined which pixels correspond to the scanned object. Such sources are normally used to determine the response uniformity of the gamma camera. For the AXIS-camera, the highest vertical rectangular area was 144 pixels wide and 222 pixels high. For the 1500 XP-camera a similar region was obtained (123 pixels wide and 215 pixels high). As the solids concentration profile is considered homogeneous in a plane parallel to the bottom of the column, the 2-dimensional data of each image were transformed into 1-dimensional data by summing the values per pixel in every plane. This results in a vector with 222 elements for the AXIS-camera,

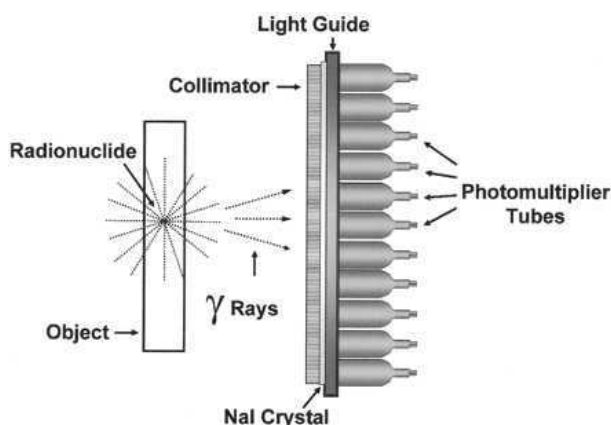


Figure 5.4: Basic principles and components of a gamma camera

resp. 215 elements for the 1500 XP-camera. The data were subsequently corrected for radioactive decay. The half-life of Tc-99m is approximately 6 hours.

5.2.2 Origin of the sludge

Sludge was taken from 2 different municipal wastewater treatment plants close to Ghent: Destelbergen and Deinze. They will be referred to as Destelbergen sludge and Deinze sludge. The two plants have the same treatment steps, i.e. screening, selector tank, biological treatment (with nitrification/denitrification and chemical phosphorous removal) and secondary clarification (and sludge treatment).

The wastewater treatment plant of **Destelbergen** is located in the East of Ghent and is designed for about 66000 PE. However, only 20 % of this capacity is used so far. The aeration tank has a volume of 8900 m³, a depth of 4 m and an aeration capacity of 132 kW. There are 3 clarifiers each with a volume of 2280 m³, a diameter of 33 m and central depth of 4 m. The average SVI of the activated sludge was 150 ml/g.

The wastewater treatment plant of **Deinze** is designed for 25500 PE. The aeration tank has a volume of 6800 m³, a depth of 3.58 m and an aeration capacity of 180 kW. There are 3 clarifiers each with a volume of 1309 m³, a diameter of 25 m and central depth of 3.5 m. The average SVI of the activated sludge was 110 ml/g.

Sludge was taken from the overflow of the aeration tank and recycle of the secondary clarifier. Effluent was used for dilution.

5.2.3 Analytical procedures

Total suspended solids concentration was determined according to method 2540 D of Standard Methods (1995). The technique consists of evaporating the water from the sample at 105 °C and a subsequent determination of the solids weight.

The **solids mass density** was determined according to a soil science method which is under approval for certification (ISO/DTS 17892-3-2003) and is called "Geotechnical investigation and testing - Laboratory testing of soil - Part 3: Determination of particle density - pycnometer method". The procedure consists of the following steps:

1. Dry an amount of sludge at 105 °C, depending on the solids concentration, so that 2 g of dry solids can be obtained. The time of this drying process can be

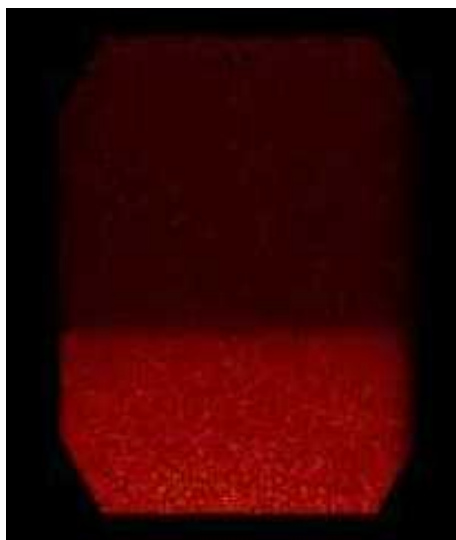


Figure 5.5: Example of an image obtained after 6 hours settling of sludge with Tc-99m Sestamibi as radiotracer. The concentration of the tracer is higher when the color is brighter; the brightest color corresponds to the sludge blanket, the darkest to the supernatant

significantly shortened by thickening the sludge and withdrawing the supernatant prior to drying.

2. The dried solids are pulverized with a mortar and shaken through a 2 mm sieve. Afterwards the grit is put in a dessicator to avoid rehydration of the solids.
3. A closed, dry pyknometer (50-100 ml) (Figure 5.6) is weighed using an analytical balance (WA g).
4. Add the ± 2 g solids to the pyknometer, close the pyknometer and withdraw any solids which have been spilled on the outside of the pyknometer. The pyknometer is weighed again using an analytical balance (WS g).
5. The pyknometer is filled with de-aired distilled water until about 1/3 of the volume. One needs to make sure that solids do not stick at the inside wall of the pyknometer.
6. The pyknometer is put for 20 minutes in a vacuum bottle, of which the bottom is filled with water. After releasing the vacuum the inside wall of the pyknometer is cleaned by adding a new small amount of de-aired distilled water to the pyknometer. Afterwards the pyknometer is put back in the vacuum bottle for another 20 minutes. This procedure is repeated two to three times to wet the solids entirely.
7. The pyknometer is filled entirely with de-aired distilled water. It is closed and the outside wall is cleaned. While doing this, water withdrawal from the capillary head should be avoided. The pyknometer is weighed using an analytical balance (WSW g) and the temperature of the de-aired distilled water ($^{\circ}\text{C}$) is determined.



Figure 5.6: Pycnometer

8. The pycnometer is cleaned thoroughly and filled with de-aerated distilled water. After drying up the outside of the pycnometer, the pycnometer is weighed using an analytical balance (WW g).
9. Finally, the density of the dried activated sludge flocs ρ_s (g/ml) is calculated

$$\rho_s = \rho_l \frac{WS - WA}{(WS - WA) - (WSW - WW)} \quad (5.1)$$

5.2.4 Experimental procedure for P- and C-set-up

Prior to each experiment, the cigarette filters of the P-set-up were renewed and both columns were filled with distilled water. The tubes were de-aired and the zero-differential pressure was checked at the different ports. Sludge (a total volume of 360 liters) was collected at the wastewater treatment plant 2 days before the actual measurements. The 3 columns of the P- and C-set-up were filled with the sludge and the columns were aerated until the start of measurements in order to get it to room temperature (to avoid temperature differences during the experiment and endogenous respiration).

Just before the experiment, all 3 columns were brought to the identical suspension height. Samples were taken for analysis of the solids concentration and solids density. The temperature of the suspension was measured.

For the P-set-up, the pressure profile measurements were started immediately after ceasing the aeration of the column to get it completely mixed. In this column, the sludge blanket height was determined visually. For the C-set-up, the 2 columns were transported to the gamma camera rooms and positioned as closely as possible to the

Table 5.1: Experimental conditions in the preliminary experiments: solids concentration, radioactivity of Tc-99m Sestamibi and gammascan measurements

C_o (g/l)	Radioactivity (mCi)	Gammascan
5.1	2.06	120 scans of 30 s and one scan of 5 minutes after 1.24 hrs of settling
5.1	0.458	10 scans of 30 s during first 5 minutes of settling and one scan of 5 minutes after 1.53 hrs of settling
6.6	0.487	10 scans of 30 s during first 5 minutes of settling and one scan of 5 minutes after 1.8 hrs of settling
10.1	1.83	10 scans of 30 s during first 5 minutes of settling and one scan of 5 minutes after 2.07 hrs of settling
10.2	0.488	10 scans of 30 s during first 5 minutes of settling and one scan of 5 minutes after 2.36 hrs of settling

gamma cameras (about 10-20mm). About 20-40 mCi Tc-99m Sestamibi was injected and the columns were aerated for about 5 minutes to get a good distribution of the radiotracer over the whole suspension. The measurements were then started and lasted between 5 and 6 hours. During the first 2 hours, images were taken every 30 seconds, for the last 4 hours, images were taken every 60 seconds.

5.3 Preliminary experiments

Preliminary experiments were needed to gain more insight in the proposed measurement technique and to answer the following questions

- Does Tc-99m Sestamibi adsorb on the sludge?
- Does Tc-99m Sestamibi change the settling properties?
- Is it possible to measure the excess pore pressure?

5.3.1 Concentration profiles (C-set-up)

Preliminary radiotracer experiments were performed at lab-scale, i.e. in 2 litre bottles (height of the sludge was 16 cm), and with varying radioactivity versus solids concentration ratios. Sludge was collected from the overflow of the aeration tank of the Destelbergen treatment plant. One of the samples was scanned for one hour, the others at the beginning and after approximately 1-2 hours of settling, as summarized in Table 5.1.

Since the radiating recipient (i.e. the 2 l bottle) is smaller than the field of view of the gamma camera, the pixels of the image corresponding to the recipient had to be determined and extracted. Subsequently, the data were converted to 1-dimensional vectors by summing all pixels corresponding to the same horizontal plane. The results of the 120 scans of the first experiment (Figure 5.7 left) show that (1) Tc-99m Sestamibi partly adsorbs onto the sludge, (2) the radioactivity in the supernatant stays constant (i.e. the adsorption does not change during the experiment), and (3) the radioactivity increases with depth in the sludge blanket (i.e. a radioactivity profile is

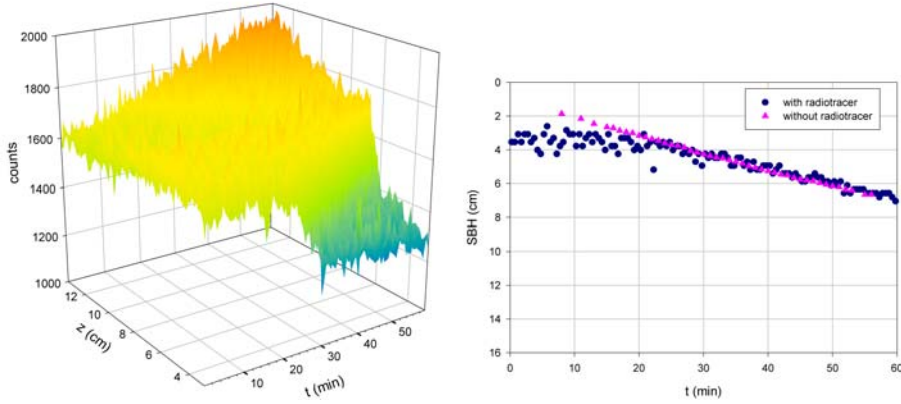


Figure 5.7: Preliminary batch settling of Destelbergen sludge ($C_o=5.1$ g/l) experiment: Time-height profile of the counts of radiating Tc-99m Sestamibi (2.06 mCi) (left) and measured SBH in the sludge with and without radiotracer (right)

observed inside the sludge blanket), just like the solids concentration increases with depth.

The partial adsorption and decreasing radioactivity profile with height are also observed in the other experiments of Table 5.1 (results shown in Appendix A). After correction for radioactive decay, the total radioactivity remained constant with time for all 5 experiments.

Figure 5.7 (right) also shows the evolution of the sludge blanket height in a sample with and without addition of Tc-99m Sestamibi. The sludge blanket height in the sample with Tc-99m Sestamibi is determined as the depth where the counts reached the counts of the completely mixed sample. The deviation during the first 20 minutes is due to the fact that the scanned images can only be collected from a certain depth (approximately 30 mm) in the recipient. It can be concluded that the settling properties do not change with the addition of the radiotracer for the Destelbergen sludge. However, it is felt that this should be verified for each experiment.

Knowing that the radioactivity remains constant in the supernatant and that the radioactivity increases with increasing solids concentration, the solids concentration at a certain depth z and time t , $C(z,t)$, can be calculated with:

$$C(z,t) = \frac{Cnts(z,t) - Cnts_l}{Cnts_o - Cnts_l} C_o \quad (5.2)$$

with $Cnts_o$ the counts of the completely mixed suspension, $Cnts_l$ the counts of the supernatant and $Cnts(z,t)$ the counts at a certain height and time. To illustrate the result of these calculations, a batch settling experiment with Destelbergen sludge ($C_o=3.3$ g/l) was performed in a column of the C-set-up, with radiotracer and with the 1500 XP-camera. The settling properties were verified in the lab without radiotracer. Scans were taken over a depth of 12 down to 62 cm. Solids concentration profiles as calculated with the above formula are shown in Figure 5.8 together with the sludge blanket heights obtained from these profiles (i.e. the depth where the solids concentration reached the initial solids concentration) and from the lab measurements. The high-resolution profile gives a nice representation of the settling process and can be

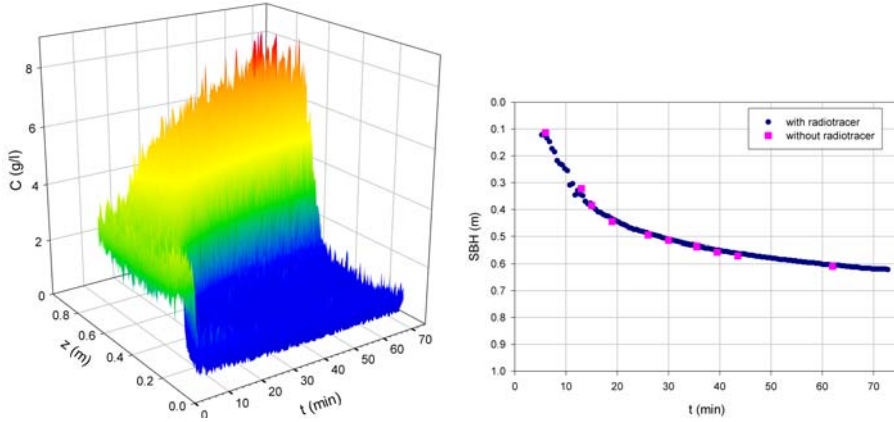


Figure 5.8: Calculated solids concentration profile according to equation 5.2 (left) and its sludge blanket height and measured sludge blanket height in sludge without radiotracer (right) during the batch settling of Destelbergen sludge ($C_o=3.3$ g/l)

used for a better understanding and modelling of the process.

The coefficient of variation for the obtained solids concentration at each time and location is calculated from the standard deviation σ of the measured counts and measured solids concentration according to the standard error propagation rule:

$$\frac{\sigma_{C(z,t)}^2}{C(z,t)^2} = \frac{\sigma_{Cnts(z,t)}^2}{(Cnts(z,t) - Cnts_t)^2} + \frac{\sigma_{Cnts_o}^2 + \sigma_{Cnts_t}^2}{(Cnts_o - Cnts_t)^2} + \frac{\sigma_{C_o}^2}{C_o^2} \quad (5.3)$$

and results in a coefficient of variation of 20 % for the initial concentration and 16 % for the maximum observed concentration. In comparison, the reported accuracy of 0.1 vol% of the CATScan measurements (Chu *et al.*, 2003) results in a coefficient of variation of 50% for the initial concentration and 7% for the maximum observed concentration. As indicated in Figure 5.8 (right), the settling properties once again did not change with the addition of the radiotracer.

In conclusion, the proposed technique, i.e. the use of the radiotracer and measuring the radiation with a gamma camera, can be used to determine a high resolution solids concentration profile during batch settling with good accuracy.

5.3.2 Pressure profiles (P-set-up)

A preliminary experiment in the P-set-up was done with Destelbergen sludge ($C_o=4.64$ g/l). The results of the differential pore pressure measurements are shown in Figure 5.9. The sludge blanket height can be clearly distinguished from the change in slopes between the 2 linear parts. This indicates that the supernatant has a slightly higher density than the distilled water in the water-filled column. Since the profile in the supernatant does not change in time, the supernatant density, ρ_{super} , remains constant and can be calculated from the measurements: 998.87 ± 0.03 kg/m³. From this density, the measured solids density and the solids concentration profile (C-set-up), the excess pore pressure p_e , i.e. the pressure solely due to the solids that are carried by the liquid,

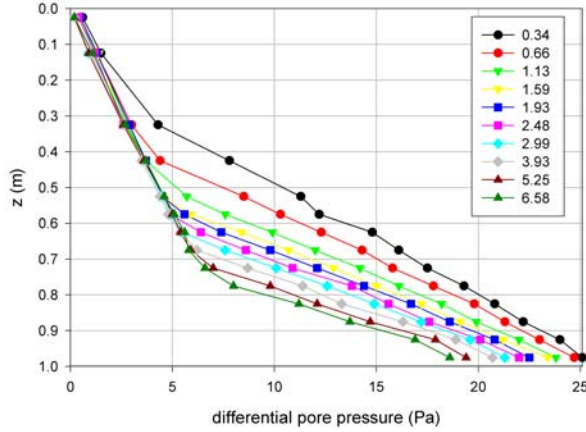


Figure 5.9: Differential pore pressure profile measurements during the batch settling of sludge ($C_o=4.64$ g/l, legend represents time in hrs)

can be calculated from the differential pore pressure p_{dif} profiles:

$$p_e(z, t) = p_{dif}(z, t) - \int_0^z \left(1 - \frac{C(z, t)}{\rho_s}\right) (\rho_{super} - \rho_l) g dz \quad (5.4)$$

The excess pore pressure at the bottom of the column decreases with time, indicating that the liquid is carrying less and less solids and, hence, solids carry each other. This result gives promising results to study compression during the settling of activated sludge. Since the highest measuring point is always in the supernatant, the standard deviation of the measurement can be determined from the different profile measurements and is 0.2 Pa, which is the same as the specifications of the transducer. In conclusion, the measurement of the differential pressure seems promising to determine an accurate excess pore pressure profile during batch settling.

5.4 Pilot-scale experiments: results and discussion

In total, six batch settling experiments were performed: three on Destelbergen sludge and three on Deinze sludge. Table 5.2 shows the initial concentrations, radiotracer adsorption, calculated coefficient of variation for the initial and maximum observed solids concentrations and solids densities for these experiments. The Deinze sludge clearly exhibits a higher affinity towards Tc-99m Sestamibi than the Destelbergen sludge, which explains the lower coefficient of variation for Deinze sludge. The coefficient of variation decreases with increasing initial solids concentration since more radiotracer is adsorbed when the initial solids concentration is higher. The total mass of solids in the column, calculated from the solids concentration profile and assuming the same concentration in the lower 2 cm as the concentration measured at the lowest point, does not deviate more than 2 % from the total mass calculated from the initial solids concentration and volume of the suspension. This suggests that mass balancing can be performed with these radiotracer data. The solids densities for each sludge did not significantly change for the 3 experiments. However, there is quite some difference in

Table 5.2: Origin of sludge, initial solids concentrations, coefficients of variation for the initial and maximum observed solids concentrations and solids density of the 6 batch settling experiments (◦: Destelbergen; *: Deinze; ⊕: pressure measurement)

C_o (g/l)	Fraction of radio-tracer adsorbed on C_o (%)	Coefficient of variation for C_o -max C (%)	Solids density (kg/m ³)
2.40±0.05◦	21	27-21	1762±19
3.23±0.05◦	26	20-16	1753±36
4.30±0.02◦	34	14-11	1714±6
3.67±0.06*⊕	74	11-9	1943±42
6.12±0.09*⊕	83	10-8	1898±57
7.29±0.04*⊕	85	6-4	1881±27

solids densities for both sludges. This should result in lower settling velocities for the same solids concentration. This will be verified in Chapter 6.

The concentration profile measurements are first shown and discussed thoroughly. After that, the results and discussion of the pressure profile measurements are given. In all experiments, settling properties and temperature did not change when radiotracer was added. Moreover, the coherence of the 2 parallel settling tests (upper and lower part of the column) was excellent and the hindered settling rates decreased with increasing initial solids concentrations, as was expected.

5.4.1 Concentration profiles

The solids concentration profiles during batch settling are shown in Figure 5.10 for both sludges. All profiles show the same trend. Initially, the solids concentration is uniform. Subsequent profiles show the accumulation of sludge at the bottom of the column as a result of settling, as well as the drop in sludge blanket height. The concentrations at the bottom are continuously increasing and higher concentrations rise to the sludge blanket height. Once concentrations in excess of the original one reach the sludge blanket height, the latter drops more slowly. The solids concentration at the bottom increases faster initially, but more slowly towards the end for the Deinze sludge in comparison with the Destelbergen sludge. This indicates that the Deinze sludge shows more resistance to further thickening. This will be verified in the next Chapter by modelling the profiles. Equilibrium seems to prevail at the end of the experiments on the Deinze sludge (the concentration profiles did not change any longer for a period of more than 20 minutes).

The equilibrium concentration profiles for the 3 different initial concentrations for the Deinze sludge are presented in Figure 5.11 (left). The equilibrated solids concentrations at the base are around 22 g/l regardless of the initial solids concentration. The fact that the observed equilibrium profiles exhibit an increasing concentration towards the bottom, indicates that besides hindered settling, compression settling is occurring too. A suspension undergoing only hindered settling has an equilibrium profile where a sludge blanket with a constant maximum concentration prevails (for which the hindered settling velocity equals zero). At the sludge blanket, the different equilibrium profiles show approximately the same jump in concentration of about 15 g/l over a height of

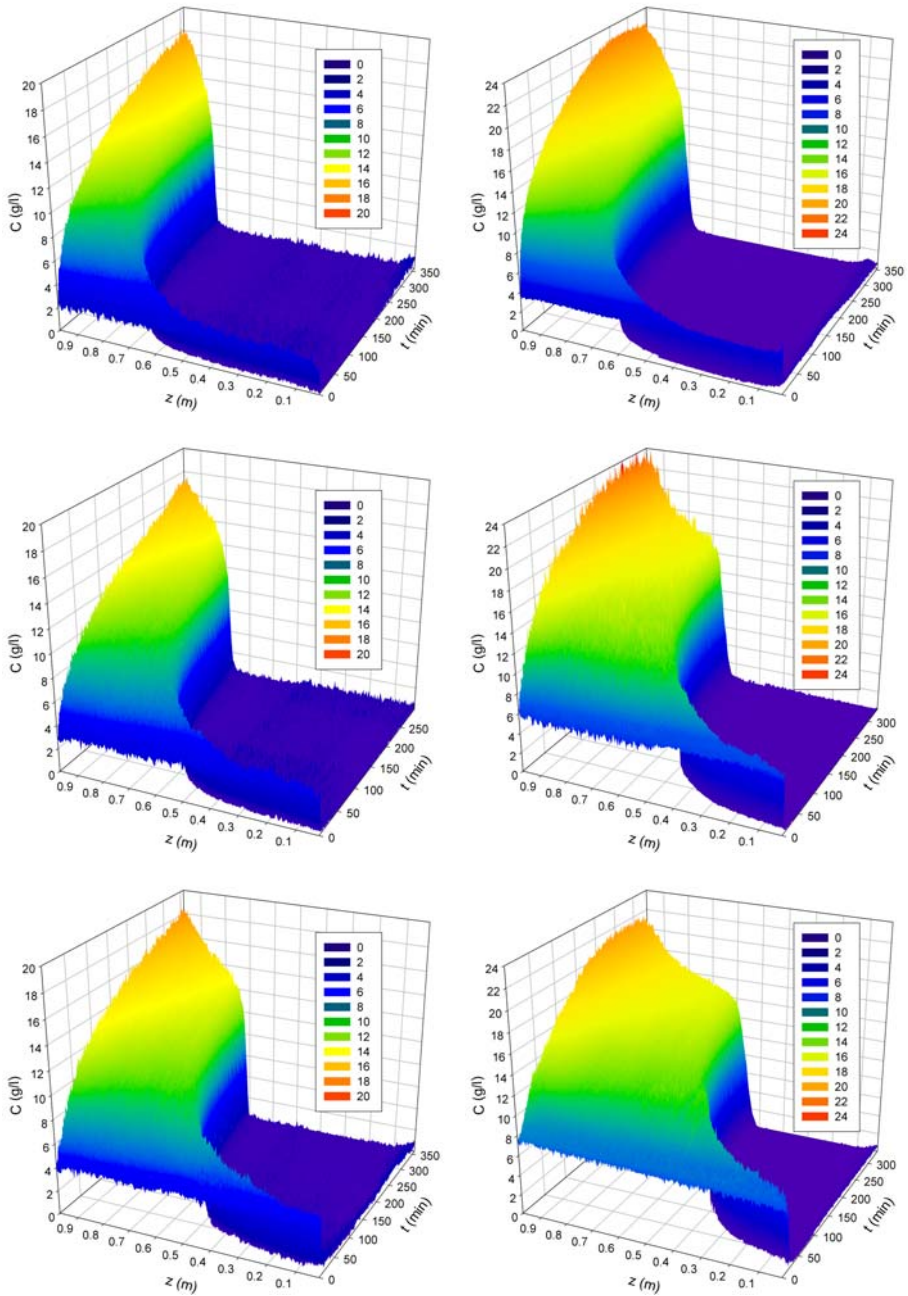


Figure 5.10: Solids concentration profile evolution during batch settling of Destelbergen sludge (left; top: $C_o=2.40$ g/l; middle: $C_o=3.23$ g/l; bottom: $C_o=4.30$ g/l) and Deinze sludge (right; top: $C_o=3.67$ g/l; middle: $C_o=6.12$ g/l; bottom: $C_o=7.29$ g/l)

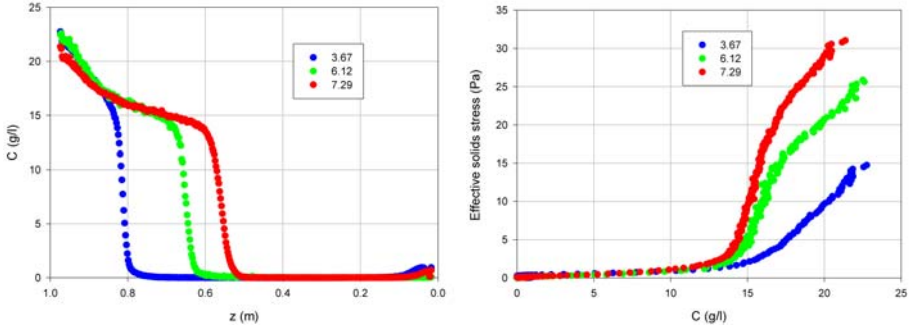


Figure 5.11: Equilibrium solids concentration profiles (left) and effective solids stress versus solids concentration (right) for different initial concentrations (shown in legend) for the Deinze sludge

about 3 cm. It can be stated that for concentrations higher than 15 g/l compression is present. The compression solids concentration (boundary between hindered and hindered+compression settling) can be estimated by averaging concentrations between 1 g/l and 15 g/l of the equilibrium profiles (Chu *et al.*, 2002), giving values of 7.71, 8.58 and 9.09 g/l for increasing initial concentration for the Deinze sludge. Although equilibrium is not reached yet for the Destelbergen experiments, the profiles at the end show the same trend as the Deinze equilibrium profiles (as can be deduced from Figure 5.10). There is a jump in concentration of about 12 g/l over a height of 4 cm. Calculating the average concentrations between 1 and 12 g/l of the Destelbergen profiles at the end gives estimated compression solids concentrations of 6.88, 7.34 and 8.85 g/l for increasing initial concentration. Again, this statement needs to be verified by modelling the concentration profiles.

Since at equilibrium the solids pressure at a certain height equals the effective solids stress at that height, the effective solids stress σ_e can be calculated as follows:

$$\sigma_e(C(z, t_{equilibrium})) = \frac{\Delta\rho g}{\rho_s} \int_0^z C(z, t_{equilibrium}) dz \quad (5.5)$$

The calculated effective solids stress is shown in Figure 5.11 (right) for the different experiments of the Deinze sludge. The effective solids stress increases with the concentration and is different for the 3 experiments. The stress calculated in this way for the highest concentration (i.e. at the base of the column) is in agreement with the pressure of the buoyant weight of solids calculated from the initial solids concentration ($\Delta\rho g C_o H / \rho_s$). This confirms again the accuracy of the proposed measurement technique. At concentrations lower than 15 g/l, the solids do not offer considerable resistance to further settling (effective solids stress lower than 5 Pa), but for concentrations higher than 15 g/l, the solids yield more slowly with the applied pressure. The results are comparable with those reported by Chu *et al.* (2002) for kaolin and clay. Figure 5.11 (right) can be used to find an empirical relationship correlating the effective solids stress and the solids concentration, as will be shown in Chapter 6. The measurements clearly show compression during the batch settling of the Deinze sludge since there is a solids concentration profile at equilibrium. The Destelbergen sludge shows the same behaviour.

The existence of compression during the batch settling is also evidenced by the shape of the iso-concentration lines observed. When only hindered settling is occurring, the iso-concentration lines are straight lines and propagate from the origin (Concha and Burger, 2002); when compression occurs too, the iso-concentration lines become curved (Concha and Burger, 2002) and the iso-concentration lines arise from the bottom of the settler at different values of time (Font and Laveda, 2000). This is clearly the case for all experiments, as shown in Figure 5.12 for both sludges. Compression is already occurring at solids concentrations just above the initial solids concentration since all iso-concentration lines starting from the bottom are not propagating from the origin. Since at the end of the experiments the compression solids concentrations are significantly higher than the initial solids concentration, the compression solids concentration increases with time for both sludges, as modelled by Diplas and Papanicolaou (1997) and suggested by Kinnear (2002).

Analysis of the experiments of the Deinze and Destelbergen sludges (Figures 5.13 and 5.14) shows that for different initial concentrations the concentration profiles inside the sludge bed (i.e. below the suspension-liquid interface) coincide both in time and height after approximately 50 minutes. This period of 50 minutes is beyond the constant rate of fall period (as explained in section 2.1.1) for all experiments. This collapse implies that settling properties are the same for all experiments performed with the same sludge and can be explained by the fact that the iso-concentration lines, which are ascending from the suspension-sediment interface (i.e. location where $C=C_C$), do not depend on the initial height and the initial solids concentration and are thus identical (Font, 1988; Font *et al.*, 1999) (see also Figure 2.11 of Chapter 2). This independency also holds for the isoconcentration lines inside the sediment (i.e. for $C \geq C_C$).

Font (1988) showed that the sediment-suspension interface can be determined from the suspension-liquid interfaces of experiments at different initial solids concentrations. This is based on the fact that iso-concentration lines arising from the sediment-suspension interface do so tangentially (Fitch, 1983; Bustos *et al.*, 1999). When straight lines are drawn on the batch settling curve graphs which are joining points with the same settling rate of the suspension-liquid interface and which pass close to the origin (rising from the bottom) or intersect the height axis on the positive part (i.e. those lines rise from the sediment), the sediment-suspension interface can be drawn tangentially to all the iso-concentration lines with positive ordinate at time zero. The method is illustrated in Figure 5.15. This was applied to the different batch settling curves of the same sludge to determine the sediment-suspension interface. Since there are 3 batch settling curves for each sludge, there are 3 points with the same settling rate of the suspension-liquid interface. This analysis shows that lines connecting those 3 points are not linear and do not pass the origin nor the height axis on the positive part. This indicates that the batch settling curve measurements show a sediment-suspension interface that is rising so fast that it cannot be determined from the measurements.

The solids concentration profile and batch settling curve measurements indicate that the compression solids concentration at the beginning is around the initial solids concentration ($C_o \approx C_C$). By inspecting the solids concentration profiles (Figures 5.10) more closely, a zone with constant initial solids concentration can be observed for each experiment. This zone, also taking the induction period into account, is however very short, i.e. around 10 minutes. At this time, the first iso-concentration line with a

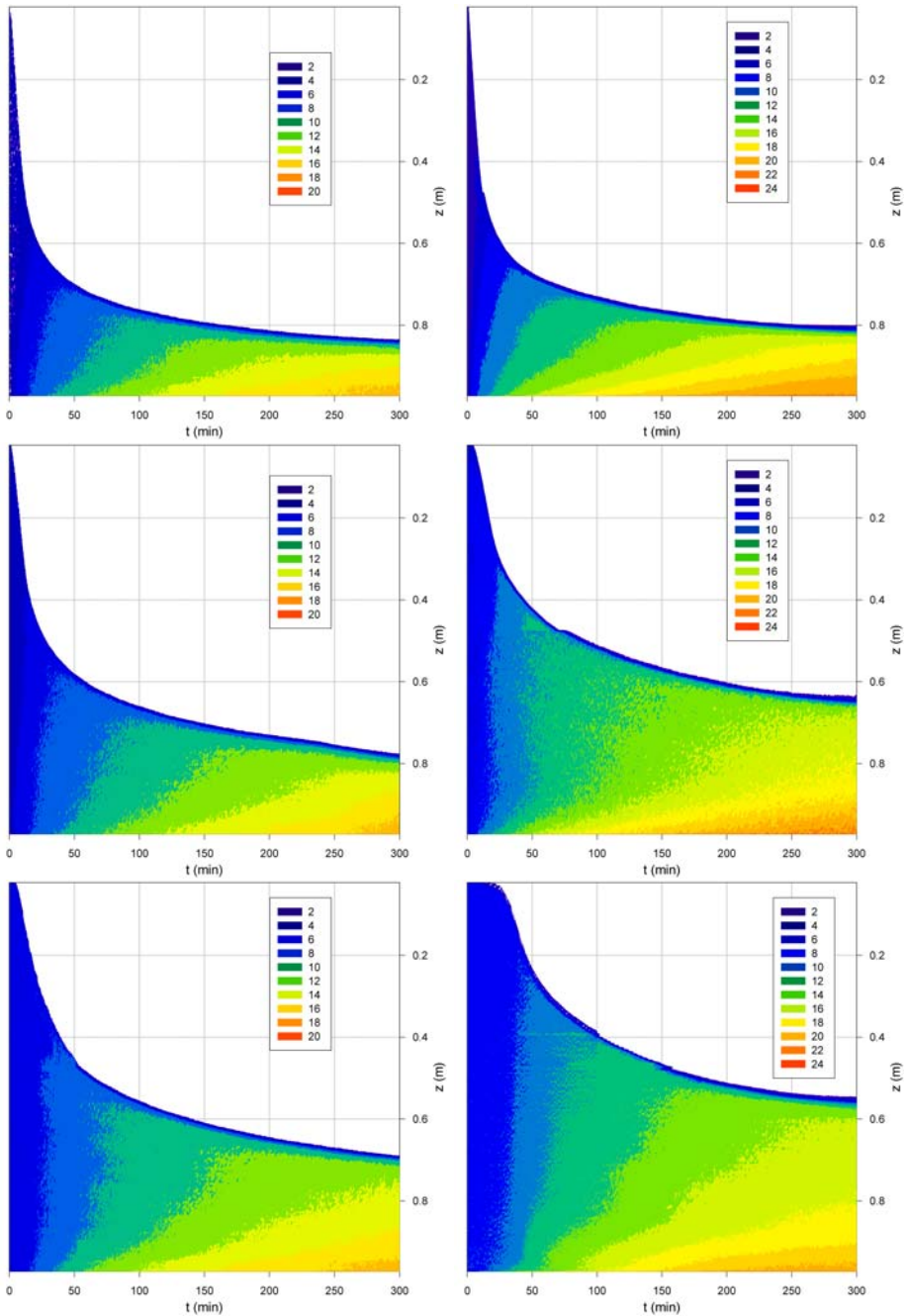


Figure 5.12: Iso-concentration contour plots (different concentrations shown in legend) during batch settling of Destelbergen sludge (left; top: $C_o=2.40$ g/l; middle: $C_o=3.23$ g/l; bottom: $C_o=4.30$ g/l) and Deinze sludge (right; top: $C_o=3.67$ g/l; middle: $C_o=6.12$ g/l; bottom: $C_o=7.29$ g/l)

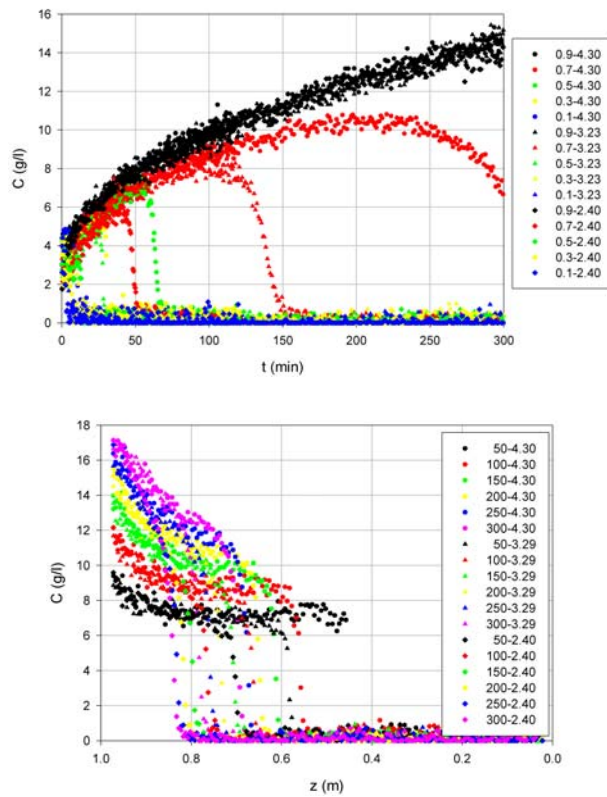


Figure 5.13: Concentration profiles in time at different depths (m) and initial solids concentrations (g/l) (see legend) (top) and concentration profiles in depth at different times (min) and initial solids concentrations (g/l) (see legend) (bottom) during batch settling of Destelbergen sludge

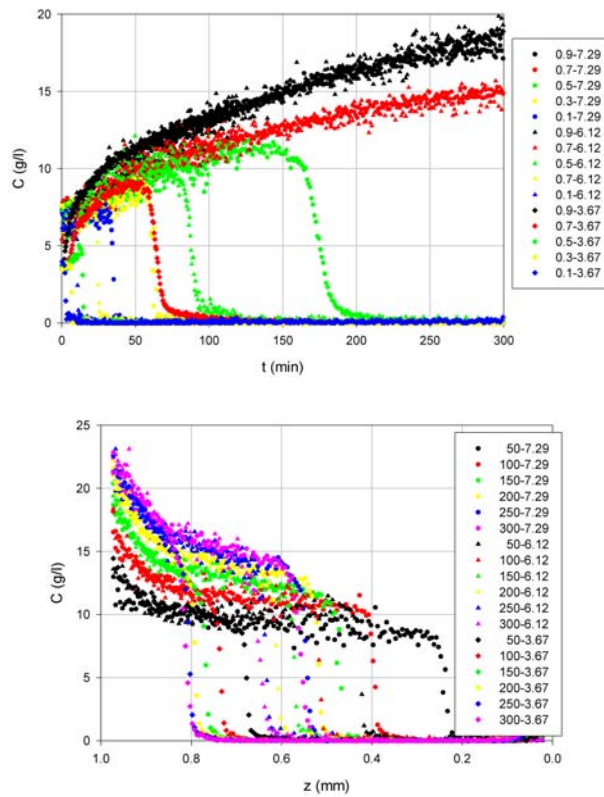


Figure 5.14: Concentration profiles in time at different depths (m) and initial solids concentrations (g/l) (see legend) (top) and concentration profiles in depth at different times (min) and initial solids concentrations (g/l) (see legend) (bottom) during batch settling of Deinze sludge

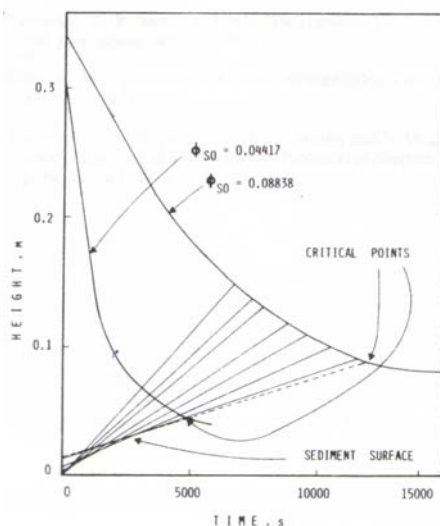


Figure 5.15: Method to estimate the height of the sediment-suspension interface versus time from two batch settling curves (with initial solids concentration ϕ_o of 0.04117 and 0.08838) according to Font (1988)

solids concentration higher than the initial one arrives at the suspension-liquid interface. This implies that there are only few points on the batch settling curve for the determination of the initial settling velocities. The batch settling curves and corresponding induction period and period of constant rate of fall are presented in Figure 5.16. The induction period is approximately nihil for the Destelbergen sludge, but increases for higher initial solids concentrations for the Deinze sludge. This increase of the induction period for higher initial solids concentration was also shown in the experiments of Vanderhasselt and Vanrolleghem (2000). An explanation for this is however still lacking. Moreover there is still quite some discussion about the origin of this period: a recovery from initial disturbances or flocculation/coagulation?

Modelling of these data needs to illuminate these observations. However, it is already obvious at this stage that the measurement of the solids concentration profiles contains a lot more information than the batch settling curves alone. This extra information is very useful in view of the modelling exercise (Chapter 6).

5.4.2 Pressure profiles

Differential pore pressure profile measurements for the batch settling experiment of Deinze sludge at an initial concentration of 6.12 g/l are shown in Figure 5.17. The measurements for the other concentrations showed the same trend. In contrast to Figure 5.9, the pressure at the top of the suspension does not remain constant, even though it is only supernatant. Why this occurred, is not clear. A possible explanation could be that part of the scum on top of the suspension (created due to the aeration before the settling) starts to rest more and more on the suspension. When the column was filled with distilled water, this phenomenon did not take place. The data were

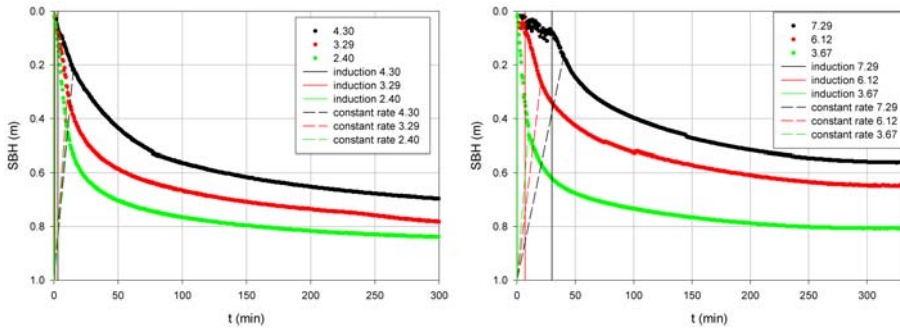


Figure 5.16: Batch settling curves and corresponding induction periods and periods of constant rate of fall for the Destelbergen sludge (left) and the Deinze sludge (right) (concentrations and periods are shown in legend)

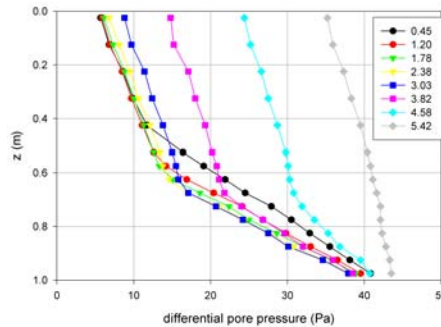


Figure 5.17: Differential pore pressure profiles during batch settling of Deinze sludge (elapsed time (hrs) is shown in legend) for $C_o=6.12$ g/l

corrected for this by subtracting the pressure measured at the top from every other measured pressure. After this correction the data appeared more acceptable because the straight lines which correspond to the supernatant, had the same tangent for each measured profile, as was also observed in Figure 5.9. The supernatant density is calculated for each experiment from these straight lines and is for all 3 experiments around 998 kg/m^3 with standard deviations in the order of 0.25 kg/m^3 .

The **excess pore pressure profiles** were calculated from the differential pore pressure profiles and the supernatant density, the solids density and the solids concentration profiles (see equation 5.4). Those profiles together with the total solids stress profiles (calculated from the solids concentration profiles and the solids density) are shown in Figure 5.18. The excess pore pressure at the bottom of the column decreases with time, indicating that the liquid is carrying less and less solids. Compression is present for each profile (i.e. excluding the induction period for the data with $C_o=7.29$ g/l) from the suspension-liquid interface on (because the excess pore pressure profile is different from the total solids stress profile). This confirms the statement of the previous section (5.4.1) that the compression solids concentration already occurs at this interface for each measurement. On Figure 5.18, some excess pore pressures are higher

than the total solids stress, which is impossible. Those points are to be considered as outliers.

The **effective solids stress**, calculated from the difference between the total solids stress and the excess pore pressure, is depicted as function of the solids concentration at each measuring point as shown in Figure 5.19. Only the data at the lowest initial solids concentration show a nice trend: the relationship effective solids stress versus solids concentration shows a changing compression solids concentration and the effective solids stress is a function of the difference between the compression solids concentration and the solids concentration. The effective solids stress, calculated from the pressure measurements at 5.9 hrs, agrees with the effective solids stress, calculated from the equilibrium solids concentration profile for the experiment at the lowest initial solids concentration. Those observations are considered in the modelling of the data. The changing compression solids concentration is seen too in the other 2 experiments, but in those experiments the effective solids stress at a constant solids concentration increases with time after 3.5 hrs. This means that the solids at a certain concentration show more resistance to further settling with respect to time. It is not clear what happened there. It appears an unrealistic phenomenon which makes that no further modelling was attempted for these conditions.

5.5 Conclusion

A solids radiotracer and 2 gamma cameras were used to obtain high time and spatial resolution solids concentration profiles during the batch settling of activated sludge in a pilot-scale column with a height of 1 m. It is the first time that such detailed pilot-scale dynamic solids concentration profiles have been reported. This non-invasive technique does not disturb the settling process, does not alter the settling characteristics, gives profiles every minute, and is capable of measuring in a range of 0-25 g/l with high accuracy.

The pilot-scale dynamic solids concentration profiles give a detailed quantitative representation of the settling process. They confirm that hindered settling rates decrease with increasing initial solids concentrations. The profiles show not only hindered settling but the equilibrium concentration profiles and the iso-concentration lines clearly show that compression is taking place. Equilibrium compression solids concentrations can be estimated from the equilibrium profiles and are between 7 and 10 g/l depending on the origin of the sludge and the initial solids concentration. The iso-concentration lines show that the compression solids concentration at the beginning should be around the initial solids concentration. Those 2 observations result in a time-dependent compression solids concentration as modelled by Diplas and Papanicolaou (1997) and suggested by Kinnear (2002). Since the concentration profiles inside the sludge bed coincide for the different experiments of the same sludge beyond the constant rate of fall period, the settling properties remained constant during the time period of the experiments.

The pressure measurements also show compression from the suspension-liquid interface downwards and give some indications about the effective-solids-stress-versus-solids-concentration relationship. Those data are however not as conclusive as the solids concentration profiles, since only one of the 3 experiments seems to be useful. More work is needed to further improve this measurement technique.

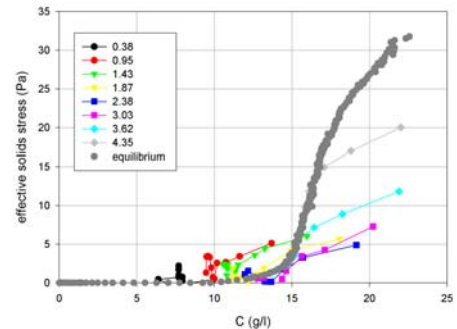
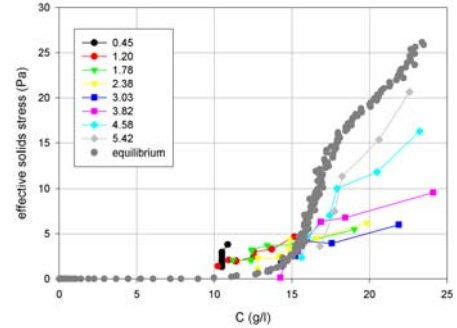
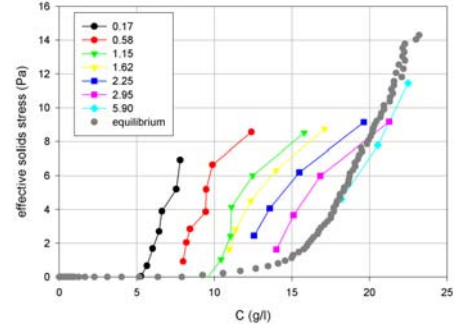
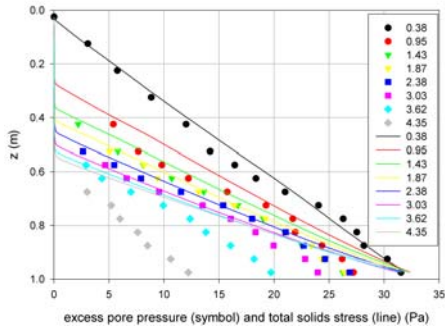
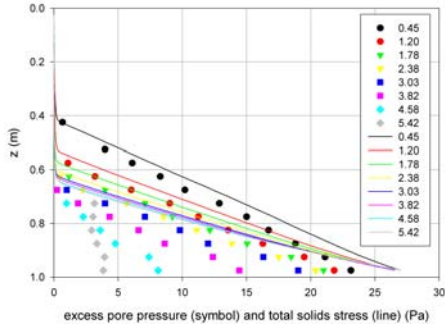
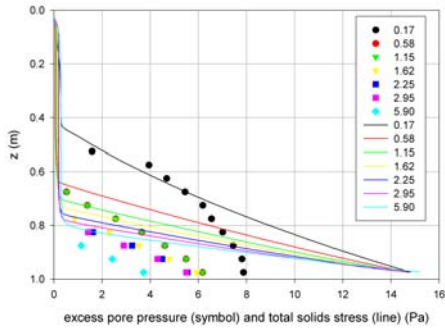


Figure 5.18: Excess pore pressure and total solids stress profiles during batch settling of Deinze sludge (elapsed time (hrs) is shown in legend) (top: $C_o=3.67$ g/l; middle: $C_o=6.12$ g/l; bottom: $C_o=7.29$ g/l)

Figure 5.19: Effective solids stress versus solids concentration during batch settling of Deinze sludge (elapsed time (hrs) is shown in legend; equilibrium is taken from Figure 5.11) (top: $C_o=3.67$ g/l; middle: $C_o=6.12$ g/l; bottom: $C_o=7.29$ g/l)

Chapter 6

Development of an activated sludge batch settling model

In this Chapter, the batch settling experiments of Chapter 5 are used as a basis for the development of a new model describing the batch settling process. The model structure is the one given in section 4.1.1:

$$\frac{\partial C}{\partial t} = -\frac{\partial f_{bk}(C)}{\partial z} + \frac{\partial}{\partial z} \left(f_{bk}(C) \frac{\rho_s}{\Delta \rho g C} \frac{d\sigma_e(C)}{dC} \frac{\partial C}{\partial z} \right) \quad (6.1)$$

with boundary conditions and initial condition

$$f_{bk}(C) \left(1 - \frac{\rho_s}{\Delta \rho g C} \frac{d\sigma_e(C)}{dC} \frac{\partial C}{\partial z} \right)_{z=0, z=H} = 0 \quad (6.2)$$

$$C_{z,0} = C_o \quad (6.3)$$

The aim of this Chapter is to find appropriate expressions for the hindered settling flux f_{bk} and effective solids stress σ_e using the experimental data collected in Chapter 5 as a source of inspiration. As stated in section 5.5, the model should be able to describe the following observations of the batch settling experiments:

- hindered and compression settling
- hindered settling rates decrease with increasing initial solids concentrations
- the compression solids concentration is time-dependent

As described in section 2.3.2, the parameters of the Kynch batch density function can be obtained from observed initial settling velocities whereas those of the effective solids stress can be obtained from observed equilibrium solids concentration profiles. The experimental data of Chapter 5 are not only used to find parameter estimates of the respective functions but also to determine the most appropriate functional relationship.

6.1 Initial settling velocity and induction period

The batch settling curves (Figure 5.16) showed an induction period. Only few people tried to incorporate this period into a batch settling model by multiplying the Kynch

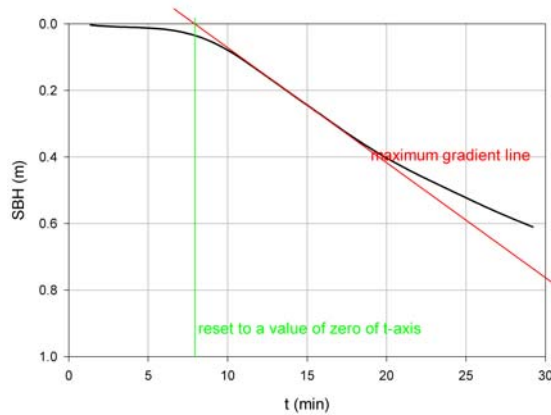


Figure 6.1: Procedure to omit the induction period from a batch settling curve

batch density function with an on-off term (Vanderhasselt and Vanrolleghem, 2000; Perez *et al.*, 1998). This is an empirical way to account for this period and it makes the model more complicated since at least one parameter is added. Moreover, there is still quite some discussion about the origin of this period: a recovery from initial disturbances or flocculation/coagulation. Hence, the modelling of this period is beyond the scope of this work, moreover since these phenomena do not need to be covered by the 1D continuous settling model. The ultimate goal of this dissertation is finding a 1D continuous settling model that can describe the (settling) behaviour of the activated sludge. In a continuous settling mode, there are no transient phenomena taking place like it is the case in batch settling, e.g. the dissipation of the energy originating from mixing the sludge. This period will therefore be omitted from the experimental data as described below.

During the induction period, the settling velocity increases to the settling velocity at the initial solids concentration (i.e. the slope becomes steeper during the initial stages of the batch settling experiment). Since the settling velocity is equal to the gradient of the batch settling curve, gradients are calculated at each point and the maximum settling velocity is determined. Then a straight line with this maximum gradient is drawn on the batch settling curve. The time corresponding to a height of 1 m of this extrapolated line is reset to a value of zero and the experimental data are retained from the point of the maximum gradient onwards. This procedure is shown in Figure 6.1. The transformed data then no longer exhibit an induction period. Initial settling velocities are given in Table 6.1. As expected the settling velocities are decreasing with higher concentrations.

6.2 Kynch batch density function $f_{bk}(C)$

The Kynch batch density function values, f_{bk} , are calculated using the initial settling velocities of Table 6.1 and the corresponding solids concentrations. Those (f_{bk} -versus- C) data are used for the selection of the functions described in Chapter 2. Those functions are given there as function of the solids volume fraction. For the conversion of solids volume fraction to solids concentration, a parameter was added to the functions

Table 6.1: Solids concentrations and corresponding initial settling velocities of the batch settling experiments

Sludge origin	$C_o(\text{g/l})$	$V_{hindered} (\text{m/d})$
Destelbergen	2.40	69.18
	3.23	44.36
	4.30	24.67
Deinze	3.67	82.93
	6.12	24.45
	7.29	15.28

because the functions were not capable to describe the flux data when the solids density is used in the conversion. Only the functions with maximum 2 parameters are retained for the selection since there are only 3 observations and the parameters are calibrated with the algorithm given in Chapter 4. The objective function for parameter estimation was the sum of squared errors (SSE) between the observed and predicted Kynch batch density values. The parameter estimates are summarized in Table 6.2. For both sludges, the Kynch batch density functions of Shirato *et al.* (1970); Kinnear (2002) and Zheng and Bagley (1998, 1999) give the best results, both for the accuracy of the calibrated parameters as for the sum of squared errors. The functions of Table 6.2 are shown graphically in Figure 6.2 together with the measured values. It is clear that among the best Kynch batch density functions, only the function of Zheng and Bagley (1998, 1999) gives acceptable results for a concentration range from 0 to 25 g/l (positive function values) and satisfies most of the conditions of Kynch (1952). This function (Zheng and Bagley, 1998, 1999) is actually the Vesilind function (Vesilind, 1968), which is one of the most frequently used functions in clarifier modelling (Takacs *et al.*, 1991; Hamilton *et al.*, 1992; Grijspeerd *et al.*, 1995; Watts *et al.*, 1996; Ekama *et al.*, 1997; Diehl and Jeppsson, 1998; Lee *et al.*, 1999; Joannis *et al.*, 1999). Consequently, this Vesilind function and its calibrated parameters will be used as basis for the further modelling. In Figures 6.3 and 6.4, simulations with this Vesilind batch settling model (using the determined parameter estimates) and no compression are shown together with the measurements of SBH's and solids concentration profiles respectively. When the constant rate of fall period is passed, it can be observed for all experiments that the settling velocities are too high giving (1) SBH's that are lower than the measured ones and (2) more thickened concentration profiles than the measured ones. Hence, the model is performing well only for the period of constant rate of fall and compression is needed to improve the model simulations: compression implies resistance to further settling, which results in a higher simulated SBH and a less thickened concentration profile.

6.3 Effective solids stress function $\sigma_e(C)$

The effective solids stress function and its parameters are usually obtained from observed equilibrium solids concentration profiles but can be obtained also from inverse modelling, in which all concentration profiles, and not only the one at equilibrium, are considered. The theory about inverse modelling is first introduced and subsequently applied to the experimental data collected in Chapter 5.

Table 6.2: Different Kynch batch density functions with calibrated parameters and SSE for the 2 experiments

Kynch batch density function	Destelbergen sludge		SSE	Deinze sludge		SSE
	a	b		a	b	
$f_{bk}(C) = \frac{a}{C-b}C$ Cacossa and Vaccari (1994)	82±14	1.2±0.3	201	76±9	2.7±0.1	250
$f_{bk}(C) = a(1-bC)^3$ Shirato et al. (1970); Kinnear (2002)	270±18	0.061±0.006	22	663±34	0.063±0.002	58
$f_{bk}(C) = a(1-bC)^{4.65}$ Font (1991)	195±6	0.084±0.002	6	303±34	0.067±0.003	282
$f_{bk}(C) = a(b-C)$ Font (1991)	31.6±2.2	7.7±0.3	9	55±7	9.1±0.5	362
$f_{bk}(C) = aC^{\frac{(2-3bC)^2}{3bC+4+3(8bC-3b^2C^2)^{0.5}}}$ Bergstrom (1992); Burger et al. (2000)	295±12	0.085±0.002	10	430±58	0.065±0.004	558
$f_{bk}(C) = ae^{-bC}C$ Zheng and Bagley (1998, 1999)	254±4	0.541±0.005	1	482±40	0.48±0.02	67
$f_{bk}(C) = ae^{-bC}C^2$ Karl and Wells (1999)	221±16	0.85±0.02	16	273±37	0.68±0.03	177
$f_{bk}(C) = ae^{\frac{b}{2}C^2}$ Burger et al. (2000)	0.90±0.36	8.4±1.1	446	0.23±0.06	17±1	358
$f_{bk}(C) = aC^2 + bC$ Burger et al. (2000)	-22±3	119±11	177	-18±5	141±33	3708

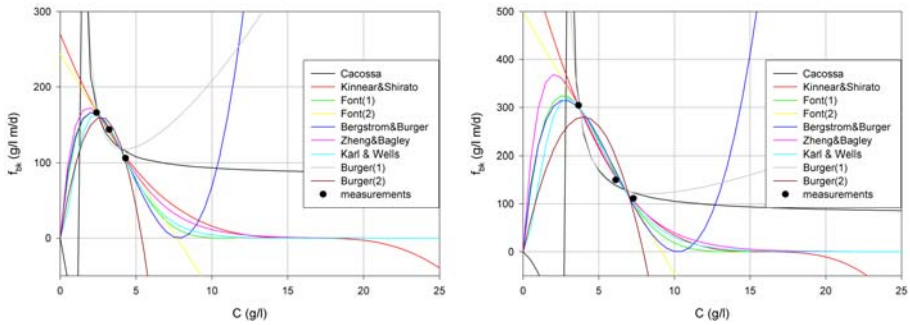


Figure 6.2: Calculated (line, different functions are shown in legend) and measured (symbol) Kynch batch density function versus solids concentration (left: Destelbergen sludge; right: Deinzee sludge)

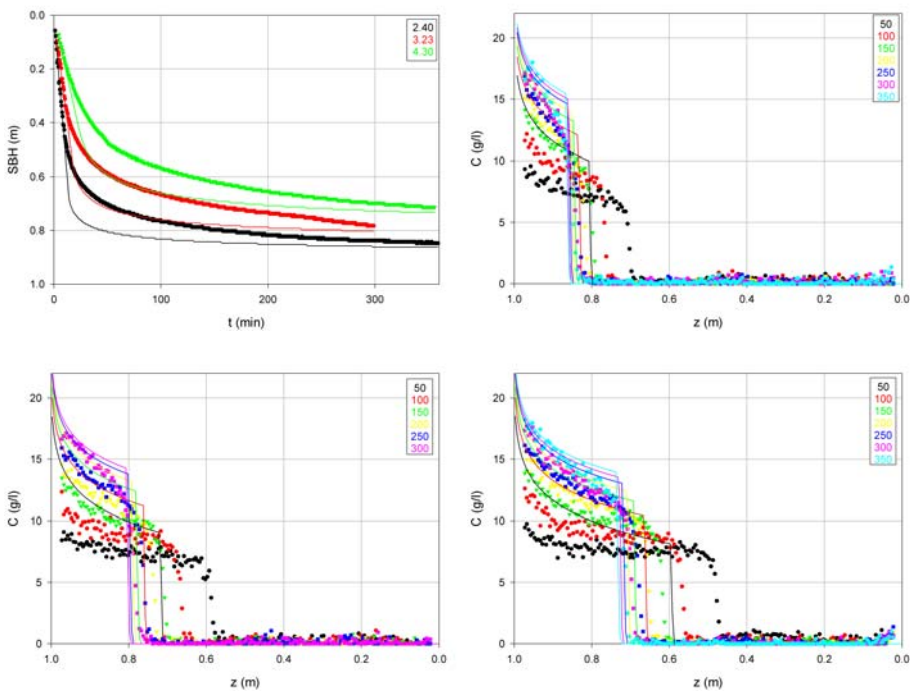


Figure 6.3: Simulated (lines) and measured (symbols) batch settling curves for different initial solids concentrations (g/l in legend) (top left) and simulated (lines) and measured (symbols) solids concentration profiles in height at different times (indicated in minutes in legend) during batch settling of Destelbergen sludge (top right: $C_o=2.40$ g/l; bottom left: $C_o=3.23$ g/l; bottom right: $C_o=4.30$ g/l); simulations are performed with the batch settling model with only the calibrated Vesilind function

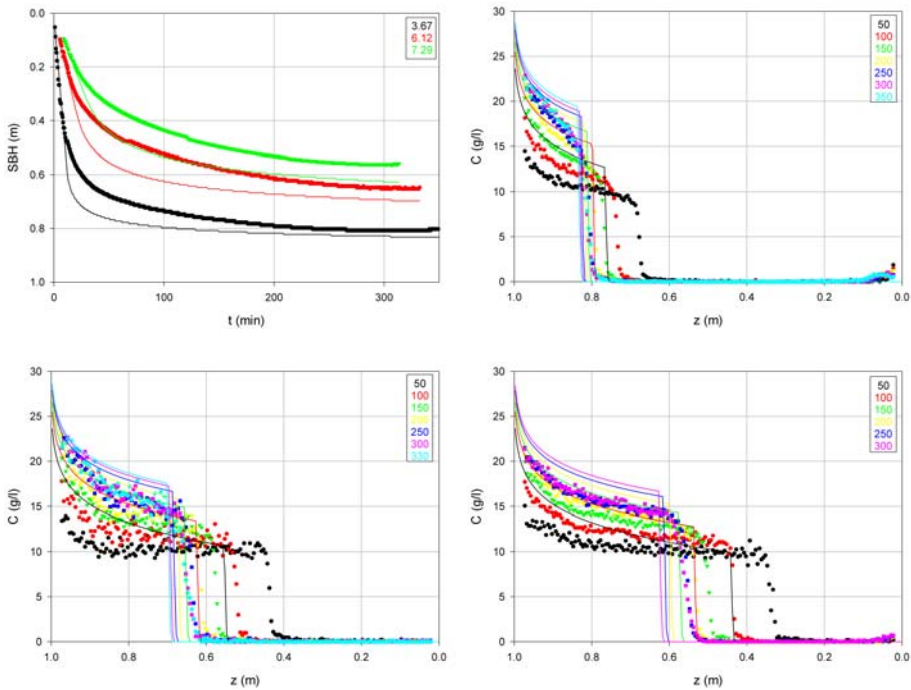


Figure 6.4: Simulated (line) and measured (symbol) batch settling curves for different initial solids concentrations (g/l in legend) (top left) and simulated (lines) and measured (symbols) solids concentration profiles in height at different times (indicated in minutes in legend) during batch settling of Deinze sludge (top right: $C_o=3.67$ g/l; bottom left: $C_o=6.12$ g/l; bottom right : $C_o=7.29$ g/l); simulations are performed with the batch settling model with the calibrated Vesilind function

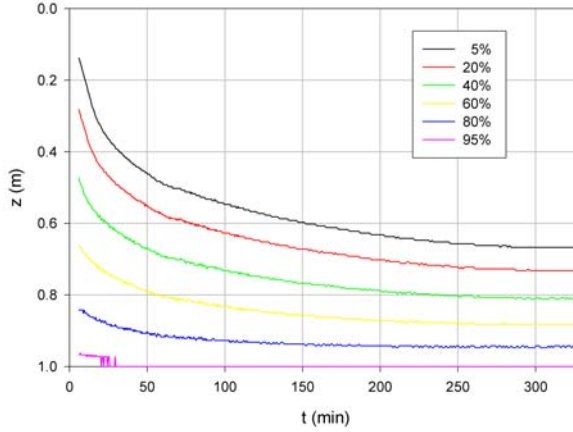


Figure 6.5: Isomass (% of initial mass above) lines calculated from the measured concentration profiles during the batch settling of the Deinze sludge ($C_o=6.12$ g/l)

6.3.1 Inverse modelling: theory and application

Following Tiller *et al.* (1991) and Been and Sills (1981), Burger *et al.* (2001) constructed Lagrangian paths to follow given sets of particle species. Integrating the concentration profiles at a given time with respect to height yields the heights above which 1%, 2%, 3%, ..., 99% of the total mass of solids is located. The succession of these points with respect to time yields curves that may be considered as trajectories of solids separated by 1% from the remaining 99% (and so on) of total mass of the sludge. These trajectories are called isomass lines and are calculated for all 6 experiments. A selection of these isomass lines computed from the measured concentration profiles of one of the 6 experiments is shown in Figure 6.5.

The settling velocity, V_S , for an element of sludge is simply the gradient of the trajectory at a specific time. For each trajectory, at each time, this settling velocity is calculated. At each point of a trajectory, the solids concentration is known from the radiotracer experiment and with the constitutive equation for the Kynch batch density function derived in section 6.2, estimates of the settling velocity can be used to obtain values of the effective solids stress σ_e with the following formula:

$$V_S(C) = ae^{-bC} \left(1 - \frac{\rho_s}{\Delta\rho g C} \frac{d\sigma_e(C)}{dC} \frac{\partial C}{\partial z} \right) \quad (6.4)$$

Since there is noise on the solids concentration, the calculation of the concentration gradient in equation 6.4 is not straightforward. Moreover, the effective solids stress function $\sigma_e(C)$ is of interest and not its gradient. Hence, to resolve these two issues, the equation is numerically integrated to:

$$\sigma_e(C(z)) = \sum_0^z \left(1 - \frac{V_S(C(z))}{ae^{-bC(z)}} \right) \frac{\Delta\rho g C(z)}{\rho_s} \Delta z \quad (6.5)$$

The results of these calculations are shown in Figure 6.6. It is clear that there is no single effective solids stress function which is able to describe all data points, even with

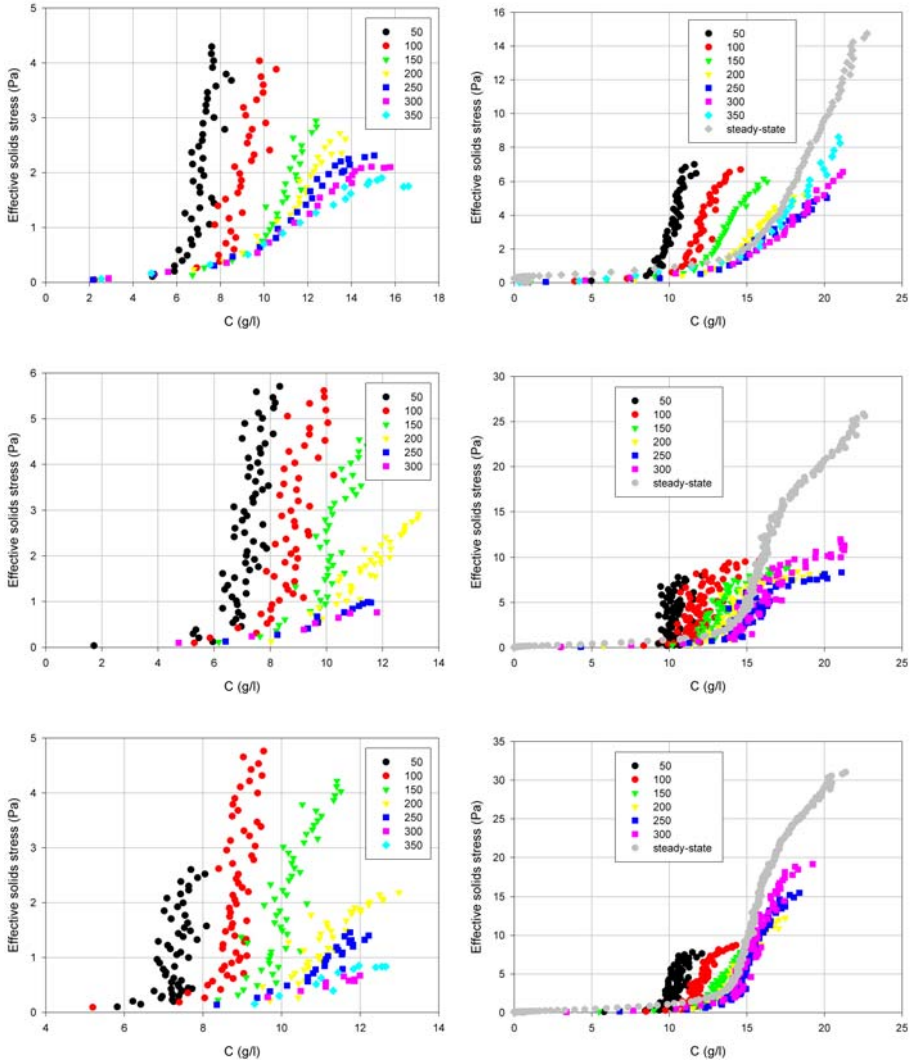


Figure 6.6: Calculated effective solids stress versus solids concentration at different times (indicated in minutes in legend) during batch settling of Destelbergen sludge (left; top: $C_o=2.40$ g/l; middle: $C_o=3.23$ g/l; bottom: $C_o=4.30$ g/l) and Deinze sludge (right, top: $C_o=3.67$ g/l; middle: $C_o=6.12$ g/l; bottom: $C_o=7.29$ g/l); calculations are performed with the Vesilind function, except for the curves at steady-state (grey symbols) which originate from Figure 5.11

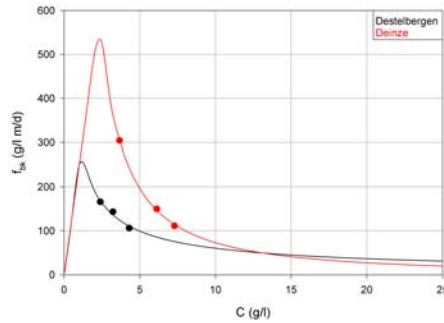


Figure 6.7: Calculated (line, power function of Cole (1968)) and measured Kynch batch density function with V_{max} (symbol) versus solids concentration for Destelbergen and Deinze sludge (for the Destelbergen sludge: $a=317\pm 57$, $b=0.72\pm 0.16$, $SSE=82$; for the Deinze sludge: $a=1944\pm 133$; $b=1.426\pm 0.046$, $SSE=18$)

a compression solids concentration that for example increases with time. Comparison of the calculated effective solids stress with the effective solids stress calculated from the equilibrium solids concentration profiles (Figure 6.6 left) also shows that the model with the Vesilind function gives too low effective solids stress values. This indicates that the Vesilind function is incorrect: a Vesilind function that gives higher hindered settling velocities for concentrations higher than the initial solids concentrations will result in higher effective solids stress values. To obtain a single effective solids stress function, with a time-dependent compression solids concentration, the settling velocity at concentrations higher than the initial concentrations should be higher than the value given by the Vesilind function. By inspecting Figure 6.2 and Table 6.2, it is clear that none of the other investigated functions is capable of giving both good initial settling velocities and higher settling velocities at concentrations higher than the initial concentrations.

However, another function, which gives higher settling velocities for higher concentrations, is the power function of Cole (1968):

$$f_{bk}(C) = aC^{-b} \quad (6.6)$$

This function was not included in the evaluation of the function of Table 6.2 because it has not been used in batch settling models that consider compression and that have been confronted with experimental batch settling data. This function was also evaluated by Cho *et al.* (1993) and Grijspeerdt *et al.* (1995). The power function however gives an infinite f_{bk} for a zero solids concentration and does not have a maximum. This can be resolved either by imposing a maximum settling velocity or by using another function for the lower solids concentrations. In the current Chapter, a maximum settling velocity of 250 m/d was imposed. The resulting best fit function is shown in Figure 6.7 together with the measurements. The Deinze sludge settles better than the Destelbergen sludge for concentrations lower than about 13 g/l but the opposite is seen for the higher concentrations. This is reflected in the higher a - and b -values for the Deinze sludge. To evaluate how this power function affects the

effective solids stress function, inverse modelling calculations performed with

$$\sigma_e(C(z)) = \sum_0^z \left(1 - \frac{V_S(C(z))}{aC(z)^{-b-1}} \right) \frac{\Delta\rho g C(z)}{\rho_s} \Delta z \quad (6.7)$$

are shown in Figure 6.8. These calculations give good agreement with the equilibrium data and show a single effective solids stress function when a time-dependent compression solids concentration (compression solids concentration is increasing with time as can be deduced from Figure 6.8) is considered. Therefore, it can be concluded that the power function is performing better than the Vesilind function and is retained as the Kynch batch density function from now on.

The time-dependent compression solids concentration, i.e. the concentration above which an effective solids stress exists, is located at the sludge blanket height, as was already shown in Chapter 5. Before determining an appropriate functional relationship for the effective solids stress, the evolution of the compression solids concentration needs to be determined from the solids concentration profiles.

6.3.2 Evolution of the compression solids concentration

Chapter 5 and section 6.3.1 showed that the time-dependent compression solids concentration C_C is located at the sludge blanket height. This concentration can be calculated from the solids concentration profiles in the following way.

At the sludge blanket height, there is a discontinuity or in reality a large concentration gradient around the initial solids concentration. Just below the sludge blanket height, the profile is much smoother (i.e. has smaller concentration gradients). An example of a concentration profile and its concentration gradient is shown in Figure 6.9. When the concentration just at the sludge blanket height, which is defined here as the initial solids concentration, would be considered as the compression solids concentration, then this compression solids concentration would remain at this initial solids concentration, i.e. would not be time-dependent, which is contradictory to the findings. Moreover, compression can be seen as some kind of dispersion (second order gradient with depth in model equation 6.1) and dispersion is known to smoothen concentration profiles. This can also be seen in Figures 2.18, 2.20 and 2.22 of Chapter 2, in which the simulations show a lower concentration gradient just below the compression solids concentration versus the gradient just above it. Therefore, the compression solids concentration has to be located just below the discontinuity of the sludge blanket height, where the concentration gradients are stabilized again. It is proposed here to define the compression solids concentration to be that concentration where the concentration gradient reaches values below 200 g/l/m and which is located below the depth of the highest concentration gradient (Figure 6.9). The concentration gradients are calculated for all 6 experiments and shown in Figure 6.10. The calculated time-dependent compression solids concentrations are shown in Figure 6.11. It can be observed that these evolutions more or less coincide for the different initial solids concentrations. With these time-evolutions, it is now tried to deduce an effective solids stress functional relationship.

6.3.3 Effective solids stress function

Figure 6.12 shows that the effective solids stress versus the difference between the solids concentration and the compression solids concentration can be considered related during each experiment. Especially the experiments at higher initial solids concentrations

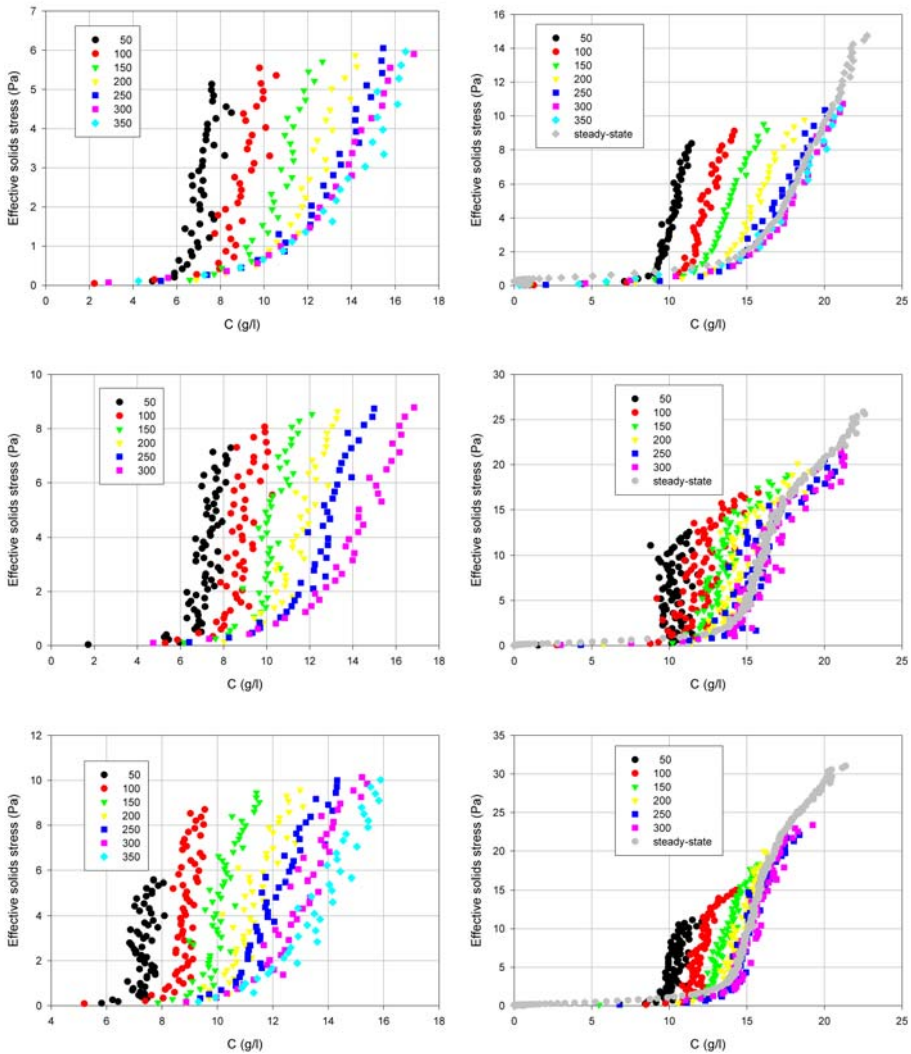


Figure 6.8: Calculated effective solids stress versus solids concentration at different times (indicated in minutes in legend) during batch settling of Destelbergen sludge (left; top: $C_o=2.40$ g/l; middle: $C_o=3.23$ g/l; bottom: $C_o=4.30$ g/l) and Deinze sludge (right; top: $C_o=3.67$ g/l; middle: $C_o=6.12$ g/l; bottom: $C_o=7.29$ g/l); calculations are performed with the power function of Cole (1968), except for the curves at steady-state (grey symbols) which originate from Figure 5.11

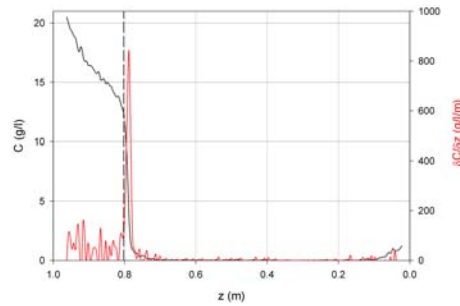


Figure 6.9: An example of a concentration profile and its concentration gradient profile (dashed line corresponds to the compression solids concentration location)

show that the most frequently used power or exponential functions (see Chapter 2, Table 2.2) are not capable of describing the calculated effective solids stresses since those functions have an increasing gradient for higher concentrations, which is opposite to the data shown in Figure 6.12.

Hence, the following logarithmic function was fitted to the calculated effective solids stress data,

$$\sigma_e(C(z, t)) = \alpha \ln \left(\frac{C(z, t) - C_C(t) + \beta}{\beta} \right) \quad (6.8)$$

with α (Pa) and β (g/l) parameters which have to be estimated (with the algorithm of Chapter 4). Moreover, it was investigated whether one or more parameters of this logarithmic function could be constant for all experiments performed with the same sludge. Statistically, this was only acceptable for the parameter α . The objective function for parameter estimation was the sum of squared errors (SSE) between the observed and predicted effective solids stresses. The results are shown in Table 6.3 and the resulting functions together with the calculated effective solids stress are presented in Figure 6.13.

It can be observed that the Deinze sludge has a higher effective solids stress than the Destelbergen sludge, which is mainly reflected in the higher α -value. The β parameter is decreasing for a higher initial concentration, i.e. the effective solids stress is increasing with an increasing initial concentration. This can be explained by the following. For the same $C - C_C$ and increasing initial concentration, there is more sludge present above the depth z corresponding to the concentration C , which results in a higher effective solids stress for an increasing initial concentration. The estimated β -value for the experiment at 3.67 g/l is rather high in comparison with the other estimates. The agreement between the function and the calculated values is satisfying, especially for the Deinze sludge.

6.4 Prediction/simulation of the batch settling experiments

The inverse modelling showed that a power function for the Kynch batch density function combined with a logarithmic function for the effective solids stress gave promising results. However, simulation of the batch settling experiments with the obtained para-

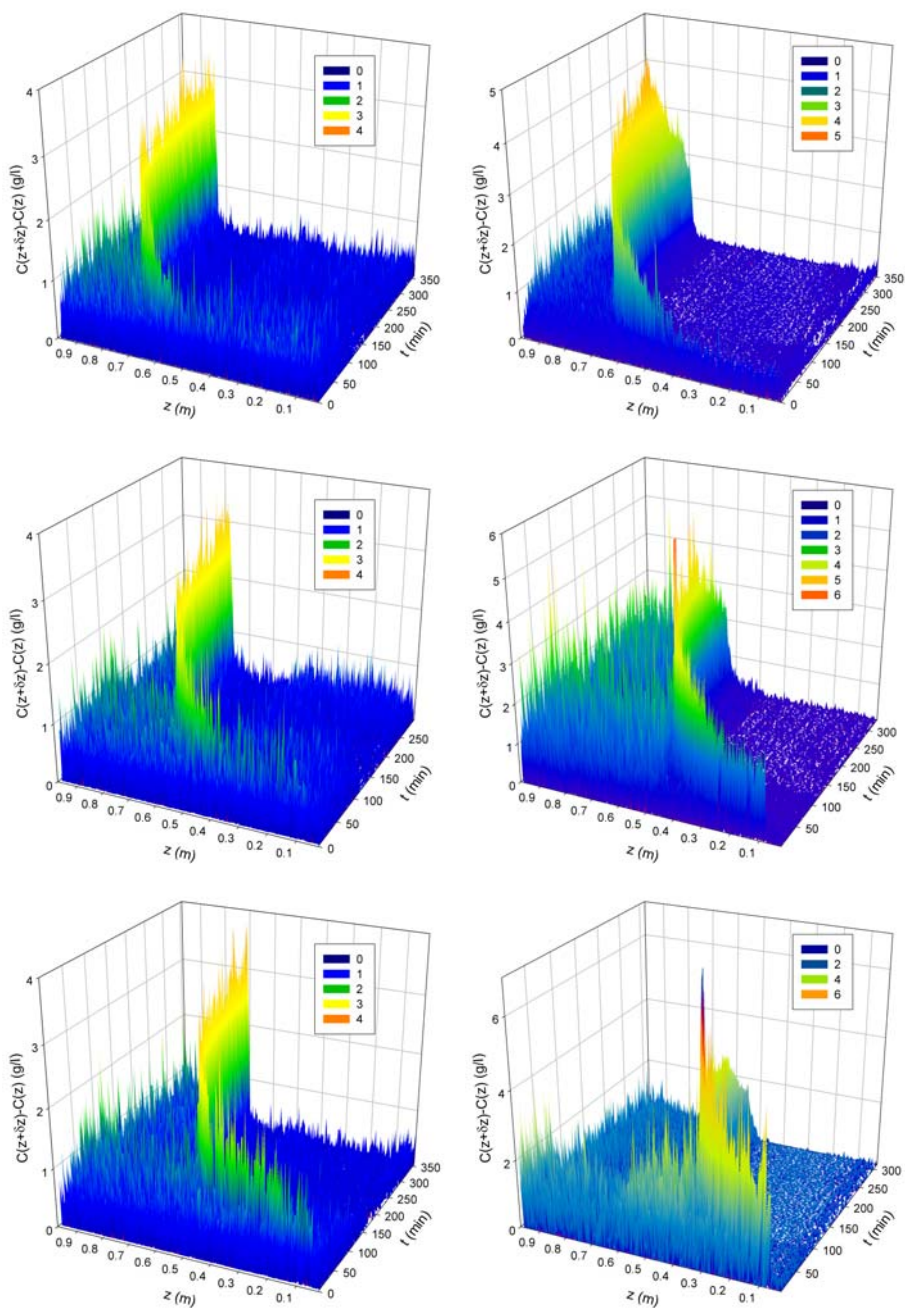


Figure 6.10: Concentration gradient profiles versus height and time during batch settling of Destelbergen sludge (left; top: $C_o=2.40$ g/l; middle: $C_o=3.23$ g/l; bottom: $C_o=4.30$ g/l) and Deinze sludge (right; top: $C_o=3.67$ g/l; middle: $C_o=6.12$ g/l; bottom: $C_o=7.29$ g/l)

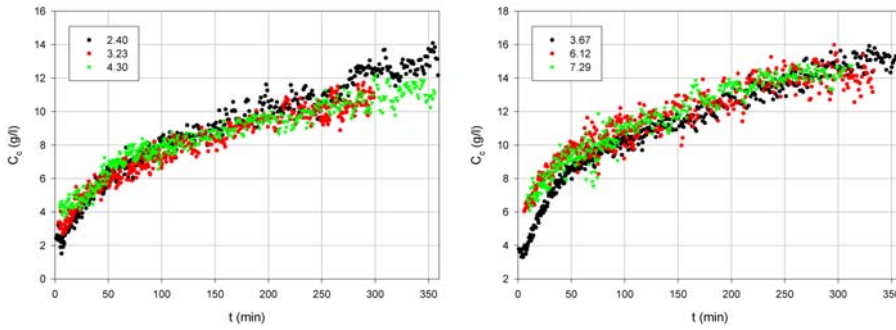


Figure 6.11: Compression solids concentration versus time during batch settling of sludge (left: Destelbergen; right: Deinze) at different initial solids concentrations (indicated in g/l in legend) determined from the concentration gradient profiles

Table 6.3: Calibrated parameters of the logarithmic effective solids stress function for the 2 batch settling experiments

	α (Pa)	β (g/l)		
Destelbergen sludge	$C_o=2.40$ g/l	$C_o=3.23$ g/l	$C_o=4.30$ g/l	
	6.69	4.37	2.52	1.64
Deinze sludge	α (Pa)	β (g/l)		
	$C_o=3.67$ g/l	$C_o=6.12$ g/l	$C_o=7.29$ g/l	
	23.45	11.62	3.76	2.96

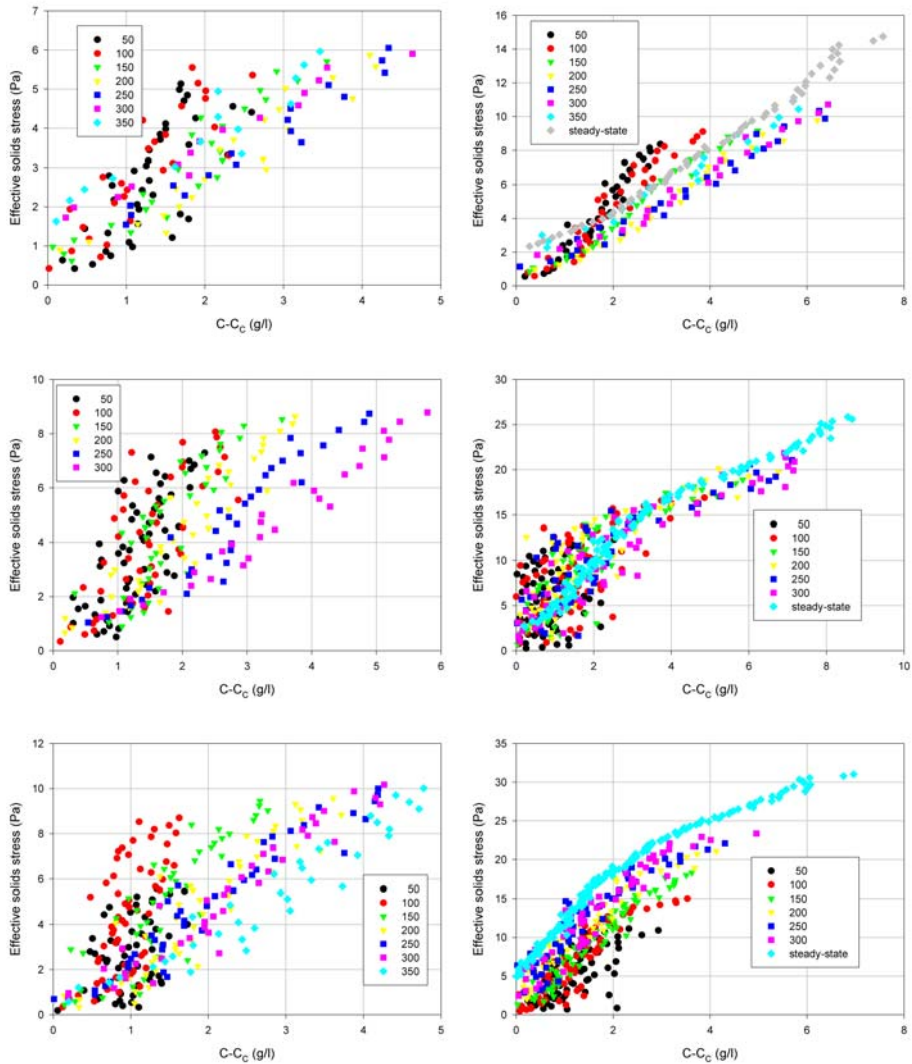


Figure 6.12: Calculated effective solids stress versus solids concentration at different times (indicated in minutes in legend) during batch settling of Destelbergen sludge (left; top: $C_o=2.40$ g/l; middle: $C_o=3.23$ g/l; bottom: $C_o=4.30$ g/l) and Deince sludge (right; top: $C_o=3.67$ g/l; middle: $C_o=6.12$ g/l; bottom: $C_o=7.29$ g/l); calculations are done with the power function of Cole (1968), except for the curve at steady-state which originates from Figure 5.11

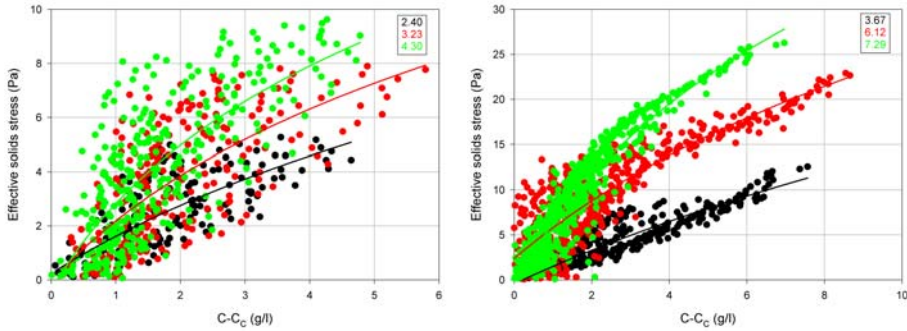


Figure 6.13: Logarithmic effective solids stress function (line) and calculated effective solids stress (symbol) versus solids concentration during batch settling (left: Destelbergen; right: Deinze) (different initial solids concentrations are given in g/l in legend)

Table 6.4: Final parameter estimates of the power batch density function (a and b) and logarithmic effective solids stress function (α and β) for the 2 batch settling experiments

Destelbergen sludge		$C_o=2.40$ g/l	$C_o=3.23$ g/l	$C_o=4.30$ g/l
a ($m/d(g/l)^{b+1}$)	433			
b (-)	0.94			
α (Pa)	7.00			
β (g/l)		2.90	1.76	1.17
Deinze sludge		$C_o=3.67$ g/l	$C_o=6.12$ g/l	$C_o=7.29$ g/l
a ($m/d(g/l)^{b+1}$)	3588			
b (-)	1.70			
α (Pa)	18.24			
β (g/l)		8.27	2.60	2.12

meter values showed unsatisfying results (Figure 6.14). Hence, parameter estimation was done using the obtained parameter values of both functions as initial guesses. The objective function for parameter estimation was the sum of squared errors (SSE) between the observed and predicted concentration profiles. For one sludge, this resulted in a total of 250 000 data points that are used for the parameter estimation. The final parameter estimates are given in Table 6.4. In comparison with the initial parameter guesses, the values changed (α increased and β 's decreased) but the change of β with initial concentration showed the same trend and the value ranges remained the same.

Measured and simulated batch settling curves are shown in Figure 6.15, solids concentration profiles in Figure 6.16. The batch settling model describes the solids concentration profiles and the batch settling curves very well (SSE decreased with at least a factor 3 in comparison with the initial parameter guesses). Comparison with the simulations performed with the Vesilind function (shown in Figures 6.3 and 6.4), which is most frequently used in clarifier modelling, clearly indicates that the proposed model and its parameters gives excellent results.

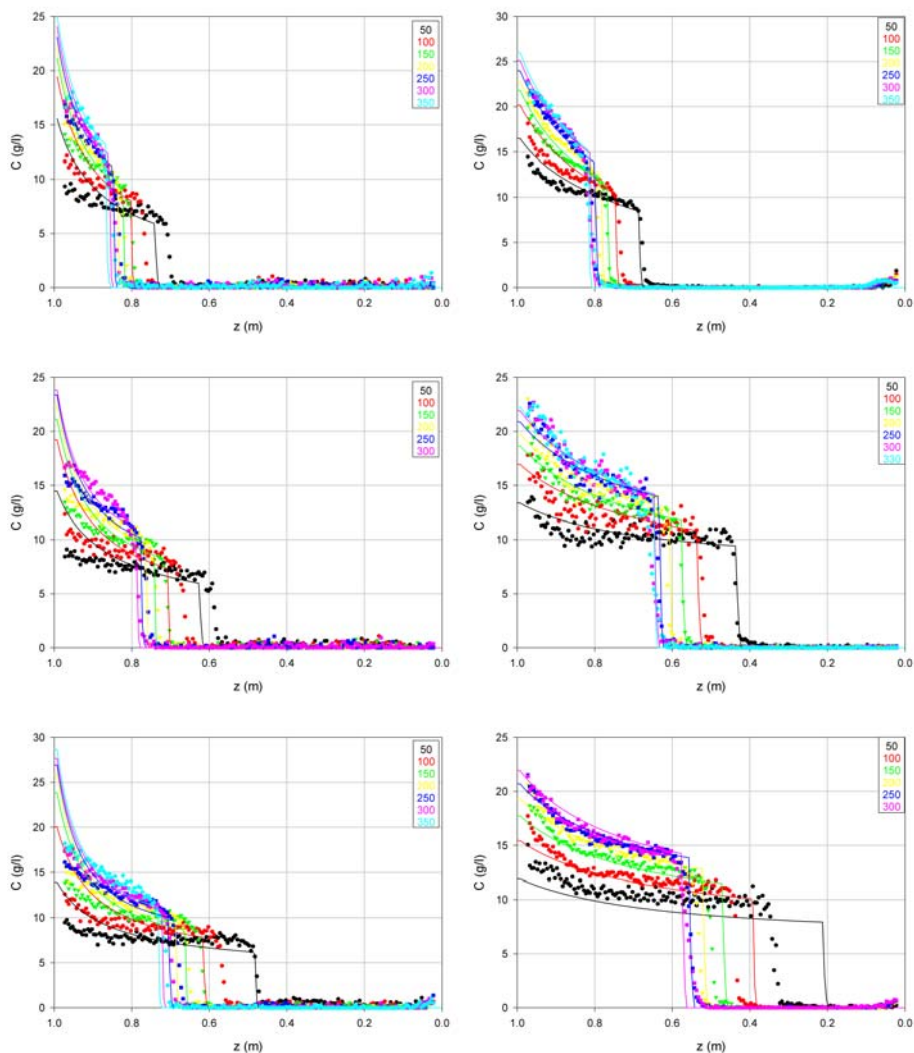


Figure 6.14: Simulated (lines) and measured (symbols) solids concentration profiles in height at different times (indicated in minutes in legend) during batch settling of Destelbergen sludge (left; top: $C_o=2.40$ g/l; middle: $C_o=3.23$ g/l; bottom: $C_o=4.30$ g/l) and Deinze sludge (right; top: $C_o=3.67$ g/l; middle: $C_o=6.12$ g/l; bottom: $C_o=7.29$ g/l); simulations are done with the batch settling model with the power function and the logarithmic function with the parameter values given in Figure 6.7 and Table 6.3

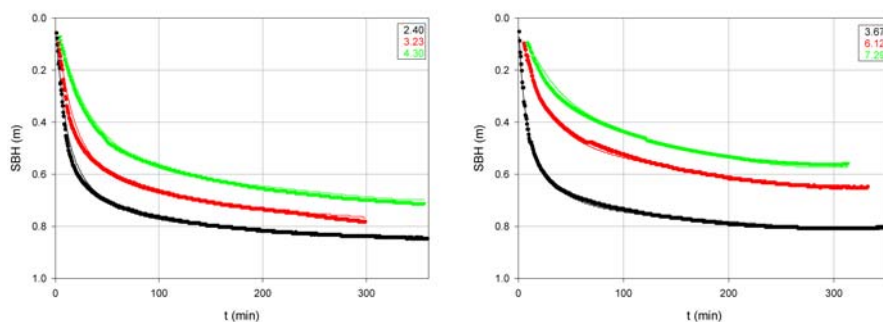


Figure 6.15: Simulated (lines) and experimental (symbols) batch settling curves (left: Destelbergen sludge; right: Deinze sludge; initial concentrations are given in g/l in legend)

Figure 6.17 shows the resulting effective solids stress function, the effective solids stress calculated from inverse modelling and the effective solids stress calculated from the measured equilibrium solids concentration profiles. There is a small overestimation of the calculated effective solids stresses for the Destelbergen sludge, which is due to the lower final β -values (compare Table 6.4 with Table 6.3). For the Deinze sludge, the agreement is still satisfying, even though the parameters did change.

The value of the resulting effective solids stress function at the bottom of the column and the calculated value of the effective solids stress at the end of the experiments approximates the pressure of the buoyant weight of solids (i.e. $C/\rho_s \Delta \rho g H$). This means that equilibrium is reached at the end for all 6 experiments. This was already shown in Chapter 5 for the Deinze sludge. The simulated equilibrium solids concentration profiles are shown in Figure 6.18. For the Deinze sludge, the profiles show the same trend, except for the one at 3.67 g/l. This is due to the much higher β -value at 3.67 g/l, in comparison with the other 2 experiments of the Deinze sludge. Since measured concentration profiles were used to find/calculate these parameters, the measurements implied this slightly different concentration profile at 3.67 g/l.

To complete the comparison with the initial parameter values and the measurements, the Kynch batch density function was evaluated for both sludges before and after parameter estimation and is compared to the calculated fluxes in Figure 6.19. The estimation with the solids concentration profiles resulted in a higher Kynch batch density function for concentrations around the lowest initial solids concentration as compared to the initial function and measurements.

A characteristic of the experiments was the shape of the iso-concentration lines: they are curved (Burger *et al.*, 2000) and rise from the bottom at different values in time (Font and Laveda, 2000). The calculated iso-concentration lines of the simulations, as shown in Figure 6.20, confirm this.

The simulated solids concentrations inside the sludge blanket for each sludge (Figures 6.21 and 6.22) coincide relatively well for the experiments with different initial concentrations, just like the experiments indicated, except for the experiment at 3.67 g/l. This was due to the higher β -value at 3.67 g/l, as already indicated.

The batch settling model characterized by the Kynch batch density function, effective solids stress function and compression solids concentration evolution is shown in Figure 6.23 for both sludges. Both sludges have a different settling behaviour, which is

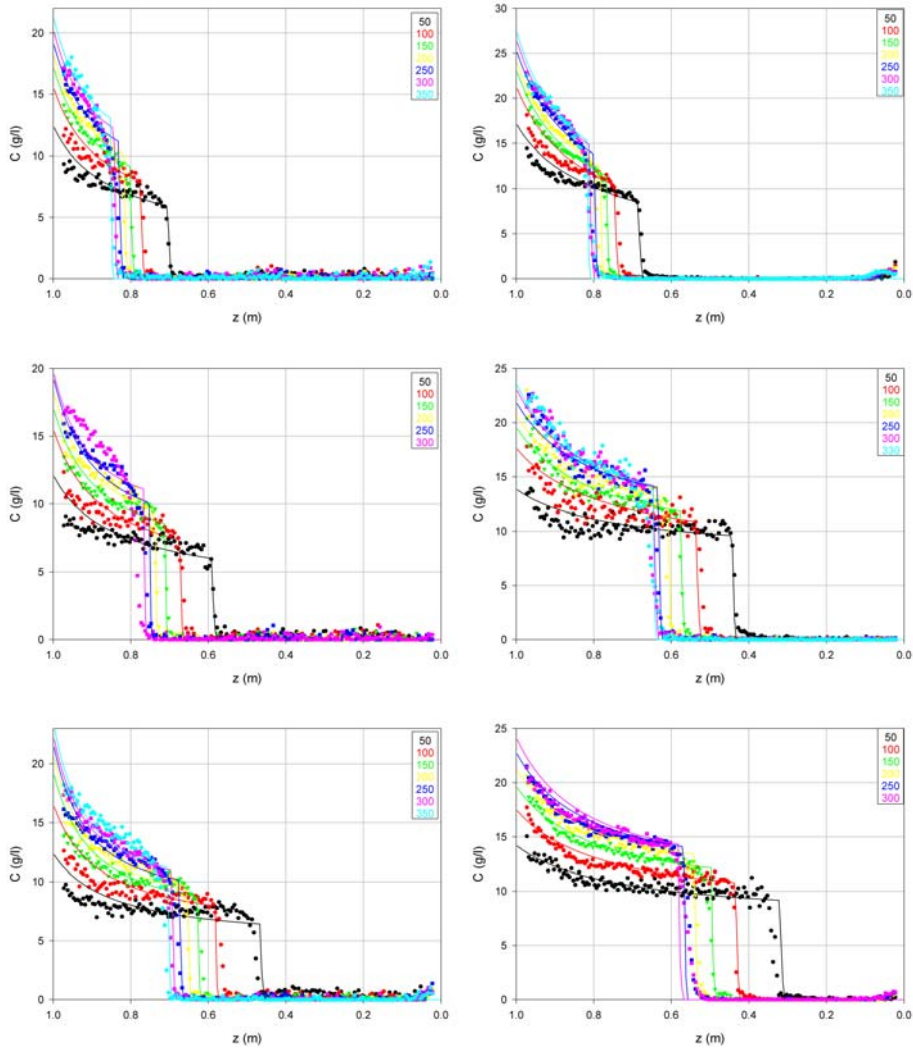


Figure 6.16: Simulated (lines) and measured (symbols) solids concentration profiles in height at different times (indicated in minutes in legend) during batch settling of Destelbergen sludge (left; top: $C_o=2.40$ g/l; middle: $C_o=3.23$ g/l; bottom: $C_o=4.30$ g/l) and Deinze sludge (right; top: $C_o=3.67$ g/l; middle: $C_o=6.12$ g/l; bottom: $C_o=7.29$ g/l); simulations are done with the batch settling model with the power function and the logarithmic function with the parameter values given in Table 6.4)

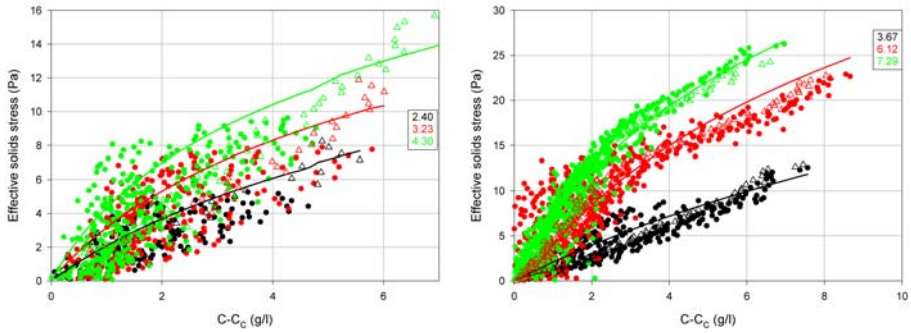


Figure 6.17: Final logarithmic effective solids stress function (line), calculated effective solids stress (circle) and steady-state effective solids stress (triangle) versus solids concentration during batch settling (left: Destelbergen; right: Deinze) (different initial solids concentrations are given in g/l in legend)

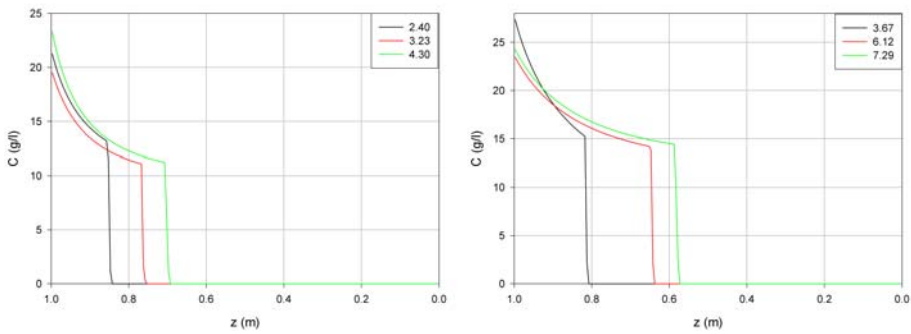


Figure 6.18: Simulated equilibrium solids concentration profiles after batch settling (left: Destelbergen; right: Deinze) (different initial solids concentrations are given in g/l in legend)

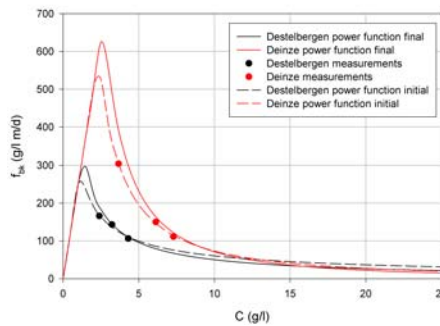


Figure 6.19: Final, measured and initial Kynch batch density function (as indicated in legend) versus solids concentration

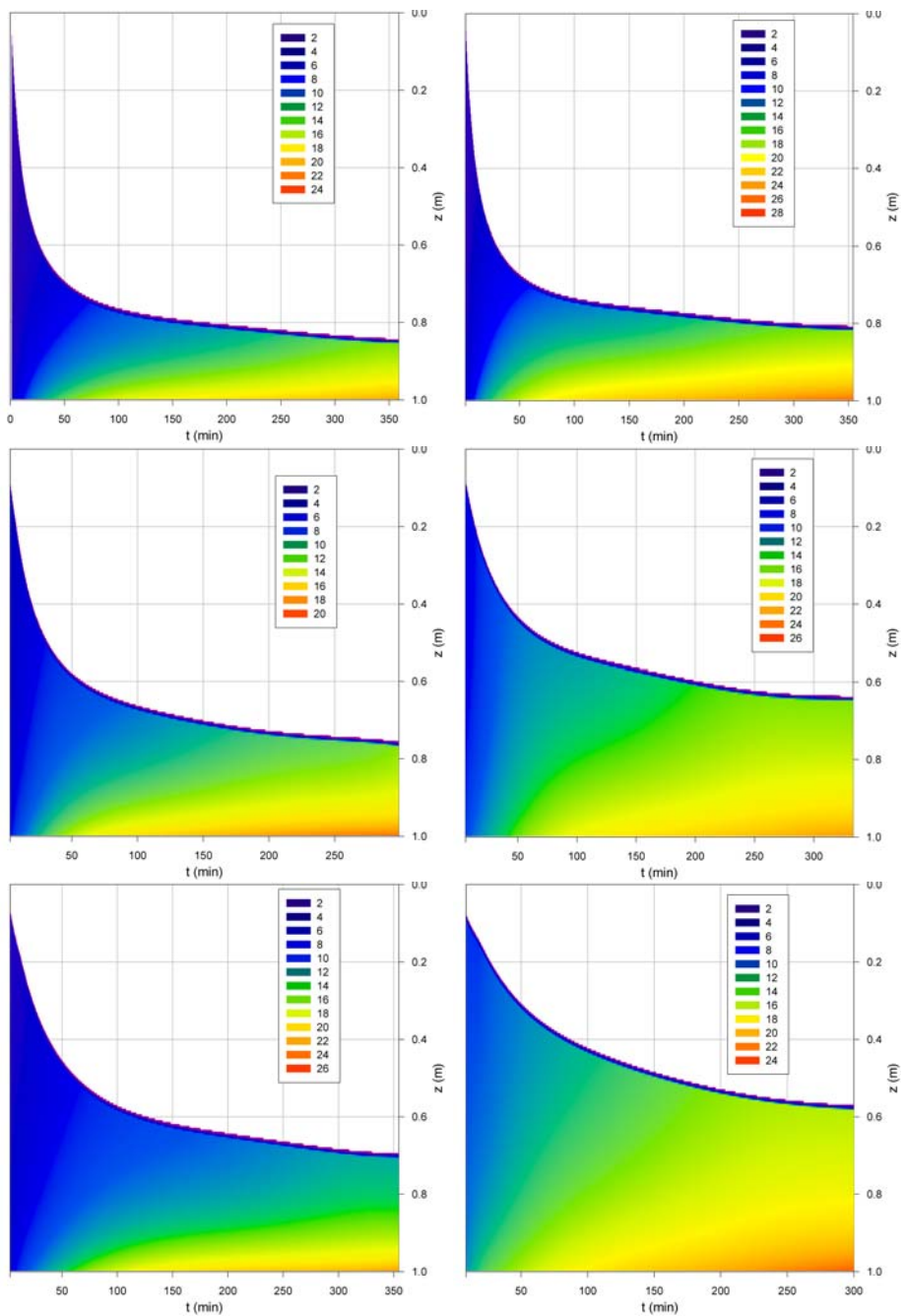


Figure 6.20: Simulated iso-concentration lines (different concentrations shown in legend) during batch settling of Destelbergen sludge (left; top: $C_o=2.40$ g/l; middle: $C_o=3.23$ g/l; bottom: $C_o=4.30$ g/l) and Deinze sludge (right; top: $C_o=3.67$ g/l; middle: $C_o=6.12$ g/l; bottom: $C_o=7.29$ g/l)

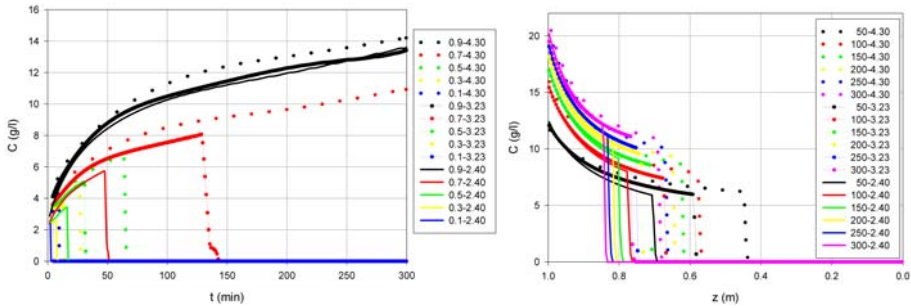


Figure 6.21: Simulated concentration profiles in time at different heights (different heights (m) and concentrations (g/l) are shown in legend) (left) and simulated concentration profiles in height at different times (different times (min) and concentrations (g/l) are shown in legend) (right) during batch settling of Destelbergen sludge

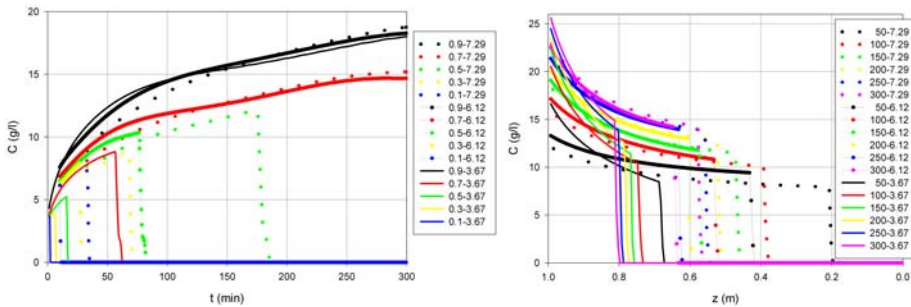


Figure 6.22: Simulated concentration profiles in time at different heights (different heights (m) and concentrations (g/l) are shown in legend) (left) and concentration profiles in height at different times (different times (min) and concentrations (g/l) are shown in legend) (right) during batch settling of Deinze sludge

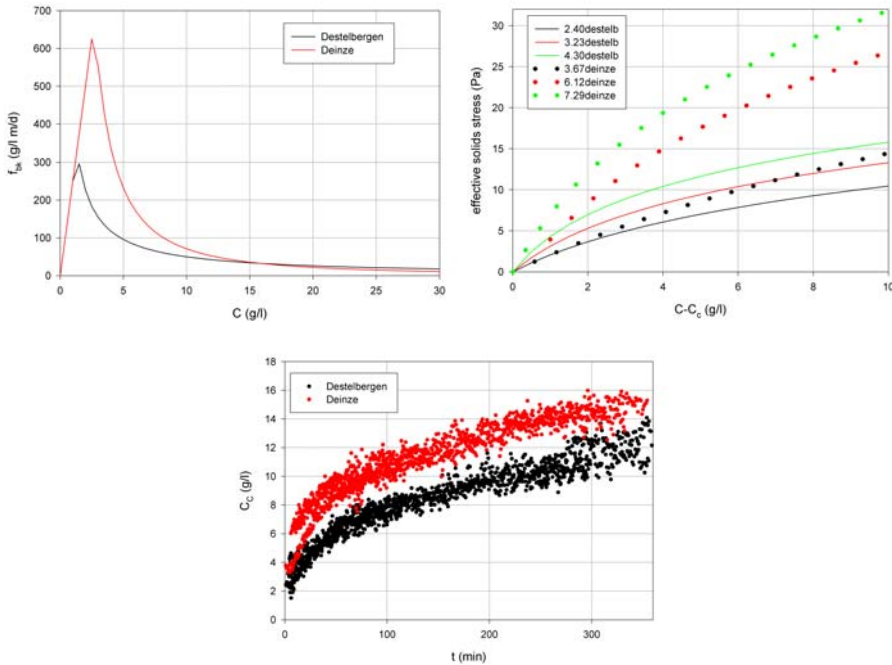


Figure 6.23: Kynch batch density function (top left), effective solids stress function (top right; different concentrations are shown in legend in g/l) and evolution of the compression solids concentration (bottom) for batch settling of Destelbergen and Deinze sludge

evidenced in the model by:

- the Kynch batch density function (higher for the Deinze than for the Destelbergen sludge for solids concentrations lower than 15 g/l)
- the effective solids stress (higher for the Deinze than for the Destelbergen sludge except for the experiment at 3.67 g/l)
- the compression solids concentration (higher for the Deinze than for the Destelbergen sludge)
- the solids density (higher for the Deinze than for the Destelbergen sludge, see Table 5.2), which is needed in the model equation 6.1

6.5 Practical use of the improved model to describe batch settling curve measurements

In practice one cannot expect to have such detailed batch settling experiments available for deriving the settling properties (i.e. the Kynch batch density and the effective solids stress functions with their parameters). Instead, batch settling curves can be frequently measured with a Settrometer (Applitek N.V., Belgium; Vanrolleghem *et al.*

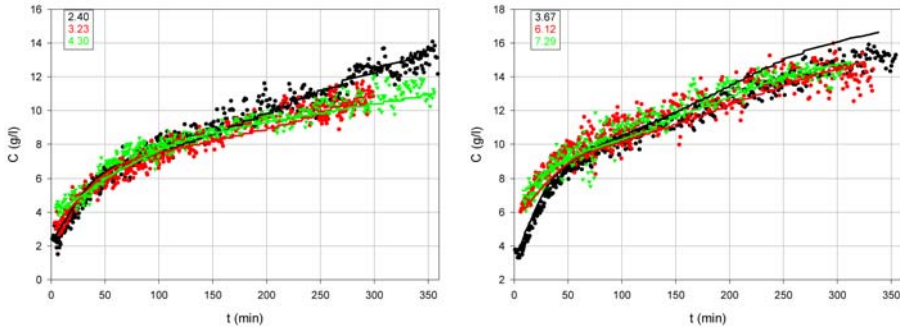


Figure 6.24: Solids concentration at the sludge blanket height according to Kynch (1952)'s theory (line) and compression solids concentration (symbol) versus time during batch settling (left: Destelbergen; right: Deinze) (different initial solids concentrations are given in g/l in legend)

(1996)). In Chapter 8, the proposed batch settling model will be applied to the numerous batch settling curve measurements presented in Chapter 7. How this application is actually performed, is explained below.

When batch settling curves are measured for different solids concentrations, the parameters of the Kynch batch density function can be estimated from the initial settling velocities. The parameters of the effective solids stress function can be estimated using the batch settling curve measurements when the evolution of the compression solids concentration, i.e. the solids concentration at the sludge blanket height in the current model, is known. To obtain this evolution of C_C the solids concentration at the sludge blanket height can be calculated according to Kynch (1952)'s theory when the settling is in the first falling rate period, as follows:

1. determine the tangent at each point i of the batch settling curve
2. draw a straight line through point i with that tangent
3. determine the intercept of this straight line: H_i
4. the solids concentration at point i equals the initial solids concentration times the initial sludge height divided by H_i

As shown in Figure 6.24, when this method is applied to the highly detailed batch settling experiments reported in this Chapter, the solids concentrations at the sludge blanket height coincide fairly well with the compression solids concentrations calculated using the maximum concentration gradient method described in section 6.3.2. Only after 250 minutes, the solids concentration was higher than the compression solids concentration for the experiment at 3.67 g/l. This time, i.e. after 250 minutes, is however a lot larger than that during which the batch settling curve is typically measured, i.e. around 30 minutes.

The current batch settling model with the β parameter depending on each particular initial solids concentration tested can be modified/simplified so that β has a functional relationship with the initial solids concentration. One such function that gives satisfying results for the batch settling experiments, is a power function (r-square value of

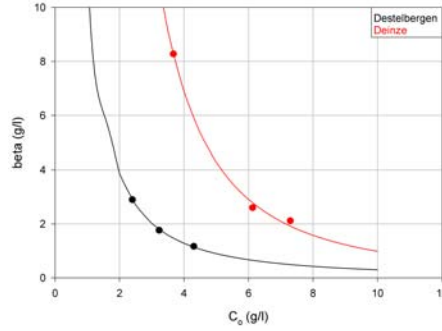


Figure 6.25: β parameter versus the initial solids concentration during batch settling of Destelbergen and Deinze sludge (symbol: parameter value, line: power function)

0.998 for the Destelbergen sludge and 0.997 for the Deinze sludge, Figure 6.25). This will be evaluated in Chapter 8.

6.6 Conclusion

The batch settling experiments of Chapter 5 were used to find appropriate functions for the Kynch batch density function and the effective solids stress. Inverse modelling and calculated initial settling velocities showed that none of the functions reviewed in Chapter 2 was capable of describing the batch settling experiments. A power function for the Kynch batch density function gives a single effective solids stress throughout the experiments with a time-dependent compression solids concentration. This time-dependency was already observed in the batch settling experiments, as well as the fact that the compression solids concentration was located at the sludge blanket height. Inspection of the batch settling experiments allows easy determination of the compression solids concentration evolution. Given the Kynch batch density function and the time-evolution of the compression solids concentration, the functional relationship of the effective solids stress can be determined from inverse modelling. The effective solids stress was shown to exhibit a logarithmic behaviour with the solids concentration. The parameters of both the Kynch batch density function and the effective solids stress function were subsequently estimated from the solids concentration profiles.

The resulting batch settling model is the following:

$$\frac{\partial C}{\partial t} = -\frac{\partial f_{bk}(C)}{\partial z} + \frac{\partial}{\partial z} \left(f_{bk}(C) \frac{\rho_s}{\Delta \rho g C} \frac{d\sigma_e(C)}{dC} \frac{\partial C}{\partial z} \right) \quad (6.9)$$

with boundary conditions and initial condition

$$f_{bk}(C) \left(1 - \frac{\rho_s}{\Delta \rho g C} \frac{d\sigma_e(C)}{dC} \frac{\partial C}{\partial z} \right)_{z=0, z=H} = 0 \quad (6.10)$$

$$C_{t=0} = C_o \quad (6.11)$$

with the Kynch batch density function

$$f_{bk}(C) = aC^{-b} \quad \text{for } \frac{f_{bk}(C)}{C} < 250 \frac{m}{d} \quad (6.12)$$

$$f_{bk}(C) = 250 \frac{m}{d} C \quad \text{for } \frac{f_{bk}(C)}{C} \geq 250 \frac{m}{d} \quad (6.13)$$

and the effective solids stress function

$$\sigma_e(C) = \alpha \ln \left(\frac{C - C_C + \beta}{\beta} \right) \quad \text{for } C > C_C \quad (6.14)$$

$$\frac{d\sigma_e(C)}{dC} = 0 \quad \text{for } C \leq C_C \quad (6.15)$$

The model describes the settling behaviour significantly better than any other model reported in literature and this for sludges originating from two different wastewater treatment plants. This indicates a good potential for wider applicability of the model. By performing batch settling experiments at lower solids concentrations with a settling velocity lower than 250 m/d (i.e. located in the increasing part of the settling flux function), a Kynch batch density function could be found which also describes the settling (and the concentration profiles) at these lower solids concentrations. In Chapter 8 the Kynch batch density function was extended with the Vesilind function to describe such behaviour since the measured batch settling curves (Chapter 7) were performed at solids concentrations which were located in the increasing part of the settling flux curve. This extension for the lower solids concentrations needs to be validated by performing and simulating extensive batch settling experiments (Chapter 5 at these concentrations).

In practice, extensive experimental data as collected in Chapter 5 are not available to identify the settling behaviour. In most cases a number of batch settling curves collected with different initial solids concentrations are. At least 3 batch settling curves need to be measured, i.e. at 3 quite different solids concentrations, in order to estimate the parameters of the model.

When the settling behaviour, i.e. the parameters of the batch settling model, is identified, this can be used to simulate continuous settling. Those 2 aspects, i.e. describing the settling behaviour by modelling batch settling curves with the batch settling model and modelling 1D continuous settling, are the subject of Chapter 8.

Since the batch settling model describes the settling behaviour better than any other reported model, 1D, 2D or 3D continuous settling models which attempt to describe the full-scale behaviour of a clarifier and which incorporate the batch settling model can be used e.g. to make better designs and set-up better control strategies.

Chapter 7

Full-scale continuous settling experiments

As stated in Chapter 3, continuous settling models require extensive testing with high-quality **full-scale dynamic data**. For that purpose, two detailed full-scale measurement campaigns were performed, providing measurements of solids concentration profiles in the clarifier, sludge blanket heights, concentrations of the relevant flows (feed, recycle and effluent), batch settling experiments and sludge volume index (SVI). One of them was performed on the secondary clarifier of the municipal WWTP of Essen and the other one on a no longer operational primary clarifier of the municipal WWTP of Heist, which was converted into a secondary clarifier. The first one is referred to as the Essen data (Le Poulichet, 2001), the second one as the Heist data (Onillon, 2003).

7.1 Experimental results obtained at the Essen WWTP

First, the material and methods are described. Next, an overview is given of the measurement results. Afterwards, the results are discussed more thoroughly in order to identify the effect of changes in load and settling properties on the behaviour of the clarifier.^{1 2}

7.1.1 Material and methods

Plant details

The municipal WWTP of Essen is designed for 11 000 PE. The plant has a biological treatment (with nitrification/denitrification and chemical phosphorous removal with

¹Part of these experimental results are published as Jeriffa De Clercq, Martijn Devisscher, Ivo Boonen, Peter A. Vanrolleghem and Jacques Defrancq (2003). A New One-dimensional Clarifier Model - Verification Using Full-scale Experimental Data. *Water Science & Technology*, 47 (12), 105-112.

²Part of these experimental results are published as Jeriffa De Clercq, Martijn Devisscher, Ivo Boonen, Peter A. Vanrolleghem and Jacques Defrancq (2005). Analysis and simulation of the sludge profile dynamics in a full-scale clarifier. *Journal of Chemical Technology & Biotechnology*, 80 (5), 523-530.

FeCl₃) and a secondary clarifier. It treats municipal wastewater and industrial wastewater from a carpet, candy and snacks producing company and a metallurgic plant. The lay-out of the plant can be summarized as follows:

1. 2 Archimedes screws; capacity: $2 \times 320 \text{ m}^3/\text{h}$
2. 2 bar screens
3. 1 grit chamber
4. 1 oxidation ditch with an average MLSS of 2.26 g/l and hydraulic residence time of 4.5 h
5. 1 clarifier with a residence time of 1 h

The WWTP has to meet the following effluent standards: BOD₅= 25 mg/l, COD= 125 mg/l, SS= 35 mg/l, N_{tot}= 15 mg/l and P_{tot}= 3 mg/l.

Clarifier specifications

The circular centre-fed clarifier is 19.3 m in diameter with a 1.88 m sidewall depth and a 2.56 m depth at the centre, and is operated in such a manner that the sludge blanket height lies between 0.1 and 0.5 m of height. The influent enters at a central feed well with a diameter of 4.5 m and a depth of 1.18 m. A baffle plate with a diameter of 4.9 m is placed below the feed well at a depth of 1.75 m to break the density currents and deflect them sideways. The sludge at the bottom is scraped to a central hopper. Two Archimedes screws with capacities of 316 m³/h and 158 m³/h respectively, recycle the sludge. Figure 7.1 shows drawings of the top-view and side-view and a picture of the clarifier.

On-line measurements

Solids concentration profiles and the **sludge blanket height** were measured every hour, respectively every 10 minutes, with a Staiger-Mohilo 7210 MTS sensor. The height of the sludge blanket was defined to be the height where the solids concentration reached 0.8 g/l. The Staiger-Mohilo 7210 MTS sensor, shown in Figure 7.2, consists of a microprocessor-based analyzer with 2 analog outputs for suspended solids and height, a stepping motor and controller and a Staiger-Mohilo 7510 SAM for optical detection of the suspended solids concentration (range 0-10 g/l). The principle of detection is based on a four-beam intensity compensation technique (Edwards, 1998).

Batch settling curves were measured using a Settrometer (Applitek N.V., Belgium; Vanrolleghem *et al.* (1996)). The Settrometer as shown in Figure 7.3 is a down-scaled version of a secondary clarifier designed in such a way to avoid wall effects and prevent solids from bridging. The down-scaled clarifier has a capacity of 10 litres, a diameter of 14 cm and a height of 70 cm. With an external light source and a moving light-intensity scanner, the sludge blanket height is continuously detected.

The **effluent flow rate** was measured with an ultrasonic meter (Swedmeter LF300/T).

Off-line measurements

A sampler system with 24 liter Polyethylene Bottles (Sigma 900), shown in Figure 7.4, was used to take samples of the inlet mixed liquor, recycle sludge and effluent every

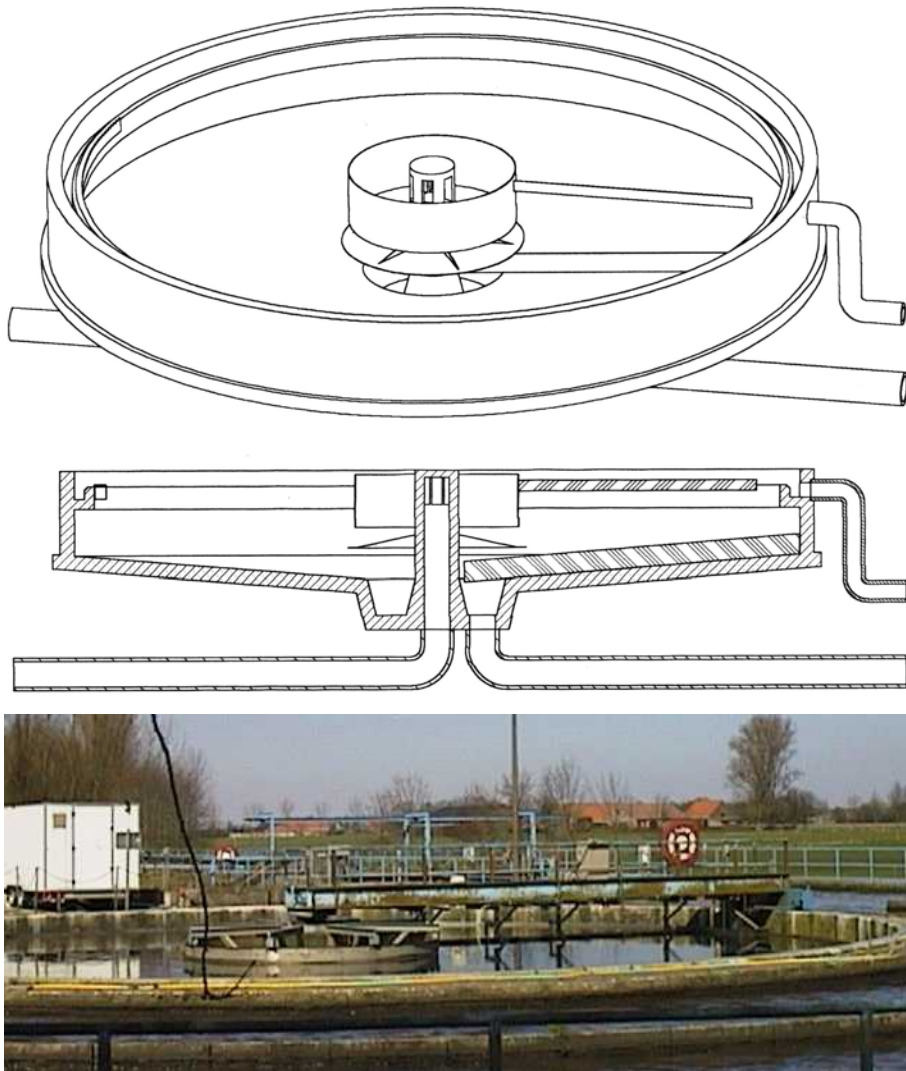


Figure 7.1: A top-view (top), side-view (middle) drawing and picture (bottom) of the clarifier of the municipal WWTP of Essen



Figure 7.2: The Staiger-Mohilo 7210 MTS sensor

2 or 4 hours. The samples were stored at 4°C. Subsequently, the total suspended solids concentration of inlet mixed liquor, recycle sludge and effluent, sludge volume index SVI and non-settleable suspended solids concentration of the mixed liquor were measured according to Standard Methods (1995).

7.1.2 Results of the measurements at the Essen WWTP

Measurements were performed from February 20th 2001 until March 22nd 2001 (30 days). During this period, there was a lot of rainfall and as a result of that the feed concentration into the clarifier increased from 2 g/l up to 5 g/l due to the accumulation of solids released from the sewer. During 3 days (March 12th until March 15th), the recycle flow rate was reduced by 50 % from 316 to 158 m³/h and during 2 days (March 21st until the end), the recycle flow rate was increased with 50%, i.e. from 316 to 475 m³/h. The changes in flow rates are shown in Figure 7.5, as well as the off-line measured solids concentrations. The change in recycle flow rate clearly had an impact on the recycle and subsequently feed solids concentrations. The effluent solids concentrations violated the yearly effluent standard (35 mg/l) a few times (but it does not necessarily violates the consents) but approximated the non-settleable solids concentrations, indicating that the clarifier is working properly.

The aforementioned changes in operation resulted in quite some variation in load to the clarifier (at the end the load was almost 4 times higher than the initial load). Figure 7.6 shows the measured sludge blanket height (SBH) and load $Q_f \cdot C_f$ versus time. The sludge blanket height and the load appear to be correlated.

Figure 7.7 shows the evolution of the measured solids concentration profiles. It is clear that sludge is accumulating as the sludge load increases. The high concentrations measured at the surface of the clarifier (below 0.5 m) are an artefact caused by scum that attaches to the sensor when it moves out of the water and returns into the water.



Figure 7.3: The Settrometer (Applitek N.V.; Vanrolleghem *et al.* (1996))



Figure 7.4: The Sigma 900 refrigerated sampler system

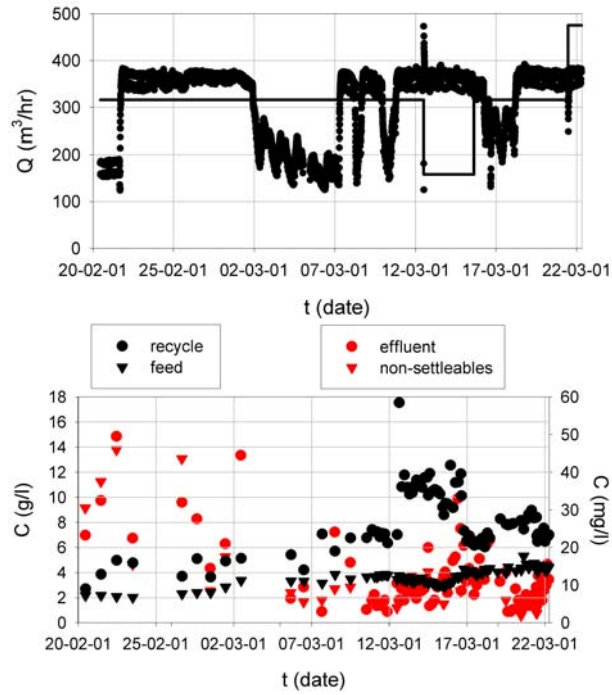


Figure 7.5: Effluent (symbol) and recycle (line) flow rates versus time (top) and recycle (left axis), feed (left axis), effluent (right axis) and non-settleable (right axis) solids concentrations versus time (bottom); Essen data

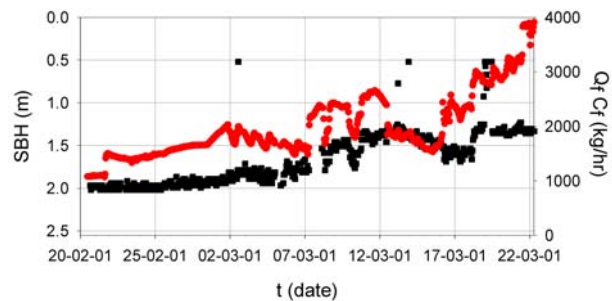


Figure 7.6: Sludge blanket height (black symbol) and sludge load (red symbol) versus time; Essen data

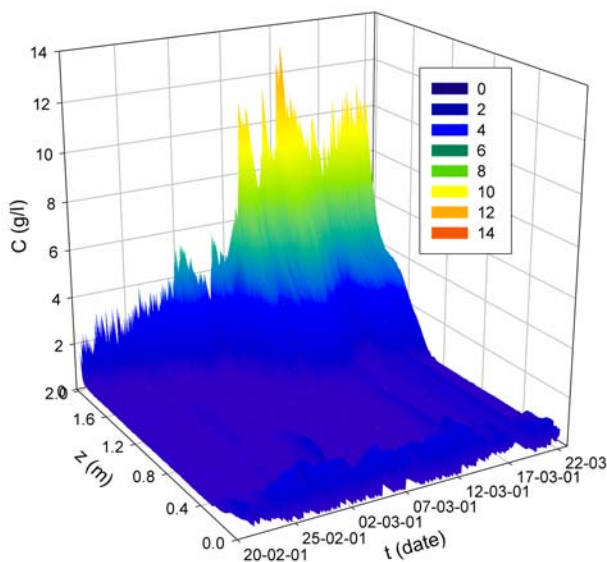


Figure 7.7: Solids concentration profile; Essen data

Only at the end of the measurements (last 5 days), a sludge blanket with a constant solids concentration zone was observed.

During 20 of the 31 days, batch settling curves were recorded with a Settrometer (Vanrolleghem *et al.*, 1996) and on 3 days of these 20, the recording was done for several solids concentrations, as shown in Table 7.1, yielding a total of 82 settling curves. The batch settling curves recorded for several concentrations are shown in Figure 7.8. The induction period and the initial settling velocity at the initial solids concentration were determined for every curve according to the method given in section 6.1. The SVI-values of Table 7.1 show that settling properties changed from good (SVI 50-100) to fair (SVI 100-200) but even became poor (SVI 200-300) (Von Sperling and Froes, 1999). The deterioration was probably due to an increase in the COD load from the industrial wastewater. The initial settling velocities confirm the changes in SVI.

7.1.3 Discussion of the measurement results at the Essen WWTP

The effect of the **load** on the recycle and effluent solids concentration, sludge blanket height and solids profiles are shown in Figure 7.6 and 7.9 together with the changes in **recycle flow rate**.

Increases in load resulted in increasing **recycle solids concentrations** and vice versa. This effect was, however, less pronounced from March 15th on. This could be explained by changes in settling properties (see below). The changing recycle flow rate had a pronounced effect on the recycle solids concentration: a decreasing recycle flow rate resulted in more time for the solids to settle and thicken, which subsequently resulted in a higher recycle solids concentration, and vice versa.

The **effluent solids concentrations** did not show any clear relationship with the load nor the recycle flow rate.

Table 7.1: Number of batch settling curves (N) measured each day (t) at a certain sludge concentration (C), the SVI measured off-line at the feed concentration ($C=C_f$, except for the \diamond -days on which batch settling curves were measured at different solids concentrations, obtained by diluting recycle or feed sludge with effluent) and the corresponding initial settling velocity $V_{hindered}$; Essen data

t (date)	N	C (g/l)	SVI (ml/g)	$V_{hindered}$ (m/d)
20/02/01	24	2.1	88	132
21/02/01	13	2.2	91	133
22/02/01	3	2.1	98	110
23/02/01	1	2.0	121	72
24/02/01	-		-	
25/02/01	-		-	
26/02/01	2	2.3	-	81
27/02/01	1	2.4	-	58
28/02/01 \diamond	6	4.3; 3.6; 3.2; 2.4; 1.7; 1.0	162	29; 36; 51; 85; 119; 150
01/03/01	2	2.9	140	48
02/03/01	-		155	
03/03/01	-		-	
04/03/01	-		-	
05/03/01	2	3.3	216	26
06/03/01 \diamond	5	4.2; 3.5; 2.4 1.6; 0.8	231	13; 24; 41; 77; 156
07/03/01	2	3.2	219	25
08/03/01	2	3.8	221	24
09/03/01	1	3.4	201	27
10/03/01	-		-	
11/03/01	-		-	
12/03/01	1	3.5	159	24
13/03/01	1	3.3	153	28
14/03/01	4	3.2	142	41
15/03/01 \diamond	6	9.2; 8.8; 6.6; 3.8; 2.0; 0.9	152	6; 6; 13; 29; 91; 138
16/03/01	2	3.8	121	44
17/03/01	-		-	
18/03/01	-		-	
19/03/01	6	4.2	98	33
20/03/01	2	4.5	96	36
21/03/01	-		101	
22/03/01	-		88	

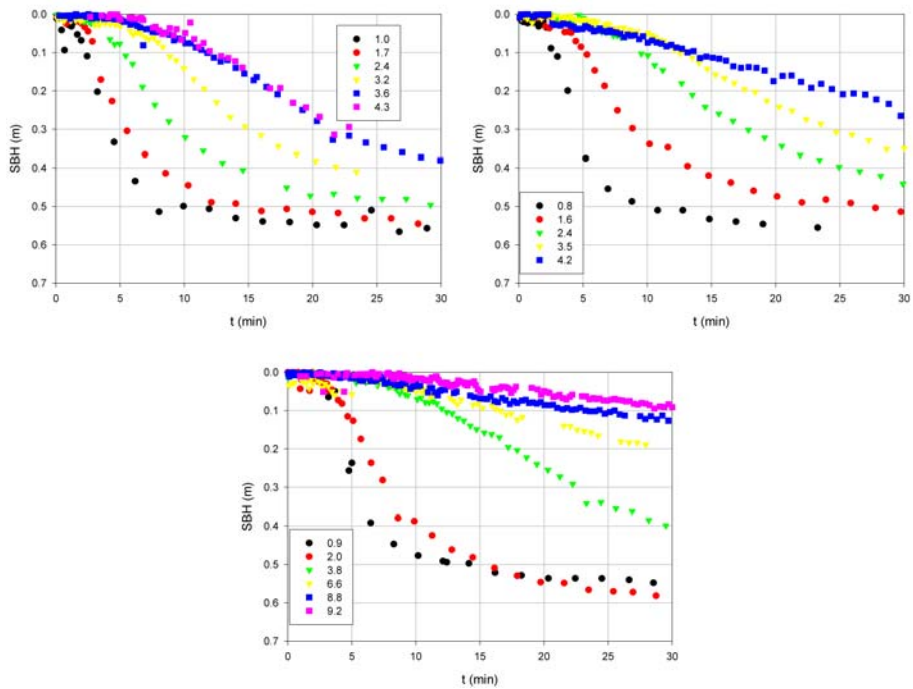


Figure 7.8: Batch settling curves measured with the Settlometer on February 28th (top left), March 6th (top right) and March 15th (bottom) for different solids concentrations (indicated in g/l in legend); Essen data

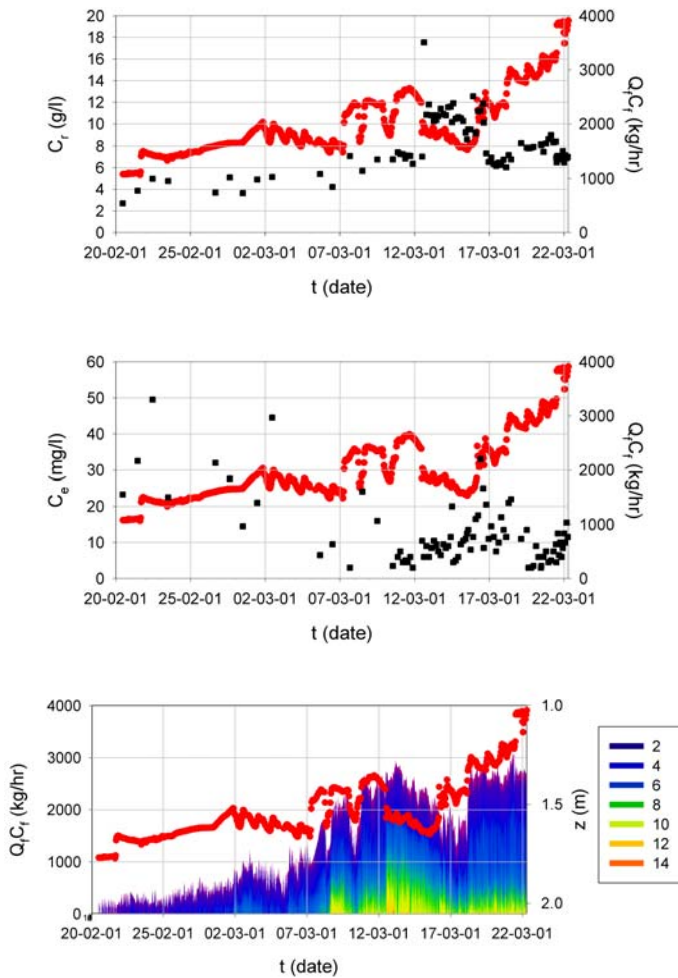


Figure 7.9: Recycle (top), effluent (middle) solids concentration (black symbol) and solids concentration profile (bottom, legend: concentration in g/l) and sludge load (red symbol) versus time; Essen data

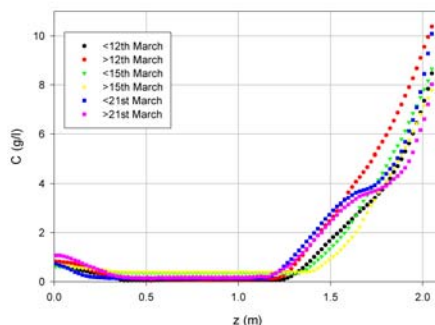


Figure 7.10: Solids concentration profile versus depth before and after changes in recycle flow rate on March 12th, March 15th and March 21st; Essen data

When the load increased, the **sludge blanket height** shifted upwards, and vice versa. However exceptions were found around March 2nd, March 5th and from March 15th onwards. Again changes in settling properties are believed to be responsible for this. The variations of the recycle flow rate did not result in a significant change of the sludge blanket height, in contrast to what was expected. Conversely, changes in recycle flow rate do result in changing residence times which enables the solids to settle and thicken better. Since no significant effects were observed in the sludge blanket height, the recycle flow rate had to affect the recycle solids concentration and **solids concentration profiles**: the profiles indeed showed more thickening when the recycle flow rate decreased. The sludge blanket with constant concentration zone which was observed during the last 5 days, had a concentration of about 3.6 g/l which was lower than the feed solids concentration of about 4 g/l.

When the load increased, the total mass of solids in the clarifier increased, and vice versa. This was clearly seen in the period from March 2nd onwards. Increases in recycle flow rate resulted in decreasing mass of solids in the clarifier and vice versa. Especially the decrease in the recycle flow rate showed a significant shift of mass from the aeration tank to the clarifier. After the decrease in recycle flow rate, the feed concentration decreased with time, which subsequently resulted in a lower sludge blanket height and recycle solids concentration, a counter-intuitive result. The effect of changing recycle flow rate is shown in more detail in Figure 7.10. The decrease in recycle flow rate at March 12th resulted in a shift upwards of the concentration profile. This shift was more pronounced for the higher concentrations than for the concentrations near the sludge blanket height. The increase in recycle flow rate at March 15th showed a shift downwards of the concentration profile. The increase in recycle flow rate at March 21st showed a similar shift downwards but the shift was again more pronounced for the higher concentrations in comparison with the concentrations at the sludge blanket height.

The effect of **SVI** on **sludge blanket height, recycle and effluent solids concentration and solids profiles** is shown in Figure 7.11. A higher SVI is expected to result in a shift upwards of the sludge blanket height, and vice versa. This is clearly seen in the evolution of the sludge blanket height (and solids concentration profile) around March 2nd (SVI increased from 140 to 155 ml/g), March 6th (SVI increased from 216 to 231 ml/g) and from March 15th (SVI decreased while sludge load in-

creased). No effect of SVI on the recycle and the effluent solids concentration and solids concentration profile could be determined from the data. Modelling of the data has to give more insight in that respect. This will be the subject of Chapter 8.

7.2 Experimental results obtained at the Heist WWTP

First, the material and methods are described. Next, an overview is given of the results of the measurements. Afterwards, the results are discussed more thoroughly in order to identify the effect of changes in flow rates, feed solids concentration and settling properties on the behaviour of the clarifier.

7.2.1 Material and Methods

Plant details

The municipal WWTP of Heist is designed for 91 800 PE. The plant has a biological treatment (with nitrification/denitrification and biological phosphorous removal) and a secondary clarifier. It solely treats municipal wastewater. The lay-out of the plant can be summarized as follows:

1. 2 Archimedes screws (1 for dry weather DWA and 1 for rain weather RWA)
2. 2 bar screens
3. 1 DWA and 2 RWA grit chambers (the water from the 2 RWA grit chambers flows to 3 rain sedimentation tanks)
4. 2 primary clarifiers which are now used for biological phosphorous removal and 2 primary clarifiers which are not used
5. 6 aeration tanks in series
6. 4 clarifiers

The WWTP has to meet the following effluent standards: $BOD_5 = 25$ mg/l, $SS = 35$ mg/l, $NH_4-N = 1$ mg/l, $NO_3-N = 5$ mg/l and $P_{tot} = 2$ mg/l.

Clarifier

One of the non-used primary clarifiers was used in the study to act as a secondary clarifier. The circular centre-fed clarifier is 18 m in diameter with a 1.92 m sidewall depth and a 2.41 m depth at the centre. The influent enters at a central feed well with a diameter of 3.6 m and a depth of 1.02 m. The sludge at the bottom is scraped to a central hopper. The feed was taken just before the aeration tank overflow, the recycle was pumped to the biological phosphorous 'removal clarifiers' and the effluent flowed to the inlet of the aeration tank. Centrifugal pumps were used for the feed and recycle flow. The feed pump had a capacity of 270 m³/hr, the recycle pump 210 m³/hr, but in reality it was observed that the maximum flow rate of the latter was 185 m³/hr. The flow rate of the feed pump was controlled with a manual butterfly valve and the flow rate of the recycle pump with a George Fisher 367 butterfly valve. Pictures of the clarifier, the feed centrifugal pump, and the controllers are shown in Figure 7.12.

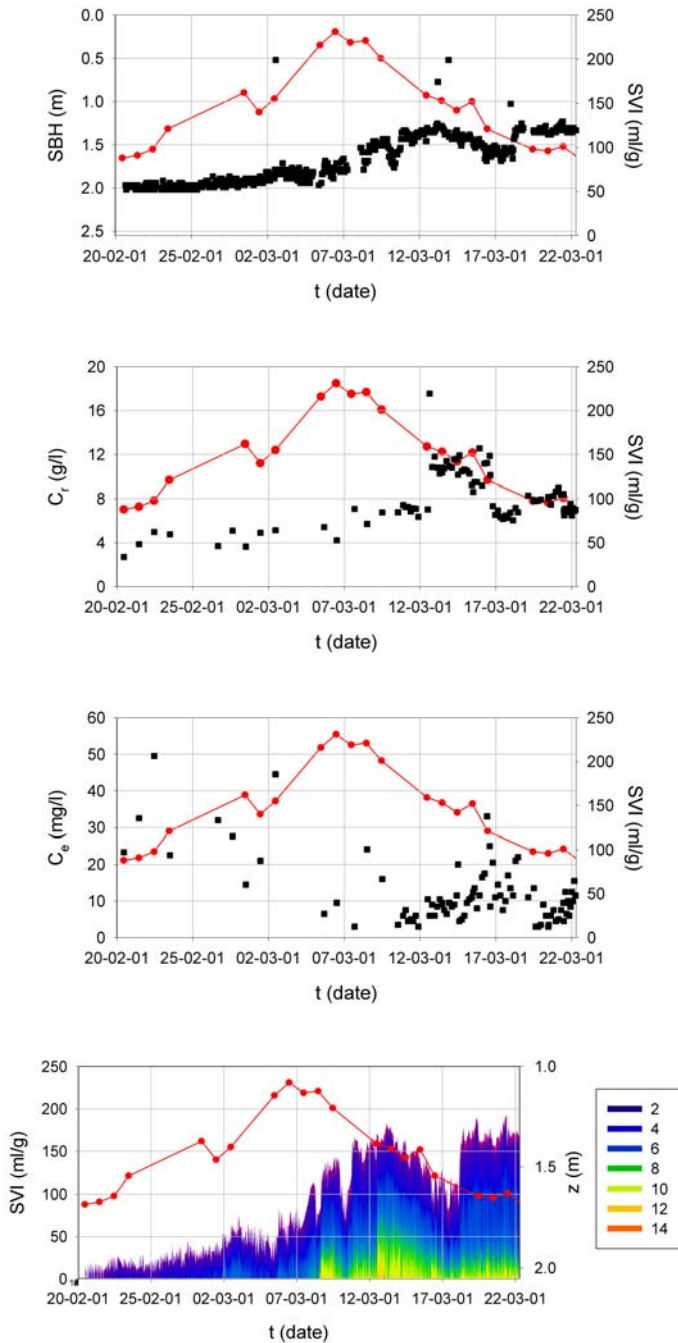


Figure 7.11: Sludge blanket height (top), recycle (second) and effluent (third) solids concentration (black symbol), solids concentration profile (bottom; legend: concentration in g/l) and sludge volume index (red symbol) versus time; Essen data



Figure 7.12: Pictures of the clarifier (top), the feed centrifugal pump (bottom left), the feed valve (bottom middle) and the recycle valve (bottom right) of the Heist WWTP

The installation of the studied clarifier among the biological treatment of the plant is shown in Figure 7.13. This unique set-up at full-scale offered a lot of opportunities because the effluent of the studied clarifier did not have to meet any standard.

On-line measurements

Feed and recycle flow rates were measured with 2 electromagnetic meters MAGFLO MAG 3100.

Solids concentration profiles and **sludge blanket height** were measured every 10 minutes with the Staiger-Mohilo 7210 MTS sensor (see section 7.1.1). The height of the sludge blanket was defined to be the height where the solids concentration reached 0.8 g/l. The sensor was placed at a radius of 4.5 m from the centre of the clarifier, at this distance the water level was situated at 2.25 m.

Batch settling curves were measured using a Settrometer (Applitek N.V., Belgium; Vanrolleghem *et al.* (1996)) (see section 7.1.1) which was programmed now to automatically dilute the sample and measure batch settling curves at different initial solids concentrations. The recycle, instead of the feed, was always fed to the Settrometer, in order to have the largest possible concentration range, and dilution was performed with effluent. The dilution were set at 0% (i.e. no dilution), 30%, 60%, 70% and 80% (i.e. 4 parts of effluent, 1 part of recycle activated sludge).

A **circuit** with different loops, shown in Figure 7.14, allowed for the measurement of **effluent, feed and recycle solids concentrations** at regular time intervals of 15 minutes. They were fed by small submerged pumps for the effluent, feed and recycle.

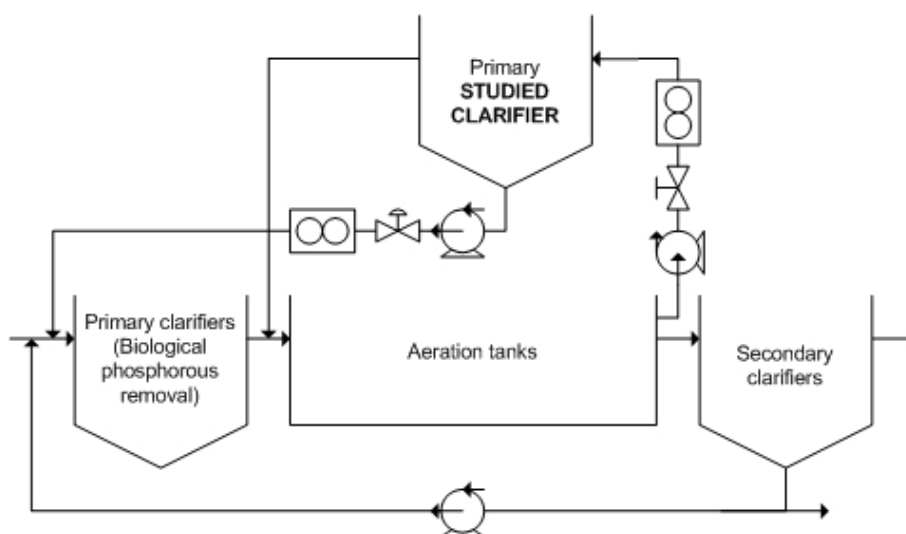


Figure 7.13: Studied clarifier and biological treatment of the Heist WWTP

The solids concentrations of the various lines were measured with a Staiger-Mohilo 7530 SSN (range 0-1000 NTU) for the effluent solids concentration and a Staiger-Mohilo 7510 SAM (range 0-10 g/l) for the feed and recycle solids concentrations for the first period. The measurement principle was explained in section 7.1.1.

The Staiger-Mohilo 7530 SSN did however not work properly, even under different circumstances (changing the direction of the probe from cocurrent to countercurrent with the flow, measuring the overflow of the clarifier, measuring in a volume of 10 liters where the effluent flowed continuously). Because of the low range of the Staiger-Mohilo 7510 SAM (under certain circumstances, the recycle solids concentrations reached values higher than 10 g/l) and of the problems encountered with the Staiger-Mohilo 7530 SSN, 2 sampler systems (Sigma 900, see section 7.1.1) were used to take samples of the effluent and recycle every 4 hours and solids concentrations were measured off-line. For the second period, 2 Dr. Lange Solitax probes were used, one for the effluent solids concentration and one for the feed and recycle solids concentration. The measuring principle of the probes (range 0-150 g/l) is based on a combined infrared absorption/scattered light process. The circuit also provided the feed necessary for the Settrometer: when this one asks for recycle sludge, the circuit is automatically changed in such way that recycle sludge is fed to the Settrometer. The effluent is permanently available for dilution and rinsing of the Settrometer.

A **T-BOX** (TechnoTrade) was installed to allow complete control of the clarifier status. The T-BOX is a programmable controller with telecontrol, it archives a very large volume of information and it includes an alarm notification system. Some of the on-line measurements were recorded and transmitted by the T-BOX to Aquafin N.V. and Ghent University.

Off-line measurements

The total suspended solids concentration of inlet mixed liquor, recycle and effluent and sludge volume index were measured according to Standard Methods (1995). The concentration sensors were calibrated frequently with off-line measurements of about

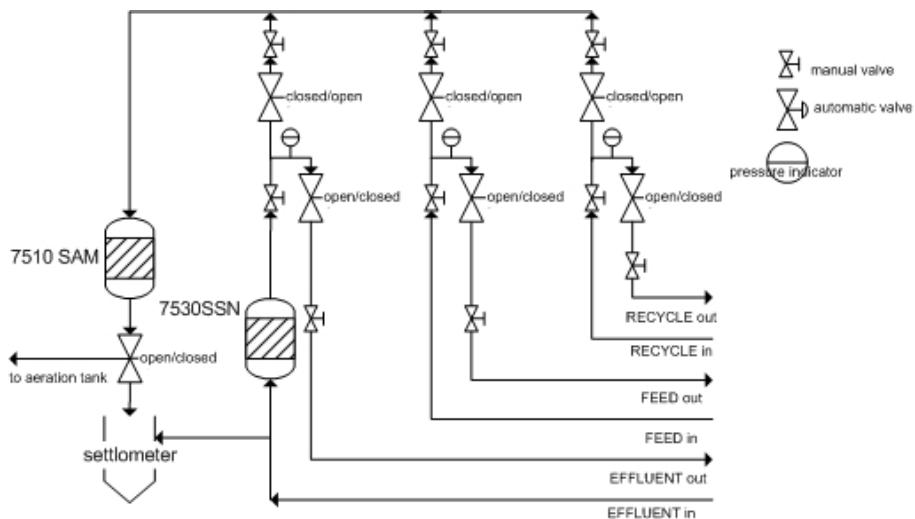


Figure 7.14: Circuit with different loops for on-line measurement of effluent, feed and recycle concentrations; Heist data

6 to 8 samples with different concentrations (Onillon, 2003).

7.2.2 Results of the measurements at the Heist WWTP

Measurements were performed from 22th January 2003 until 28th February 2003, which will be called the first period, and from March 21th 2003 until April 15th 2003, referred to as the second period. During the first period, a lot of problems with the sensors were encountered, whereas during the second period, less problems occurred. The problems are summarized in Table 7.2. Unreliable data were omitted from the results.

Independent variables

It was intended to change the **feed and recycle flow rates** frequently (i.e. every 1-3 days). The changes in feed and recycle flow rate, together with the resulting effluent flow rate, surface load and recycle ratio are given in Table 7.3. The surface load was always lower than 1 m/hr, which is recommended for sludge with poor settling properties. The recycle ratio even became higher than 1, which is hardly ever encountered. This was due to the fact that the 2 centrifugal pumps had approximately the same capacities and that for a surface load of 1 m/hr, the recycle flow rate should almost be nihil. Figure 7.15 gives a clear overview of the set-up of the flow rates.

The **settling properties**, expressed by SVI, are shown in Figure 7.16 and changed from fair (SVI 100-200) to poor (SVI 200-300) and even became very poor (SVI 300-400) (Von Sperling and Froes, 1999). A lot of filamentous organisms were observed with the microscope when the SVI was higher than 300. Around these times, maintenance works were conducted on the secondary clarifiers of the WWTP. The settling properties were worse in the second period as compared to the first. In total, 415 batch settling curves were recorded by the Settrometer. Per day, this means an average of 14

Table 7.2: Problems encountered in the operation and measurements of the Heist data

FIRST PERIOD	
29/01/03 16:30 until 31/01/03 16:30	no reliable data: scraper mechanism failed several times
31/01/03 19:00 until 03/02/03 16:30	transmission of profile and SBH measurements failed
07/02/03 01:00 until 07/02/03 12:00	no reliable feed and recycle solids concentration measurements: sludge stuck on Staiger-Mohilo 7510 SAM sensor
10/02/03 13:00 until 10/02/03 17:30	no reliable data: problems with feed and recycle pump: clarifier operation was stopped
10/02/03 19:30 until 11/02/03 13:30	transmission of profile and SBH measurements failed
11/02/03 17:30 until 21/02/03 14:30	1.recycle pump failed when increasing its flow rate to 200 m ³ /hr: clarifier operation was stopped
	2.transmission of profile and SBH measurements failed
	3.clarifier operation was stopped again
	4.transmission of profile and SBH measurements failed
	5.Staiger-Mohilo 7510 SAM sensor of the Staiger-Mohilo 7210 MTS sensor was torn off
	6.clarifier operation was stopped and drained on 18/02/03 until 21/02/03 14:30 (sensor was repaired)
21/02/03 14:30 until 25/02/03 12:30	problems with recycle sampling pump
21/02/03 14:30 until 28/02/03 13:30	only few data available of Staiger-Mohilo 7210 MTS sensor due to problems with transmission and broken electronic cards
SECOND PERIOD	
21/03/03 13:00 until 25/03/03 13:00	repaired electronic cards of Staiger-Mohilo 7210 MTS sensor do not work due to mistake of supplier
05/04/03 00:00 until 08/04/03 9:50	no concentration profile measurements: sludge stuck onto Staiger-Mohilo 7210 MTS sensor
07/04/03 9:30 until 08/04/03 9:50	no effluent solids concentration measurements: sludge stuck on Solitax sensor
09/04/03 until 14/04/03	problems with calibration and depth-measurement of Staiger-Mohilo 7210 MTS sensor
10/04/03 13:00 until 11/04/03 13:00	No feed solids concentration and flow rate measurements
11/04/03 14:10 until 15/04/03 end	Solitax for effluent solids concentration gave unrealistically fluctuating values
11/04/03 18:00 until 15/04/03 9:30	sludge stuck on the Staiger-Mohilo 7210 MTS sensor
15/04/03 00:00 until 15/04/03 7:50	No Solitax data

Table 7.3: Feed, recycle and effluent flow rate, surface load v_o and recycle ratio R; Heist data

Time	Q_f (m ³ /hr)	Q_r (m ³ /hr)	Q_e (m ³ /hr)	v_o (m/hr)	R (-)	
First period A						
1	22/01 ⇒ 24/01 16:00	250	150	100	0.39	1.50
2	24/01 16:00 ⇒ 28/01 11:30	250	100	150	0.59	0.67
3	28/01 11:30 ⇒ 29/01 15:00	250	40	210	0.83	0.19
4	29/01 15:00 ⇒ 01/02 10:00	250	75	175	0.69	0.43
	03/02 ⇒ 05/02 10:45	250	75	175	0.69	0.43
5	05/02 10:45 ⇒ 11/02 16:30	175	125	50	0.20	2.50
6	11/02 19:00 ⇒ 13/02 14:00	250	185	65	0.26	2.85
7	13/02 14:00 ⇒ 15/02	250	125	125	0.49	1.00
8	21/02 14:00 ⇒ 28/02 13:00	175	125	50	0.20	2.50
Second period B						
1	21/03 14:00 ⇒ 25/03 15:30	175	135	40	0.16	3.38
2	25/03 16:00 ⇒ 27/03 14:00	250	185	65	0.26	2.85
3	27/03 14:00 ⇒ 28/03 10:00	250	50	200	0.79	0.25
4	28/03 10:00 ⇒ 1/04 12:00	100	50	50	0.20	1.00
5	1/4 12:30 ⇒ 3/04 9:30	175	50	125	0.49	0.40
6	3/04 9:30 ⇒ 8/04 10:30	175	125	50	0.20	2.50
7	8/04 10:30 ⇒ 10/04 10:00	250	185	65	0.26	2.85
8	10/04 10:00 ⇒ 15/04 11:45	250	125	125	0.49	1.00
9	15/04 11:45 ⇒ 16/04 10:00	250	50	200	0.79	0.25

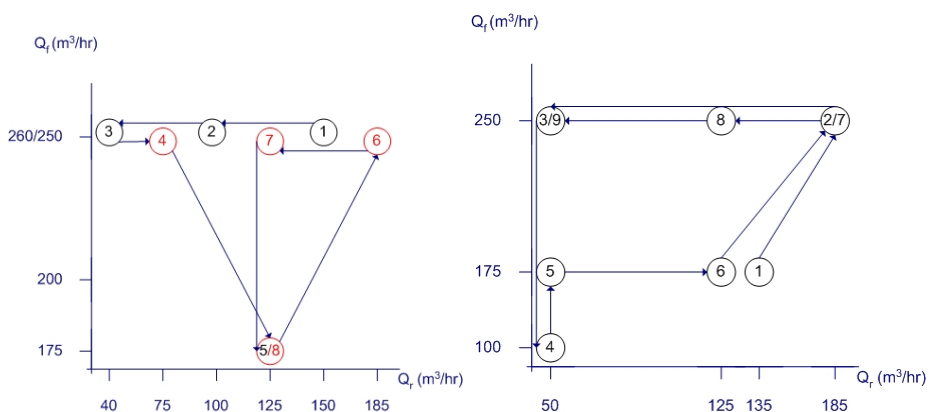


Figure 7.15: Set-up of the feed and recycle flow rates (numbers are related with those of Table 7.3, red points indicate unavailable or unreliable measurement data) (left: first period; right: second period); Heist data

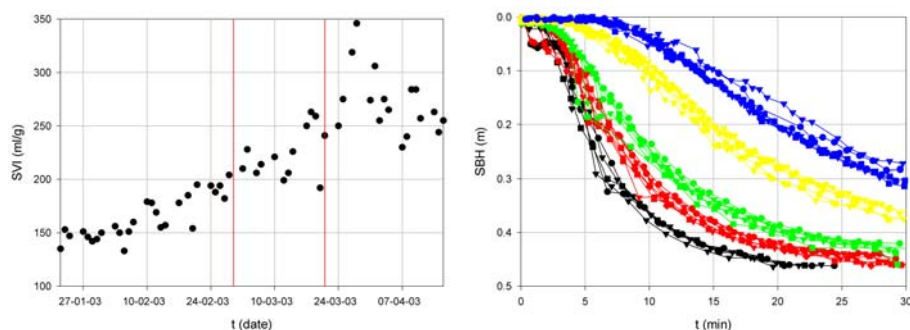


Figure 7.16: Time evolution of the sludge volume index (left; red lines give end of first and beginning of second period) and different batch curves measured on April 4th 2003 (right) (black: 80% dilution, red: 70%, green: 60%, yellow: 30% and blue: 0%); Heist data

batch curves. Figure 7.16 shows the recording on April 4th (24 curves were recorded on that day). The effect of dilution is clearly seen and the induction period is smaller for a higher dilution. The settling properties (and solids concentration) did not change during the whole day because the different curves at the same dilution coincide. The induction period and the initial settling velocity at the initial solids concentration were determined for every curve according to the method given in section 6.1. The settling velocities versus solids concentration for each batch settling curve, as shown in Figure 7.17, confirmed the changing settling properties. The data showed that settling properties did change on a daily basis. Moreover, by investigating the data of each day, it was determined, on an hourly basis, when the settling properties changed. Such changes were found on March 24th and April 3rd.

Because the feed, the recycle and effluent flow are originating from, respectively sent back to the aeration tank, the **feed solids concentration** was not coupled with the

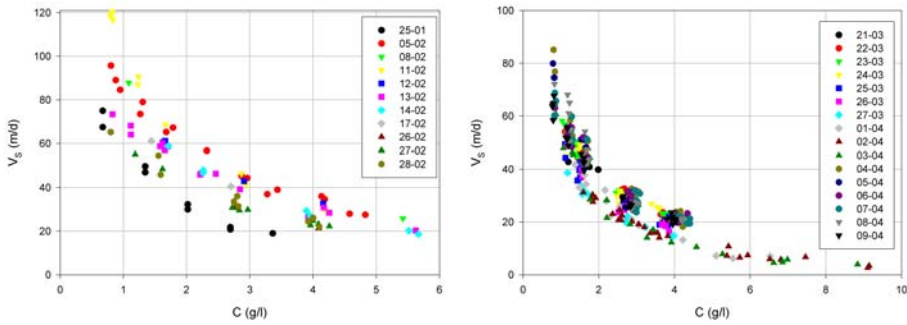


Figure 7.17: Initial settling velocity versus initial solids concentration for different days (date indicated in legend) (left: first period; right: second period); Heist data

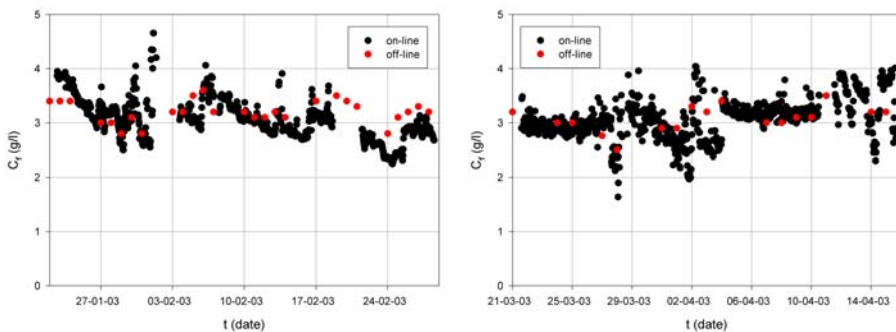


Figure 7.18: On-line and off-line measured feed solids concentration versus time (left: first period; right: second period); Heist data

recycle solids concentration. The evolution of the feed solids concentration with time is shown in Figure 7.18. The feed solids concentration did not vary much with time and in most cases the off-line measured solids concentrations corresponded very well with the on-line ones.

Dependent variables

The evolution of the **recycle solids concentration** is shown in Figure 7.19. The recycle solids concentration varied quite much as expected from the changes in flow rates. The concentrations even exceeded 10 g/l which is out of the measuring range of the Staiger-Mohilo sensor. The off-line measured solids concentrations corresponded very well with the on-line measured solids concentrations, except for concentrations higher than 10 g/l and for the first off-line measured concentration. The latter is discussed more thoroughly further on.

The evolution of the **effluent solids concentration** is shown in Figure 7.20. The on-line concentration measurements of the first period were, as mentioned in section 7.2.1, unreliable. The off-line concentration measurements of the first period did not show much variation with time and were only higher than 35 mg/l for 3% of the mea-

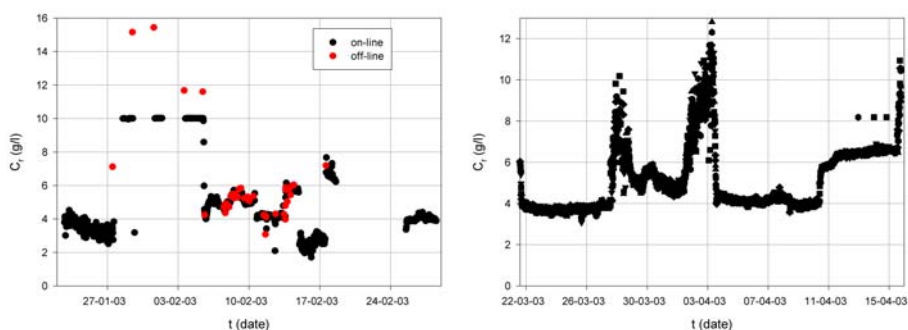


Figure 7.19: On-line and off-line measured recycle solids concentration versus time (left: first period; right: second period); Heist data

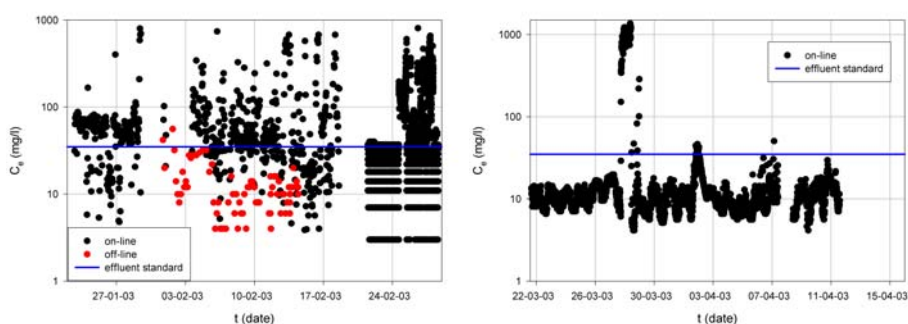


Figure 7.20: On-line and off-line measured effluent solids concentration versus time (left: first period; right: second period); Heist data

measurements. The second period gave more reliable on-line concentrations. The peak in effluent solids concentrations was related with low recycle and high feed flow rates (see Table 7.3).

The evolution of the **sludge blanket height** and the **solids concentration profiles** are shown in Figure 7.21 and 7.22. Quite some variation is seen in both measurements, mostly due to changes in the flow rates of feed, recycle and effluent.

7.2.3 Discussion of the measurement results at the Heist WWTP

The effect of the independent variables (i.e. Q_r , Q_f , C_f , settling properties) on the dependent variables (i.e. C_e , C_r , SBH, $C(z)$) is discussed in more detail now.

First, the days on which flow rates were changed, are discussed chronologically. The evolution of the effluent solids concentrations is only discussed when changes were observed. Steady state solids concentration profiles were calculated over a period of 8 hours.

A decrease/increase in recycle flow rate is expected to result in an increase/decrease of the recycle solids concentration and a shift upwards/downwards of the solids concentration profile. A decrease/increase in feed flow rate is expected to result in a

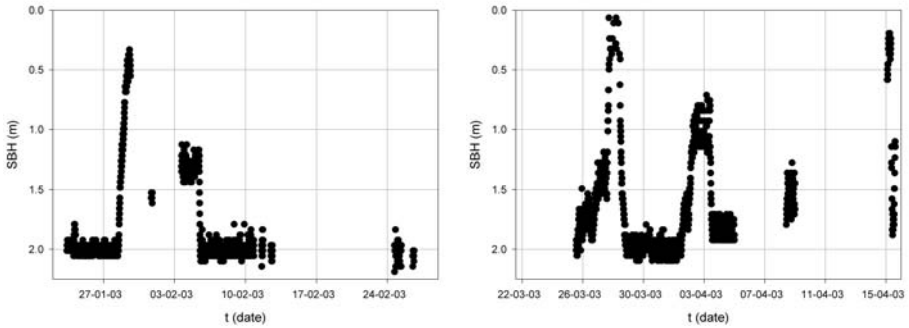


Figure 7.21: Measured sludge blanket height versus time (left: first period; right: second period); Heist data

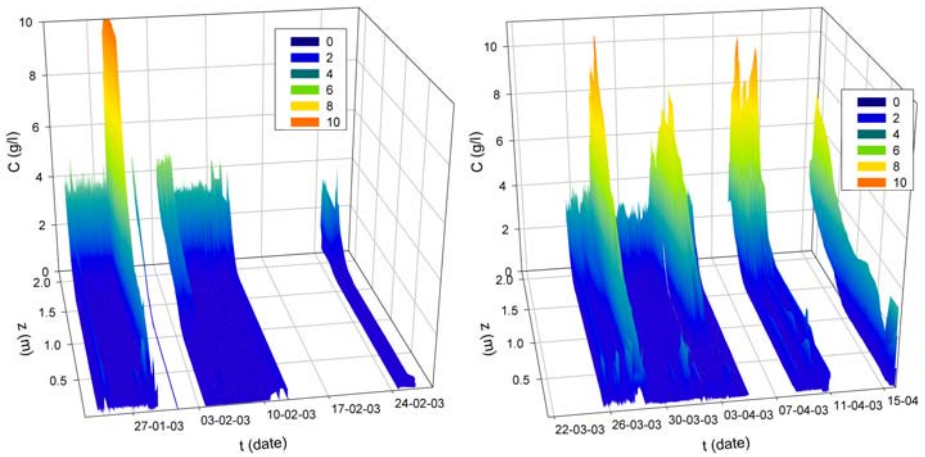


Figure 7.22: Measured solids concentration profiles (left: first period; right: second period); Heist data

decrease/ increase of the recycle solids concentration and a shift downwards/upwards of the solids concentration profile.

Finally, the days in between the changes in flow rates are discussed to identify the effect of changes in feed solids concentrations and settling properties.

A decrease/increase in feed solids concentration is expected to result in a decrease/increase of the recycle solids concentration and a shift downwards/upwards of the solids concentration profile. Changes in the settling properties should result in a change of the recycled solids concentration and a shift of the solids concentration profile and sludge blanket height.

The batch settling curves are used in Chapter 8 to identify the parameters of the settling velocity function of Chapter 6.

Change in recycle flow rate from 150 m³/hr to 100 m³/hr (January 24th) (period A 1→2 of Table 7.3) Figure 7.23

Apparently, the feed and recycle solids concentration approximately coincided. However this is impossible because of the mass balance over the clarifier (mass of solids coming in = mass of solids going out + accumulation). The sludge concentration profile measurement did not show any accumulation, i.e. the mass of solids coming in should equal the mass of solids going out. The measured feed solids concentrations were considered correct since they were validated with off-line measurements. In contrast, the measured recycle solids concentrations were considered incorrect (and this for the period in which these concentrations were not validated with off-line measurements). Before the change, the stationary recycle solids concentration should be around 6 g/l; after the change, 8.6 g/l according to the mass balance. This difference could be due to the fact that the circuit for the solids measurement (switching between recycle and feed) was not working properly.

The decrease in recycle flow rate should result in a higher solids concentration profile and sludge blanket height. However, this effect was very small as observed in the steady-state profiles. The solids concentration profile below 2.25 m should therefore show more changes. This should be confirmed by the modelling of the experiments, which is the subject of Chapter 8. The high solids concentration profiles around 4:00 were due to sludge attached to the Staiger-Mohilo 7210 MTS sensor.

Change in recycle flow rate from 100 m³/hr to 40 m³/hr (January 28th) (period A 2→3 of Table 7.3) Figure 7.24

There were no reliable recycle solids concentrations for that day but there were off-line recycle solids concentration measurements on 27th and 29th January: 7.12 g/l before and 15.16 g/l after the change. Hence, the recycle solids concentration increased by a factor 2 with the decrease in recycle flow rate. The solids concentration profile and sludge blanket height increased quite a lot: the concentrations at the lowest detection point reached values higher than the measuring range of the sensor and the sludge blanket height rose to a depth of 0.5 m. It lasted about 20 hrs before steady state was reached after the imposed change. The steady state profile after the change showed a sludge blanket with a constant concentration of about 2 g/l, below which there was a very steep concentration gradient. It is expected though that the constant concentration zone would coincide with the feed solids concentration of about 3 g/l (Larsen, 1977) which was also observed in the batch settling experiments.

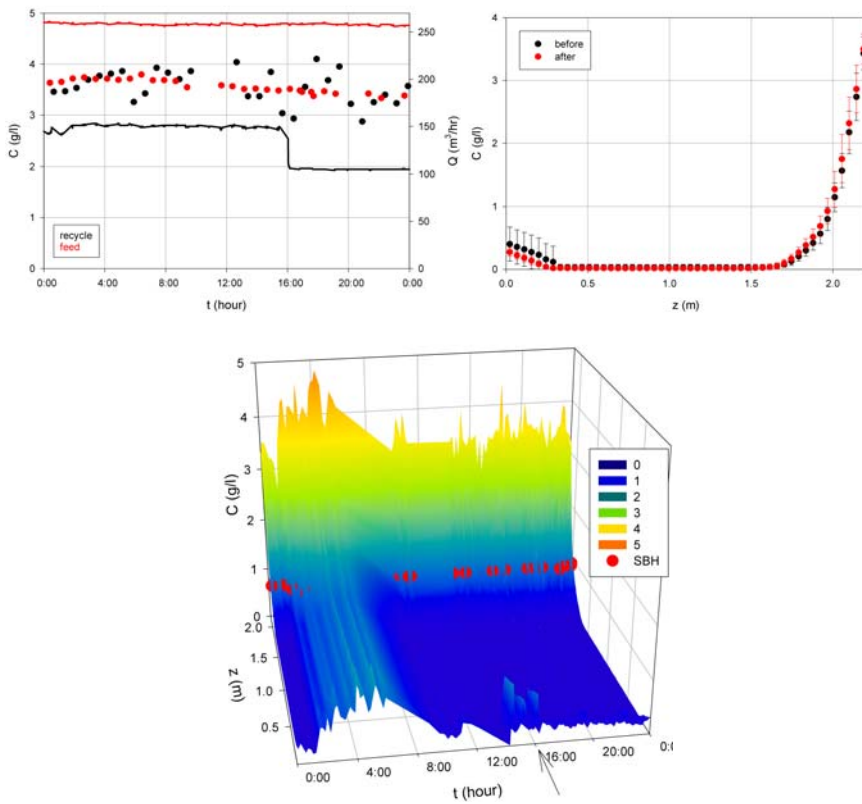


Figure 7.23: Recycle and feed solids concentration (symbol), feed and recycle flow rate (line) versus time (top left), steady state concentration profiles before and after the change in recycle flow rate (top right), and solids concentration profiles and sludge blanket height (bottom) on January 24th; Heist data

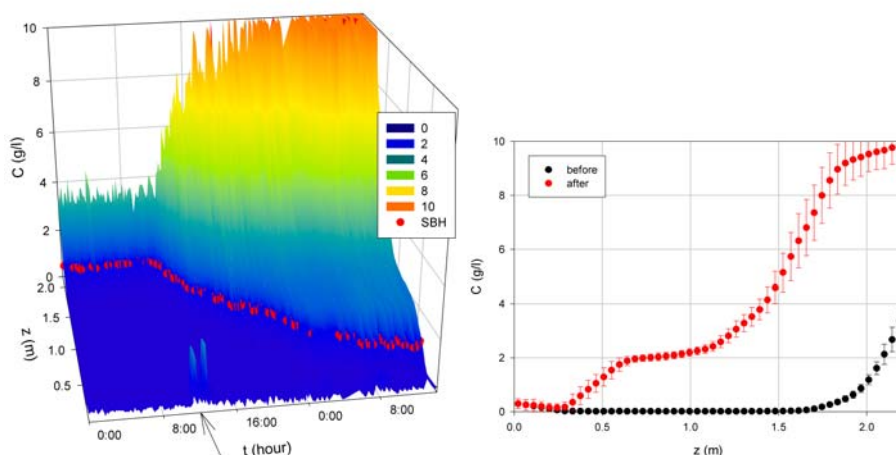


Figure 7.24: Solids concentration profiles and sludge blanket height (left), and steady state concentration profiles before and after the change in recycle flow rate (right) on January 28th; Heist data

In summary, the decrease of the recycle flow rate showed the expected shift upwards of the solids concentration profile and sludge blanket height.

Change in recycle flow rate from 40 m³/hr to 75 m³/hr (January 29th) (period A 3→4 of Table 7.3)

Due to failures of the scraper mechanism on that day, the measurements were not reliable and are therefore not discussed further.

Changes in feed flow rate from 250 m³/hr to 175 m³/hr and recycle flow rate from 75 m³/hr to 125 m³/hr (February 5th) (period A 4→5 of Table 7.3) Figure 7.25

Less sludge was entering the clarifier (lower feed flow rate) and more sludge was leaving the clarifier (higher recycle flow rate). Hence, in about 2 hrs, the recycle solids concentration decreased from a value higher than 10 g/l (upper range of sensor) to about 5 g/l. The changes resulted in a decrease of sludge mass in the clarifier as is also observed in the solids concentration profiles. The sludge blanket height declined very fast: a shift of depth of 1.2 m to a depth of 2.1 m. About 3.5 hrs after the change, steady state was reached. The steady state profile before the change had the tendency to form a sludge blanket with a constant solids concentration of about 1.5 g/l, whereas after the change, almost no sludge was remaining in the clarifier. It is expected though that the constant concentration zone would coincide with the feed solids concentration of about 3 g/l (Larsen, 1977), which was also observed in the batch settling experiments. The recycle solids concentrations were much higher than the concentrations at the lowest detection point in the clarifier. Therefore, there had to be a steep concentration gradient in the lowest 0.2 m (thickening), especially before the change in flow rate. At steady state, the mass balances of incoming and outgoing sludge were correct.

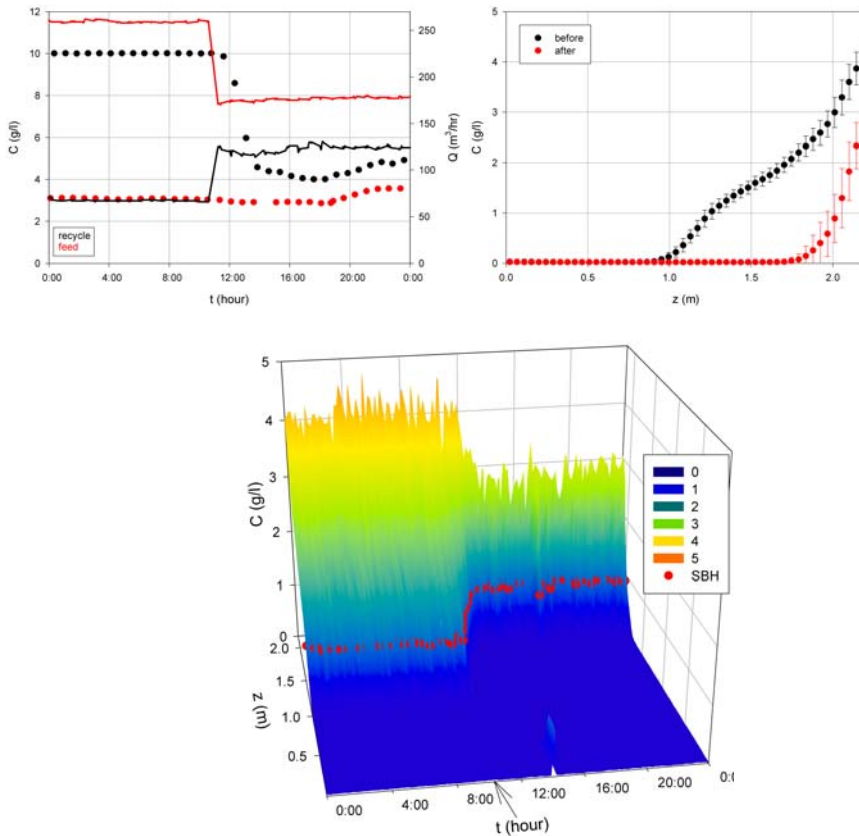


Figure 7.25: Recycle and feed solids concentration (symbol), feed and recycle flow rate (line) versus time (top left), steady state concentration profiles before and after the changes in flow rates (top right), and solids concentration profiles and sludge blanket height (bottom) on February 5th; Heist data

The increase of the recycle flow rate and decrease of the feed flow rate showed the expected decrease of the recycle solids concentration and shift downwards of the solids concentration profile and sludge blanket height.

Changes in flow rates from February 10th until 28th (period A 5→8 of Table 7.3)

Because of a variety of problems, the effect of the changes made to the operation of the clarifier could not be investigated.

Changes in feed flow rate from 175 m³/hr to 250 m³/hr and recycle flow rate from 135 m³/hr to 185 m³/hr (March 25th) (period B 1→2 of Table 7.3) Figure 7.26

Just before the change in flow rates, the feed solids concentration decreased and increased again after the change. The recycle solids concentration reacted instantaneously.

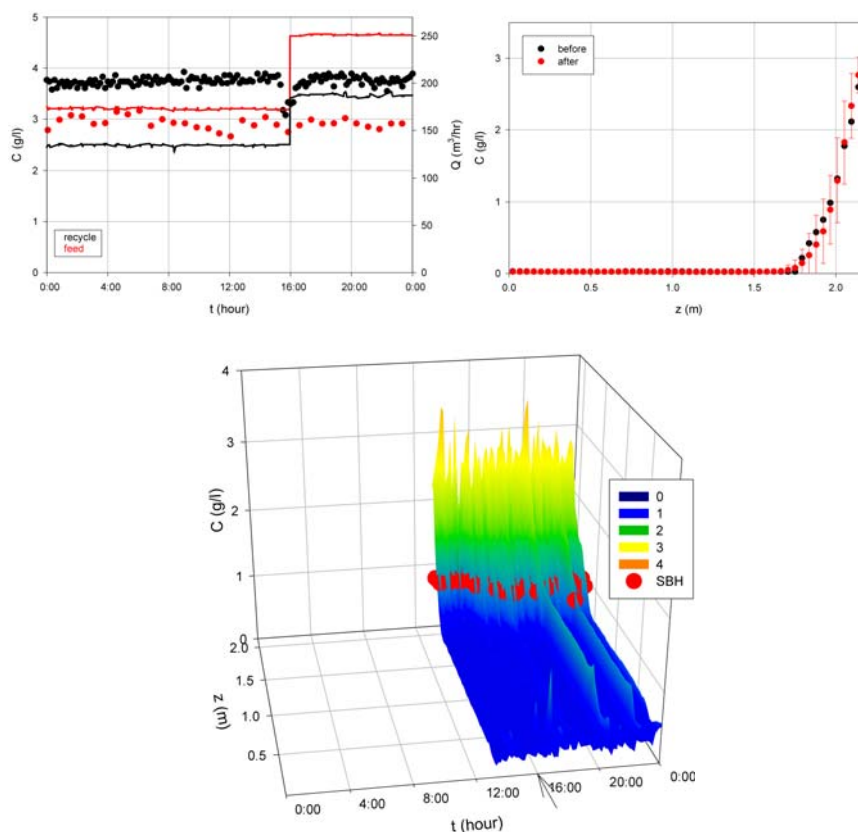


Figure 7.26: Recycle and feed solids concentration (symbol), feed and recycle flow rate (line) versus time (top left), steady state concentration profiles before and after the change in flow rates (top right), and solids concentration profiles and sludge blanket height (bottom) on March 25th; Heist data

neously to this variation in feed solids concentration (although there were also changes in feed solids concentration around 12:00) but was not remarkably influenced by the change in flow rates. At this stage, it is not clear why this happened. Modelling of the experiments has to give more insight in that behaviour. This will be the subject of Chapter 8. The solids concentration profile increased slightly and the sludge blanket height shifted a bit upwards. This was also observed in the steady state concentration profiles. After about 3 hrs, steady state was reached. The lower concentrations (i.e. below 1 g/l) did increase, whilst the higher ones remained constant. At steady state, the mass balances of incoming and outgoing sludge were correct. Because the recycle and feed flow rate were both increased, the effect of these changes on the recycle solids concentration and the solids concentration profile and sludge blanket height was not pronounced.

Change in recycle flow rate from 185 m³/hr to 50 m³/hr (March 27th) (period B 2→3 of Table 7.3) Figure 7.27

On March 26th and 27th, there were maintenance works on the secondary clarifiers of the WWTP and on March 27th, a huge amount of filamentous organisms were observed with the microscope. This resulted in worse settling properties on March 27th.

The recycle solids concentration gradually increased to a value of 8 g/l and more. These high values showed quite a lot of fluctuations, especially in comparison to the values before the changes. The sludge blanket height and solids concentration profile increased to such levels that an overflow of sludge occurred with an effluent solids concentration of about 1 g/l. Steady state was reached 6 hrs after the change. Before the change, the constant concentration zone of the sludge blanket was around 1.7 g/l, after the change around 2.5 g/l. The concentration of about 1.7 g/l was lower than the feed solids concentration, whilst the concentration of 2.5 g/l coincided with the feed solids concentration. It is expected that the constant concentration zone would coincide with the feed solids concentration (Larsen, 1977), which was also observed in the batch settling experiments. There could not be much thickening in the lowest 0.2m when recycle concentrations are compared with concentration profiles. At steady-state, mass balancing of the ingoing and outgoing sludges resulted in recycle solids concentrations of about 11 g/l. This indicates that the fluctuating measurements were probably underpredicting the real recycle solids concentrations.

Summarizing, the decrease of the recycle flow rate showed the expected increase of the recycle solids concentration and shift upwards of the solids concentration profile and sludge blanket height.

Change in feed flow rate from 250 m³/hr to 100 m³/hr (March 28th) (period B 3→4 of Table 7.3) Figure 7.28

The flow rate evolution depicted in Figure 7.28 (top left) shows that the changes in flow rates could not always be performed as straightforward.

Just before the change, the fluctuating recycle solids concentration measurements already decreased to about 6 g/l. This was, however, not observed in the solids concentration profiles which attained values of about 8 g/l at the lowest detection point. A possible explanation for the decrease in recycle solids concentration could be short-circuiting (Dupont and Dahl, 1995). Since there were no indications that other variables changed, the recycle solids concentration measurements of 6 g/l and higher were questioned. After the change, the recycle solids concentration measurement was still fluctuating until the values became less than 6 g/l. It took about 11 hrs before the concentration profiles reached steady state.

The sludge blanket height and solids concentration profile decreased to a level of about 2 m and the effluent solids concentration returned to its original value of about 20 mg/l. After the change, only a very small amount of sludge remained in the clarifier and the constant concentration zone of the sludge blanket had disappeared.

The decrease of the feed flow rate showed the expected shift downwards of the solids concentration profile and sludge blanket height. A decrease of the recycle solids concentration was expected too, but this could not be determined here since the recycle solids concentration measurements were doubtful.

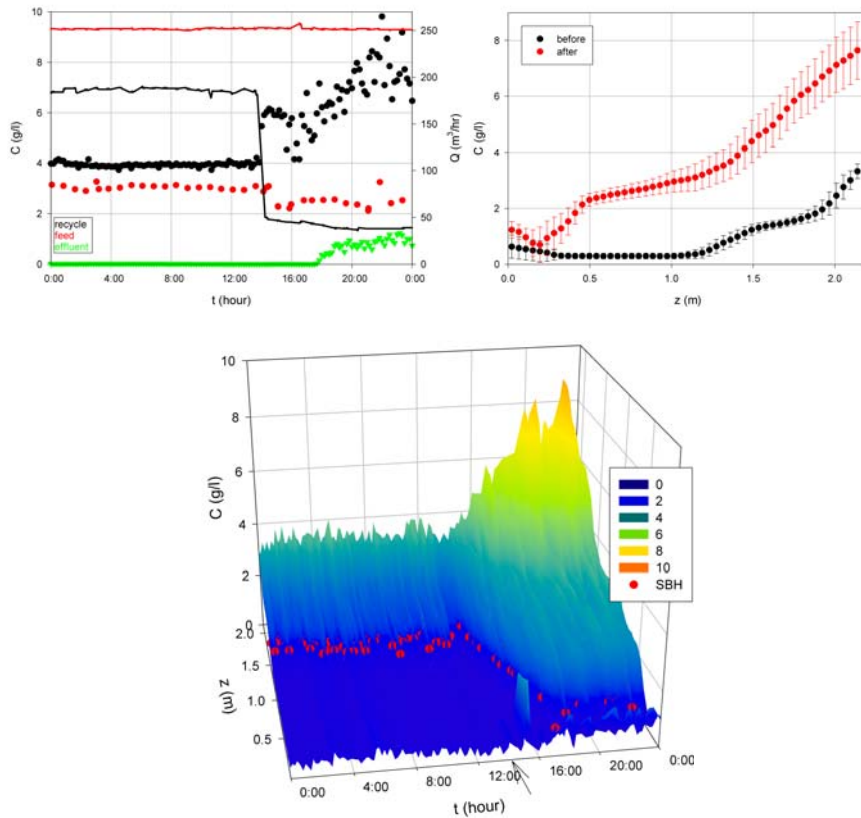


Figure 7.27: Recycle, feed and effluent solids concentration (symbol), feed and recycle flow rate (line) versus time (top left), steady state concentration profiles before and after the change in recycle flow rate (top right), and solids concentration profiles and sludge blanket height (bottom) on March 27th; Heist data

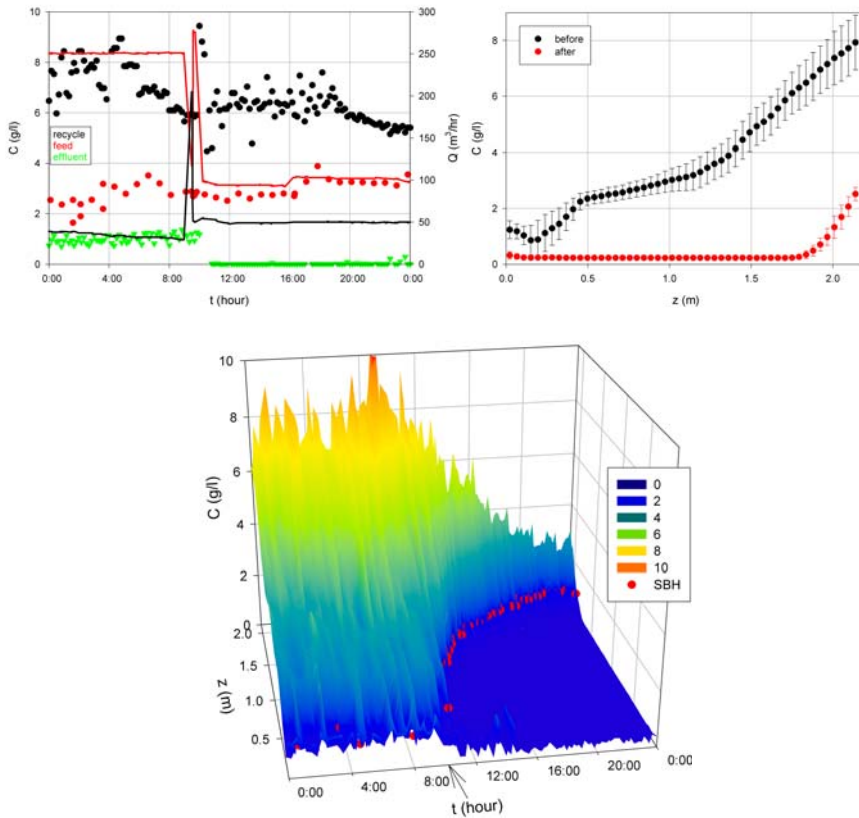


Figure 7.28: Recycle, feed and effluent solids concentration (symbol), feed and recycle flow rate (line) versus time (top left), steady state concentration profiles before and after the change in feed flow rate (top right), and solids concentration profiles and sludge blanket height (bottom) on March 28th; Heist data

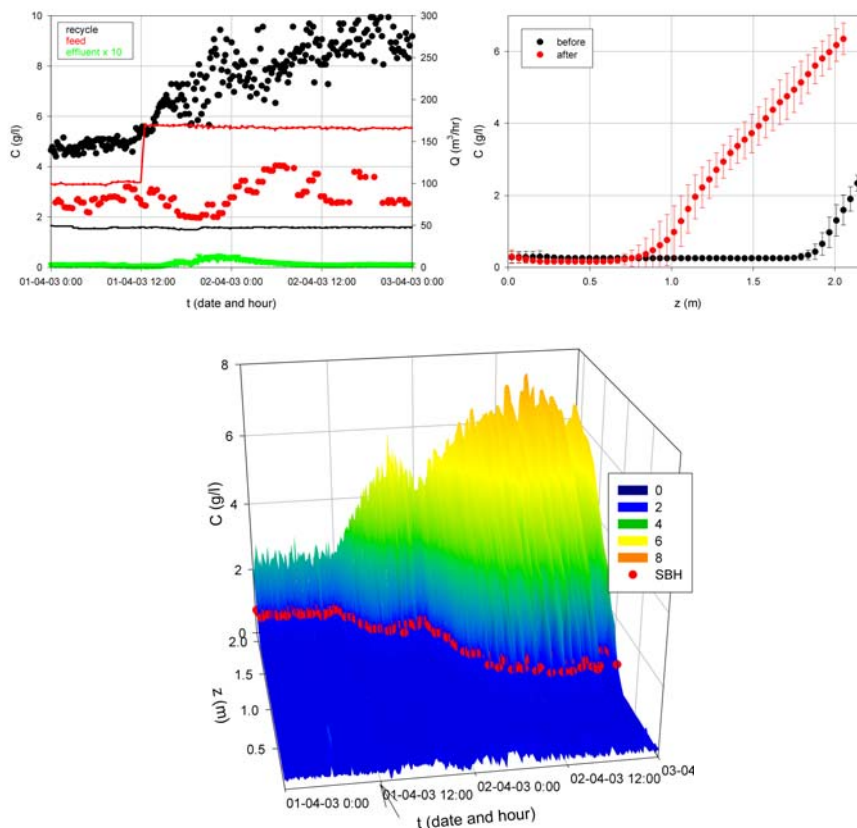


Figure 7.29: Recycle, feed and effluent solids concentration (symbol), feed and recycle flow rate (line) versus time (top left), steady state concentration profiles before and after the change in feed flow rate and feed solids concentration (top right), and solids concentration profiles and sludge blanket height (bottom) on April 1st and 2nd; Heist data

Change in feed flow rate from $100 \text{ m}^3/\text{hr}$ to $175 \text{ m}^3/\text{hr}$ (April 1st) (period B 4→5 of Table 7.3) Figure 7.29

The feed solids concentration decreased on April 1st and increased again on April 2nd. This was due to the rainfall on April 1st (the flow rate to the WWTP was doubled). The SVI also showed a peak on April 1st.

The recycle solids concentration increased from 5 g/l to about $8\text{--}10 \text{ g/l}$. The sludge blanket height and solids concentration profile increased to a level of about 1 m . The changing feed solids concentration clearly had an impact on the concentration profile and sludge blanket height. The effluent solids concentration showed a peak of about 40 mg/l , probably due to the worse settling properties. Steady state was reached on April 2nd after the change in flow rate and feed solids concentration. At steady state, the mass balances of incoming and outgoing sludge were correct.

The increase of the feed flow rate showed the expected increase of the recycle solids concentration and the shift upwards of the solids concentration profile and sludge blanket height.

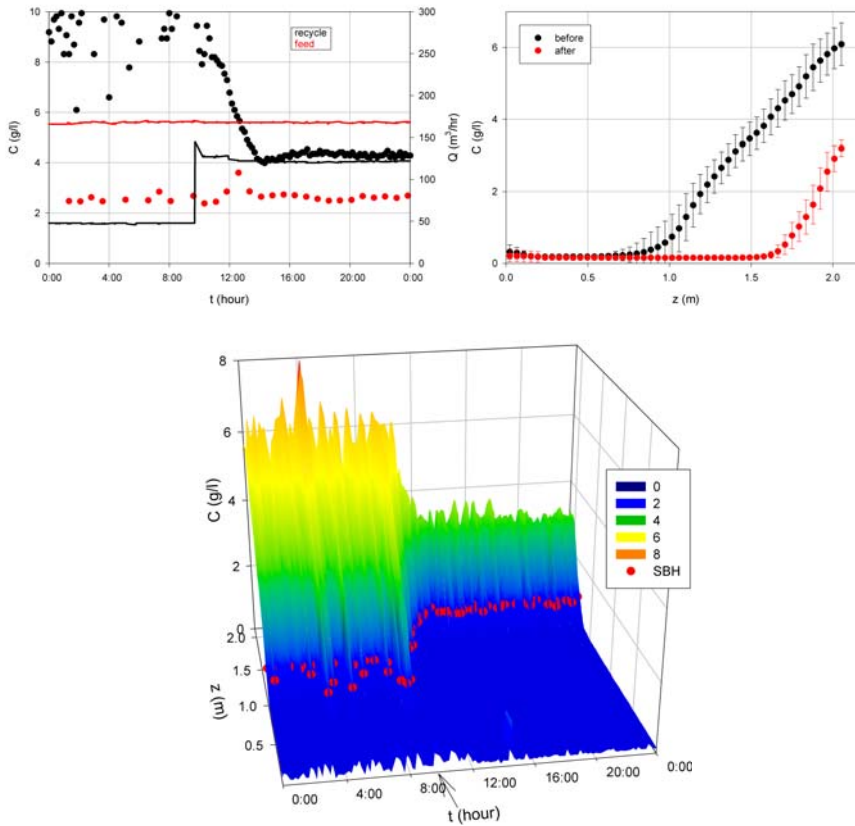


Figure 7.30: Recycle and feed solids concentration (symbol), feed and recycle flow rate (line) versus time (top left), steady state concentration profiles before and after the change in recycle flow rate (top right), and solids concentration profiles and sludge blanket height (bottom) on April 3rd; Heist data

Change in recycle flow rate from 50 m³/hr to 125 m³/hr (April 3rd) (period B 5→6 of Table 7.3) Figure 7.30

The recycle solids concentration decreased in about 5 hrs from 8-10 g/l to 4 g/l. The sludge blanket height and solids concentration profile decreased to a level of about 1.8 m. Steady state was reached after about 5 hrs after the change in flow rate. After the change, not much sludge remained in the clarifier. At steady state, the mass balance of incoming and outgoing sludge was correct. Around 13:00, the settling properties improved (as shown in section 7.2.2). This effect could not clearly be identified from the measurements, modelling of the data has to give more insight in that. In summary, the increase of the recycle flow rate showed the expected decrease of the recycle solids concentration and shift downwards of the solids concentration profile and sludge blanket height.

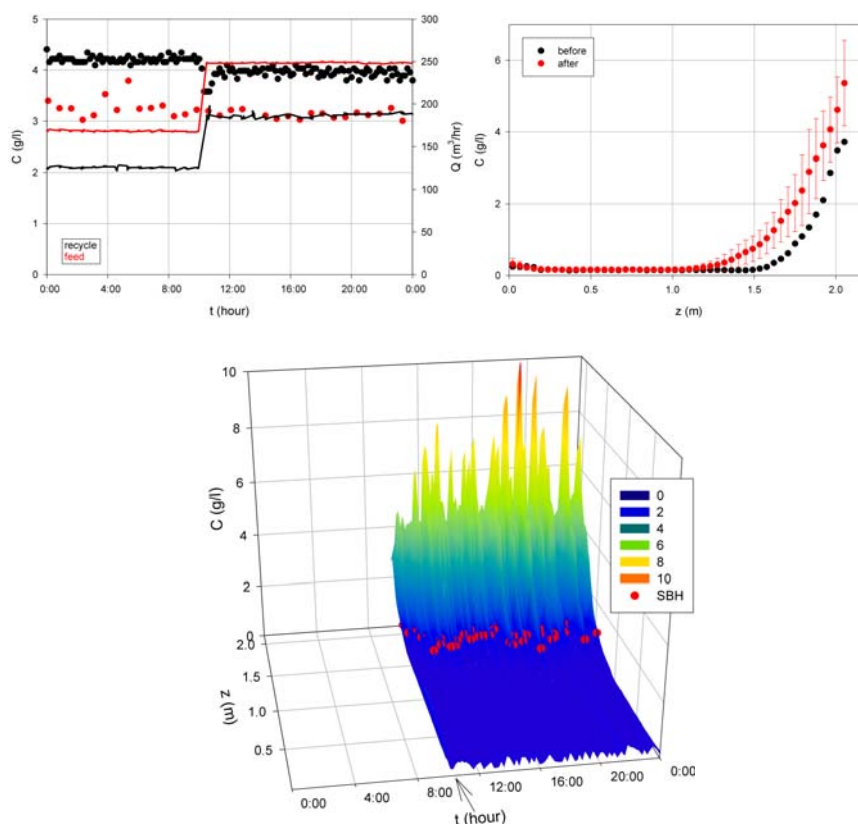


Figure 7.31: Recycle and feed solids concentration (symbol), feed and recycle flow rate (line) versus time (top left), steady state concentration profiles before and after the change in flow rates (top right), and solids concentration profiles and sludge blanket height (bottom) on April 8th; Heist data

Changes in feed flow rate from 175 m³/hr to 250 m³/hr and recycle flow rate from 125 m³/hr to 185 m³/hr (April 8th) (period B 6→7 of Table 7.3) Figure 7.31

Unfortunately, in this experiment, only one solids concentration profile measurement was available before the change was made. The recycle solids concentration decreased almost instantaneously from 4.2 g/l to 3.5 g/l and increased again after 0.5 hrs to 4 g/l. The sludge blanket height and solids concentration profile increased with 0.1 m. Steady state was reached after about 2 hours after the changes in flow rates. After the change, more sludge accumulated. There were however quite some fluctuations in the concentration profile measurements (the concentrations at the lowest detection point showed changes of 100%). The steady state concentration at the lowest detection level of the profile sensor was higher than the recycle solids concentration. Because at steady state, the mass balances of incoming and outgoing sludge were correct, the concentration profile measurements were believed to be incorrect.

The effect of the increases of the recycle and feed flow rate were counteracting and resulted in the very small decrease of the recycle solids concentration.

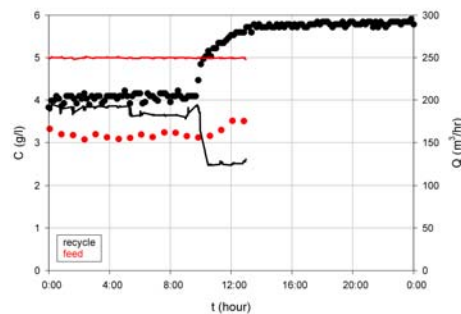


Figure 7.32: Recycle and feed solids concentration (symbol) and feed and recycle flow rate (line) versus time on April 10th; Heist data

Change in recycle flow rate from 185 m³/hr to 125 m³/hr (April 10th) (period B 7→8 of Table 7.3)

The changes of recycle and feed solids concentrations induced by the change in recycle flow are shown in Figure 7.32. The recycle solids concentration increased from 4 g/l to 5.8 g/l in 3.5 hrs. Unfortunately, there were no reliable solids concentration profile measurements due to problems with the calibration and depth measurement of the Staiger-Mohilo 7210 MTS sensor.

The decrease of the recycle flow rate showed the expected increase of the recycle solids concentration.

Change in recycle flow rate from 125 m³/hr to 50 m³/hr (April 15th) (period B 8→9 of Table 7.3) Figure 7.33

The recycle solids concentration gradually increased from 6.6 g/l to values higher than 10 g/l (above detection limit). The sludge blanket height and solids concentration profile increased from a level of 1.4 m to the overflow (no measurements available). Since steady state was not yet reached at the end of measurements, the last profile measurement after the change is shown. Before the change, the constant concentration zone of the sludge blanket was around 1.8 g/l, after the change around 2 g/l. Both values were lower than the feed solids concentration (which was expected to equal the concentration of the constant concentration zone (Larsen, 1977), as observed also in the batch settling experiments).

The decrease of the recycle flow rate showed the expected increase of the recycle solids concentration and shift upwards of the solids concentration profile and sludge blanket height.

Periods with constant flow rates

For the days on which no changes in flow were carried out, it was examined whether the feed and recycle concentration, concentration profile, SBH and SVI measurements exhibited any changes.

From January 25th until 27th, from February 3rd until 4th and from February 6th until 9th, the flow rates, SVI and feed solids concentration could reasonably be as-

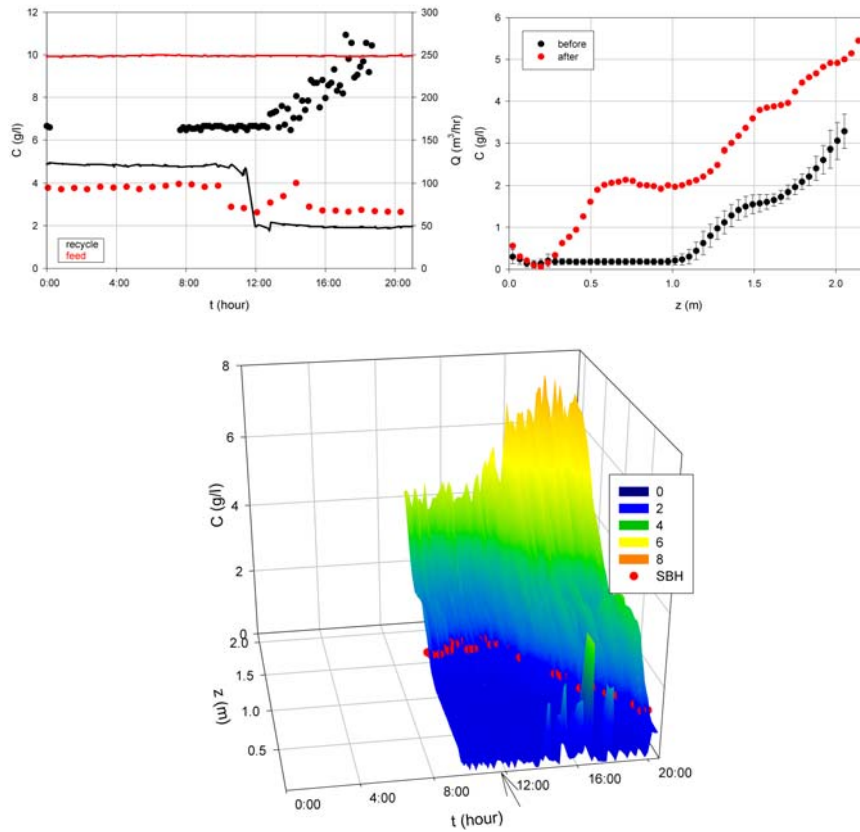


Figure 7.33: Recycle and feed solids concentration (symbol), feed and recycle flow rate (line) versus time (top left), steady state concentration profiles before change in recycle flow rate and final non-steady state profile (top right), and solids concentration profiles and sludge blanket height (bottom) on April 15th; Heist data

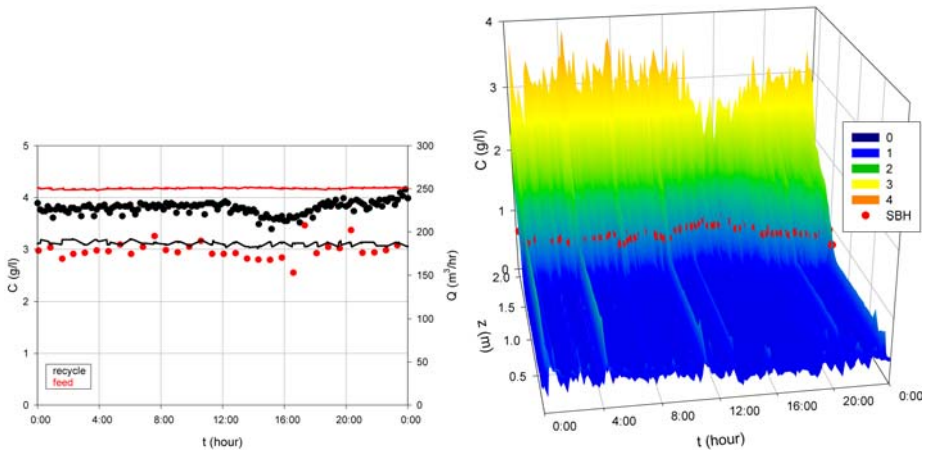


Figure 7.34: Recycle and feed solids concentration (symbol), feed and recycle flow rate (line) versus time (left), solids concentration profiles and sludge blanket height (right) on March 26th; Heist data

sumed constant which resulted in constant solids concentration profiles and recycle solids concentrations.

On March 26th, the solids concentration profiles and recycle solids concentration did show some dynamics around 16:00, as shown in Figure 7.34. There was a very small decrease (about 8%) in feed solids concentration around 12:00-16:00. Afterwards, the sludge blanket height shifted upwards to 1.5 m. This SBH increase was probably due to the deterioration of the settling properties because maintenance works on the secondary clarifiers of the WWTP were started on that day. The effect of deteriorating settling properties around this period is shown in Figure 7.35, which compares the steady state concentration profile of March 25th with the one before the change of March 27th. The sludge blanket height is shifted upwards while the concentration profile showed a constant concentration zone of about 1.5 g/l. It is expected though that the constant concentration zone would coincide with the feed solids concentration of about 3 g/l (Larsen, 1977), which was also observed in the batch settling experiments. Concentrations of about 0.5 g/l in the clarification zone all the way to the top on March 26th are not realistic and are an artefact caused by sludge attached to the Staiger-Mohilo 7210 MTS sensor.

The deterioration of the settling properties showed a shift upwards of the solids concentration profile and sludge blanket height.

From March 29th until 31st, the feed flow rate varied between 95 and 110 m³/hr while the feed solids concentration gradually decreased from 3.5 to 2.5 g/l. There were no data available on the settling properties but they probably improved since the SVI was 346 ml/g on 28th March and decreased to 274 ml/g on March 31st. All these changes (feed and SVI) resulted in quite some dynamics in the solids concentration profiles and recycle solids concentrations as shown in Figure 7.36.

The decrease of the feed solids concentration resulted in the expected decrease of the recycle solids concentration and shift downwards of the solids concentration profile

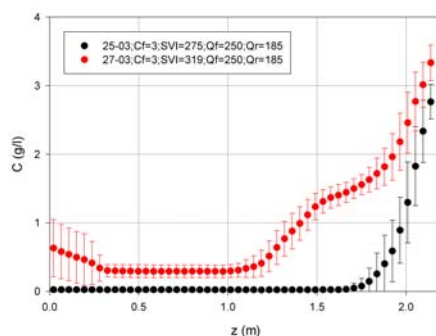


Figure 7.35: Steady state concentration profiles on March 25th and March 27th (legend gives date, feed solids concentration in g/l, SVI in ml/g, feed and recycle flow rate in m^3/hr); Heist data

and sludge blanket height.

From April 4th until 7th, the flow rates and feed solids concentration were constant but the SVI however changed from a value of 265 ml/g on April 4th to 230 ml/g on April 7th. Since only few concentration profile measurements were available in this period, the steady state concentration profile after the change of April 3th is compared with the concentration profile just before the change of April 8th. The improvement of the settling properties resulted in a small increase of the recycle solids concentration and solids concentration profile as shown in Figure 7.37.

The improvement of the settling properties showed an increase of the recycle solids concentration and a small shift upwards of the concentration profiles at the bottom.

From April 11th until 14th, the feed solids concentration fluctuated, the flow rates were kept constant, the SVI had approximately the same value at April 11th and April 14th and the recycle solids concentration gradually increased (Figure 7.38). There were no solids concentration profile measurements available for this period. Moreover, insufficient data (especially on the settling properties) were available to explain or confirm (solids concentration profiles) the observed variation of the recycle solids concentration.

Steady states at different times with approximately the same flow rates could also be compared. There were 3 such occasions with reliable measurements:

- point 3 of first period, points 3 and 9 of second period (see Figure 7.15)
- points 2 and 7 of second period (see Figure 7.15)
- point 5 of first period, points 1 and 6 of second period (see Figure 7.15)

Points 2 and 7 of the second period of Figure 7.15 could however not be compared because of the questionable solids concentration profiles at point 7. However the recycle solids concentrations could be compared: the recycle solids concentration was higher at point 7 ($C_f = 3 \text{ g/l}$; $\text{SVI} = 240 \text{ ml/g}$; $Q_f = 250 \text{ m}^3/\text{hr}$; $Q_r = 190 \text{ m}^3/\text{hr}$) than at point 2 ($C_f = 3 \text{ g/l}$; $\text{SVI} = 275 \text{ ml/g}$; $Q_f = 250 \text{ m}^3/\text{hr}$; $Q_r = 185 \text{ m}^3/\text{hr}$) which

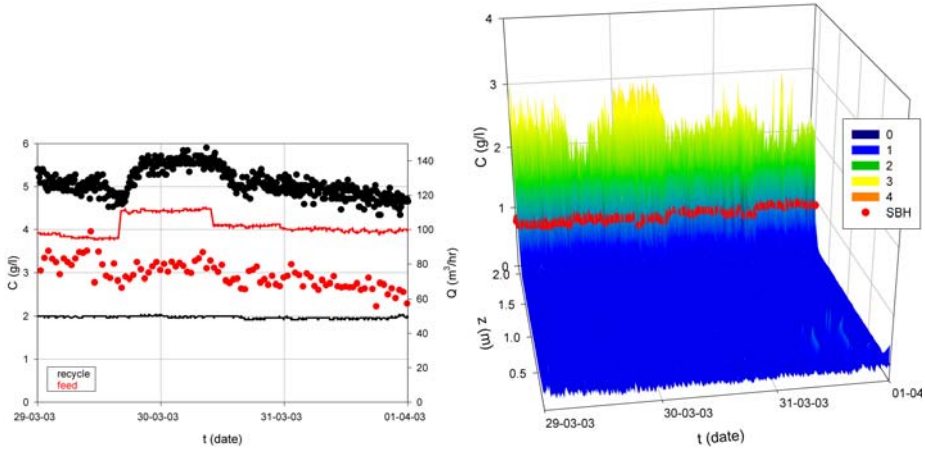


Figure 7.36: Recycle and feed solids concentration (symbol), feed and recycle flow rate (line) versus time (left), solids concentration profiles and sludge blanket height (right) from March 29th until 31th; Heist data

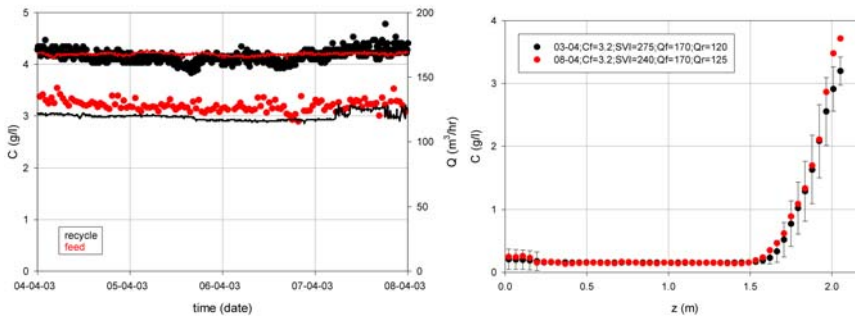


Figure 7.37: Recycle and feed solids concentration (symbol), feed and recycle flow rate (line) from April 4th until 7th (left) and concentration profiles on March 3rd and March 8th (legends give date, feed solids concentration in g/l, SVI in ml/g, feed and recycle flow rate in m³/hr)(right); Heist data

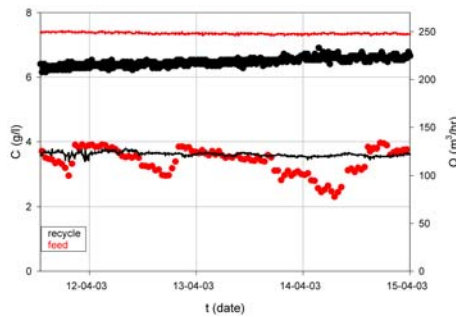


Figure 7.38: Recycle and feed solids concentration (symbol), feed and recycle flow rate (line) from April 11th until 14th; Heist data

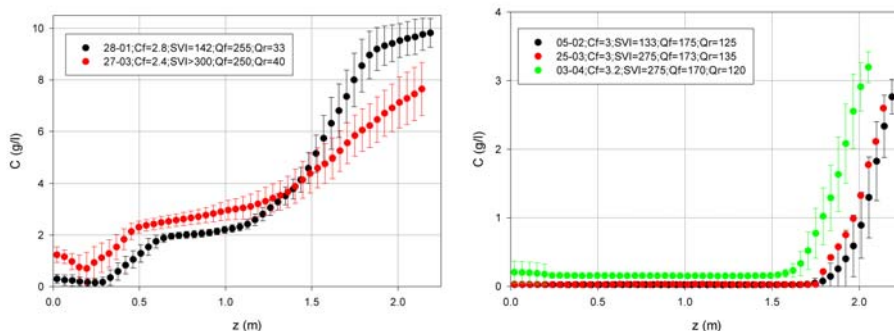


Figure 7.39: Steady state concentration profiles on January 28th and March 27th (left) and concentration profile on March 25th and steady state concentration profiles on February 5th and April 3rd (right) (legends give date, feed solids concentration in g/l, SVI in ml/g, feed and recycle flow rate in m^3/hr); Heist data

is probably due to the better settling properties at point 7.

The (steady state) profiles of the other 2 similar situations are shown in Figure 7.39.

On January 28th, March 27th and April 15th (point 3 of the first period and points 3 and 9 of the second period), the feed flow rate was around $250 \text{ m}^3/\text{hr}$ and the recycle flow rate around $40 \text{ m}^3/\text{hr}$. On April 15th however no steady state solids concentration profile was available. There was a difference in feed solids concentration and SVI for the other 2 profiles (January 28th and April 27th). Although there was a higher load entering the clarifier on January 28th and there was less recycle, the steady state profile had a lower sludge blanket height and higher concentrations (including recycle concentration) than the one on March 27th. This was caused by the better settling properties prevailing on January 28th. This is a very nice illustration of the difference between the experiments of the first period and the ones of the second period.

On February 5th, March 25th and April 3rd (point 5 of first period, points 1 and 6 of the second period), the feed flow rate was around $170 \text{ m}^3/\text{hr}$ and the recycle flow rate around $130 \text{ m}^3/\text{hr}$. The higher SVI on March 25th as compared to February 5th should result in a higher sludge blanket height and concentration profile. However, the higher recycle flow rate on March 25th (as compared to February 5th) counteracted this effect. On April 3rd, there was a slightly higher load entering the clarifier and there was less recycle. The lower recycle flow rate and the higher sludge load resulted, as expected, in a higher sludge blanket height, concentration profile and recycle solids concentration on April 3rd as compared to March 25th (SVI was the same for both days).

7.3 Conclusion

It is clear that it is not straightforward to perform full-scale experiments: it is impossible to control all variables (feed solids concentration, settling properties), the daily operation of the WWTP may not be disturbed but on the other hand also influences the experiments (e.g. maintenance works on Heist WWTP had effect on settling pro-

erties and feed solids concentration). There is not always someone present on-site to solve problems, one needs reliable and appropriate sensors/pumps that remain stable with time, Nevertheless, the results are very satisfying: solids concentration profiles, sludge blanket heights, solids concentrations in feed, effluent and recycle flows and settling properties characterised by SVI and batch settling tests were measured. For the experiments at the Heist WWTP in particular, the full-scale set-up made it possible to have overflow of sludge because there were no effluent restrictions. The independent variables (recycle and feed flow, feed solids concentrations and SVI) showed quite some variation which resulted in a highly dynamic operation of the clarifier. The effect of these variations could in most cases be clearly identified and confirmed the expectations:

- A decrease/increase in recycle flow rate resulted in an increase/decrease of the recycle solids concentration and a shift upwards/downwards of the solids concentration profile and sludge blanket height.
- A decrease/increase in feed flow rate resulted in a decrease/increase of the recycle solids concentration and a shift downwards/upwards of the solids concentration profile and sludge blanket height.
- A decrease/increase in feed solids concentration resulted in a decrease/increase of the recycle solids concentration and a shift downwards/upwards of the solids concentration profile and sludge blanket height.
- Changes in the settling properties resulted in a change of the recycle solids concentration and a shift of the solids concentration profile and sludge blanket height.

It was remarkable that it took longer to reach steady state when the recycle flow rate is decreased as compared to other changes in flow rates as shown in the Heist data. When sludge blankets with a constant concentration zone were observed, the solids concentration of this zone was always lower than the feed solids concentration. This is however contradictory with what is observed in batch settling experiments. In the next Chapter, these 2 sets of full-scale experimental data will be used to build, test and validate a 1D continuous settling model.

Chapter 8

Development of an activated sludge 1D continuous settling model

In this Chapter, the 2 sets of full-scale experimental data of Chapter 7 are used to build, test and validate a 1D continuous settling model. The batch settling model of Chapter 6 is used to describe the settling behaviour of the full-scale experimental data. With this continuous settling model, the continuous settling experiments of the full-scale experimental data are subsequently simulated and the need for a dispersion term to account for the other processes occurring besides settling and advection is shown.

8.1 Building and testing

The experimental results obtained at the Heist WWTP were used to build and test a 1D continuous settling model.

8.1.1 Determining the settling behaviour of the Heist data

The batch settling model of Chapter 6 is used to describe the measured batch settling curves. In total, 415 batch settling curves were recorded. The calculated f_{bk} -values from the initial solids concentration and its initial settling velocity (Figure 8.1) reveal that the limitation of the initial settling velocity (at e.g. 40 m/d) which results in a linear relationship between f_{bk} and C , is not valid for the settling behaviour of the Heist data. The initial f_{bk} -values are mostly located in the increasing part of the f_{bk} -versus- C curve. These data are out of the concentration range of the batch settling experiments of Chapter 5. Instead of using a maximum settling velocity (as in Chapter 5), another function has to be used for the lower solids concentration, as suggested in section 6.3.1. The Vesilind function (Vesilind, 1968) is preferred, since it was already used in Chapter 6 (but it gave too low settling velocities for higher solids concentrations) and since it is one of the most frequently used functions in clarifier modelling (Takacs *et al.*, 1991; Hamilton *et al.*, 1992; Grijspeerdt *et al.*, 1995; Watts *et al.*, 1996; Ekama *et al.*, 1997; Diehl and Jeppsson, 1998; Lee *et al.*, 1999; Joannis

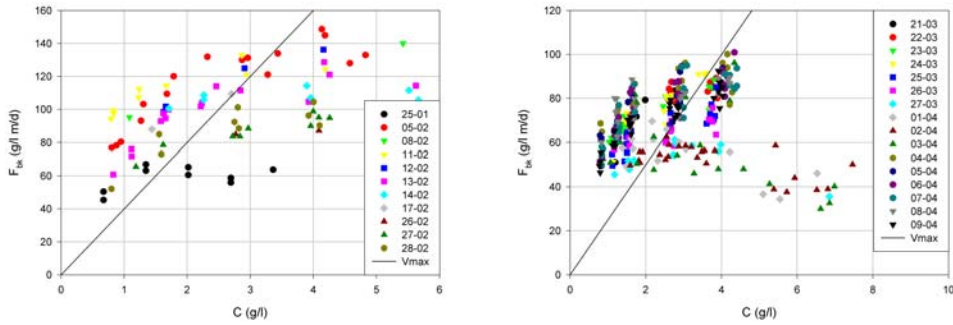


Figure 8.1: Initial Kynch batch density function versus initial solids concentration for different days (date indicated in legend)(left: first period; right: second period); Heist data

et al., 1999). The 2 parameters of the power function, a and b , are calculated from the condition that the Kynch batch density function is differentiable at the transition solids concentration C_{tr} , i.e. the function values and first derivatives of the Vesilind function, $a_1 e^{-b_1 C}$, and power function, $a C^{-b}$, are equal at C_{tr} :

$$b = -1 + b_1 C_{tr} \quad (8.1)$$

$$a = a_1 C_{tr}^{b+1} e^{-b_1 C_{tr}} \quad (8.2)$$

The settling parameters were kept constant on a daily basis, except for March 24th and March 27th, where the settling properties changed during the day. The parameters a_1 and b_1 were estimated from the calculated initial settling velocities and initial solids concentrations. The transition concentration and compression parameters were estimated from measured sludge blanket heights. The simulated sludge blanket height was determined from the simulated solids concentration profile (the batch settling model calculates solids concentration profiles) and was taken as the height where the solids concentration reaches the initial solids concentration. The evolution of C_C for each batch settling curve was determined according to the procedure described in section 6.5.

The results of the estimation (Tables 8.1 and 8.2) show that the parameters of the Vesilind function and the proportionality factor of the compressive solids stress function could be accurately predicted. As expected, the a_1 -parameter decreases and the b_1 -parameter increases for increasing SVI. The β -parameter calculated for a C_o of 3 g/l increases for increasing SVI; the fluctuating C_{tr} -parameter and the α -parameter are not related to the SVI. Appendix B shows the agreement between the calculated initial Kynch batch density values and the Kynch batch density function. The second period clearly exhibits worse settling behaviour as evidenced also by the higher SVI. The sludge blanket heights are simulated with an average standard deviation of 0.015 m. The simulated and measured batch settling curves are shown in Figures 8.2, 8.3 and 8.4. The agreement with the experimental data is excellent. Comparing the results with simulations with the Vesilind function (Appendix C) demonstrates that the batch settling model is capable of describing batch settling curves for different initial concentrations. The concentrations in the current case ranged from about 1 g/l to the value of the recycle solids concentration.

In summary, the settling properties of the Heist sludge can be described with the

Table 8.1: Number of batch settling curves (N) measured each day (t), estimated settling parameters with their standard deviation, number of observations (NOB), estimate of the standard deviation of the sludge blanket heights (s) and sludge volume index (SVI): first period of Heist data

t (date)	N (-)	a_1 (m/d)	b_1 (l/g)	C_{tr} (g/l)	$\frac{\alpha \beta s}{\Delta p g}$ (kg/m ²)	β (g/l)	NOB (-)	s (m)	SVI (ml/g)
05/02/03	14	112.3±2.8	0.295±0.013	10.68±0.96	0.0846±0.0045	(0.701 ± 0.056)C _o ⁻ (0.499±0.053)	302	0.016	133
08/02/03	2	119.2	0.282	7.84±0.57	0.3574±0.0368	(3.500 ± 0.424)C _o ⁻ (0.083±0.039)	34	0.013	
11/02/03	9	156.3±8.5	0.422±0.039	5.95±0.29	0.1132±0.0081	(0.821 ± 0.090)C _o ⁻ (0.123±0.051)	159	0.020	178
12/02/03	5	91.0±2.7	0.249±0.013	10.29±1.15	0.1487±0.0083	(0.655 ± 0.056)C _o ⁻ (0.338±0.046)	77	0.010	169
13/02/03	17	89.5±2.2	0.273±0.012	15.22±2.64	0.1164±0.0052	(0.724 ± 0.046)C _o ⁻ (0.211±0.038)	293	0.016	155
14/02/03	7	89.7±4.2	0.280±0.016	11.43±2.36	0.1024±0.0064	(0.421 ± 0.045)C _o ⁻ (0.594±0.093)	145	0.015	157
17/02/03	2	97.9	0.326	8.14±1.09	0.0925±0.0071	(0.457 ± 0.048)C _o ⁻ (0.206±0.023)	43	0.0095	178
26/02/03	2	65.7	0.275	>30	0.1278±0.0068	(0.853 ± 0.074)C _o ⁻ (0.212±0.049)	41	0.0055	194
27/02/03	10	73.8±3.8	0.291±0.019	7.57±0.96	0.1442±0.0135	(0.864 ± 0.110)C _o ⁻ (0.062±0.025)	201	0.022	182
28/02/03	9	81.2±4.0	0.306±0.022	8.61±1.02	0.1155±0.0086	(1.065 ± 0.114)C _o ⁻	170	0.015	204

Table 8.2: Number of batch settling curves (N) measured each day (t), estimated settling parameters with their standard deviation, number of observations (NOB), estimate of the standard deviation of the sludge blanket heights (s) and sludge volume index (SVI); second period period of Heist data

t (date)	N (-)	a_1 (m/d)	b_1 (l/g)	C_{tr} (g/l)	$\frac{\alpha D_s}{\Delta \rho g}$ (kg/m ²)	β (g/l)	NOB (-)	s (m)	SVI (ml/g)
21/03/03	10	74.0±3.2	0.321±0.024	10.53±1.25	0.1136±0.0060	(0.717 ± 0.062)C ₀ ⁻ (0.327±0.036)	172	0.010	241
22/03/03	21	77.7±1.8	0.341±0.012	9.93±0.71	0.1114±0.0032	(0.814 ± 0.036)C ₀ ⁻ (0.177±0.016)	449	0.010	
23/03/03	20	76.3±2.3	0.329±0.016	9.67±0.73	0.0912±0.0035	(0.822 ± 0.046)C ₀ ⁻ (0.860±0.051)	403	0.011	
24/03/03	9	70.3±5.5	0.297±0.030	10.43±1.18	0.1318±0.0065	(1.004 ± 0.065)C ₀ ⁻ (0.321±0.034)	189	0.010	250
24/03/03	6	63.5±3.0	0.313±0.025	9.36±1.79	0.1109±0.0074	(0.902 ± 0.086)C ₀ ⁻ (0.616±0.090)	113	0.013	
25/03/03	20	62.5±2.8	0.314±0.020	9.27±0.84	0.1028±0.0034	(0.694 ± 0.034)C ₀ ⁻ (0.295±0.024)	438	0.011	275
26/03/03	18	63.4±4.6	0.340±0.027	4.19±0.11	0.1942±0.0120	(1.208 ± 0.085)C ₀ ⁻ (0.643±0.064)	378	0.017	
27/03/03	15	55.1±1.9	0.345±0.016	8.07±1.06	0.1209±0.0049	(0.877 ± 0.049)C ₀ ⁻ (0.036±0.012)	352	0.011	319
01/04/03	15	64.9±5.3	0.388±0.036	7.14±1.08	0.1158±0.0073	(0.839 ± 0.070)	347	0.015	306
02/04/03	27	48.4±1.9	0.309±0.013	8.78±1.19	0.1222±0.0040	(0.865 ± 0.039)C ₀ ⁻ (0.060±0.009)	807	0.011	255
03/04/03	13	44.8±4.7	0.309±0.031	6.82±0.86	0.1120±0.0110	(1.147 ± 0.134)	384	0.014	275
03/04/03	14	74.7±3.8	0.315±0.028	9.99±1.27	0.1148±0.0057	(0.784 ± 0.059)C ₀ ⁻ (0.337±0.039)	335	0.015	
04/04/03	24	88.1±4.6	0.348±0.028	9.97±1.03	0.0922±0.0035	(0.603 ± 0.036)C ₀ ⁻ (0.024±0.008)	531	0.015	265
05/04/03	26	85.0±4.6	0.358±0.030	9.08±0.80	0.1146±0.0043	(0.865 ± 0.050)C ₀ ⁻ (0.149±0.021)	600	0.016	
06/04/03	25	78.9±2.6	0.325±0.016	14.70±3.89	0.1074±0.0035	(0.770 ± 0.042)C ₀ ⁻ (0.058±0.009)	539	0.015	
07/04/03	24	81.0±2.7	0.330±0.019	10.29±1.10	0.1021±0.0040	(0.754 ± 0.046)C ₀ ⁻ (0.211±0.027)	542	0.016	230
08/04/03	24	84.6±5.3	0.352±0.032	9.52±0.79	0.1096±0.0041	(0.846 ± 0.049)C ₀ ⁻ (0.178±0.024)	555	0.015	240
09/04/03	27	76.5±2.4	0.342±0.017	13.98±5.25	0.0977±0.0034	(0.716 ± 0.041)C ₀ ⁻ (0.470±0.037)	610	0.015	284

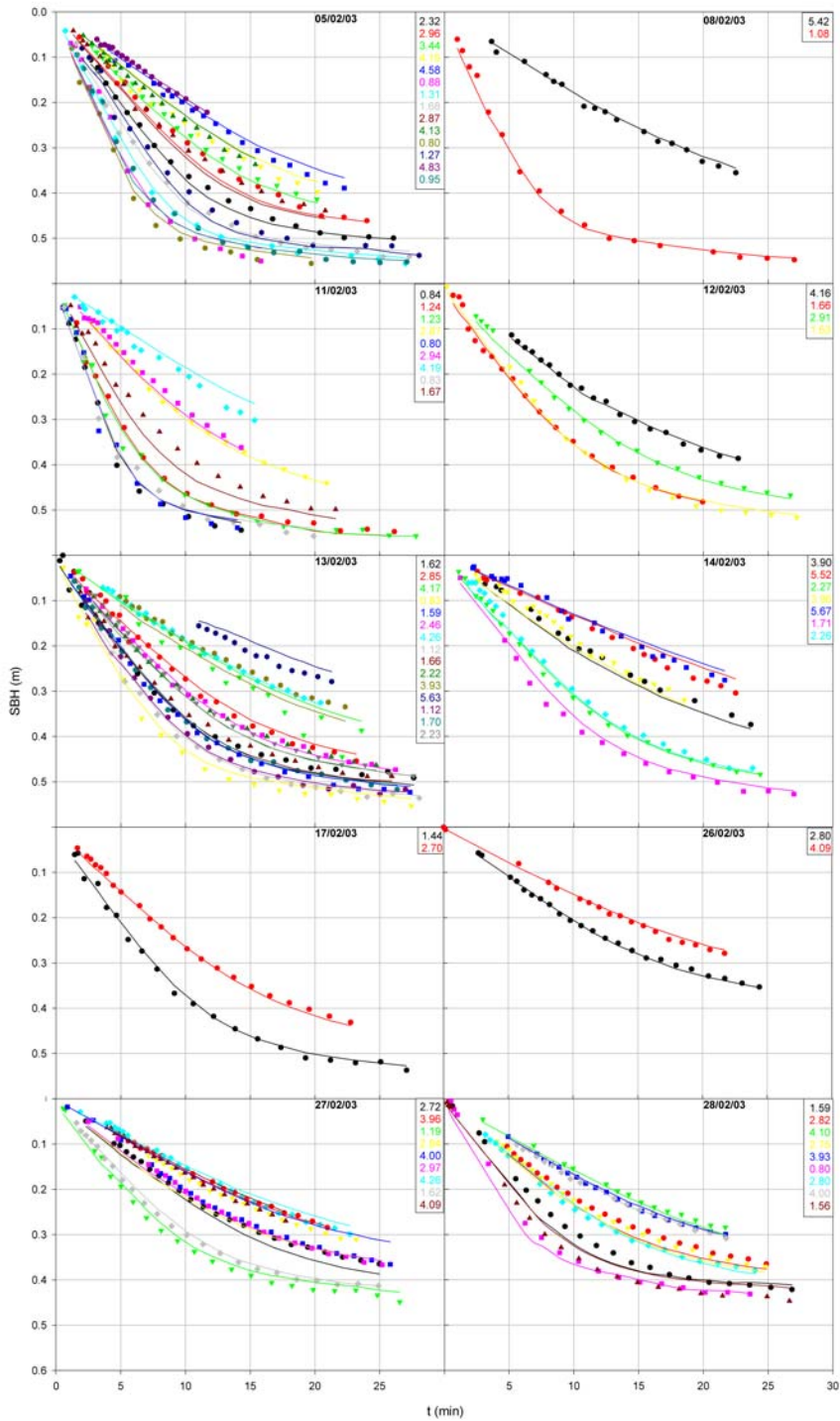


Figure 8.2: Measured (symbol) and simulated (line) batch settling curves (date and concentrations (g/l) in legend), first period Heist data

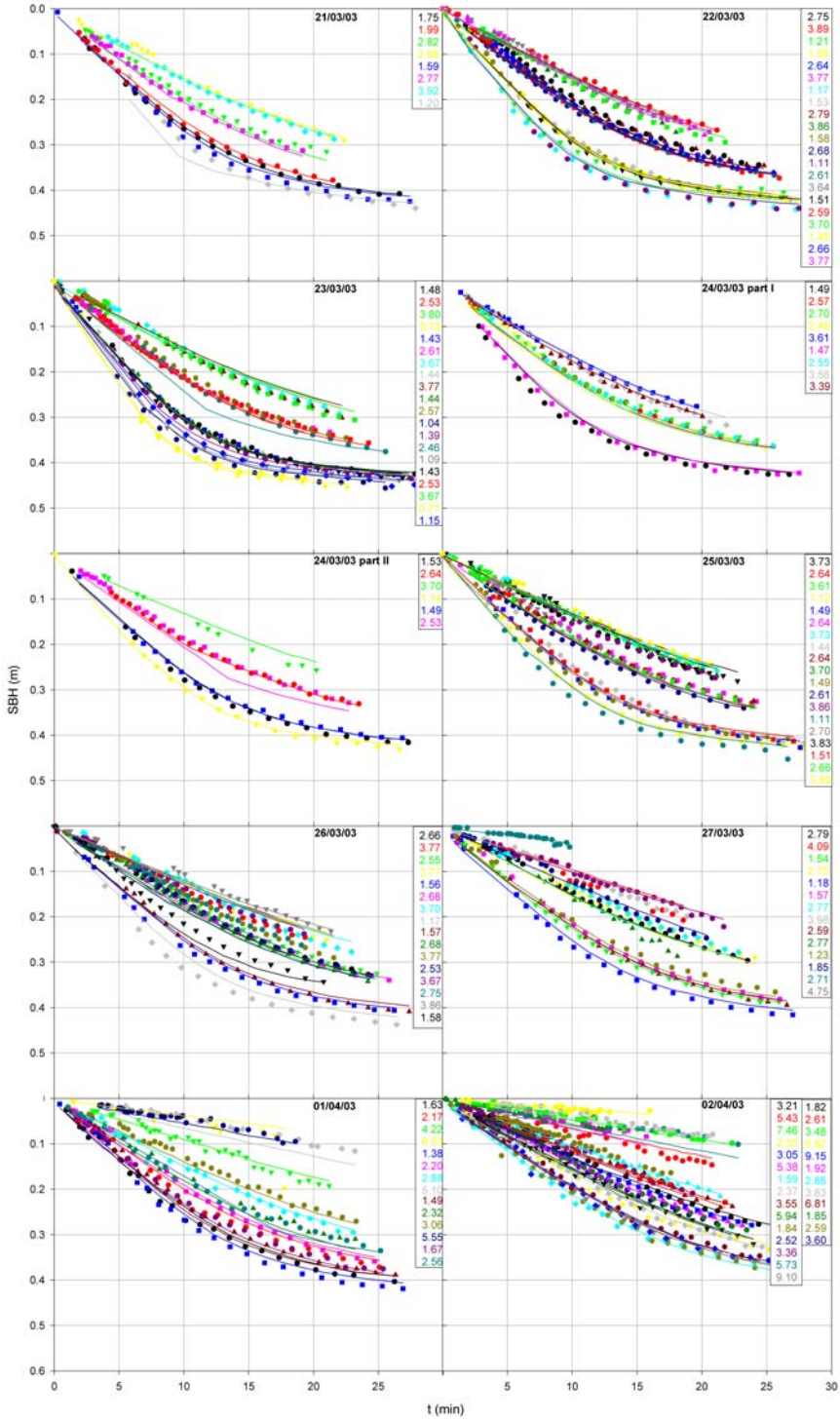


Figure 8.3: Measured (symbol) and simulated (line) batch settling curves (date and concentrations (g/l) in legend), first part second period Heist data

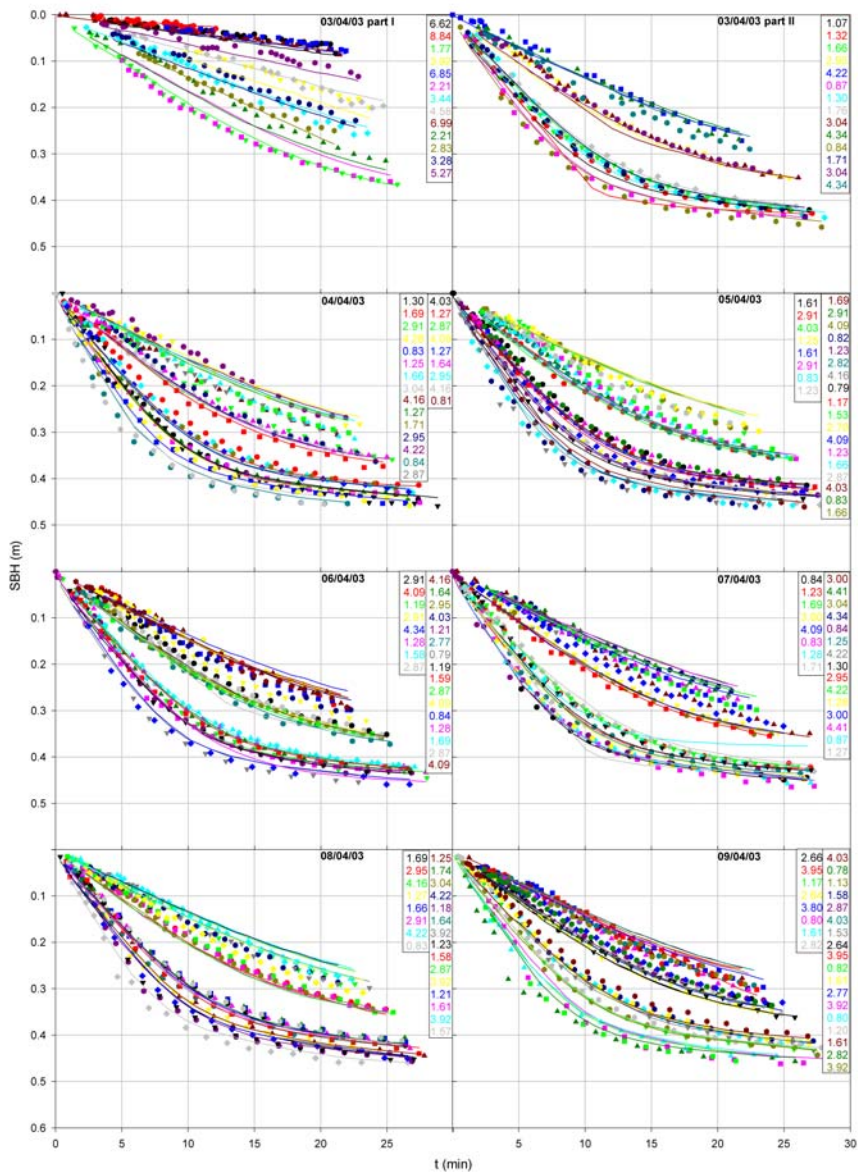


Figure 8.4: Measured (symbol) and simulated (line) batch settling curves (date and concentrations (g/l) in legend), second part second period Heist data

following batch settling model:

$$\frac{\partial C}{\partial t} = -\frac{\partial f_{bk}(C)}{\partial z} + \frac{\partial}{\partial z} \left(f_{bk}(C) \frac{\rho_s}{\Delta \rho g C} \frac{d\sigma_e(C)}{dC} \frac{\partial C}{\partial z} \right) \quad (8.3)$$

with boundary conditions and initial condition

$$f_{bk}(C) \left(1 - \frac{\rho_s}{\Delta \rho g C} \frac{d\sigma_e(C)}{dC} \frac{\partial C}{\partial z} \right)_{z=0, z=H} = 0 \quad (8.4)$$

$$C_{t=0} = C_o \quad (8.5)$$

with the Kynch batch density function

$$f_{bk}(C) = a_1 e^{-b_1 C} C \quad \text{for } C \leq C_{tr} \quad (8.6)$$

$$f_{bk}(C) = a C^{-b} \quad \text{for } C > C_{tr} \quad (8.7)$$

with

$$b = -1 + b_1 C_{tr} \quad (8.8)$$

$$a = a_1 C_{tr}^{b+1} e^{-b_1 C_{tr}} \quad (8.9)$$

and the effective solids stress function

$$\sigma_e(C) = \alpha \ln \left(\frac{C - C_C + \beta}{\beta} \right) \quad \text{for } C > C_C \quad (8.10)$$

$$\frac{d\sigma_e(C)}{dC} = 0 \quad \text{for } C \leq C_C \quad (8.11)$$

The obtained settling parameters are now input to a 1D continuous settling model in order to simulate the full-scale solids concentration profiles.

8.1.2 Building a 1D continuous settling model

The second period of the Heist data is used to build a 1D continuous settling model; the first period is subsequently used to test the resulting model. The basic 1D continuous settling model with dispersion is given by the following equations:

$$\frac{\partial C}{\partial t} = -\frac{\partial F(C)}{\partial z} + \frac{\partial}{\partial z} \left(D \frac{\partial C}{\partial z} \right) + s \quad (8.12)$$

with $F(C) =$

$$\begin{cases} f_{bk}(C) \left(1 - \frac{\rho_s}{\Delta \rho g C} \frac{\partial \sigma_e(C)}{\partial C} \frac{\partial C}{\partial z} \right) - \frac{Q_e}{A} C & 0 \leq z < z_f \\ f_{bk}(C) \left(1 - \frac{\rho_s}{\Delta \rho g C} \frac{\partial \sigma_e(C)}{\partial C} \frac{\partial C}{\partial z} \right) - \frac{Q_e}{A} C + \frac{Q_u}{A} C & z = z_f \\ f_{bk}(C) \left(1 - \frac{\rho_s}{\Delta \rho g C} \frac{\partial \sigma_e(C)}{\partial C} \frac{\partial C}{\partial z} \right) + \frac{Q_u}{A} C & z_f < z \leq H_{centre} \end{cases} \quad (8.13)$$

$$s = \frac{Q_f}{A \partial z} C_f \Delta(z - z_f) \quad (8.14)$$

with boundary conditions and initial condition

$$f_{bk}(C) \left(1 - \frac{\rho_s}{\Delta \rho g C} \frac{d\sigma_e(C)}{dC} \frac{\partial C}{\partial z} \right) - D \frac{\partial C}{\partial z} \Big|_{z=0, z=H_{centre}} = 0 \quad (8.15)$$

$$C_{t=0} = C_o \quad (8.16)$$

The **cross sectional area A** is dependent on the geometry of the clarifier. The compression solids concentration C_C and feed layer location z_f still need to be determined. The measurements showed that the solids concentration of the sludge blanket with constant concentration was always lower than the feed solids concentration C_f . This is however contradictory with what is observed in batch settling experiments. It is actually not surprising since the feed solids concentration C_f in continuous settling does not give any information about the solids mass or concentration inside the clarifier as compared to batch settling. The location of the sludge blanket height (not the measured SBH, which was determined at a concentration of 0.8 g/l and compared with the simulated SBH at the same concentration value) was therefore calculated from the simulated solids concentration profile as being the height where the concentration gradient versus z , calculated from the surface of the clarifier, starts to decrease (the gradient was calculated at each layer and compared with the one of the layer above it). Since the batch settling experiments showed that the time-dependent compression solids concentration was located around the sludge blanket height, the **compression solids concentration C_C** in the continuous settling model at each time step was the concentration that is found at a location of 5 layers below the location of the highest gradient. To account for density currents, the **feed layer location z_f** was chosen equal to the location of the compression solids concentration because (i) the experiments of Chapter 7 showed that when sludge blankets with a constant concentration zone were observed, the solids concentration of this zone was always lower than the feed solids concentration and (ii) Anderson (1945) mentioned that the feed flow falls down to the sludge blanket height.

In the batch settling model, the **β -parameter** of the effective solids stress function is dependent (power function) on the initial solids concentration C_o . This is translated in the continuous settling model as being the average solids concentration $C_{average}$ in the clarifier:

$$\beta = \beta_1 C_{average}^{\beta_2} \quad (8.17)$$

with β_1 and β_2 parameters which have to be calibrated. The average solids concentration is calculated at each time step from the simulated solids concentration profile.

Because the settling properties are known from March 21st until April 10th, only the solids concentration profiles collected within this period are used here. At first, simulations with the model without dispersion term were performed with the settling properties estimated from the batch settling curves, and with the measured feed and recycle flow rate, the feed solids concentration and the clarifier's geometry. To analyse the dynamics, the measured and simulated sludge blanket heights and recycle solids concentrations are shown in Figure 8.5. The sludge blanket height is underpredicted but shows the same trend as the measurements. The higher recycle solids concentrations are overpredicted but show the same trend as the measurements. It is clear that dispersion may expand the sludge blanket and decrease the recycle solids concentration and in this way improve the simulation results.

The **dispersion** term has to be considered as a lumped term of all processes that affect the sludge profile besides convection and settling, such as turbulent diffusivity, 2D and 3D dispersion, anomalies in the particulates transport and the sludge removal procedure (Ekama *et al.*, 1997). In the approach of Hamilton *et al.* (1992) and Joannis *et al.* (1999), the dispersion coefficient was a constant, whereas Lee *et al.* (1999)

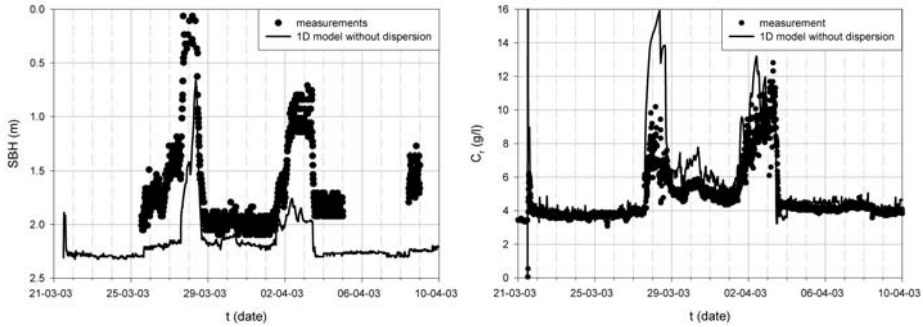


Figure 8.5: Measured (symbol) and simulated (line) sludge blanket height (left) and recycle solids concentration (right) versus time; second period; Heist data

proposed two dispersion coefficients, one for the clarification and one for the thickening zone. Watts *et al.* (1996) made the dispersion coefficient dependent on solids concentration and feed velocity. Lakehal *et al.* (1999) showed that the flow pattern in a clarifier can exhibit several recirculation zones, mainly located in the clarification zone. A higher dispersion coefficient in the clarification zone as compared to the thickening zone can account for this. Therefore, a model with two dispersion coefficients was developed here, one in the clarification zone and the other in the thickening zone. The objective function for estimation of the two dispersion coefficients is the sum of squared errors (SSE) between the observed and predicted solids concentration profiles (80 400 data points, i.e. 1608 profiles each with 50 measurements). Compared to the original model, the sum of squared errors is more than halved by adding dispersion to the model, giving a better fit of the solids concentration profiles and the sludge blanket height. As was expected, the dispersion in the clarification zone ($6.41 \frac{m^2}{d}$) is larger than in the thickening zone ($1.07 \frac{m^2}{d}$). The estimated standard deviation of the solids concentrations is 0.89 g/l. The measured and simulated solids concentration profiles are compared in Figure 8.6. The simulated profiles approximate the trends well, but overpredict the higher concentrations, except at the end of the second period. This confirms the statement of Chapter 7, namely that the concentration profile measurements are believed to be incorrect. Figure 8.7 presents the measured and simulated sludge blanket heights and recycle solids concentrations. The simulated sludge blanket height is of course higher than the simulations with the model without dispersion. The simulations give a fairly good prediction of the measurements with periods of overprediction as well as underprediction.

The calculated compression solids concentration $C_C(t)$ is always lower than the feed solids concentration $C_f(t)$ as shown in Figure 8.8. This confirms the choice of the feed layer since the experimental data also showed that the sludge blanket is located above the location of the feed solids concentration.

To compare the measurements in more detail with the simulations, the effect of the changing flow rates, feed solids concentrations and settling properties on the solids concentration profiles and recycle solids concentrations is discussed.

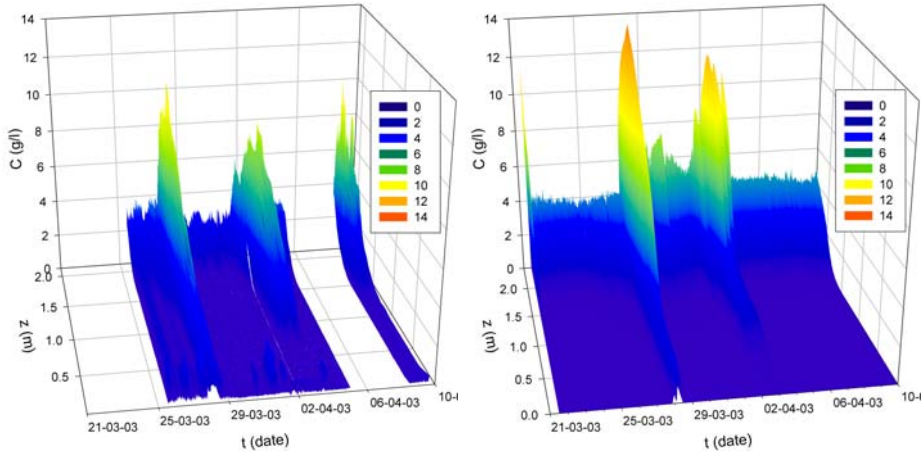


Figure 8.6: Measured (left) and simulated (right) solids concentration profiles; second period; Heist data

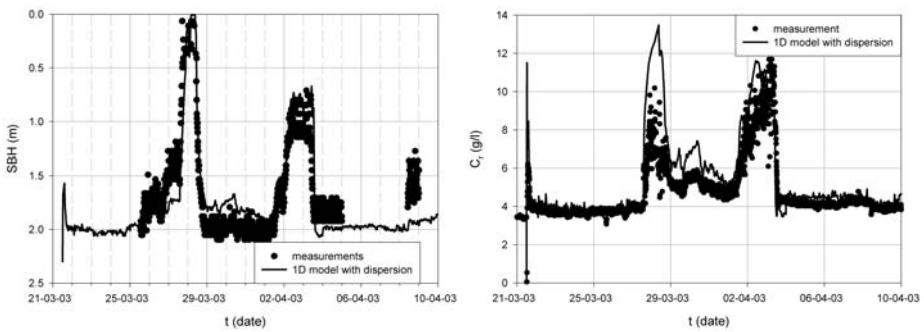


Figure 8.7: Measured (symbol) and simulated (line) sludge blanket height (left) and recycle solids concentration (right) versus time; second period; Heist data

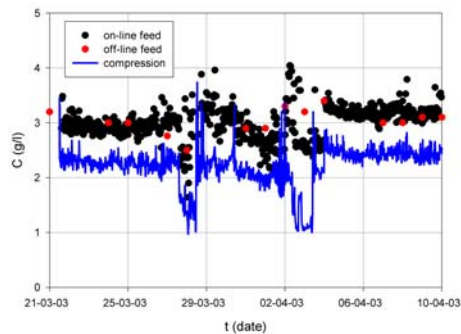


Figure 8.8: Calculated compression (line) and measured feed (symbol) solids concentration versus time; second period; Heist data

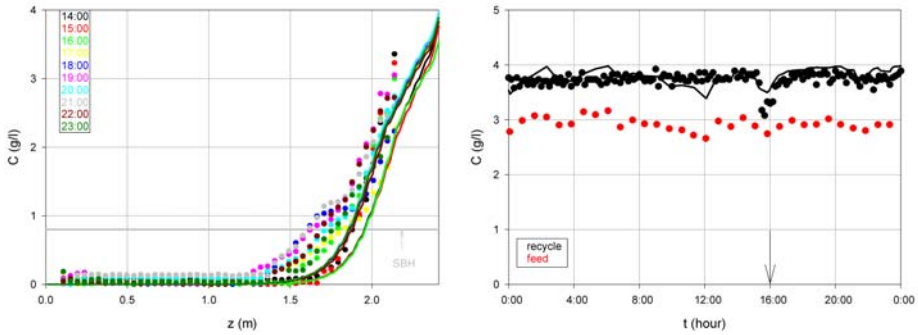


Figure 8.9: Measured (symbol) and simulated (lines) solids concentration profile (left) and recycle and feed solids concentration (right) versus time on March 25th, changes in flow rate indicated with arrow; Heist data

Changes in feed flow rate from $175 \text{ m}^3/\text{hr}$ to $250 \text{ m}^3/\text{hr}$ and recycle flow rate from $125 \text{ m}^3/\text{hr}$ to $185 \text{ m}^3/\text{hr}$ (March 25th) (period B 1→2 of Table 7.3) Figure 8.9

The simulated solids concentration profiles react more pronounced to the change in flow rates than the measurements and the simulated profile reaches a new steady state within one hour after this change. The measured solids concentration profiles showed quite some variation and were mostly underpredicted. The simulated recycle solids concentration responds almost instantaneously to changes in the feed solids concentration. The measurements showed this response only around 16:00 (and not around 12:00). This could be due to the fact that the feed solids concentration measurements, which are used as input to the model, are less stable than the recycle solids concentration measurements.

Change in recycle flow rate from $185 \text{ m}^3/\text{hr}$ to $50 \text{ m}^3/\text{hr}$ (March 27th) (period B 2→3 of Table 7.3) Figure 8.10

The simulations respond instantaneously to the change in flow rate. The higher concentrations (including recycle) are overpredicted after the change while the lower concentrations are underpredicted for the whole day. No overflow of sludge occurs in the simulations and steady state is not yet reached at the end of the day. The simulations confirm the doubtful fluctuating recycle solids concentration measurements.

Change in feed flow rate from $250 \text{ m}^3/\text{hr}$ to $100 \text{ m}^3/\text{hr}$ (March 28th) (period B 3→4 of Table 7.3) Figure 8.11

The fluctuating flow rate evolution of Figure 7.28 has a direct impact on the simulated recycle solids concentration, which decreases as a consequence of a sudden jump in the recycle and decrease of the feed flow rate. After this fluctuation, the lower feed flow rate results in lower sludge blanket heights, concentration profiles and recycle solids concentrations. The simulations show a small overflow of sludge just before the fluctuations and change in flow rate. The higher solids concentrations (including recycle) are overpredicted for the whole day and the lower ones are underpredicted before the change. Steady state is not yet reached in the simulations at the end of

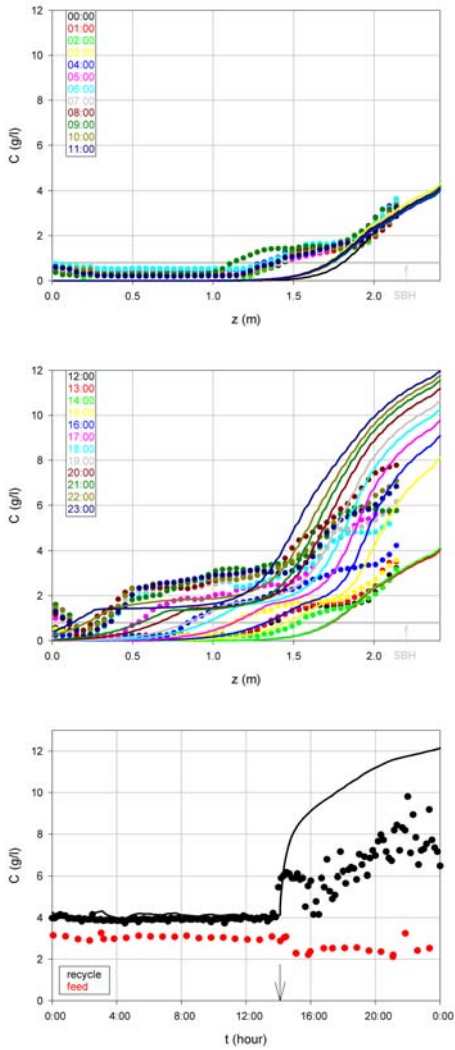


Figure 8.10: Measured (symbol) and simulated (lines) solids concentration profile (top and middle; legend: time in hours) and recycle and feed solids concentration (bottom) versus time on March 27th, change in flow rate indicated with arrow; Heist data

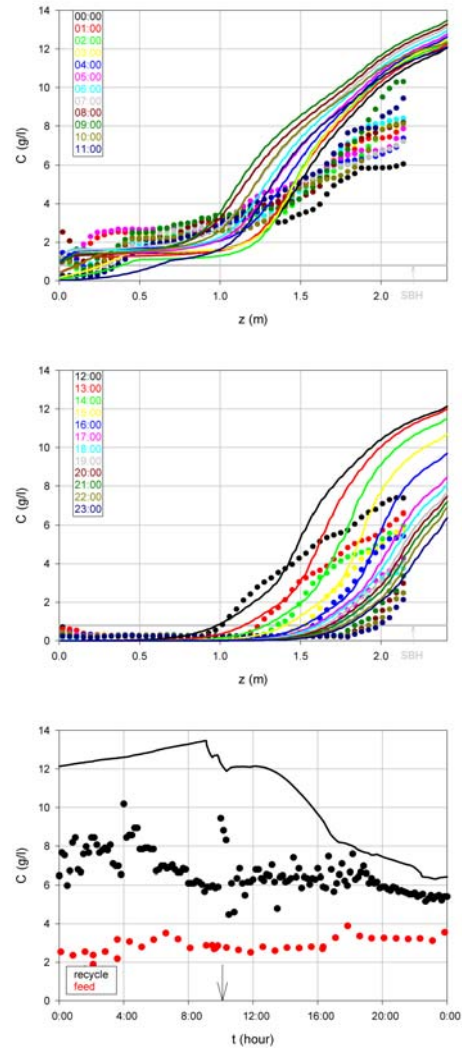


Figure 8.11: Measured (symbol) and simulated (lines) solids concentration profile (top and middle; legend: time in hours) and recycle and feed solids concentration (bottom) versus time on March 28th, change in flow rate indicated with arrow; Heist data

the day. Once again, the simulations confirm the doubtful fluctuating recycle solids concentration measurements.

Change in feed flow rate from 100 m³/hr to 175 m³/hr (April 1st) (period B 4→5 of Table 7.3) Figure 8.12

On April 1st, the simulated solids concentration profiles agree well with the measured ones. The recycle solids concentrations are overpredicted. This is probably due to the fluctuating recycle solids concentration measurements which are considered doubtful. The changing feed solids concentration on April 1st and 2nd clearly influences the simulated solids concentration profiles (and recycle solids concentrations). Steady-state is not yet reached in the simulations on April 2nd.

Change in recycle flow rate from 50 m³/hr to 125 m³/hr (April 3rd) (period B 5→6 of Table 7.3) Figure 8.13

The simulations show a decrease of the recycle solids concentration due to the increase of the recycle flow rate. The improvement of the settling properties and the jump in the feed solids concentration around 13:00 influence the simulated recycle solids concentration and solids concentration profile. Steady state is reached in the simulations about 5 hrs after the change in flow rate. The agreement with the measurements is poor.

Changes in feed flow rate from 175 m³/hr to 250 m³/hr and recycle flow rate from 125 m³/hr to 185 m³/hr (April 8th) (period B 6→7 of Table 7.3) Figure 8.14

The simulated sludge blanket height and solids concentration profile respond to the changes by an increase with 0.1 m. After the change, more sludge is present in the clarifier. Steady state is reached after about 2 hrs after the changes in flow rates. The simulations show the same trend as the measurements, but confirm the statement in Chapter 7 that the concentration profile measurements were incorrect. The simulated recycle solids concentration reacts instantaneously to the change in flow rates, by first decreasing due to the higher recycle flow rate and increasing immediately afterwards because more feed is entering. The simulated recycle solids concentration nicely follows the varying feed solids concentration.

Periods with constant flow rates

On March 26th, the simulated recycle solids concentrations and solids concentration profiles follow the trend of the varying feed solids concentrations, as shown in Figure 8.15. The solids concentration profiles are underpredicted. The effect of deteriorating settling properties around this period is presented in Figure 8.16. The simulations underpredict the measurements, show a less pronounced effect of the changes than the measurements and are not characterized by a sludge blanket height with constant concentration zone. Measured concentrations of about 0.5 g/l in the clarification zone are an artefact (as mentioned in Chapter 7).

From March 29th until 31st, the variation of the feed solids concentration and the feed flow rate around March 30th influences the simulated solids concentration profiles and recycle solids concentrations. Both overpredict the measured ones as shown in Figure 8.17.

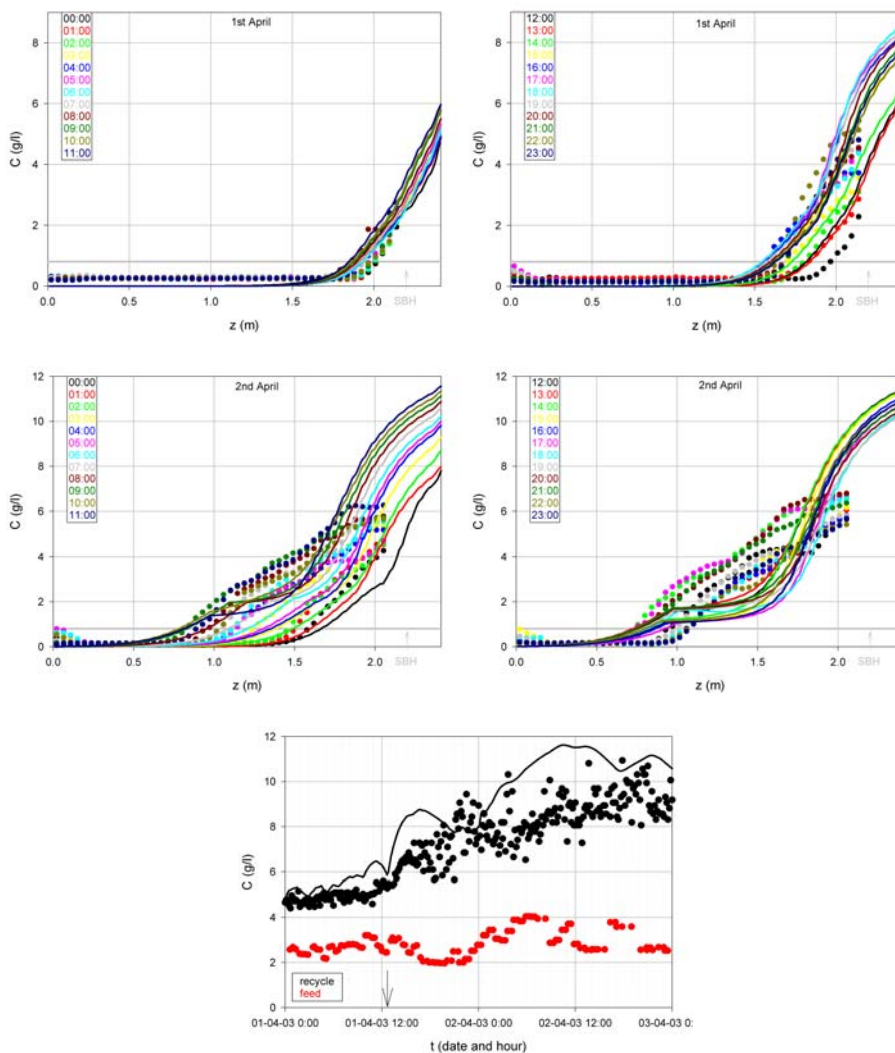


Figure 8.12: Measured (symbol) and simulated (lines) solids concentration profile (April 1st: top; April 2nd: middle; legend: time in hours) and recycle and feed solids concentration (bottom) versus time on April 1st and April 2nd, change in flow rate indicated with arrow; Heist data

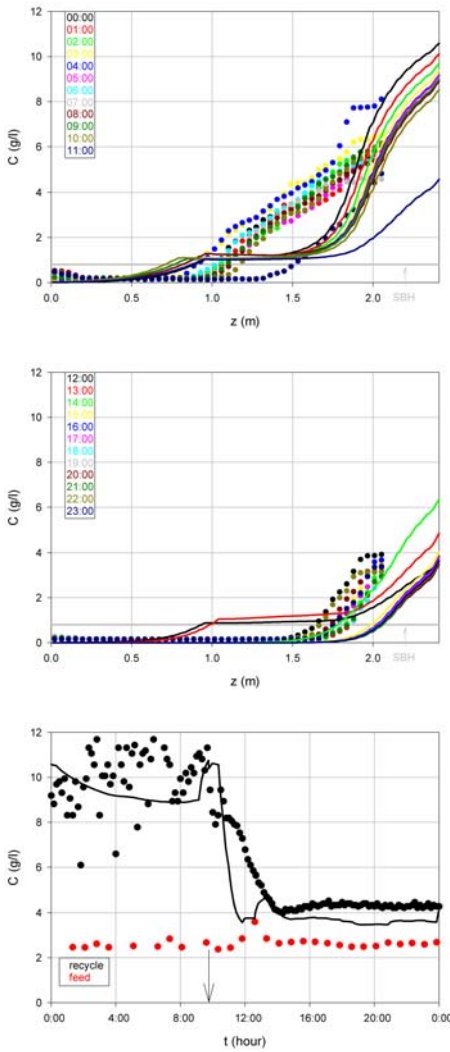


Figure 8.13: Measured (symbol) and simulated (lines) solids concentration profile (top and middle; legend: time in hours) and recycle and feed solids concentration (bottom) versus time on April 3rd, change in flow rate indicated with arrow; Heist data

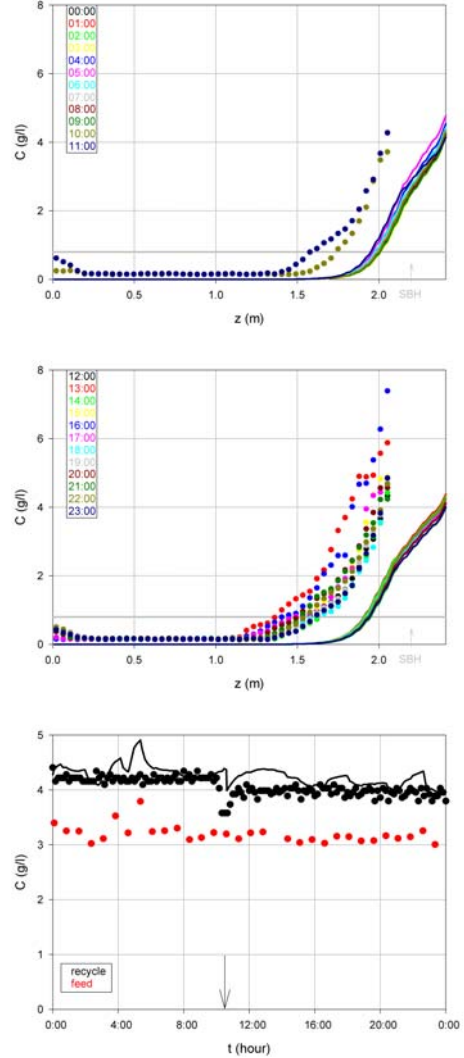


Figure 8.14: Measured (symbol) and simulated (lines) solids concentration profile (top and middle; legend: time in hours) and recycle and feed solids concentration (bottom) versus time on April 8th, change in flow rate indicated with arrow; Heist data

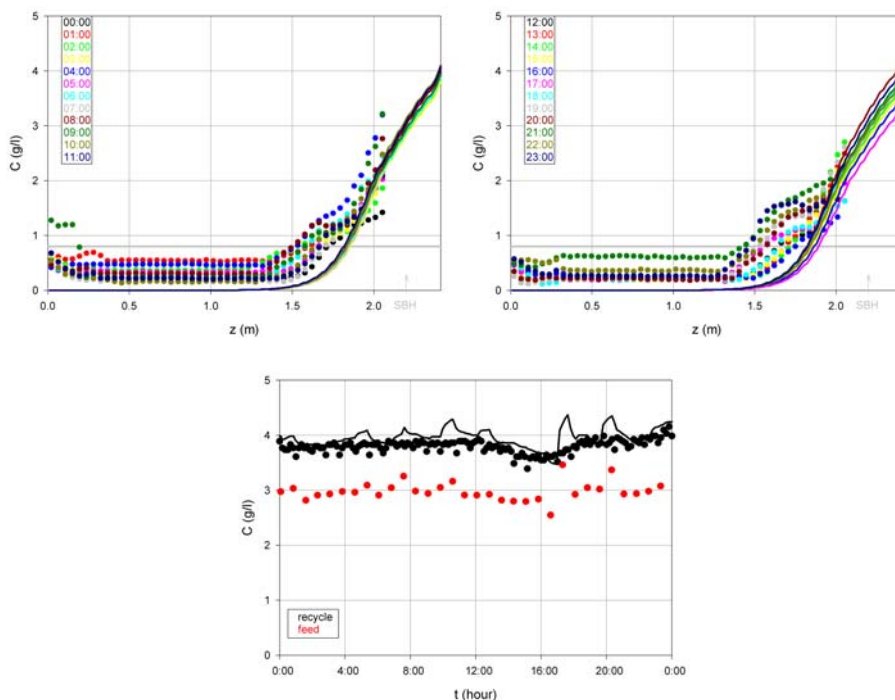


Figure 8.15: Measured (symbol) and simulated (lines) solids concentration profile (top; legend: time in hours) and recycle and feed solids concentration (bottom) versus time on March 26th; Heist data

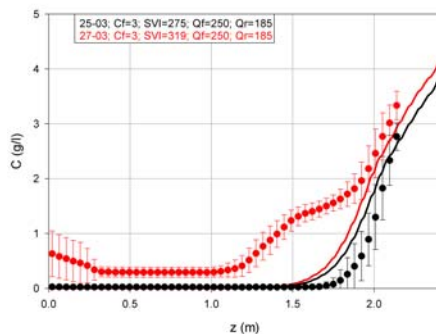


Figure 8.16: Measured (symbol) and simulated (lines) steady state concentration profiles on March 25th and 27th (legend gives date, feed solids concentration in g/l, SVI in ml/g, feed and recycle flow rate in m^3/hr); Heist data

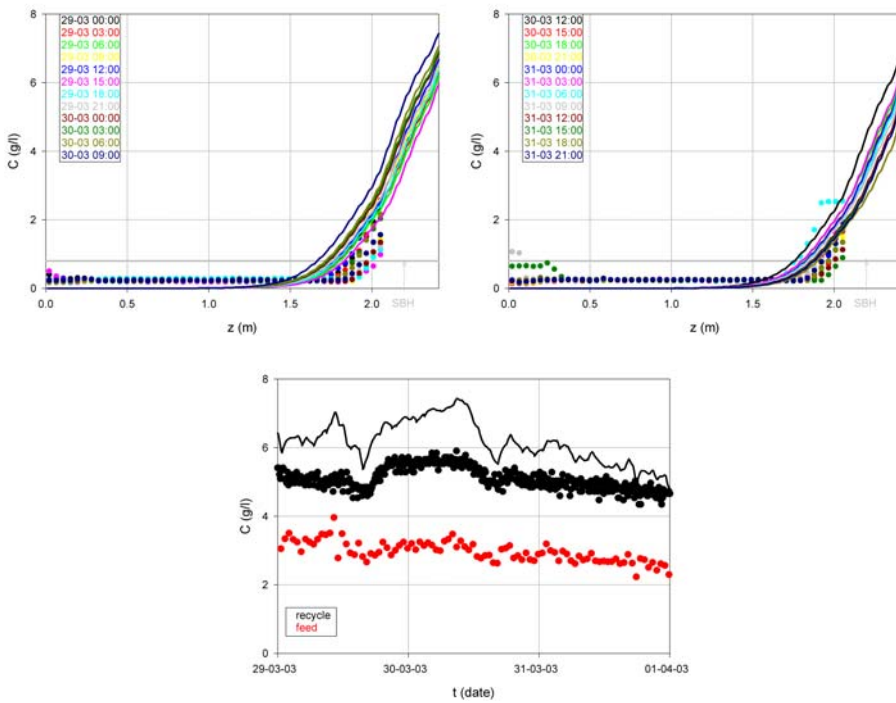


Figure 8.17: Measured (symbol) and simulated (lines) solids concentration profile (top; legend: time in hours) and recycle and feed solids concentration (bottom) versus time from March 29th until 31st; Heist data

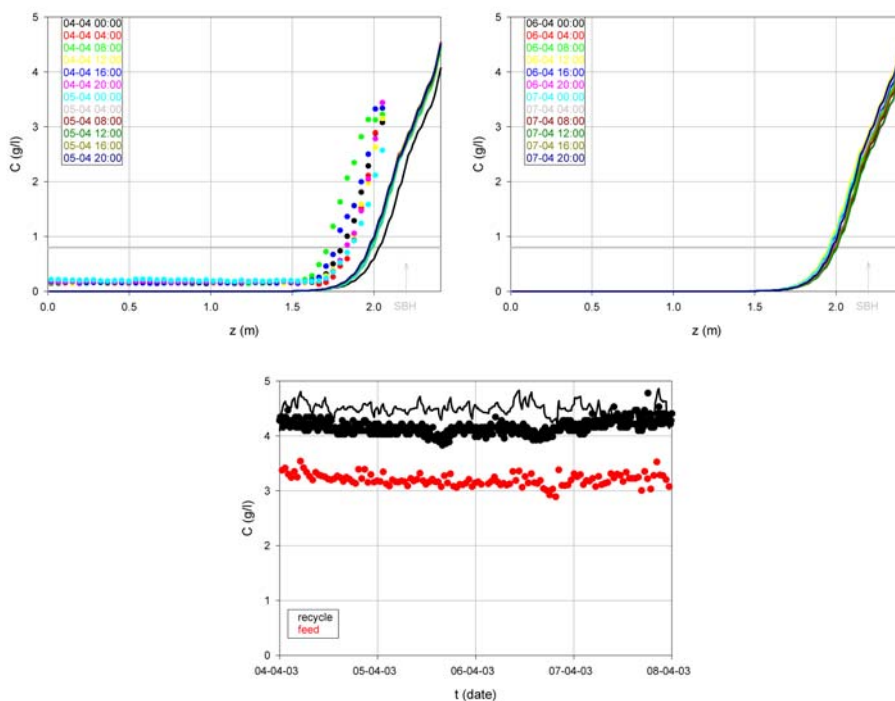


Figure 8.18: Measured (symbol) and simulated (lines) solids concentration profile (top; legend: time in hours) and recycle and feed solids concentration (bottom) versus time from April 4th until 7th; Heist data

From April 4th until 7th, the batch settling curves and modelled settling properties do not show the changes which were seen in the SVI (from a value of 265 ml/g on April 4th to 230 ml/g on April 7th). The simulated solids concentration profiles and recycle solids concentrations exhibit the expected effect of the small variation of the feed solids concentrations. The solids concentration profiles are underpredicted and the recycle solids concentrations are slightly overpredicted.

The **steady states of points 2 and 7** of Figure 7.15 (which presents an overview of the set-up of the flow rates of the experiments performed at the Heist WWTP) are compared in Figure 8.19. The improvement of the settling properties (modelled as well as expressed by SVI) is reflected in the lower simulated solids concentration profile.

The **steady states of points 1 and 6** of Figure 7.15 are compared in Figure 8.20. Although the SVI was the same for both periods, the batch settling curves showed better settling properties at point 6. This counteracts with the slightly higher load entering the clarifier and the lower recycle flow rate.

8.1.3 Testing a 1D continuous settling model

The first period of the Heist data was used to test the resulting model. A simulation was performed with the dispersion coefficients obtained in section 8.1.2, i.e. a value of $6.41 \frac{m^2}{d}$ for the dispersion in the clarification zone and a value of $1.07 \frac{m^2}{d}$ in

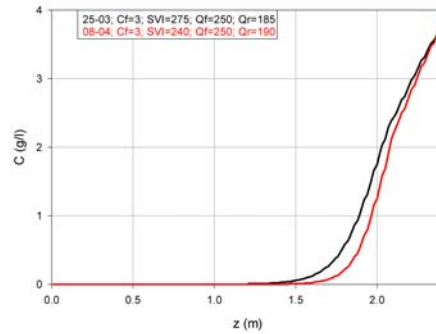


Figure 8.19: Simulated steady state concentration profiles of points 2 and 7 of Figure 7.15 (legend gives date, feed solids concentration in g/l, SVI in ml/g, feed and recycle flow rate in m³/hr); Heist data

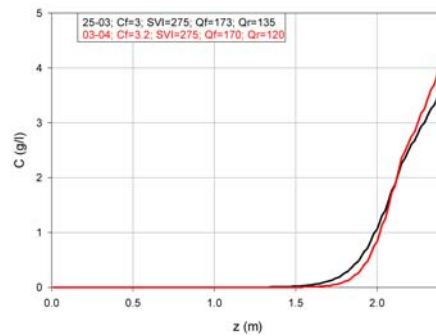


Figure 8.20: Simulated steady state concentration profiles of points 1 and 6 of Figure 7.15 (legend gives date, feed solids concentration in g/l, SVI in ml/g, feed and recycle flow rate in m³/hr); Heist data

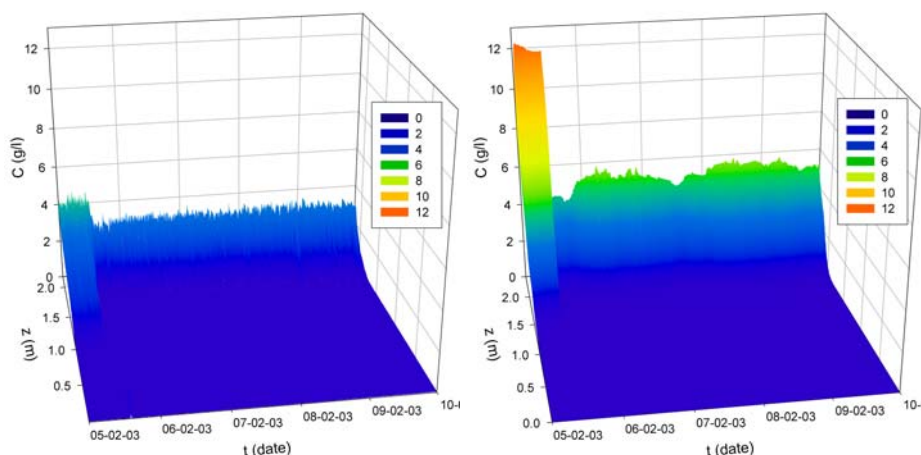


Figure 8.21: Measured (left) and simulated (right) solids concentration profiles; first period; Heist data

the thickening zone. The settling properties estimated from the batch settling curves (obtained in section 8.1.1), the measured feed and recycle flow rate, feed solids concentration and clarifier's geometry are also input to the 1D continuous settling model. Because the settling properties are known from February 5th and the measurements are not reliable from February 10th on due to a variety of problems (see section 7.2.3), simulations are only performed from February 5th until 10th.

There are 550 measured solids concentration profiles each with 50 measurements (i.e. 33300 data points). The estimated standard deviation of the solids concentrations is 0.57 g/l. The measured and simulated solids concentration profiles are compared in Figure 8.21. The simulated profiles approximate the trends well. Figure 8.22 gives the measured and simulated sludge blanket heights and recycle solids concentrations. The sludge blanket height is predicted nicely except at the beginning (underprediction). The recycle solids concentrations are predicted nicely as well. The measured values of 10 g/l are incorrect because the upper range of the sensor used in the first period was 10 g/l (see section 7.2.1). The simulated and measured recycle solids concentration follow the trend of the varying feed solids concentration nicely.

Changes in feed flow rate from 250 m³/hr to 175 m³/hr and recycle flow rate from 75 m³/hr to 125 m³/hr (February 5th) (period A 4→5 of Table 7.3) Figure 8.23

The solids concentration profiles are underpredicted, especially before the change. About 2 hrs after the changes in flow rate, steady state is reached in the simulation. The simulations do not show a tendency to form a sludge blanket, as compared to the measurements. The trends are well predicted, but quantitatively the model is not performing very well, especially before the change. The subsequent days are shown in more detail in Figure 8.24.

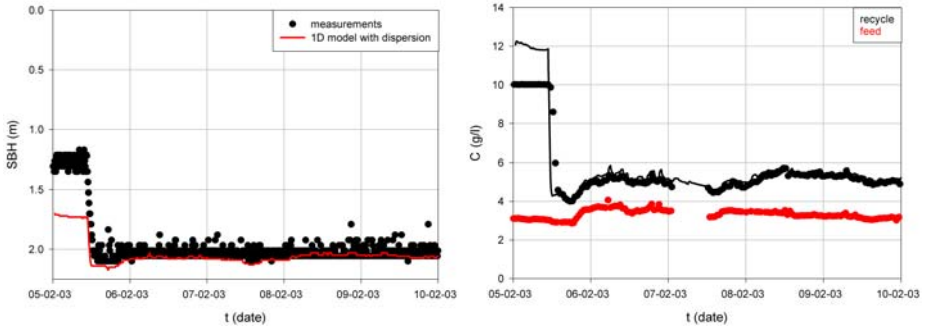


Figure 8.22: Simulated (line) and measured (symbol) sludge blanket height (left) and recycle solids concentration (right) versus time; first period; Heist data

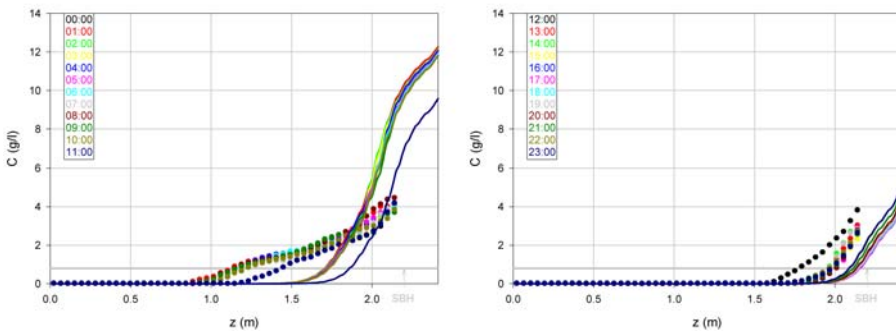


Figure 8.23: Measured (symbol) and simulated (lines) solids concentration profile (legend: time in hours) on February 5th; Heist data

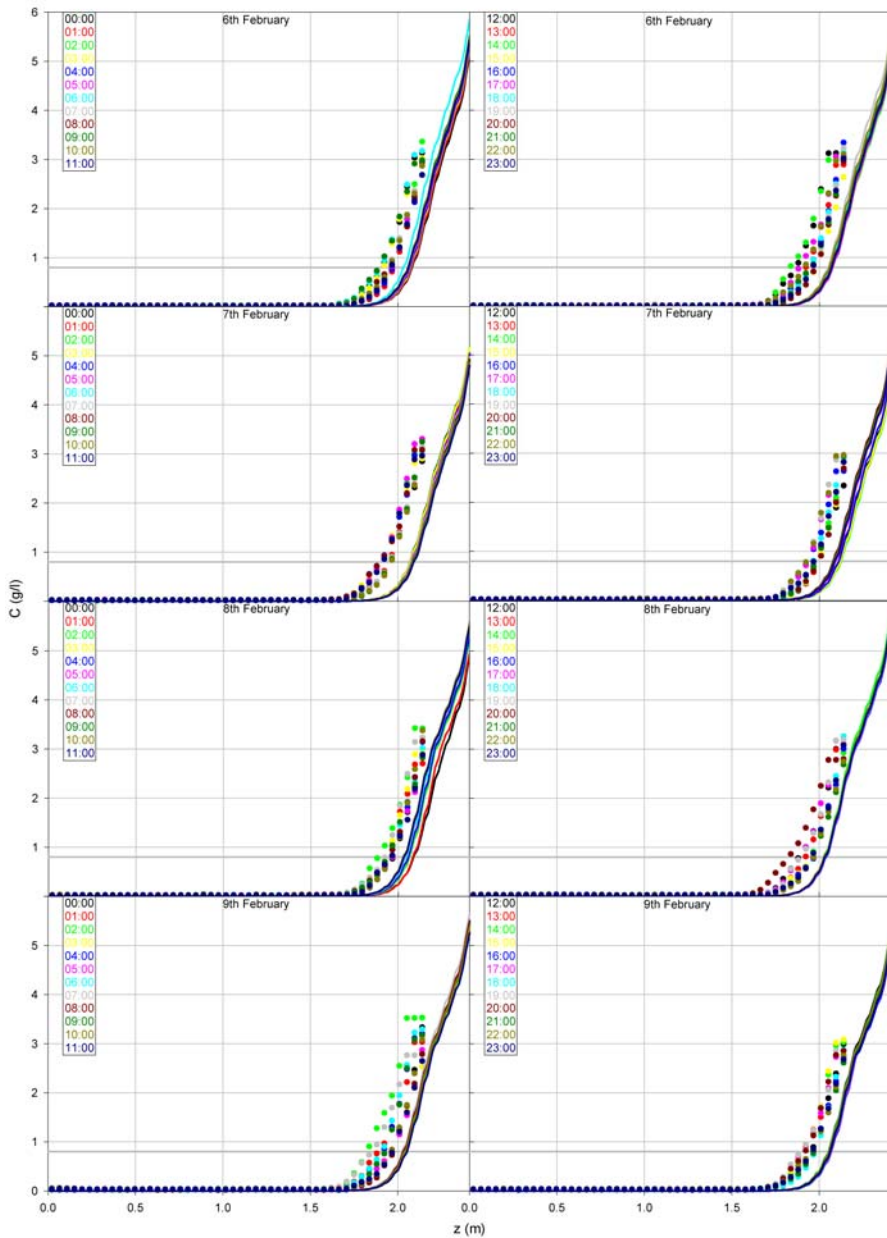


Figure 8.24: Measured (symbol) and simulated (lines) solids concentration profile (legend: time in hours) from February 6th until 10th; Heist data

8.2 Validation using the Essen data

The experimental results obtained at the Essen WWTP (see Chapter 7) were used to further validate the 1D continuous settling model with dispersion.

8.2.1 Determining the settling behaviour of the Essen data

By inspecting Table 7.1, 13 of the 20 days on which batch settling curves were recorded with a Settrometer (Vanrolleghem *et al.*, 1996), contained only one or two curves measured at one solids concentration. In view of this, the settling parameters were kept constant for consecutive days if the batch settling curves measured at approximately the same concentration overlapped. For the other days, the settling parameters were kept constant on a daily basis. When curves are only available at a certain solids concentration, it is impossible to estimate the power of β (which shows the dependency of β on the initial solids concentration). The results of the estimation are presented in Table 8.3. Again the parameters of the Vesilind function could be accurately estimated. The sludge blanket heights could be simulated with an average standard deviation of 0.016 m. The simulated and measured batch settling curves are shown in Figures 8.25 and 8.26. The agreement with the experimental data is excellent.

Even though the SVI's (varying between 80 to 240) were in the same range as the ones of the Heist sludge (varying between 130 to 350), the average settling parameters were quite different from the ones of the Heist sludge. This emphasizes the need to estimate the settling properties for each sludge from batch settling curve measurements.

8.2.2 Simulating the Essen data with the 1D continuous settling model

All the measured solids concentration profiles of the Essen data were used. The settling properties estimated from the batch settling curves (Table 8.3), the measured feed and recycle flow rate, the feed solids concentration and the clarifier's geometry were used as input to the 1D continuous settling model. For the days on which no batch settling curves were measured, the settling properties were assumed constant. The two dispersion coefficients were estimated from the measured solids concentration profiles. The objective function for this estimation was the sum of squared errors (SSE) between the observed and predicted solids concentration profiles (33 300 data points, i.e. 555 profiles each with 60 measurements). The dispersion in the clarification zone ($14.39 \frac{m^2}{d}$) is higher than in the thickening zone ($0.30 \frac{m^2}{d}$), as was expected. The estimated standard deviation of the solids concentrations is 1.20 g/l.

The measured and simulated solids concentration profiles are compared in Figure 8.27. The simulated profiles approximate the trends well but overpredict the higher concentrations, except at the end of the measurement campaign. Figure 8.28 gives the measured and simulated sludge blanket heights and recycle solids concentrations. The sludge blanket height is well predicted for the first 15 days, but afterwards the sludge blanket height is mostly overpredicted. The recycle solids concentration is nicely predicted for the whole period.

The simulated sludge blanket heights and solids concentration profiles follow the changes in load more pronouncedly than the measured ones. The decrease in recycle flow rate on March 12th influences the simulated recycle solids concentration and solids concentration profile as observed in the measurements. The sludge loss via the effluent is not reduced in the simulations. The simulated sludge blanket shifts

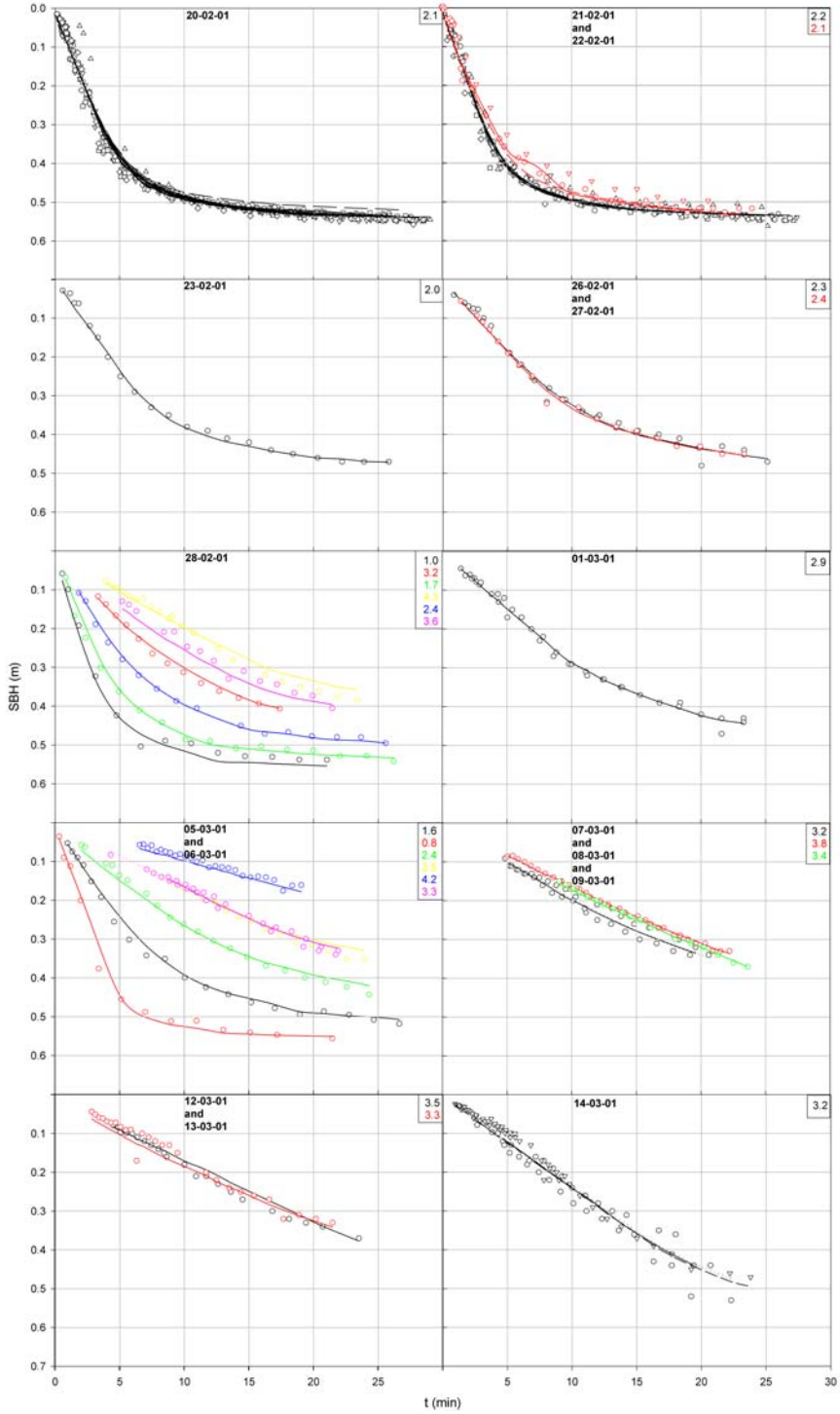


Figure 8.25: Measured (symbol) and simulated (line) batch settling curves (date and concentrations (g/l) in legend); Essen data

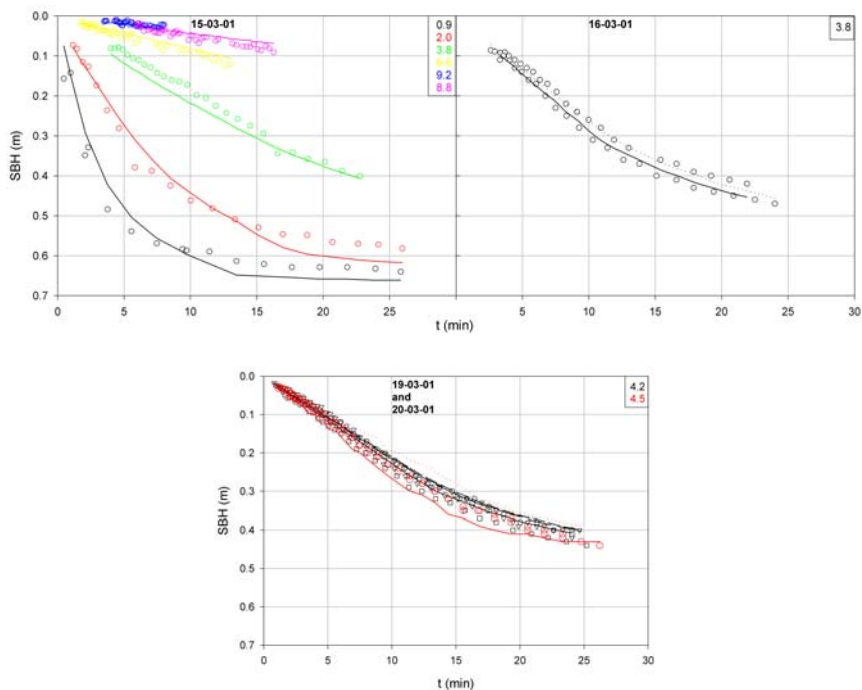


Figure 8.26: Measured (symbol) and simulated (line) batch settling curves (date and concentrations (g/l) in legend); Essen data

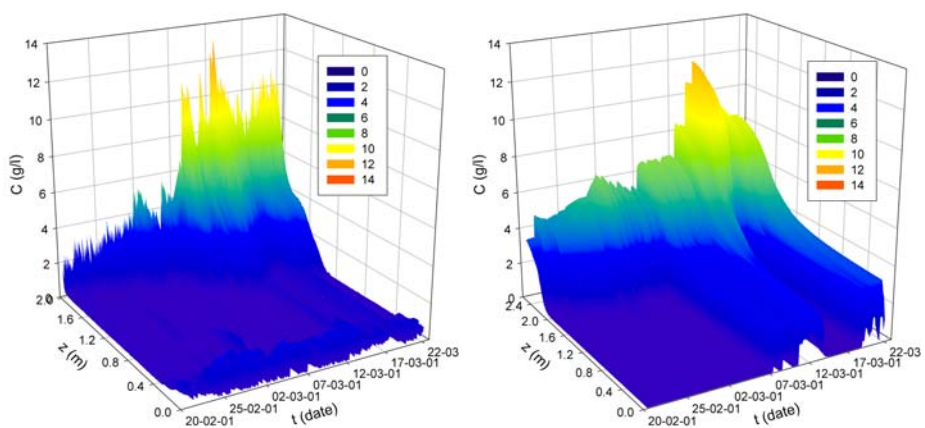


Figure 8.27: Measured (left) and simulated (right) solids concentration profiles; Essen data

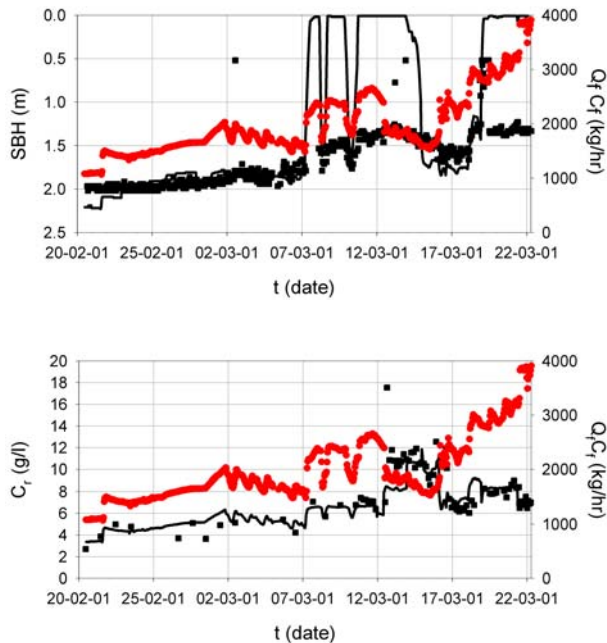


Figure 8.28: Measured (symbol) and simulated (line) sludge blanket height (top) and recycle solids concentration (bottom) versus time; Sludge load (red symbol) versus time; Essen data

downwards and the solids concentration profile shows more thickening on March 14th, due to improved settling properties (though not observed in the measured concentration profiles). The increase in recycle flow rate on March 15th results in a shift downwards of the simulated sludge blanket height and solids concentration profile (as observed qualitatively but not quantitatively in the measured concentration profiles). From March 19th on, the settling improved for the lower concentrations (lower than about 4.5 g/l) but worsened for the higher concentrations. This results in an upward shift of the solids concentration profiles and subsequently the sludge blanket height (not observed in the measured solids concentration profiles). The increase in recycle flow rate on March 21st influences the higher concentrations of the simulated solids concentration profiles (also observed in the measured solids concentration profiles). The model is not performing well, especially quantitatively. This could be due to the not so numerous measurements available for determination of the settling properties.

8.3 Conclusion

The presented activated sludge batch settling model describes the settling characteristics in an adequate way. First, the parameters of the Vesilind function are estimated from the initial settling velocities. Second, the parameters of the effective solids stress function and the transition concentration are estimated from the batch settling curve measurements. In this study, these curves are measured with a Settrometer (Applitek N.V., Belgium; Vanrolleghem *et al.* (1996)), but it can be done with every device that

is able to measure batch settling curves which only reflect the settling behaviour (i.e. are not dependent on the measurement device itself). Batch settling curves at different initial solids concentrations are required to get a reliable and good prediction of the settling behaviour (i.e. all its parameters). For that purpose, the Settrometer was extended with an automatic dilution system that mixes recycle activated sludge with clarified effluent. The experimental batch settling curves can be described excellently. This confirms the practical use of the batch settling model as concluded in Chapter 6.

The estimated settling properties are subsequently used as input for the following 1D continuous settling model with dispersion:

$$\frac{\partial C}{\partial t} = -\frac{\partial F(C)}{\partial z} + \frac{\partial}{\partial z} \left(D \frac{\partial C}{\partial z} \right) + s \quad (8.18)$$

with $F(C) =$

$$\begin{cases} f_{bk}(C) \left(1 - \frac{\rho_s}{\Delta \rho g C} \frac{\partial \sigma_e(C)}{\partial C} \frac{\partial C}{\partial z} \right) - \frac{Q_e}{A} C & 0 \leq z < z_f \\ f_{bk}(C) \left(1 - \frac{\rho_s}{\Delta \rho g C} \frac{\partial \sigma_e(C)}{\partial C} \frac{\partial C}{\partial z} \right) - \frac{Q_e}{A} C + \frac{Q_u}{A} C & z = z_f \\ f_{bk}(C) \left(1 - \frac{\rho_s}{\Delta \rho g C} \frac{\partial \sigma_e(C)}{\partial C} \frac{\partial C}{\partial z} \right) + \frac{Q_u}{A} C & z_f < z \leq H_{centre} \end{cases} \quad (8.19)$$

$$s = \frac{Q_f}{A} C_f \Delta(z - z_f) \quad (8.20)$$

with the hindered settling flux function

$$f_{bk}(C) = a_1 e^{-b_1 C} C \quad \text{for } C \leq C_{tr} \quad (8.21)$$

$$f_{bk}(C) = a C^{-b} \quad \text{for } C > C_{tr} \quad (8.22)$$

with

$$b = -1 + b_1 C_{tr} \quad (8.23)$$

$$a = a_1 C_{tr}^{b+1} e^{-b_1 C_{tr}} \quad (8.24)$$

with the effective solids stress function

$$\sigma_e(C) = \alpha \ln \left(\frac{C - C_C + \beta}{\beta} \right) \quad \text{for } C > C_C \quad (8.25)$$

$$\frac{d\sigma_e(C)}{dC} = 0 \quad \text{for } C \leq C_C \quad (8.26)$$

with boundary conditions and initial condition

$$f_{bk}(C) \left(1 - \frac{\rho_s}{\Delta \rho g C} \frac{d\sigma_e(C)}{dC} \frac{\partial C}{\partial z} \right) - D \frac{\partial C}{\partial z} \Big|_{z=0, z=H_{centre}} = 0 \quad (8.27)$$

$$C_{t=0} = C_o \quad (8.28)$$

The experimental results obtained at the Heist WWTP were used to build and test a 1D continuous settling model, the ones obtained at the Essen WWTP were used to validate the resulting 1D continuous settling model.

A model with two dispersion coefficients, one in the clarification zone and the other in the thickening zone, gives a fairly good prediction of the sludge blanket height and

recycle solids concentrations measurements obtained at the Heist WWTP. In some cases, the solids concentration profiles are nicely predicted, whereas in other cases, there is an overprediction of the higher concentrations and an underprediction of the lower concentrations in the concentration profiles. A hypothesis is that this may be due to a too low effective solids stress or to another process which is not considered in the current 1D continuous settling model. The time needed to reach steady-state after a change differs in the simulated versus measured data. To improve the results, it could e.g. be investigated whether the dispersion coefficients could be related to one or more independent variables. Another way to improve the model results could be based on another full-scale measuring campaign together with extensive batch settling experiments (as in Chapter 5) at various initial solids concentrations and modelling these data, in order to identify whether the settling properties are really accurately determined with batch settling curve measurements (e.g. do both measurements result in the same settling properties? What is the relationship between the β -parameter and the initial solids concentration?). Another point that requires further investigation is whether the dependency of the β -parameter in the effective solids stress function on the initial solids concentration in batch settling is correctly translated for the continuous settling model. The calculation of the compression solids concentration needs to be further investigated, e.g. it could be determined as the concentration in the sludge blanket at which a value of 90% or less of the maximum concentration gradient is reached.

The trends observed in the data (obtained at the Heist WWTP) used for testing the model with the obtained dispersion coefficients were well predicted by the simulations but quantitatively the model is not performing very well.

The same conclusion is reached for the model validation with data obtained at the Essen WWTP. These data did not include such extensive measurements for determination of the settling properties as the data obtained at the Heist WWTP: there were less batch settling curves available and the automatic dilution system was not yet operational. The solids concentration in the concentration profiles ranges from zero g/l to the recycle solids concentration whereas the batch settling curves were mainly measured at the feed solids concentrations. On the other hand the available batch settling curves were excellently described with the batch settling model (and its estimated parameters).

Chapter 9

Conclusions and perspectives

In municipal wastewater treatment, the wastewater is transformed in clean water and solid matter. In order to get the clean water the solids are most often separated from it by gravity in a clarifier. The clarifier is therefore crucial for the overall performance; improper operation results in a washout of solids, increasing the concentration of effluent particulate pollutants and involuntarily wasting mixed liquor. Violation of effluent permits and deterioration of the receiving waters is then the unavoidable result, with long-term release of nitrogen, phosphorus and COD as the solids degrade. The settling characteristics of activated sludge are obviously important for the performance of the clarifier and, hence, the efficiency of the wastewater treatment plant. The operation of a clarifier can be improved by a better understanding and modelling of the settling properties and the development of a full-scale 1D continuous settling model.

9.1 Batch settling of activated sludge

A thorough review on batch settling (not limited to the field of activated sludge but expanded to other application areas) revealed that more information can be gained on the well-known hindered and compression activated sludge settling by performing more in-depth measurements and that batch settling can be modelled more fundamentally (based on the fundamental mass and force balances for water and solids) as opposed to the commonly applied empirical approaches in the field of activated sludge.

9.1.1 Non-invasive monitoring of batch settling

In this work, novel measurement techniques were developed which give solids concentration profiles and pressure profiles with sufficient accuracy during the batch settling of activated sludge.

Non-invasive techniques, such as gamma-ray (Bergstrom, 1992; Scott, 1968; Dreher, 1997) and X-ray (Shih *et al.*, 1986; Been, 1980; Been and Sills, 1981; Wells, 1990; Tiller *et al.*, 1991), have been applied for the measurement of solids concentration profiles during batch settling of suspensions other than activated sludge. However, those suspensions all have a higher solids concentration and solids density than activated sludge which, given the accuracy of the measurement, i.e. 0.5 (Bergstrom, 1992)

and 0.25 vol% (Been and Sills, 1981) and 0.1 vol% (Chu *et al.*, 2003), is too low for studying activated sludge settling (with solids concentration of only 0.1-0.4 vol%).

Optical devices, ultrasound and dielectric spectrometry have been used for the measurement of the solids concentration in wastewater treatment (Vanrolleghem and Lee, 2003). However, such sensors cannot be used for monitoring the solids concentration profile during batch settling since they are commonly positioned inside the clarifier, disturbing the settling process.

Since the reported techniques cannot be used, the idea of measuring a characteristic of a substance which adsorbs to the solids in a non-invasive way, arose. Solids tracers have already been used before to determine sludge residence time distributions: MnCl_2 (Lumley and Horkeby, 1989), radioactive Au-198 (Bailey and Harkness, 1978; Audic *et al.*, 1993), La-140 (IAEA, 2001) and pyrene (Grijpspeerd and Verstraete, 1995). Radioactive tracers have the advantage over Mn and pyrene that they can be measured on-line, rather than off-line after sampling. The most commonly used radioisotope in nuclear medicine is Tc-99m. This popularity is due to its good half-life, the monochromatic gamma-ray energy it emits, and its existence in oxidation states from +1 to +7. Hence, since the activated sludge solids are negatively charged, a cationic Tc-99m complex could be used to trace them. One such positively charged complex is Tc-99m Sestamibi (Methoxy IsoButyl Isonitritil). It is shown that Tc-99m Sestamibi adsorbs well onto activated sludge, and, very importantly, does not alter its settling properties. It can therefore be used to monitor solids concentration profiles during batch settling. The radiotracer Tc-99m Sestamibi and 2 gamma cameras were used to obtain high time and spatial resolution solids concentration profiles during the batch settling of activated sludge in a pilot-scale column with a height of 1 m and an inner diameter of 386 mm, large enough to avoid wall effects. The gamma camera detects the 140 keV photons emitted from Tc-99m during a chosen time interval and produces a 2-dimensional projection of the radioactivity of the emitting object, i.e. an image. Images are produced every 30 or 60 seconds, which results in radiotracer profiles over time. The images have a resolution of 256 by 256 pixels, each pixel sizing 2.33 by 2.33 mm. As the solids concentration profile is considered homogeneous in a horizontal plane, the 2-dimensional data of each image is transformed into a 1-dimensional vertical profile by summing the values per pixel in every plane. The data are subsequently corrected for radioactive decay (Tc-99m's half-life is approximately 6 hours).

Sludge was collected from 2 different municipal wastewater treatment plants close to Ghent: Destelbergen and Deinze. Solids concentration profiles with 3 different initial concentrations for each sludge were obtained. The high-resolution profile gives a nice representation of the settling process and can be used for a better understanding and modelling of the process. The coefficient of variation of the obtained solids concentration, calculated from the ratio of the standard deviation of the measured counts and the measured solids concentration, is about 10-15 %. In comparison, the reported accuracy of 0.1 vol% of the CATScan measurements (Chu *et al.*, 2003) corresponds to a coefficient of variation of 50%. It is the first time that such detailed pilot-scale dynamic solids concentration profiles have been reported. This non-invasive technique does not disturb the settling process, does not alter the settling characteristics, gives profiles every minute and is capable of measuring in a range of 0-25 g/l with high accuracy.

The pilot-scale dynamic solids concentration profiles show the same trend: initially, the solids concentration is uniform but subsequent profiles show the accumulation of sludge at the base as a result of settling, as well as a decrease of the sludge blanket height. The concentrations at the base are continuously increasing and higher

concentrations move towards the sludge blanket height. The profiles not only show hindered settling but the equilibrium concentration profiles and the iso-concentration lines clearly show that compression is taking place. Equilibrium compression solids concentrations can be estimated from the equilibrium profiles and are between 7 and 10 g/l depending on the origin of the sludge and the initial solids concentration. The iso-concentration lines show that the compression solids concentration at the beginning should be around the initial solids concentration. Those 2 observations result in a time-dependent compression solids concentration as modelled by Diplas and Papanicolaou (1997) and suggested by Kinnear (2002).

For determining the excess pore pressure profiles during batch settling of suspensions other than activated sludge, pore pressure profiles have been measured with manometers (Shirato *et al.*, 1970; Dreher, 1997) and pressure transducers (Been and Sills, 1981). Subsequently, the excess pore pressure profiles were determined by subtracting the pore pressure from the hydrostatic pressure. Only Been and Sills (1981) and Sills (1998) mentioned the accuracy of this measurement, i.e. 10-30 Pa. This accuracy is however too low for determining the excess pore pressure profiles of activated sludge. For example, if the activated sludge has a solids density of 1800 kg/m³ and a solids concentration of 0.2 vol%, and settling is performed in a column of 1 m height, then the excess pore pressure at the bottom at the beginning of the settling experiment is about 20 Pa ($\Delta\rho g\phi H$) while the hydrostatic pressure is about 10 kPa. Since there is a big difference in absolute value between the excess pore pressure and the hydrostatic pressure, the idea arose to directly measure the excess pore pressure by measuring the pressure difference between the activated sludge settling column and a water-filled column. For that purpose, a differential pressure transducer (Druck LPX9481, Dimed electronic engineering, Ghent) with a range of 200 Pa and an accuracy of 0.2 Pa was used.

The set-up consists of a settling column, a water-filled column and the differential pressure transducer. Fifteen holes were drilled in the settling column at specified heights and in those ports a cigarette filter was inserted to ensure that only the pressure of the water in the sludge is transmitted, i.e. the pore pressure. Tubes with valves connect the ports in the columns with a distributor. The latter is connected to the high pressure port of the transducer. Each of the fifteen ports in the column is connected in turn with the transducer. The low pressure port of the transducer is connected to the water-filled column.

The measurements are however not as good and as detailed as the concentration profile measurements and show some phenomena which could not be explained currently: the pressure at the top of the suspension does not remain constant, even though it is only supernatant and some excess pore pressure measurements are higher than the total solids stress (considered as outliers). When the data are corrected for these phenomena, they confirm compression settling from the suspension-liquid interface downwards: the excess pore pressure at the bottom of the column decreases with time and the total solids stress is higher than the excess pore pressure in the sludge blanket. The calculated effective solids stress versus solids concentration only shows realistic results for 1 of the 3 experiments: a changing compression solids concentration and an effective solids stress which is a function of the difference between the compression solids concentration and the solids concentration. The agreement with the equilibrium solids concentration profile data confirms the correction and rejection of some of the data. More work is needed to improve this measurement technique.

With the solids concentration profiling technique both hindered and compression settling can be studied more thoroughly at an unprecedented level of spatial and temporal resolution. The presented technique can be optimized and analyzed further, by e.g. studying the effect of suspension height, suspension temperature and additives on settling, the adsorption kinetics of the radiotracer, ... A disadvantage of the technique is that the measurements need to be performed at a site where the radiotracer can be produced and where gamma cameras are available. The technique is at this stage not applicable at full-scale.

The excess pore pressure profiling technique shows some nice potential but needs to be studied more thoroughly. When the observed unrealistic phenomena are understood, the technique can be automated so that for instance each of the ports in the column is automatically connected to the transducer.

Detailed batch settling experiments as presented in this dissertation give much more information about the process of activated sludge batch settling and are therefore the most appropriate data for a better and more fundamental model of the settling process. For instance, an accurate prediction of a batch settling curve does not necessarily imply that the solids concentration profiles are correctly described.

9.1.2 Batch settling model

In this dissertation, a new activated sludge batch settling model was developed, which is based on the fundamental mass and force balances for water and solids and which excellently describes batch settling experiments and this for sludges originating from two different wastewater treatment plants.

A review on flocculated slurry settling models (not limited to activated sludge) was the basis to model the activated sludge settling process. The main difference between the reviewed models was the use of different expressions for the hindered settling flux f_{bk} and/or effective solids stress σ_e . The primary goal of the research was to find the appropriate expressions which could describe the activated sludge batch settling experiments.

First, the appropriate hindered settling flux function was selected on the basis of observed initial settling velocities. Next, the effective solids stress function and its parameters were obtained from inverse modelling, in which all concentration profiles, and not only the one at equilibrium (as in common practice), were considered. This method was applicable here since dynamic solids concentration profiles (not only at equilibrium) were measured. The results of these inverse modelling calculations however showed (1) that it was not possible to come up with a single effective solids stress function and (2) that discrepancies existed with the effective solids stress calculated from the equilibrium solids concentration profiles. This implied that the hindered settling flux function gave too low settling velocities at the higher solids concentrations. Because none of the other discussed hindered settling flux functions was capable of giving both good initial settling velocities and higher settling velocities at higher solids concentrations, another hindered settling flux function was selected: the power function of Cole (1968). This function was already evaluated by Cho *et al.* (1993) and Grijpspeerdt *et al.* (1995) and yields higher settling velocities at higher solids concentrations. Disadvantages of the function are (1) an infinite value for a zero solids concentration and (2) the lack of a maximum in the hindered settling flux. This is resolved here by imposing a maximum settling velocity. The inverse modelling calcu-

lations with the Cole (1968) function (1) gave good agreement with the equilibrium data and (2) showed a single effective solids stress function when a time-dependent compression solids concentration is considered that can be readily calculated.

The batch settling experiments and the inverse modelling calculations showed a time-dependent compression solids concentration which is found just below the sludge blanket height and is readily calculated from the solids concentration profiles. Knowing these time-evolutions, the effective solids stress values showed a uniform relationship with the difference between the solids concentration and the compression solids concentration, which could not be described with one of the discussed effective solids stress expressions but exhibited a logarithmic behaviour. A logarithmic function was therefore fitted to the calculated effective solids stress data.

The resulting activated sludge batch settling model is the following:

$$\frac{\partial C}{\partial t} = -\frac{\partial f_{bk}(C)}{\partial z} + \frac{\partial}{\partial z} \left(f_{bk}(C) \frac{\rho_s}{\Delta \rho g C} \frac{d\sigma_e(C)}{dC} \frac{\partial C}{\partial z} \right) \quad (9.1)$$

with boundary conditions and initial condition

$$f_{bk}(C) \left(1 - \frac{\rho_s}{\Delta \rho g C} \frac{d\sigma_e(C)}{dC} \frac{\partial C}{\partial z} \right)_{z=0, z=H} = 0 \quad (9.2)$$

$$C_{t=0} = C_o \quad (9.3)$$

with the hindered settling flux function

$$f_{bk}(C) = aC^{-b} \quad \text{for } \frac{f_{bk}(C)}{C} < 250 \frac{m}{d} \quad (9.4)$$

$$f_{bk}(C) = 250 \frac{m}{d} C \quad \text{for } \frac{f_{bk}(C)}{C} \geq 250 \frac{m}{d} \quad (9.5)$$

and the effective solids stress function

$$\sigma_e(C) = \alpha \ln \left(\frac{C - C_C + \beta}{\beta} \right) \quad \text{for } C > C_C \quad (9.6)$$

$$\frac{d\sigma_e(C)}{dC} = 0 \quad \text{for } C \leq C_C \quad (9.7)$$

The model excellently describes the settling and this for sludges originating from two different wastewater treatment plants. This indicates a good potential for wider applicability of the model. The relationship between the β -parameter and the initial solids concentration should be further investigated by performing batch settling experiments at more than 3 initial solids concentrations.

By performing batch settling experiments at solids concentrations which are located in the increasing part of the settling flux function, a Kynch batch density function could be found which also describes the settling (and the concentration profiles) at these solids concentrations. In Chapter 8 the Kynch batch density function was extended with the Vesilind function to describe such behaviour but this needs to be validated by performing and simulating extensive batch settling experiments at these concentrations.

In practice one cannot expect however to have such detailed batch settling experiments available to identify the settling behaviour (i.e. the hindered settling flux and the effective solids stress functions with their parameters). Instead, a number of

batch settling curves collected with different initial solids concentrations, can be frequently measured with e.g. a Settlometer (Applitek N.V., Belgium; Vanrolleghem *et al.* (1996)). At least 3 batch settling curves need to be measured at quite different solids concentrations in order to estimate the parameters of the batch settling model. First, the parameters of the hindered settling flux function can be estimated from the initial settling velocities. Second, the parameters of the effective solids stress function can be estimated using the batch settling curve measurements after the calculation of the evolution of the compression solids concentration according to Kynch (1952)'s theory. When the settling behaviour, i.e. the parameters of the batch settling model, is identified, it can be used as the basis for (1D, 2D or 3D) models which attempt to describe the full-scale behaviour of a clarifier. Since the batch settling model describes the settling behaviour better than any other reported model, these (1D, 2D or 3D) models can be used e.g. to make better designs and set-up better control strategies.

9.2 Continuous settling of activated sludge

A discussion of the current 1D continuous settling models together with their characteristics and their ability to predict the full-scale behaviour showed that none of these models combines a fundamental description of the hindered and compression settling, a suitable numerical algorithm and a calibration and validation with full-scale dynamic data.

The fundamental description of the hindered and compression settling was developed in section 9.1.1.

The 1D continuous settling model is an initial-boundary value problem of a partial differential equation of second order parabolic type for the solids concentration as a function of height and time. Due to the discontinuous fluxes and the non-linearity of the Kynch batch density function, the solutions of the model equations are discontinuous and a suitable numerical algorithm is required. For the first order spatial terms, upwind differencing is used, and more specific the generalised upwind flux of Engquist and Osher (1981) for the Kynch batch density function. The second order spatial terms are discretised with central differencing. This numerical algorithm is also applied for the activated sludge batch settling model integration.

For calibration and validation of the 1D continuous settling model, 2 detailed full-scale measuring campaigns were performed.

9.2.1 Full-scale continuous settling experiments

Two detailed full-scale measurement campaigns provided measurements of solids concentration profiles in the clarifier, sludge blanket heights, concentrations of the relevant flows (feed, recycle and effluent), batch settling curves and sludge volume index (SVI).

One of the campaigns was performed on the secondary circular centre-fed clarifier of the municipal WWTP of Essen. During the studied period, the settling properties changed and there was a lot of rainfall which resulted in an increase of feed solids concentration. The recycle flow rate was deliberately changed twice (a decrease for a few days and an increase at the end).

Increases in load resulted in increasing recycle solids concentrations and a shift upwards of the sludge blanket height, and vice versa. The changing recycle flow rate had a pronounced effect on the recycle solids concentration and solids concentration

profiles but did not result in a significant change of the sludge blanket height. Worse settling properties resulted in a shift upwards of the sludge blanket height but showed no effect on the recycle solids concentration and solids concentration profile.

The second measurement campaign was performed on a no longer operational primary clarifier of the municipal WWTP of Heist, that was converted into a secondary clarifier. Since the effluent of this clarifier flowed into the activated sludge tanks of the WWTP, this set-up allowed to have overflow of sludge (no effluent restrictions). The Settrometer (Applitek N.V., Belgium; Vanrolleghem *et al.* (1996)) for the measurement of the batch settling curves was modified with an automatic dilution system that mixes return activated sludge with clarified effluent. The dilutions were set at 0% (i.e. no dilution), 30%, 60%, 70% and 80% (i.e. 4 parts of effluent, 1 part of recycle activated sludge). During the studied period, the feed and recycle flow rates were changed frequently and on top of that the settling properties changed. The study showed that it is not straightforward to perform experiments in full-scale conditions: it is impossible to set all variables to desired values (feed solids concentration, settling properties), the daily operation of the WWTP may not be disturbed but on the other hand it influences the experiments (e.g. maintenance works had effect on settling properties and feed solids concentration). There is not always someone present on-site to solve problems, one needs reliable and appropriate sensors/pumps that remain stable with time, etc. Nevertheless, the results were very satisfying.

The effect of variations in recycle and feed flow, feed solids concentrations and settling properties could in most cases be clearly identified and confirmed the expectations:

- A decrease/increase in recycle flow rate resulted in an increase/decrease of the recycle solids concentration and a shift upwards/downwards of the solids concentration profile and sludge blanket height.
- A decrease/increase in feed flow rate resulted in a decrease/increase of the recycle solids concentration and a shift downwards/upwards of the solids concentration profile and sludge blanket height.
- A decrease/increase in feed solids concentration resulted in a decrease/increase of the recycle solids concentration and a shift downwards/upwards of the solids concentration profile and sludge blanket height.
- Changes in the settling properties resulted in a change of the recycle solids concentration and a shift of the solids concentration profile and sludge blanket height.

9.2.2 1D Continuous settling model

The 2 sets of full-scale experimental data were used to build, test and validate a 1D continuous settling model.

The experimental results obtained at the Heist WWTP were used to build and test a 1D continuous settling model. The batch settling model of section 9.1.2 was first used to predict the settling behaviour from the set of measured batch settling curves. Instead of using a maximum settling velocity to account for the deficiency of the Cole (1968) power function that leads to an infinite settling velocity for a zero solids concentration, the Vesilind function (Vesilind, 1968) was used for the lower solids

concentrations together with the condition that the hindered settling flux function is differentiable at the transition solids concentration C_{tr} . First, the parameters of the Vesilind function were estimated from the initial settling velocities. Second, the parameters of the effective solids stress function and the transition concentration were estimated from the batch settling curve measurements. The agreement with the experimental batch settling curves was excellent.

The Heist data were divided into 2 periods: one for building a 1D continuous settling model and one for testing the resulting model.

The basic 1D continuous settling model with dispersion is given by the following equations:

$$\frac{\partial C}{\partial t} = -\frac{\partial F(C)}{\partial z} + \frac{\partial}{\partial z} \left(D \frac{\partial C}{\partial z} \right) + s \quad (9.8)$$

with $F(C) =$

$$\begin{cases} f_{bk}(C) \left(1 - \frac{\rho_s}{\Delta \rho g C} \frac{\partial \sigma_e(C)}{\partial C} \frac{\partial C}{\partial z} \right) - \frac{Q_e}{A} C & 0 \leq z < z_f \\ f_{bk}(C) \left(1 - \frac{\rho_s}{\Delta \rho g C} \frac{\partial \sigma_e(C)}{\partial C} \frac{\partial C}{\partial z} \right) - \frac{Q_e}{A} C + \frac{Q_u}{A} C & z = z_f \\ f_{bk}(C) \left(1 - \frac{\rho_s}{\Delta \rho g C} \frac{\partial \sigma_e(C)}{\partial C} \frac{\partial C}{\partial z} \right) + \frac{Q_u}{A} C & z_f < z \leq H_{centre} \end{cases} \quad (9.9)$$

$$s = \frac{Q_f}{A} C_f \Delta (z - z_f) \quad (9.10)$$

with the hindered settling flux function

$$f_{bk}(C) = a_1 e^{-b_1 C} C \quad \text{for } C \leq C_{tr} \quad (9.11)$$

$$f_{bk}(C) = a C^{-b} \quad \text{for } C > C_{tr} \quad (9.12)$$

with

$$b = -1 + b_1 C_{tr} \quad (9.13)$$

$$a = a_1 C_{tr}^{b+1} e^{-b_1 C_{tr}} \quad (9.14)$$

with the effective solids stress function

$$\sigma_e(C) = \alpha \ln \left(\frac{C - C_C + \beta}{\beta} \right) \quad \text{for } C > C_C \quad (9.15)$$

$$\frac{d\sigma_e(C)}{dC} = 0 \quad \text{for } C \leq C_C \quad (9.16)$$

with boundary conditions and initial condition

$$f_{bk}(C) \left(1 - \frac{\rho_s}{\Delta \rho g C} \frac{d\sigma_e(C)}{dC} \frac{\partial C}{\partial z} \right) - D \frac{\partial C}{\partial z} \Big|_{z=0, z=H_{centre}} = 0 \quad (9.17)$$

$$C_{t=0} = C_o \quad (9.18)$$

The compression solids concentration C_C was the concentration that is found at a location of 5 layers below the location of the highest concentration gradient of the simulated solids concentration profile. The feed layer location z_f was set equal to the location where the compression solids concentration occurred. The β -parameter of the effective solids stress function was made dependent on the average solids concentration in the clarifier.

A simulation with the model without a dispersion term showed a too compact sludge blanket, an unpredicted sludge blanket height and the need for dispersion. As proposed by others, a model with two dispersion coefficients, one in the clarification zone and the other in the thickening zone, gave a fairly good prediction of the measurements (estimated standard deviation of the predicted solids concentrations is 0.89 g/l). The dispersion coefficients were estimated from the measured solids concentration profiles. The simulation data showed that the profiles reacted instantaneously to changes in independent variables (flow rates, feed solids concentrations and settling properties). When neither the simulations nor the measurements showed a constant concentration zone in the sludge blanket height, the solids concentration profiles were nicely predicted, except at the end of the studied period. In the other cases, there was an overprediction of the higher concentrations and an underprediction of the lower concentrations in the concentration profiles. A hypothesis is that this may be due to a too low effective solids stress or to another process which is not considered in the current 1D continuous settling model. To improve the results, it could e.g. be investigated whether the dispersion coefficients could be related to one or more independent variables. Since the dispersion terms are a lumped term of all processes that affect the solids profile besides convection and settling and a 2D continuous settling model describes most of these processes, such a 2D model incorporating the batch settling model could result in a better prediction of the experimental data. Another way to improve the model results could be pursued by performing another full-scale measuring campaign together with extensive batch settling experiments at various initial solids concentrations and modelling these data, in order to identify whether the settling properties could really be accurately determined from batch settling curves (e.g. do both measurements result in the same settling properties? What is the relationship between the β -parameter and the initial solids concentration?). Another point that needs more attention, is whether the dependency of the β -parameter of the effective solids stress function on the initial solids concentration in batch settling is currently correctly translated to a system with continuous settling. The calculation of the compression solids concentration needs to be further investigated, e.g. it could be determined as the concentration in the sludge blanket at which a value of 90% or less of the maximum concentration gradient is reached. The recycle solids concentrations are predicted nicely. However, the time it takes to reach a new steady-state after changes differs between simulations and measurements.

The trends observed in the data, which were used for testing the resulting model (with the original values for the dispersion coefficients), were well predicted by the simulations (estimated standard deviation of the solids concentrations is 0.57 g/l), but quantitatively the model is not performing very well.

The experimental results obtained at the Essen WWTP were used to validate the 1D continuous settling model with dispersion. First, the batch settling model was used to characterise the settling behaviour from measured batch settling curves. Since less curves were available and the automatic dilution system was not yet operational, the settling properties (and all the parameters) could not be determined as accurately as with the Heist data. This however did not influence the excellent prediction of the batch settling curves with the batch settling model.

The two dispersion coefficients of the 1D continuous settling model were estimated with the measured solids concentration profiles collected at the Essen WWTP. The resulting model could predict the trends observed in the Essen data but quantitatively the model is not performing very well.

When the 1D continuous settling model is improved e.g. by the research lines suggested above, the model could be used for operation and control in the following way. The settling properties are estimated by regularly fitting the model to on-line measured batch settling curves. Every measured batch settling curve is used as input to the activated sludge batch settling model for estimation of the settling parameters. Measuring a batch settling curve takes about 40 minutes while simulating/estimating takes about 1 minute. The current settling properties are subsequently used as input for the 1D continuous settling model (next to flow rates and feed solids concentration) that simulates/predicts the (expected) solids concentration profiles. For each specific clarifier, the two dispersion coefficients probably need to be estimated once from some profile measurements. Knowing the settling properties and the dispersion coefficients, simulations with the 1D continuous settling model can be used to predict the clarifier behaviour during normal and abnormal (e.g. high flow rates, bad settling properties) operation and to develop and test control strategies. Devisscher & Boonen (2003) also showed that simulation of the concentration profiles visualises the effect of certain operational regimes. For instance, when a clarifier is critically loaded (i.e. the clarifier will be overloaded during peak flows), simulations can be performed to investigate which control strategy (for instance manipulating flow rates) prevents massive wash-out of sludge from the clarifier.

Both the batch and continuous settling model can be improved by incorporating the activated sludge settling behaviour at low concentrations (discrete and flocculent settling). In this way, they can predict and simulate the low concentrations above the sludge blanket height and the effluent solids concentrations. In future studies, the influence of the biology of the activated sludge on the settling behaviour could be investigated and modelled.

Appendix A

Radioactivity profiles

This appendix shows the radioactivity profiles for 4 of the 5 experiments given in Table 5.1, resulting from the scan after about 2 hrs settling.

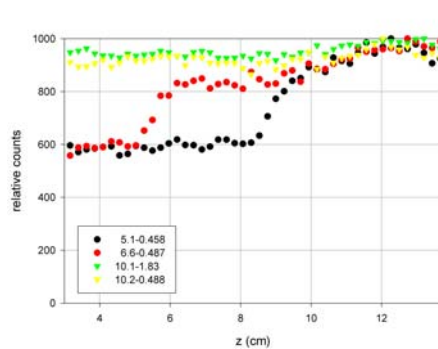


Figure A.1: Profile of the relative counts of radioactive Tc-99m Sestamibi after about 2 hours of batch settling for different initial solids concentrations (g/l) and different radioactivities (mCi) (see legend)

Appendix B

Initial Kynch batch density values: calculations and functions

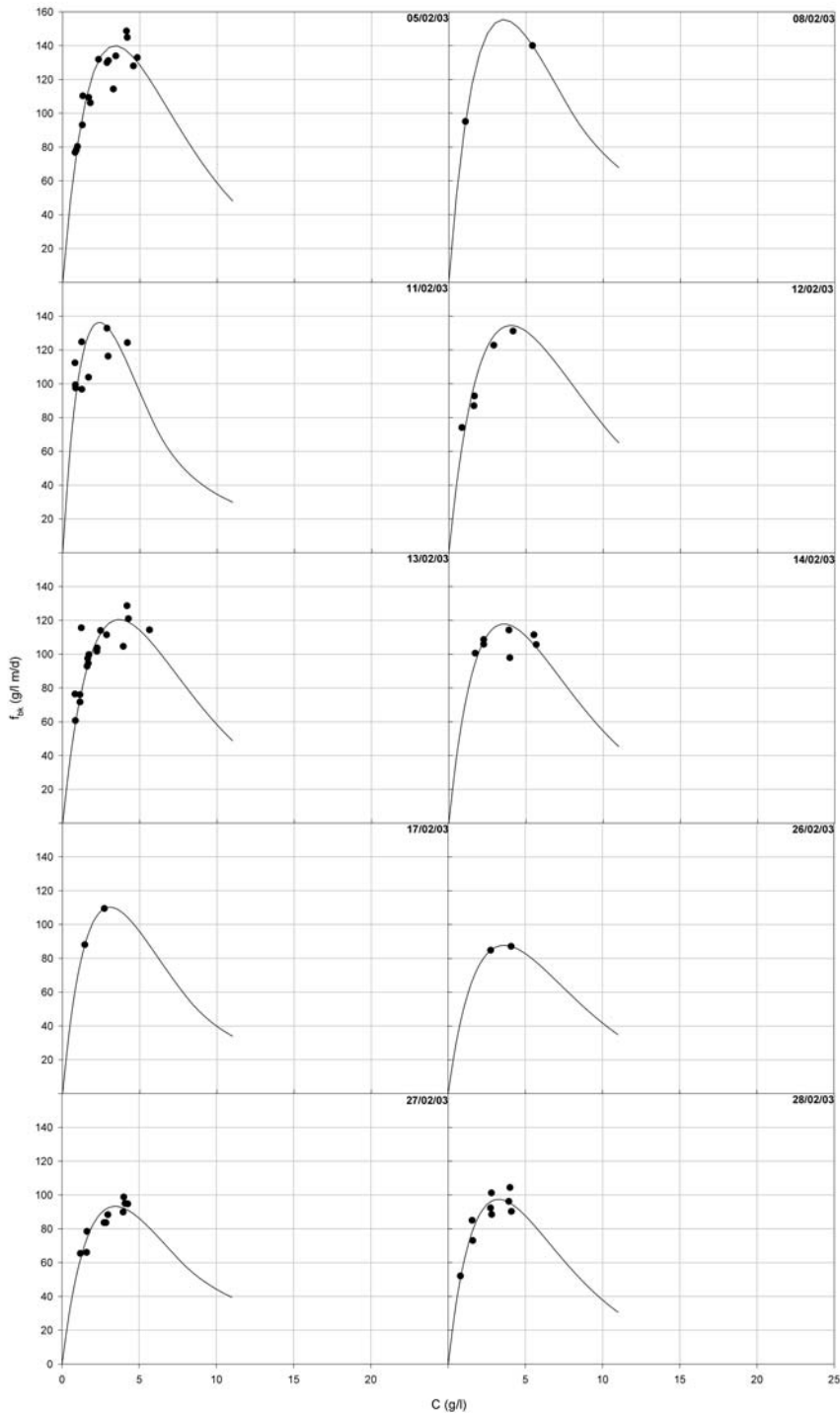


Figure B.1: Calculated Kynch batch density values (symbols) and Kynch batch density function (lines) (date in legend), first period Heist data

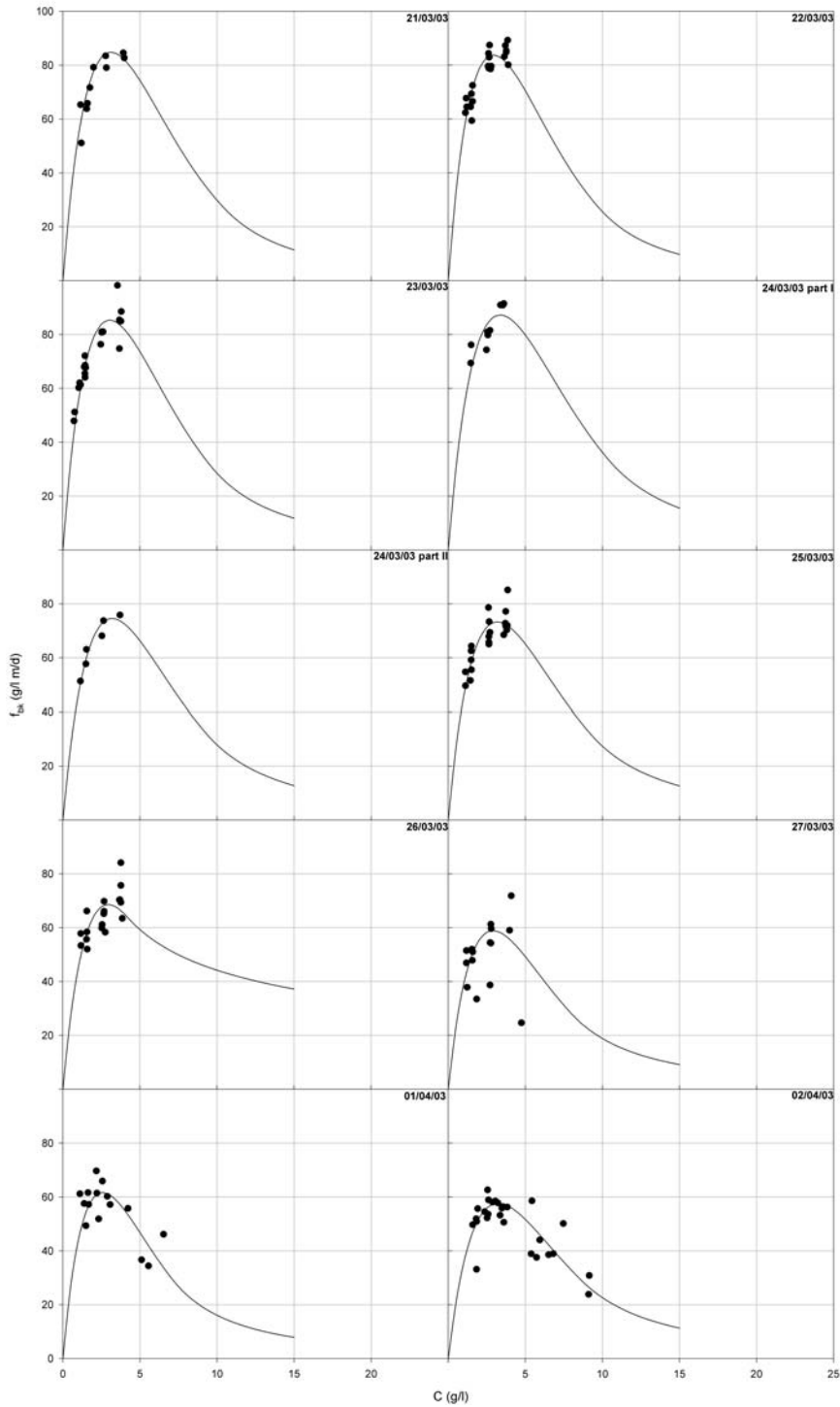


Figure B.2: Calculated Kynch batch density values (symbols) and Kynch batch density function (lines) (date in legend), first part second period Heist data

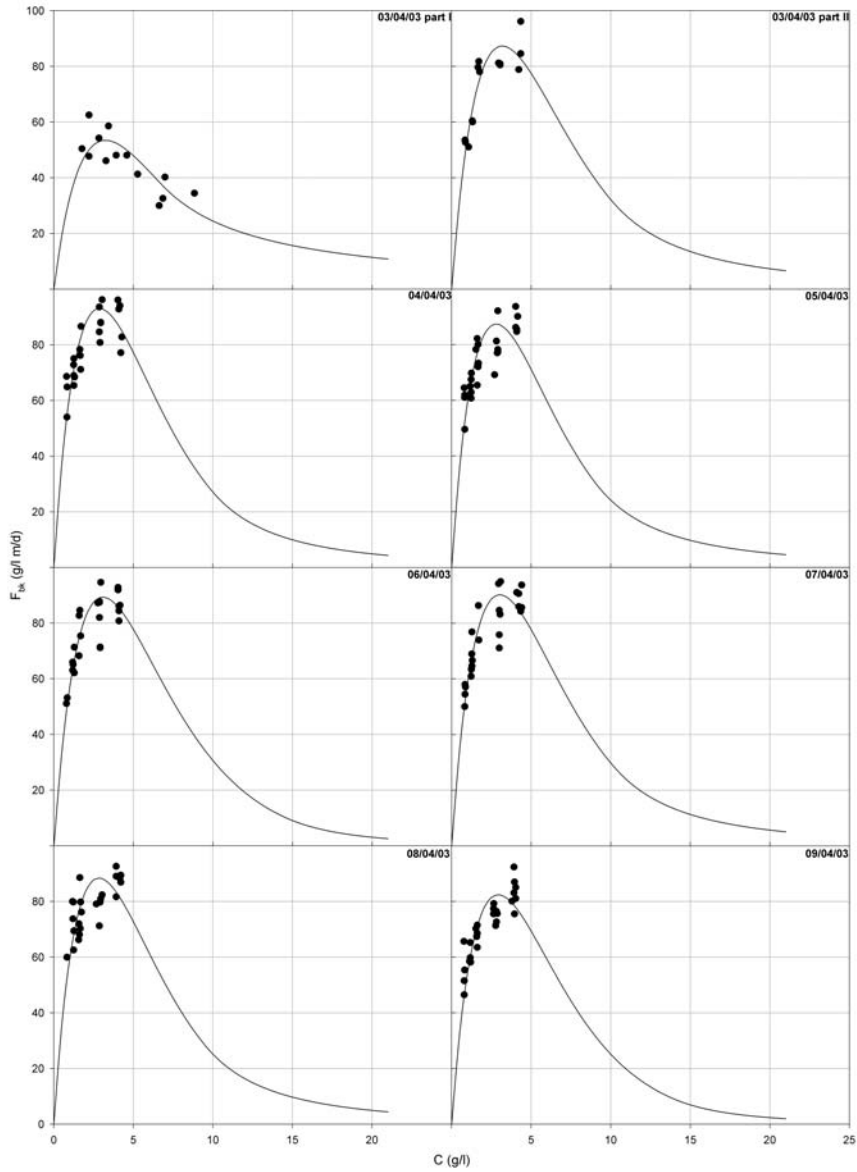


Figure B.3: Calculated Kynch batch density values (symbols) and Kynch batch density function (lines) (date in legend), second part second period Heist data

Appendix C

Batch settling curves Heist data: measurements and simulations with Vesilind function

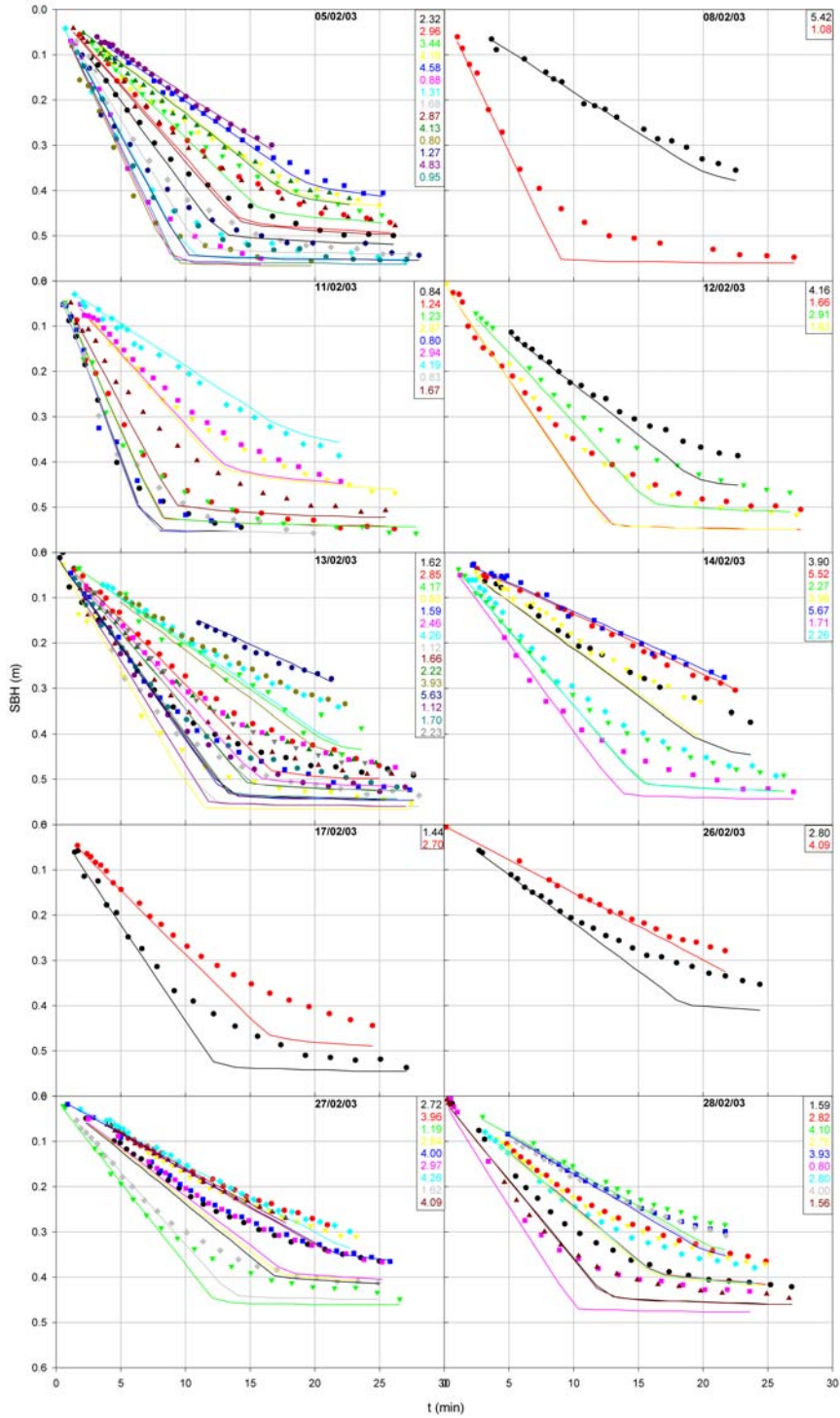


Figure C.1: Measured (symbol) and simulated (line) batch settling curves (date and concentration (g/l) in legend), first period Heist data

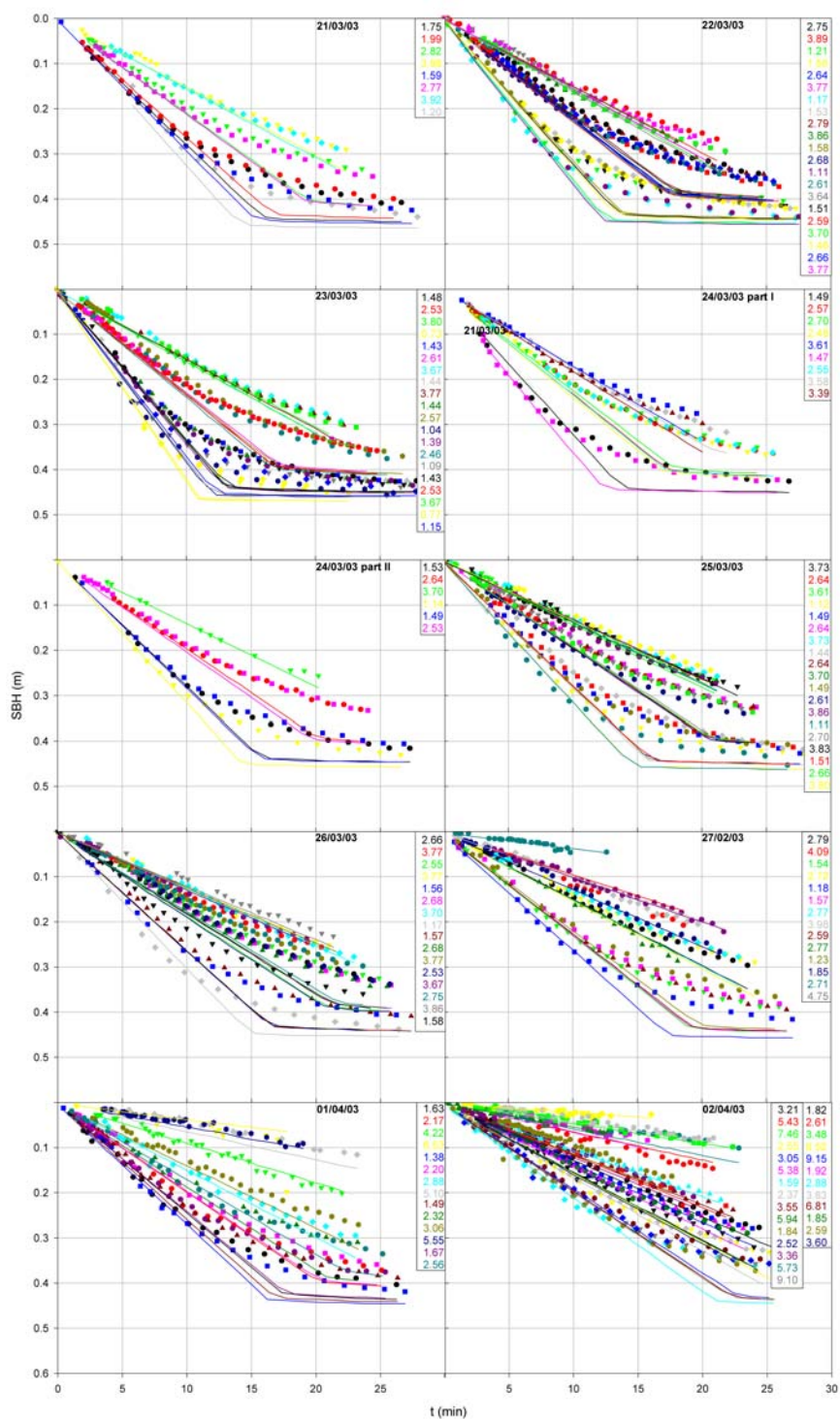


Figure C.2: Measured (symbol) and simulated (line) batch settling curves (date and concentrations (g/l) in legend), first part second period Heist data

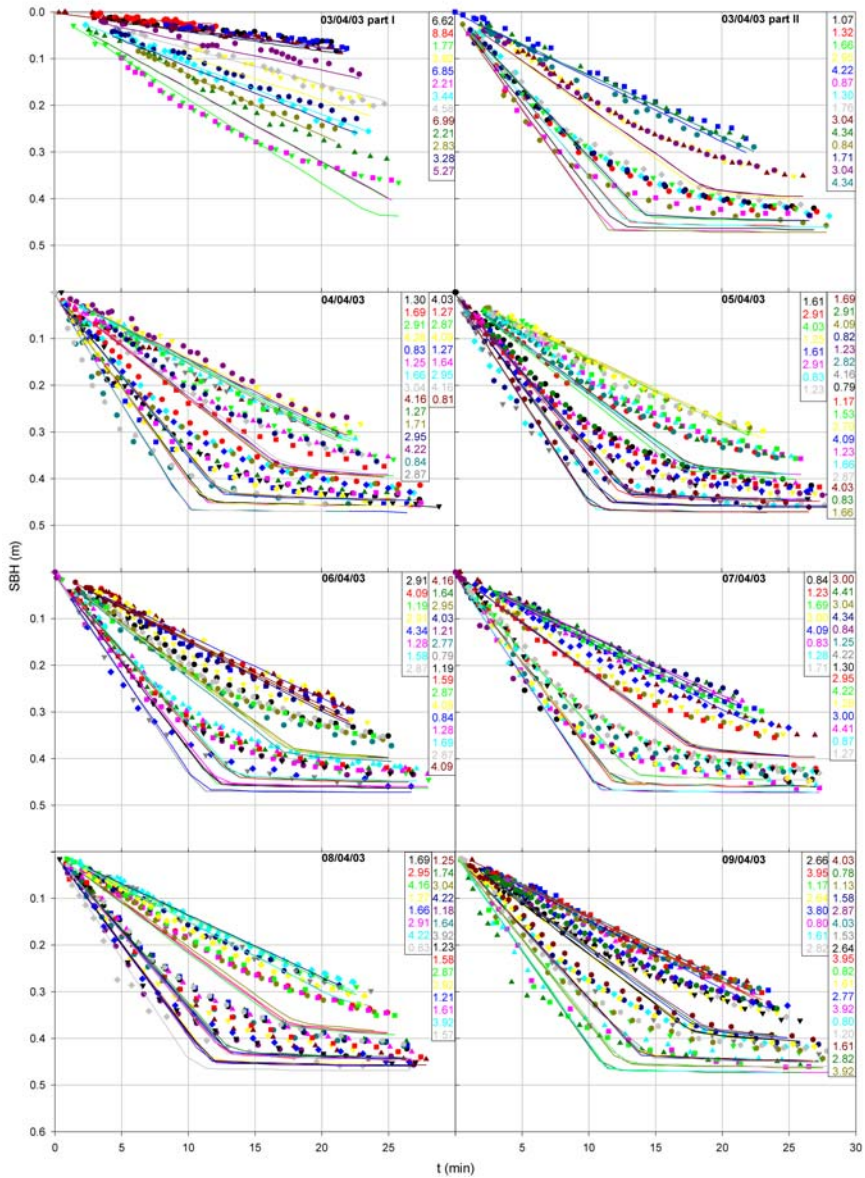


Figure C.3: Measured (symbol) and simulated (line) batch settling curves (date and concentrations (g/l) in legend), second part second period Heist data

Bibliography

- Anderson N.E. (1945). Design of final settling tanks for activated sludge. *Sewage Works Journal*, 17, 50-65.
- Arden E. and Lockett W.T. (1914). Experiments on the Oxidation of Sewage without the Aid of Filters. *J.Soc.Chem.Ind.*, 33, 523-1122.
- Audic J.M., Fayoux C., Lesty Y. and Brisset P. (1993). Sludge retention times distribution in clarifier: a key point for population dynamic and nutrients removal control. First International Specialized Conference on Microorganisms in Activated Sludge and Biofilm Processes, september 27-28, 523-526.
- Bailey L.V. and Harkness N. (1978). Determination of sludge residence time in primary sedimentation tanks. *Effluent and Water Treatment Journal*, October 1978, 497-509.
- Been K. (1980). Stress strain of a cohesive soil deposited under water. PhD thesis, Balliol College, Oxford.
- Been K. and Sills G.C. (1981). Self-weight consolidation of soft soils: an experimental and theoretical study. *Géotechnique*, 31, 519-535.
- Behn V.C. (1957). Settling behavior of waste suspensions. *Journal of the sanitary engineering division ASCE*, 83 (SA5), 1423-1 1423-20.
- Bergström L. (1992). Sedimentation of Flocculated Alumina Suspensions: γ -Ray Measurements and Comparison with Model Predictions. *Journal of the Chemical society. Faraday transactions*, 88 (21), 3201-3211.
- Bhargava D.S. and Rajagopal K. (1990). Modelling in zone settling for different types of suspended materials. *Water Research*, 24 (6), 675-683.
- Billmeier E. (1978). Verbesserte bemessungsvorschläge für horizontal durchströmte nachklärbecken von belebungsanlagen. *Berichte aus Wassergütewirtschaft and Gesundheitsingenieurwesen*, TU München, Band 21.
- Borroto J.I., Dominquez J., Griffith J., Fick M. and Leclerc J.P. (2003). Technetium-99m as a tracer for the liquid RTD. *Chemical Engineering and Processing*, 42, 857-865.
- Brinkman H.C. (1947). A calculation of the viscous force exerted by a flowing fluid on a dense swarme of particles. *Applied Science Research*, A1, 27-34.

- Brouckaert C.J. and Buckley C.A. (1999). The use of computational fluid dynamics for improving the design and operation of water and wastewater treatment plants. *Water Science & Technology*, 40 (4-5), 81-89.
- Bürger R. and Concha F. (1998). Mathematical model and numerical simulation of the settling of flocculated suspensions. *International Journal of Multiphase Flow*, 24, 1005-1023.
- Bürger R. and Wendland W.L. (1998). Entropy boundary and jump conditions in the theory of sedimentation with compression. *Mathematical Methods in the Applied Sciences*, 21, 865-882.
- Bürger R., Evje S., Karlsen K.H., Lie K.-A. (2000). Numerical methods for the simulations of the settling of flocculated suspensions. *Chemical Engineering Journal*, 80, 91-104.
- Bürger R., Concha F. and Tiller F.M. (2000). Applications of the phenomenological theory to several published experimental cases of sedimentation processes. *Chemical Engineering Journal*, 80, 105-117.
- Bürger R. and Karlsen K.H. (2001). On some upwind difference schemes for the phenomenological sedimentation-consolidation model. *Journal of Engineering Mathematics*, 41, 145-166.
- Bürger R., Concha F., Fjelde K.-K. and Karlsen K.H. (2001). Numerical simulation of the settling of polydisperse suspensions of spheres. *Power Technology*, 113, 30-54.
- Bürger R., Damasceno J.J.R., and Karlsen K. H. (2004). A mathematical model for batch and continuous thickening of flocculent suspensions in vessels with varying cross section. *International Journal of Mineral Processing*, 73, 183-208.
- Buscall R. and White L.R. (1987). The consolidation of concentrated suspensions, Part 1 - The Theory of Sedimentation. *Journal Chemical Society Faraday I*, 83, 873-891.
- Bustos M.C., Concha F., Bürger R. and Tory E.M. (1999). *Sedimentation and Thickening, Phenomenological Foundation and Mathematical Theory. Mathematical Modelling: Theory and Applications Volume 8.* Kluwer Academic Publishers, Dordrecht.
- Cacossa K.F. (1994). Calibration and validation of a compressive gravity thickening model from continuous and batch experiments with activated sludge. PhD-thesis, Faculty of the Stevens Institute of Technology, Hoboken, New Jersey.
- Cacossa K.F. and Vaccari D.A. (1994). Calibration of a compressive gravity thickening model from a single batch settling curve. *Water Science & Technology*, 30 (8), 107-116.
- Chen G.W., Chang I.L., Hung W.T. and Lee D.J. (1996). Regimes for zone settling of waste activated sludges. *Water Research*, 30 (8), 1844-1850.
- Chmielewski A.G., Owczarczyk A. and Palige J. (1998). Radiotracer investigations of industrial wastewater equalizer-clarifiers. *Nukleonika*, 43 (2), 185-194.
- Cho S.H., Colin F., Sardin M. and Prost C. (1993). Settling velocity of activated sludge. *Water Research*, 27, 1237-1242.

- Chu C.P., Ju S.P., Lee D.J. and Mohanty K.K. (2002). Batch gravitational sedimentation of slurries. *Journal of Colloid and Interface Science*, 245, 178-186.
- Chu C.P., Lee D.J. and Tay J.H. (2003). Gravitational sedimentation of flocculated waste activated sludge. *Water Research*, 37, 155-163.
- Clauss F., Helaine D., Balavoine C., Bidault A. (1998). Improving activated sludge floc structure and aggregation for enhanced settling and thickening performances. *Water Science & Technology*, 38 (8-9), 35-44.
- Cole R.F. (1968). Experimental evaluation of the Kynch theory. PhD thesis, University of North Carolina, Chapel Hill.
- Concha F and Burger R. (2002). A century of research in sedimentation and thickening. *KONA Powder and Particle*, 20, 38-70.
- De Clercq B. (2003). Computational fluid dynamics of settling tanks: development of experiments and rheological, settling, and scraper submodels. PhD-thesis, Department of Applied Mathematics, Biometrics and Process Control (Biomath), Ghent University.
- Deininger A., Günthert F.W. and Wilderer P.A. (1996). The influence of currents on circular secondary clarifier performance and design. *Water Science & Technology*, 34(3-4), 405-412.
- Deininger A., Holthausen E. and Wilderer P.A. (1998). Velocity and solids distribution in circular secondary clarifiers: Full scale measurements and numerical modelling. *Water Research*, 32 (10), 2951-2958.
- Diehl S. (1995). On scalar conservation laws with point source and discontinuous flux function. *Siam Journal on Mathematical Analysis*, 26 (6), 1425-1451.
- Devisscher M. and Boonen I. (2003). Simple operational tools for secondary settler operation—conceptual validation on an extended full-scale data set. *Communications in Agricultural and Applied Biological Sciences*, 68(2PtA), 151-154.
- Diehl S. (1996). A conservation law with point source and discontinuous flux function modelling continuous sedimentation. *SIAM Journal on Applied Mathematics*, 56 (2), 388-419.
- Diehl S. and Jeppsson U. (1998). A model of a settler coupled to the biological reactor. *Water Research*, 32(2), 331-342.
- Diplas P. and Papanicolaou A.N. (1997). Batch Analysis of Slurries in Zone Settling Regime. *Journal of Environmental Engineering*, 123 (7), 659-667.
- Dreher T. (1997). Preprint 97/34, Sonderforschungsbereich 404, University of Stuttgart.
- Dupont R. and Dahl C. (1995). A one-dimensional model for a secondary settling tank including density current and short-circuiting. *Water Science & Technology*, 31(2), 215-224.
- Dupont R. and Henze M. (1992). Modelling of the secondary clarifier combined with the activated sludge model no. 1. *Water Science & Technology*, 25 (6), 285-300.

- Edwards H.O. (1998). An instrument for the measurement of colour and turbidity in natural waters. *Water Science & Technology*, 37 (12), 263-267.
- Ekama G.A. and Marais P. (2004). Assessing the applicability of the 1D flux theory to full-scale secondary settling tank design with a 2D hydrodynamic model. *Water Research*, 38, 495-506.
- Ekama G.A., Barnard J.L., Gnther F.W., Krebs P., McCorquodale J.A., Parker D.S. and Wahlberg E.J. (1997). Secondary settling tanks: theory, modelling, design and operation. IAWQ Scientific and Technical reports: no.6, London.
- Engquist B. and Osher S. (1981). One-sided difference approximations for nonlinear conservation laws. *Math. Comput.* 36, 154, 321-352.
- Evje S. and Karlsen K.H. (2000). Monotone difference approximations of BV solutions to degenerate convection-diffusion equations. *SIAM Journal on Numerical Analysis*, 37 (6), 1838-1860.
- Farooq M., Khan I.H., Ghiyas-ud-Din, Gul S., Palige J. and Dobrowolski A. (2003). Radiotracer investigations of municipal sewage treatment stations. *Nukleonika*, 48 (1), 57-61.
- Fitch B. (1983). Kynch theory and compression zones. *AIChE Journal*, 29(6), 940-947.
- Font R. (1988). Compression Zone Effect in Batch Sedimentation. *AIChE Journal*, 34 (2), 229-238.
- Font R. (1991). Analysis of the batch sedimentation test. *Chemical Engineering Science*, 46 (10), 2473-2482.
- Font R., Garcia P. and Rodriguez M. (1999). Sedimentation test of metal hydroxides: hydrodynamics and influence of pH. *Colloids and Surfaces A: Physicochemical and Engineering Aspects*, 157, 73-84.
- Font R. and Laveda M.L. (2000). Semi-batch test of sedimentation. Application to design. *Chemical Engineering Journal*, 80, 157-165.
- Geatti O. (1999). Parathyroid scintigraphy. *Quarterly Journal of Nuclear Medicine*, 43 (3), 207-216.
- Govoreanu R. (2004). Activated sludge flocculation dynamics: on-line measurement methodology and modelling. PhD-thesis, Department of Applied Mathematics, Biometrics and Process Control (Biomath), Ghent University.
- Grijpspeerdt K., Vanrolleghem P. and Verstraete W. (1995). Selection of one-dimensional sedimentation models for on-line use. *Water Science & Technology*, 31 (2), 193-204.
- Grijpspeerdt K. and Verstraete W. (1995). Residence time distribution measurement for activated-sludge using pyrene as a tracer element. *Environmental Technology*, 16 (5), 483-488.
- Hamilton J., Jain R., Antoniou P., Svoronos S.A., Koopman B. and Liberatos G. (1992). Modeling and pilot-scale experimental verification for predenitrification process. *Journal of Environmental Engineering*, 118 (1), 38-55.

- Härtel L. and Pöpel H.J. (1992). A dynamic secondary clarifier model including processes of sludge thickening. *Water Science & Technology*, 25 (6), 267-284.
- Holdich R.G. and Butt G. (1997). Experimental and Numerical Analysis of a Sedimentation Forming Compressible Compacts. *Separation Science and Technology*, 32 (13), 2149-2171.
- IAEA (2001). Radiotracer technology as applied to industry.
- Jeppsson U. and Diehl S. (1996). An evaluation of a dynamic model of the secondary clarifier. *Water Science & Technology*, 34 (5-6), 19-26.
- Jin B., Wilén B.-M., and Lant P. (2003). A comprehensive insight into floc characteristics and their impact on compressibility and settleability. *Chemical Engineering Journal*, 95 (1-3) , 221-234.
- Joannis C., Aumond M., Dauphin S., Ruban G., Deguin A. and Bridoux G. (1999). Modeling activated sludge mass transfer in a treatment plant. *Water Science & Technology*, 39 (4), 29-36.
- Karl J.R. and Wells S.A. (1999). Numerical Model of Sedimentation/Thickening with Inertial Effects. *Journal of Environmental Engineering*, 125 (9), 792-806.
- Kinnear D.J. (2002). Biological solids sedimentation: a model incorporating fundamental settling parameters. PhD thesis, Department of Civil and Environmental Engineering, University of Utah.
- Köhne M.K., Hoen K. and Schuhen M. (1995). Modelling and simulation of final clarifiers in wastewater treatment plants. *Mathematics and Computers in Simulation*, 39 (5-6), 609-616.
- Kynch G.J. (1952). A theory of sedimentation. *Transactions of the Faraday society*, 48, 166-176.
- Lakehal D., Krebs P., Krijgsman J. and Rodi W. (1999). Computing shear flow and sludge blanket in secondary clarifiers. *Journal of hydraulic engineering-ASCE*, 125 (3), 253-262.
- Larsen P. (1977). On the hydraulics of rectangular settling basins. Report no. 1001, Department of Water Resources Engineering, Lund Institute of Technology, University of Lund, Sweden.
- Lee T.T., Wang F.Y. and Newell R.B. (1999). Distributed parameter approach to the dynamics of complex biological processes. *AIChE Journal*, 45 (10), 2245-2268.
- Le Poulichet M. (2001). Suivi détaillé d'un clarificateur secondaire par des analyses de terrain et à l'aide d'appareils en ligne: effet du débit de recirculation et courbe de flux. Internal report, Aquafin NV. pp. 59.
- Lumley D.J. and Horkeby G. (1989). Detention time distribution of sludge in rectangular secondary settlers. *Water Science & Technology*, 21, 1763-1766.
- Lumley D.J. and Balmér (1990). Solids transport in rectangular secondary clarifiers. *Water Supply*, 8, 123-132.

- Lyn D.A., Stamou A.I. and Rodi W. (1992). Density currents and shear-induced flocculation in sedimentation tanks. *Journal of Hydraulic Engineering*, 118 (6), 849-867.
- Malisse K., De Clercq J. and Vanrolleghem P.A. (2004). Sludge Density Technical Report. BIOMATH, Ghent University, Ghent, Belgium. Internal Report.
- Marquardt D.W. (1963). An algorithm for the least squares estimation of non-linear parameters. *Journal of the Society for Industrial and Applied Mathematics on Control*, 11, 431-441.
- Matsui S., Tanka F. and Shibata S. (1978). The control method of activated sludge system(I)-Evaluation of the sludge volume in the secondary settling tank. *Journal of Japan Sewage Works Association*, 15, 33-39.
- Mines R.O., Vilagos J.L., Echelberger W.F. and Murphy R.J. (2001). Conventional and AWT Mixed-Liquor Settling Characteristics. *Journal of Environmental Engineering*, 127 (3), 249-258.
- Muller E., Kriebitzsch K., Wilderer P.A. and Wuertz S. (2002). Community structure of micro- and macroflocs in pin-point sludge and the influence of sludge age and potassium addition on microfloc formation. *Water Science & Technology*, 46 (1-2), 405-412.
- Murthy S.N. and Novak J.T. (1998). Effects of potassium ion on sludge settling, dewatering and effluent properties. *Water Science & Technology*, 37 (4-5), 317-324.
- Nopens I. (2005). Modelling the activated sludge flocculation process: a population balance approach. PhD-thesis, Department of Applied Mathematics, Biometrics and Process Control (Biomath), Ghent University.
- Novak J.T., Love N.G., Smith M.L. and Wheeler E.R. (1998). The effect of cationic salt addition on the settling and dewatering properties of an industrial activated sludge. *Water Environment Research*, 70 (5), 984-996.
- Olsson G. and Newell B. (1999). *Wastewater Treatment Systems, Modelling, Diagnosis and Control*. IWA Publishing, London.
- Olsson L. and Nielsen J. (1997). On-line and in-situ monitoring of biomass in submerged cultivations. *Trends in Biotechnology*, 15, 517-522.
- Onillon C. (2003). Recherche sur la clarification secondaire: Mise au point d'une installation de mesures a pleine échelle. Internal report, Aquafin N.V. pp. 43.
- Otterpohl R. and Freund M. (1992). Dynamic models for clarifiers of activated sludge plants with dry and wet weather flows. *Water Science & Technology*, 26 (6), 1391-1400.
- Ozinsky A.E. and Ekama G.A. (1995). Secondary settling tank modelling and design Part 1 : Review of theoretical and practical developments. *Water SA*, 21 (4), 325-332.
- Papanicolaou A.N. and Diplas P. (1999). Numerical solution of a non-linear model for self-weight solids settlement. *Applied Mathematical Modelling*, 23, 345-362.

- Parker D.S. (1983). Assessment of secondary clarification design concepts. *Journal Water pollution control federation*, 55 (4), 349-359.
- Parker D.S. (1995). Assessment of secondary clarification design concepts. *Journal Water pollution control federation*, 55 (4), 349-359.
- Parker D.S., Kinnear D.J. and Wahlberg E.J. (2001). Review of folklore in design and operation of secondary clarifiers. *Journal of Environmental Engineering*, 127 (6), 476-484.
- Patry G.G. and Takács I. (1992). Settling of flocculent suspensions in secondary clarifiers. *Water Research*, 26, 473-479.
- Perez M., Font R. and Pastor C. (1998). A mathematical model to simulate batch sedimentation with compression behavior. *Computers & Chemical Engineering*, 22(11), 1531-1541.
- Pflanz P. (1969). Performance of (activated sludge) secondary sedimentation basins. In Jenkins S.H. (Ed.) *Advances in water pollution research*. London, Pergamon Press, 569-581.
- Press W.H., Flannery B.P., Teukolsky S.A. and Vetterling W.T. (1992). *Numerical recipes in Fortran 77: The art of scientific computing*. 2nd edition, Cambridge, Cambridge University Press.
- Richardson J.F. and Zaki W.N. (1954). Sedimentation and Fluidisation: Part I. *Transactions of the Institute of Chemical Engineers*, 32, 35-53.
- Rietema K. and Musters S.P.M. (1973). The Effect of Interparticle Forces on the Expansion of a Homogeneous Gas-Fluidized Bed. Paper presented at the International Symposium on Fluidization, Toulouse, France.
- Rushton A., Ward A.S and Holdich R.G. (2000). *Solid-Liquid Filtration and Separation Technology*, Second, Completely Revised Edition. Wiley-Vch Verlag GmbH, Weinheim.
- Samstag R.W., Dittmar D.F., Vitasovic Z. and McCorquodale J.A. (1992). Underflow geometry in secondary clarifiers. *Water Environment Research*, 64 (3), 204-212.
- Scott K.J. (1968). Theory of thickening: factors affecting settling rate of solids in flocculated pulps. *Transactions of the Institution of Mining and Metallurgy*, 77, C85-C97.
- Shih Y.T., Gidaspow D. and Wasan D.T. (1986). Sedimentation of Fine Particles in Nonaqueous Media: Part I - Experimental, Part II - Modeling. *Colloids and Surfaces*, 21, 393-429.
- Shirato M., Kato H., Kobayashi K. and Sakazaki H. (1970). Analysis of settling of thick slurries due to consolidation. *Journal of Chemical Engineering of Japan*, 3 (1), 98-104.
- Sills G. (1998). Development of structure in sedimenting soils. *Philosophical transactions of the Royal Society of London A*, 356, 2515-2534.

- Eaton A.D., Clesceri L.S. and Greenberg A.E. (1995). Standard methods for the examination of water and wastewater. 19th Edition 1995. American Public Health Association, American Water Works Association, Water Environment Federation.
- Taebi-Harandy A. and Schroeder E.D. (2000). Formation of density currents in secondary clarifier. *Water Research*, 34 (4), 1225-1232.
- Takács I., Patry G.G. and Nolasco D. (1991). A dynamic model of the clarification-thickening process. *Water Research*, 25 (10), 1263-1271.
- Tchobanoglous G. and Burton F.L. (1991). *Wastewater engineering Treatment, Disposal and Reuse*. 3rd Edition, Metcalf & Eddy, Inc.
- Tiller F.M. (1981). Revision of Kynch sedimentation theory. *AIChE Journal*, 27 (5), 823-829.
- Tiller F.M. and Khatib Z. (1984). The theory of sediment volumes of compressible, particulate structures. *Journal of Colloid and Interface Science*, 100 (1), 55-67.
- Tiller F.M. (1985). Unifying the theory of thickening, filtration and centrifugation. *Proc. Engrg. Found. Conf.*, B.M. Moudgil and B.J. Schneider, eds., American Institute Of Chemical Engineers, New York, 89-141.
- Tiller F.M., Hsyung N.B., Shen Y.L. (1991). *Catscan Analysis of Sedimentation in Constant Pressure Filtration*. Proceedings of the Fifth World Congress on Filtration 2, 80, Socit Franaise de Filtration, Nice, France.
- Tracy K.D. (1973). *Mathematical modelling of unsteady-state thickening*. PhD Thesis. Clemson University.
- Ueberl J. and Hager W.H. (1997). Improved design of final settling tanks. *Journal of Environmental Engineering*, 123 (3), 259-268.
- Vaccari D.A. (1984). *Modeling and Simulation of Compressive Gravity Thickening of Activated Sludge*. PhD thesis, Rutgers University.
- Vanderhasselt A. and Vanrolleghem P.A. (2000). Estimation of sludge sedimentation parameters from single batch settling curves. *Water Research*, 34 (2), 395-406.
- Vanrolleghem P.A., Van der Schueren D., Krikilion G., Grijspeerdt K., Willems P. and Verstraete W. (1996). On-line quantification of settling properties with In-Sensor-Experiments in an automated settlometer. *Water Science & Technology*, 33(1), 37-51.
- Vanrolleghem P.A. and Lee D.S. (2003). On-line monitoring equipment for wastewater treatment processes: state of the art. *Water Science & Technology*, 47 (2), 1-34.
- Vesilind P.A. (1968). Discussion of 'Evaluation of activated sludge thickening theories' by Dick R.I. and Ewing B.B. *Journal of the sanitary engineering division ASCE*, 94 (SA1), 185-191.
- Vitasovic Z.Z. (1989). Continuous settler operation: a dynamic model. In Patry, G.G. & Chapman, D. (Ed.) *Dynamic modelling and expert systems in wastewater engineering*. Chelsea, Michigan, U.S.A., Lewis, 59-81.

- Vitasovic Z.C., Zhou S.P., McCorquodale J.A. and Lingren K. (1997). Secondary clarifier analysis using data from the Clarifier Research Technical Committee protocol. *Water Environment Research*, 69 (5), 999-1007.
- Von Sperling M. and Froes C.M.V. (1999). Determination of the required surface area for activated sludge final clarifiers based on a unified database. *Water Research*, 33(8), 1884-1894.
- Vucina J. and Lukic D. (2002). Radionuclidic generators for the production of technetium-99m and rhenium-188. *Facta Universitatis, Series Physics, Chemistry and Technology*, 2 (4), 235-243.
- Wahlberg E.J., Keinath T.M., Parker D.S. (1994). Influence of activated-sludge flocculation time on secondary clarification. *Water Environment Research*, 66 (6), 779-786.
- Wahlberg E.J., Merrill D.J. and Parker D.S. (1995). Trouble-shooting activated sludge secondary clarifier performance using simple diagnostic tests. In: *Proceedings of the 68th Annual WEF Conference and Exposition, Miami, Vol. 1*, 435-444. WEF, Alexandria, Virginia.
- Wang J.M., Huang C.P. and Allen H.E. (2000). Surface physical-chemical characteristics of sludge particulates. *Water Environment Research*, 72 (5), 545-553.
- Watts R.W., Svoronos S.A. and Koopman B. (1996). One-dimensional modeling of secondary clarifiers using a concentration and feed velocity-dependent dispersion coefficient. *Water Research*, 30 (9), 2112-2124.
- Wells S.A. (1990). Permeability, liquid and solid velocity, and effective stress variations in compressible cake filtration. *Advances in filtration and separation*, W. Leung, ed., vol. 7, American Filtration and Separation Society, 9-12.
- Wells S.A. and Laliberté D.M. (1998). Winter temperature gradients in circular tanks. *Water Environment Research*, 70 (7), 1274-1279.
- Yamaguchi S. (1996). New type of sludge density meter using microwaves for application in sewage treatment plants. *Water Science & Technology*, 33 (1), 53-60.
- Zheng Y. and Bagley D.M. (1998). Dynamic Model for Zone Settling and Compression Gravity Thickeners. *Journal of Environmental Engineering*, 124 (10), 953-958.
- Zheng Y. and Bagley D.M. (1999). Numerical Simulation of Batch Settling Process. *Journal of Environmental Engineering*, 125 (11), 1007-1013.
- Zhou S.P. and McCorquodale J.A. (1992). Influence of skirt radius on performance of circular clarifier with density stratification. *International Journal for numerical methods in fluids*, 14 (8), 919-934.

Curriculum Vitae

Personalia

Jeriffa De Clercq

Heirbaan 9

9240 ZELE

052/45.90.99

jeriffa.declercq@hogent.be

geboren te Oudenaarde op 5 september 1973

gehuwd, moeder van Cas (24/07/2003) en Nande (25/03/2006)

Studies

- 1985-1991 O.-L.-Vrouwinstituut Zusters Bernardinnen te Oudenaarde
Latijn-Wiskunde
- 1991-1996 Universiteit Gent
Burgerlijk scheikundig ingenieur (onderscheiding)
Thesis: Thermische reductie van stikstofmonoxide in rookgassen:
kinetiek.
Promotor: prof. dr. ir. L. Hosten
- 1996-1997 Katholieke Universiteit Leuven
Aanvullende opleiding milieubeheer-milieukunde
Subrichting: milieutechnologie (grote onderscheiding)
Thesis: Bepaling van de BBT voor de behandeling van percolaat
van het Interleuven-stort te Pellenberg.
Promotor: prof. dr. ir. J. Baeyens
- 1998-2005 Universiteit Gent
Doctoraatsopleiding

Werkervaring

- 1997-1998 IWT-beurs: Gevludiseerde bed reactoren voor intensieve methaan-
resp. sulfideproductie
Universiteit Gent
Promotoren: prof. dr. ir. W. Verstraete en
prof. dr. ir. P.A. Vanrolleghem
- 1998-2005 Assistent, Vakgroep Chemische Proceskunde en Technische Chemie

Faculteit Toegepaste Wetenschappen, Universiteit Gent
 Doctoraatsonderzoek: Batch en continue bezinking van actief slib:
 doorgedreven experimenten en 1D compressie modellering
 Promotoren: prof. dr. ir. J. Defrancq en
 prof. dr. ir. P.A. Vanrolleghem
 2005 Milieubtenaar
 2006-present Assistent Industriële Chemie
 Hogeschool Gent, Departement Industriële Wetenschappen

Publicaties

Internationaal Tijdschrift

- De Clercq J., Devisscher M., Boonen I., Vanrolleghem P.A. and Defrancq J. (2003). A New One-dimensional Clarifier Model - Verification Using Full-scale Experimental Data. *Water Science & Technology*, 47 (12), 105-112.
- De Clercq J., Devisscher M., Boonen I., Defrancq J. and Vanrolleghem P.A. (2005). Analysis and simulation of the sludge profile dynamics in a full-scale clarifier. *Journal of Chemical Technology & Biotechnology*, 80 (5), 523-530.
- De Clercq J., Jacobs F., Kinnear D.J., Nopens I., Dierckx R.A., Defrancq J. and Vanrolleghem P.A. (2005). Detailed spatio-temporal solids concentration profiling during batch settling of activated sludge using a radiotracer. *Water Research*, 39(10), 2125-2135.
- Vanrolleghem P.A., De Clercq B., De Clercq J., Devisscher M., Kinnear D.J. and Nopens I. (2006). New Measurement Techniques for Secondary Settlers: A Review. *Water Science & Technology*, 53 (4-5), 419429.

Proceedings Internationale Conferentie

- De Clercq J., Devisscher M., Boonen I., Vanrolleghem P.A. and Defrancq J. A New One-dimensional Clarifier Model - Verification Using Full-scale Experimental Data. IWA 3rd World Water Congress, Melbourne, Australia, 7-12 April 2002, Proceedings CD-rom.
- Vanrolleghem P.A., De Clercq B., De Clercq J., Devisscher M., Kinnear D.J. and Nopens I. New Measurement Techniques for Secondary Settlers: A Review. The 2nd International Conference on Instrumentation, Control and Automation, May 29 - June 2, 2005, Korea, Proceedings.

Reviews

- Giokas D.L., Daigger G.T., Kim Y. and Paraskevas P.A. (2002). Comparison and evaluation of empirical zone settling velocity parameters based on sludge volume index using a unified settling characteristics database. *Water Research*.
- Makinia J. and Wells S.A. (2004). Evaluation of Empirical Formulae for Estimation of the Longitudinal Dispersion in Activated Sludge Reactors. *Water Research*.

- Zhanga D., Li Z., Lu P., Zhang T. and Xu D. (2005). A method for characterizing a complete settling process of activated sludge. *Water Research*.

Thesissen

- De Clercq J. (1996). Thermische reductie van stikstofmonoxide in rookgassen: kinetiek. Afstudeerwerk burgerlijk scheikundig ingenieur, Universiteit Gent.
- De Clercq J. (1997). Bepaling van de BBT voor de behandeling van percolaat van het Interleuven-stort te Pellenberg. Afstudeerwerk aanvullende opleiding milieubeheer-milieukunde, Katholieke Universiteit Leuven.